BIBLIOGRAPHIC INFORMATION

PB94-206000

Report Nos:

Title: Markov Model for Local and Global Damage Indices in Seismic Analysis.

Date: 18 Feb 94

Authors: S. Rahman and M. Grigoriu.

Performing Organization: Cornell Univ., Ithaca, NY. School of Civil and Environmental Engineering.

Performing Organization Report Nos: NCEER-94-0003

Sponsoring Organization: *National Center for Earthquake Engineering Research, Buffalo, NY.*National Science Foundation, Arlington, VA *New York State Science and Technology Foundation, Albany.

Contract Nos: NSF-BCS-90-25010, NYSSTF-NEC-91029

Type of Report and Period Covered: Technical rept.

NTIS Field/Group Codes: 89D (Structural Analyses)

Price: PC A12/MF A03

Availability: Available from the National Technical Information Service, Springfield, VA. 22161

Number of Pages: 258p

Keywords: *Markov processes, *Structural reliability, *Earthquake damage, Earthquake resistant structures, Structural analysis, Soil structure interactions, Earthquake engineering, Stochastic processes, Structural engineering, Structural vibration, Hysteresis, Building codes, Risk assessment, Mathematical models.

Abstract: Research in the study has focused on several important issues regarding probabilistic seismic performance of structural systems. Three major directions of research have been pursued. They include (1) evaluation of effects of simplifications in reliability-based design codes, (2) development of a new methodology based on Markov model for seismic reliability of degraded structures, and (3) development of analytical relations between local and global damage indices for seismic analysis of shear type buildings. Static and dynamic analyses are performed to evaluate reliability based-design codes. Both strength- and damage-based failure criteria are used to determine seismic reliability of several code-design structures. Results suggest that reliability depends on the mean arrival rate and the intensity of seismic load process. Sites with frequent small earthquakes have very different reliability indices than those at sites with infrequent large earthquakes, although the sites are characterized by the same value of a(sub 10). Comparisons between the reliability indices from the static and dynamic methods indicate that the seismic reliability can be significantly underestimated by the static method especially at sites with low seismicity.

PB94-206000

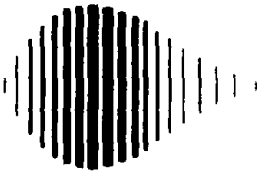

NATIONAL CENTER FOR EARTHQUAKE ENGINEERING RESEARCH

State University of New York at Buffalo

A Markov Model for Local and Global Damage Indices in Seismic Analysis

by

S. Rahman and M. Grigoriu

Cornell University
School of Civil and Environmental Engineering
Ithaca, New York 14853

Technical Report NCEER-94-0003

February 18, 1994

This research was conducted at Cornell University and was partially supported by the National Science Foundation under Grant No. BCS 90-25010 and the New York State Science and Technology Foundation under Grant No. NEC-91029.

NOTICE

PB94-206000

A Markov Model for Local and Global Damage Indices in Seismic Analysis

by

S. Rahman[1] and M. Grigoriu[2]

February 18, 1994

Technical Report NCEER-94-0003

NCEER Task Numbers 86-3033B, 87-1007, 88-1004 and 89-1103

NSF Master Contract Number BCS 90-25010
and
NYSSTF Grant Number NEC-91029

1 Research Scientist, Engineering Mechanics Department, Battelle Memorial Institute. Former Graduate Research Assistant, School of Civil and Environmental Engineering, Cornell University
2 Professor, School of Civil and Environmental Engineering, Cornell University

NATIONAL CENTER FOR EARTHQUAKE ENGINEERING RESEARCH
State University of New York at Buffalo
Red Jacket Quadrangle, Buffalo, NY 14261

PREFACE

The National Center for Earthquake Engineering Research (NCEER) was established to expand and disseminate knowledge about earthquakes, improve earthquake-resistant design, and implement seismic hazard mitigation procedures to minimize loss of lives and property. The emphasis is on structures in the eastern and central United States and lifelines throughout the country that are found in zones of low, moderate, and high seismicity.

NCEER's research and implementation plan in years six through ten (1991-1996) comprises four interlocked elements, as shown in the figure below. Element I, Basic Research, is carried out to support projects in the Applied Research area. Element II, Applied Research, is the major focus of work for years six through ten. Element III, Demonstration Projects, have been planned to support Applied Research projects, and will be either case studies or regional studies. Element IV, Implementation, will result from activity in the four Applied Research projects, and from Demonstration Projects.

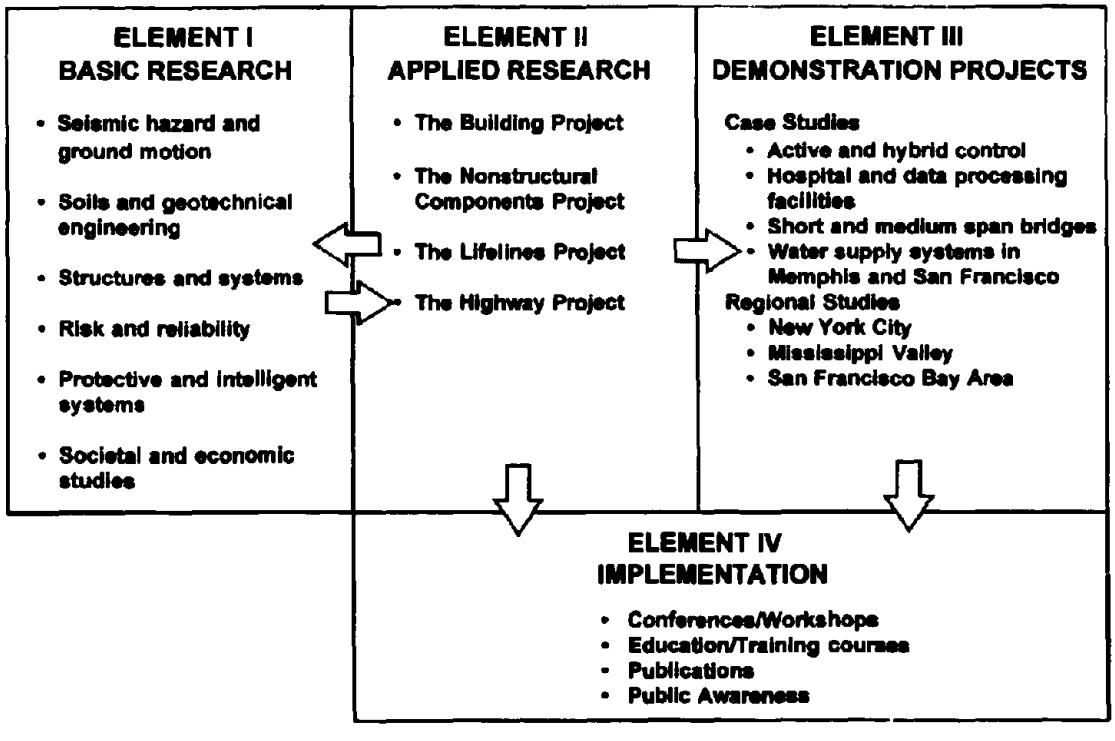

Research in the **Building Project** focuses on the evaluation and retrofit of buildings in regions of moderate seismicity. Emphasis is on lightly reinforced concrete buildings, steel semi-rigid frames, and masonry walls or infills. The research involves small- and medium-scale shake table tests and full-scale component tests at several institutions. In a parallel effort, analytical models and computer programs are being developed to aid in the prediction of the response of these buildings to various types of ground motion.

Two of the short-term products of the **Building Project** will be a monograph on the evaluation of lightly reinforced concrete buildings and a state-of-the-art report on unreinforced masonry.

The **risk and reliability program** constitutes one of the important areas of research in the **Building Project**. The program is concerned with reducing the uncertainty in current models which characterize and predict seismically induced ground motion, and resulting structural damage and system unserviceability. The goal of the program is to provide analytical and empirical procedures to bridge the gap between traditional earthquake engineering and socioeconomic considerations for the most cost-effective seismic hazard mitigation. Among others, the following tasks are being carried out:

1. Study seismic damage and develop fragility curves for existing structures.
2. Develop retrofit and strengthening strategies.
3. Develop intelligent structures using high-tech and traditional sensors for on-line and real-time diagnoses of structural integrity under seismic excitation.
4. Improve and promote damage-control design for new structures.
5. Study critical code issues and assist code groups to upgrade seismic design code.
6. Investigate the integrity of nonstructural systems under seismic conditions.

This report examines current codified methods for seismic analysis and develops a new method for evaluating the seismic performance of buildings. The current codified methods for seismic analysis are generally based on an incomplete characterization of the seismic hazard, the static method for estimating structural response, and elementary failure criteria. On the other hand, the proposed method is based on a realistic characterization of the seismic hazard, accurate estimates of structural response that can be obtained by nonlinear dynamic analysis, and failure criteria accounting for the damage process that occurs during seismic events. A Markov model is developed for evaluating the seismic performance and reliability of buildings. The model can be applied to characterize the evolution of the global damage indices during the lifetime of a building. Moreover, a simple relationship is developed between local and global indices for the case of shear type buildings.

ABSTRACT

Current methods for evaluating the overall seismic performance of structural systems are based on global damage indices which are usually obtained by heuristic combinations of local damage indices. The local indices are related to the parameters of restoring force defined at the critical cross-sections of structural system. However, a global measure of damage can not characterize structural state uniquely, provides only a crude estimate of structural performance during seismic events, and cannot be used to assess structural vulnerability to future loadings. In addition to the above limitations, current estimates of seismic reliability analysis of building structures are based on (*i*) incomplete representations of seismic hazard, *e.g.*, by the peak ground acceleration a_{10} that is exceeded at least once in 50 years with probability 10%, (*ii*) static method for estimating structural response, and (*iii*) elementary failure criteria that do not account for damage accumulation between consecutive seismic events. It is suspected that the reliability analysis based on above simplifications may not provide a satisfactory measure of structural performance.

Research in this study has focused on several important issues regarding probabilistic seismic performance of structural systems. Three major directions of research have been pursued. They include (*i*) evaluation of effects of simplifications in reliability-based design codes, (*ii*) development of a new methodology based on Markov model for seismic reliability of degraded structures, and (*iii*) development of analytical relations between local and global damage indices for seismic analysis of shear type buildings.

Reliability-Based Design Codes: Static and dynamic analyses are performed to evaluate reliability based-design codes. Both strength- and damage-based failure criteria are used to determine seismic reliability of several code-designed structures. Results suggest that reliability depends on the mean arrival rate and the intensity of seismic load process. Sites with frequent small earthquakes have very different reliability indices than those at sites with infrequent large earthquakes, although the sites are characterized by the same value of a_{10}. Comparisons between the reliability indices from the static and dynamic methods indicate that the seismic reliability can be significantly underestimated by the static method especially at sites with low seismicity.

A Markov Model for Seismic Reliability Analysis: A new methodology based on a Markov model is proposed to evaluate seismic performance and sensitivity to initial state of structural systems and determine the vulnerability of structures exposed to one or more earthquakes. The analysis involves simple but realistic characterization of seismic hazard, nonlinear dynamic analysis for estimating structural response, uncertainty in the initial state of structural systems, and failure conditions incorporating damage accumulation during consecutive seismic events. From the proposed model, both *event* and *lifetime* reliabilities can be calculated thus providing a designer more control in seismic performance evaluation. It can be used to determine the damage probability evolution during several earthquakes allowing investigation on seismic vulnerability of new and existing structures. The model can be used to compute mean first passage time determining average number of seismic events before the structure will suffer potential damage. It can also evaluate sensitivity of seismic reliability due to the variability in the initial state of structural systems.

Local and Global Damage Indices: A global hysteretic model is developed and the relations between the parameters of local and global models are established for seismic analysis of multi-story shear buildings. In both models, the analyses involve hysteretic constitutive laws commonly used in earthquake engineering to represent restoring forces and nonlinear dynamic analysis for estimating seismic structural response. From the proposed relations, the local hysteretic behavior and damage can be recovered from analysis based on global models. Both nondegrading and degrading systems are considered and several numerical examples on single- and multi-degree-of-freedom systems of shear beam models are presented to illustrate the proposed methodology. The correlation equations are also applied to implement the Markov model for estimating seismic performance of multi-story degrading structures. Results from this study indicate that the seismic reliability based on lifetime largest load effects can differ significantly from that obtained from seismic hazard based on damage accumulation between seismic events and the uncertainty in initial condition can yield significant variation in the seismic reliability estimate.

ACKNOWLEDGEMENTS

This report is based on the dissertation of Dr. Sharif Rahman that was submitted to the faculty of the graduate school of Cornell University in partial fulfillment of the requirements for the degree of Doctor of Philosophy.

The authors wish to express their thanks to Professors Peter Gergely, Andrei Reinhorn, and Luis Esteva for their suggestions on inelastic dynamic analysis and seismic damage assessment and to Professors Bruce Ellingwood and Fabio Casciati for their advice and useful insights in structural reliability.

This research was supported by the National Center for Earthquake Engineering Research (NCEER) under the NCEER Contract Numbers 86-3033B, 87-1007, 88-10004, and 89-1103. The computer time and service were provided by the Cornell National Supercomputing Facility (CNSF), a resource of the Center for Theory and Simulation in Science and Engineering at Cornell University. They are all gratefully acknowledged.

TABLE OF CONTENTS

LIST OF ILLUSTRATIONS

LIST OF TABLES

SECTION 1
Introduction

1.1 Overview

A major objective of seismic design is the generation of structures that can survive earthquakes. Traditional building structures are usually designed in accordance with provisions in building codes and standards such as *Uniform Building Code* (UBC) [100,101,102,103,104], *Standard Building Code* (SBC) [198], *The National Building Code* [37], *The BOCA/Basic Building Code* [36], and *American National Standard ANSI A58.1* [10]. Current code provisions for seismic design are usually based on simplified methods for estimating seismic hazard (*e.g.*, the zone factor Z of *Uniform Building Code*), seismic load effects (*e.g.*, the static method for stress analysis) and elementary simplified failure criteria (*e.g.*, failure occurs when load effects exceed resistance at any one structural component). Effects of frequency content and duration of ground motions, structural dynamic characteristics, nonlinear dynamic analysis, and structural redundancy are not explicitly accounted for in seismic design. There is no doubt that building codes should utilize simplified rules and formulas to facilitate operational convenience of design process. However, the validity of these rules and formulas and their impact on building safety and reliability should also be investigated.

The code provisions are intended to achieve satisfactory performance of structural systems due to seismic loads during the lifetime of structures. Thus, it is essential to evaluate the adequacy of simplified methods of buildings codes and their effects on the actual performance of structural systems under earthquakes. Ideally, this will require exact knowledge of material characteristics and lifetime seismic loadings on the structure. However, for buildings located in seismically active regions, the ground motions can not be modeled with absolute certainty. Furthermore, the variability in structural and material models constitutes another major source of uncertainty in the evaluation of seismic performance. Two sources can be identified [174,175] and they correspond to the uncertainty in (*i*) the mathematical idealization (model) of hysteretic restoring forces and (*ii*) the parameters of restoring

force characteristics given a hysteretic model. Thus, it is difficult to speak of assessment of structural performance solely by deterministic terms.

A realistic evaluation of structural performance can be conducted only if the uncertainty in structural loads, resistances, and hence responses are taken into consideration. While the load and resistance parameters are not *deterministic*, they nevertheless show *statistical regularity* and the statistical information necessary to describe their probability laws are available. This suggests that the probability theory and structural reliability methods can be applied to assess seismic performance of structural systems. The reliability analysis may then be performed by computing the probability that the structural responses of interest will not violate a set of performance criteria during its lifetime.

1.2 Static Reliability Analysis

The static reliability analysis is based on (*i*) elementary models of seismic hazard, *e.g.* by the 50-year maximum peak ground acceleration, (*ii*) stress analysis by static method, and (*iii*) limit states defined by strength-related failure criteria at a particular structural component. The corresponding component reliability index can be computed from $\Phi^{-1}(P_s)$ where P_s is the probability that the lifetime largest load effect obtained from static analysis does not exceed strength at a specific structural component and $\Phi(\cdot)$ is the cumulative distribution function of standard Gaussian random variable. Effects of structural redundancy, nonlinear dynamic response, and damage accumulation during consecutive seismic events are not explicitly included in this analysis.

These simplified methods have been used in recent studies [149,173,179] to perform reliability analysis of code-designed buildings subject to seismic ground shaking. Resultant reliability indices have much lower values than those for gravity loads. It is suspected that the seismic reliability indices obtained from static analysis do not provide satisfactory means of structural performance, because their determination involves several gross approximations. For example, it is assumed that:

- seismic hazard at a site is completely characterized by 50-year maximum peak ground acceleration. The cumulative distribution function of this acceleration depends only

on the 10% upper fractile of peak ground acceleration a_{10}. Frequency, duration, and occurrence rate of earthquakes are not considered in the analysis. Moreover, if a structure is designed to resist several seismic events in its lifetime without consideration of repairs between any two consecutive earthquakes, the lifetime peak ground acceleration may not be meaningful as a design load parameter due to accumulation of damage;

- load effects can be estimated by the equivalent static method which may provide inaccurate results in many practical cases;

- failure occurs when load effects exceed resistance in at least one structural component. Thus, in addition to using an elementary failure criterion for components, the approach completely ignores structural redundancy; and

- seismic loads E can be obtained from a_{10} reported in hazard maps developed by Algermissen and Perkins and structural strength can be derived from the nominal base shear E_n in the 1985 *Uniform Building Code*. This code is based on a seismic zone map characterizing seismic environment in terms of seismic zone factor Z which accounts for the maximum Modified Mercalli intensity observed historically in each zone. However, a_{10} is mapped considering site seismicity and design lifetime . As a result, the consequent reliability analyses based on E and E_n can be inconsistent.

1.3 Dynamic Reliability Analysis

The dynamic reliability analysis is based on (*i*) random process representation of seismic ground acceleration, (*ii*) nonlinear dynamics for structural stress analysis, and (*iii*) damage-related limit states. Since earthquake-resistant design aims at mitigating extensive damage and minimizes collapse probability, it has been proposed to evaluate the overall structural performance by *global damage indices*. These global indices are usually obtained from heuristic combinations of local damage measures which can be related to the parameters governing local restoring forces. The reliability analysis involves (*i*) nonlinear dynamic analysis to yield global damage indices (*ii*) determination and calibration of global indices, and (*iii*) assessment of seismic performance from the probability that the global indices do not exceed

admissible values. As in the static method, the seismic hazard is specified by the largest load effect during the lifetime of the structure. Effects of damage accumulation during consecutive seismic events are not taken into account in the current dynamic analysis.

The current measure of global damage has several shortcomings. For example, it (*i*) can not characterize structural state uniquely, (*ii*) provides only a crude estimate of structural performance during seismic events, and (*iii*) can not be used to assess structural vulnerability to future loadings. Furthermore, the definitions of such global indices are largely based on arbitrary considerations and do not account for any mechanistic aspects of seismic structural performance.

Another important issue in the evaluation of seismic performance is the uncertainty in the initial state of structural systems. This can be caused by manufacturing processes, errors in design, inadequate construction, unsatisfactory quality control for new structures and lack of information concerning damage caused by previous seismic events for existing structures. Reliability analysis based solely on current definitions of global damage indices cannot be applied to determine sensitivity to initial state of structural systems. Hence, any rational assessment of structural performance should simultaneously account for the mechanical degradation process of all critical cross-sections and components.

1.4 Objectives Of The Study

Research in this study focuses on several important issues regarding probabilistic evaluation of seismic performance of structural systems. Three major directions of research have been pursued. They include (*i*) evaluation of effects of simplifications in the current reliability-based design codes, (*ii*) development of a new methodology based on a Markov model for seismic reliability analysis, and (*iii*) development of an analytical approach to establish relations between local and global damage indices in seismic analysis.

1.5 Outline Of The Study

Performance and safety of structures under severe environmental loads like earthquakes strongly depend on nonlinear response of structures. Both qualitative and quantitative

natures of this response in turn are significantly related to the accuracy in the modeling of structural systems, restoring forces, seismic load processes, and obviously the seismic damage. Section 2 provides a comprehensive state-of-the-art review on the above issues describing recent progress and limitations.

Section 3 performs the static reliability analysis to obtain seismic reliability indices of structures designed according to current building codes. First- and Second-Order Reliability Methods (FORM/SORM) and Importance Sampling technique are applied to obtain the reliability measures. The reliability analysis is carried out based on component failure criteria describing structural performance at the critical cross-sections. It also involves sensitivity analysis due to different models of seismic hazard.

Section 4 carries out the dynamic reliability analysis of nondegrading models of structural systems. Various failure criteria are used to (*i*) calculate reliability indices for simple code-designed structures, (*ii*) evaluate sensitivity of reliability indices to static and dynamic methods, and (*iii*) investigate the adequacy of current code provisions for seismic design.

Section 5 continues to examine the validity of static reliability indices by conducting seismic analysis of nonlinear degrading systems. The analysis accounts for (*i*) stochastic process representation of seismic ground acceleration, (*ii*) nonlinear dynamics of structural systems, and (*iii*) damage-related limit states. Various failure criteria based on maximum deformation combined with cumulative load effects and interstory drift are employed to obtain seismic reliability measures of reinforced concrete frame structures designed by *1985 Uniform Building Code*. These analyses provide benchmark results against which the static reliability estimates of the above frames obtained in the previous phase of this study are compared.

Section 6 proposes a new methodology based on a Markov model for stochastic evaluation of seismic performance of structural systems. The method of analysis involves (*i*) complete characterization of seismic hazard, (*ii*) nonlinear dynamic analysis for estimating structural response to earthquakes, (*iii*) failure conditions incorporating damage accumulation during consecutive seismic events, and (*iv*) uncertainty in the initial state of structural systems. Simple degrading systems representing code-designed structures are presented to illustrate the capabilities of the proposed Markov model.

Section 7 develops a rational analytical tool to establish relations between parameters of local and global hysteretic models for deterministic seismic analysis of shear type buildings. The proposed method of analysis is based on (*i*) state-of-the-art endochronic model for restoring forces and (*ii*) nonlinear dynamic analysis for estimating structural response to earthquakes. Both nondegrading and degrading systems are considered and several numerical examples are presented to validate the proposed methodology. The correlation equations proposed in this section are then applied to implement the Markov model for realistic structural systems.

Section 8 summarizes the principal contributions made from this study and finally, draws conclusions regarding seismic performance of structural systems.

SECTION 2
State-Of-The-Art Review

2.1 Introduction

The behavior of all engineering systems under severe loads which typify environmental hazards like earthquakes strongly depends on nonlinear response of structures. Both qualitative and quantitative natures of this nonlinearity in turn are significantly related to the accuracy in the modeling of structural systems, restoring force, and obviously the seismic load process. Since earthquake resistant design aims at mitigating extensive damage and minimizes collapse probability, damage indices are currently used to evaluate seismic performance of structural systems. In recent years, significant progress in these areas has been achieved both in terms of the development of methodologies and the applications to earthquake engineering problems. The objective of this section is to summarize and discuss the state-of-the-art of several subject areas related to seismic analysis. The review is organized to include issues related to (*i*) material mechanical models, (*ii*) structural models, (*iii*) seismic hazard, and (*iv*) seismic damage assessment.

2.2 Material Mechanical Models

While linear elastic constitutive law provides much valuable insight into the nature of structural response due to earthquake excitation, it is now widely recognized that most real structures exhibit nonlinear behavior, particularly for levels of response which correspond to structural damage. A variety of nonlinearities may be encountered in structural applications. These range from geometric and other elastic nonlinearities to nonlinearities associated with inelastic behavior. Broadly, the nonlinear systems can be classified into (*i*) conservative systems and (*ii*) nonconservative systems.

2.2.1 Conservative Models

The simplest models of nonlinearity are those describing nonlinear elastic behavior. These models are conservative, because they do not include any form of energy dissipation. Figure 2.1(a) shows the generalized force-displacement relation of a so-called hardening elastic system for which the frequency of free oscillation increases with amplitude of oscillation. This trend is reversed for the softening system illustrated in Fig. 2.1(b). Both types of generalized force-displacement relation may be modeled by a power series expansion in generalized displacement or by a piecewise linear representation. The well-known Duffing oscillator [63] is the lowest order nonlinear power series representation of the elastic system. Hardening systems often arise as a result of geometric nonlinearities as in the case of deflection of suspension bridge cables [144]. Most equipment isolation devices also behave as hardening elastic systems for large deflection [55]. A softening elastic model may be used as a first approximation to the behavior of prestressed concrete [200]. It may also be used to characterize the behavior of axially loaded column [135] and to interpret the destabilizing effect of gravity on simple structures [95].

Due to the presence of friction (or damping forces) and other dissipative forces, most structural systems do not exhibit conservative behavior. Another major cause is the large deformation experienced by structures during earthquakes. More attention has thus been focused here on modeling nonconservative systems.

2.2.2 Nonconservative Models

A more complicated and realistic form of nonlinearity encountered in large amplitude oscillation of structures is that associated with inelastic hysteretic behavior. In structural dynamics, the term "hysteresis" is used to describe a nonconservative system behavior in which the generalized force is a functional depending not only on instantaneous generalized displacement, but also on its entire past history. For reinforced concrete structures, this type of behavior may result from opening and closing of cracks, yielding of reinforcing steel together with the Bauschinger effect, nonlinearity of concrete in compression, bond-slip of steel bars, sliding shear at open cracks, and obviously the load history. For steel structures, on the other hand, because of the uniformity of material the hysteretic behavior is considerably

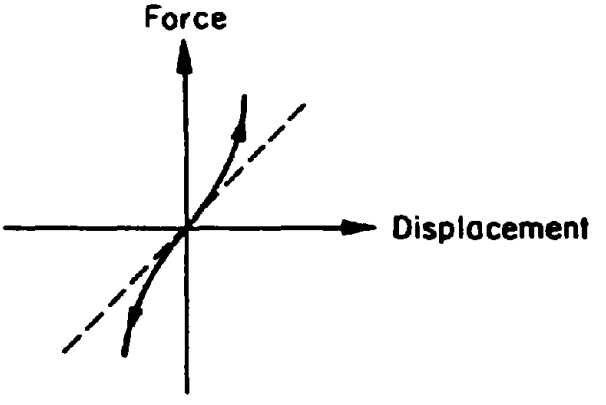

(a) Hardening System

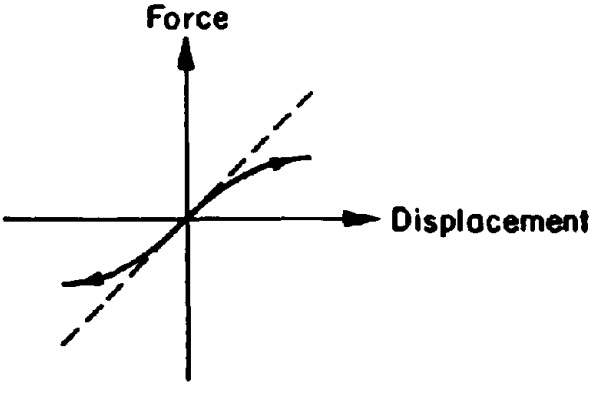

(b) Softening System

Figure 2.1: Generalized Force-Displacement Relation

simpler than that for reinforced concrete. Any complicacies arise from yielding of various elements within the structure or due to slippage of bolts at connections or due to failure of nonstructural elements and welds. The hereditary nature of this hysteretic behavior is usually described by smooth curves or piecewise linear segments which are essentially the plots of restoring forces (*e.g.*, moments, shears, etc.) versus deformations (*e.g.*, curvatures, displacements, etc.). These restoring force-deformation models can be defined for the material at the level of member usually concentrated at its ends (*e.g.*, end joints of beams and columns), subassemblages of structure (*e.g.*, the shear beam model), and structure itself.

Univariate Hysteretic Law

Consider the relative displacement response X_t of a general hysteretic oscillator with mass m which is subjected to seismic ground acceleration W_t. The equation of motion is governed by a second-order differential equation given by

$$m\ddot{X}_t + g\left(\{X_s, \dot{X}_s,\ 0 \le s \le t\}; t\right) = -mW_t \tag{2.1}$$

In Eq. 2.1, g is a general restoring force which is usually chosen to admit an additive decomposition of nonhysteretic component

$$g_{nh}(X_t, \dot{X}_t) = c\dot{X}_t + \alpha k X_t \tag{2.2}$$

and hysteretic component

$$g_h\left(\{X_s, \dot{X}_s,\ 0 \le s \le t\}; t\right) = (1-\alpha)kZ_t \tag{2.3}$$

in which c is the constant damping (viscous) coefficient, α is the parameter defining participation of linear restoring force, k is the stiffness, and Z_t is the hysteretic (auxiliary) variable, the evolution of which can be modeled by a first order nonlinear ordinary differential equation

$$\dot{Z}_t = F(X_t, \dot{X}_t, Z_t; t) \tag{2.4}$$

or, by the nondimensionalized version

$$\dot{z}_t = f(x_t, \dot{x}_t, z_t; t) \tag{2.5}$$

via the transformation

$$x_t = \frac{X_t}{X^*}, \quad z_t = \frac{Z_t}{X^*} \tag{2.6}$$

in which X^* is a characteristic displacement usually taken as the yield displacement x_y, F and f are general nonlinear functions depending on a particular constitutive law. Following the state vector approach [67,94,136] with the designation of $\theta_{1,t} = X_t$, $\theta_{2,t} = \dot{X}_t$, and $\theta_{3,t} = Z_t$, the equivalent system of first-order differential equations in state variables becomes

$$\begin{aligned} \dot{\theta}_{1,t} &= \theta_{2,t} \\ \dot{\theta}_{2,t} &= -\frac{1}{m}[c\theta_{2,t} + \alpha k\theta_{1,t} + (1-\alpha)k\theta_{3,t}] - W_t \\ \dot{\theta}_{3,t} &= F(\theta_{1,t}, \theta_{2,t}, \theta_{3,t}; t) \end{aligned} \tag{2.7}$$

which can be recast in a more compact form

$$\dot{\boldsymbol{\theta}}(t) = \mathbf{h}\left(\boldsymbol{\theta}(t), t\right) \tag{2.8}$$

with the initial conditions

$$\boldsymbol{\theta}(0) = \mathbf{0} \tag{2.9}$$

where $\mathbf{h}(\cdot)$ is a vector function, and $\boldsymbol{\theta}(t) = \{\theta_{1,t}, \theta_{2,t}, \theta_{3,t}\}^T$ is a complete 3-dimensional response state vector. Thus, the computational effort in determining the response characteristics of a nonlinear dynamical system can be viewed as the solution of the nonlinear initial-value problem in Eqs. 2.8 and 2.9.

When the functions f or F are explicitly prescribed, a wide variety of mathematical models of hysteretic characteristics can be produced. However, there is no rigorous theoretical investigation in determining these functions. Currently, they are selected on the basis of experimental and empirical studies of hysteretic behavior of structural systems subject to

repeated load processes during earthquakes. Quite arbitrarily, they are classified here into (*i*) piecewise linear hysteresis, and (*ii*) smooth hysteresis.

Piecewise Linear Hysteresis

The piecewise linear hysteretic models are conceptually simple, but they do not allow analytical treatment to be simple as well. The abrupt change in slopes of these models are obviously not very realistic and it requires very small time steps to avoid overshooting in the numerical integration of equations of motion. Nevertheless, many such models exist and are widely used in current seismic analysis.

Bilinear Model: The simplest model for hysteretic behavior and one which has received by far the widest use in earthquake engineering is the bilinear hysteretic model (including the well-known elasto-plastic system) as indicated in Fig. 2.2. The constitutive law of the

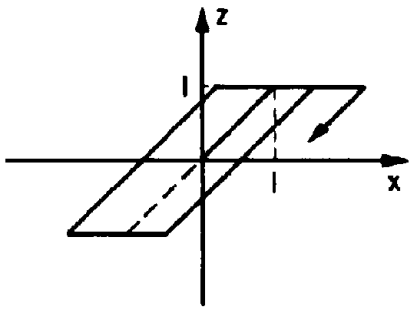

Figure 2.2: Bilinear Model

hysteretic component is given by the following differential form [118]

$$\dot{z} = \dot{x}\,[1 - H(\dot{x})H(z-1) - H(-\dot{x})H(-z-1)] \tag{2.10}$$

where $H(\cdot)$ denotes the unit step function, i.e., $H(u) = 1$ for $u \geq 0$ and 0 for $u < 0$. The constitutive law of bilinear hysteretic model is completely described by the Eqs. 2.1-

2.10. Similarly, by introducing additional state variables one can describe the hysteresis of a higher multi-linear model. The major drawback of the bilinear model is that it does not reflect system degradation, pinching effects or Bauschinger effects exhibited by various engineering materials.

Kato-Akiyama Model: The hysteretic model presented by Kato and Akiyama [115] has the stiffening or degrading characteristics of yield strength with the cumulative plastic deformation as shown in Fig. 2.3. The differential form of this model is [208]

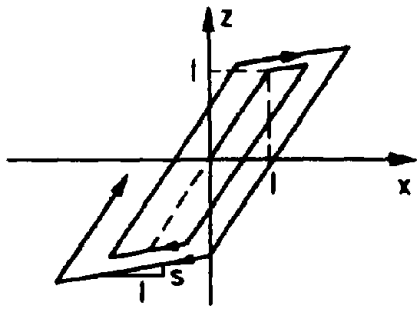

Figure 2.3: Kato-Akiyama Model

$$\dot{z} = \dot{x}\left[1 - (1-s)H(\dot{x})H\left(z - 1 - \frac{sx_p}{1-s}\right) - (1-s)H(-\dot{x})H\left(-z - 1 - \frac{sx_n}{1-s}\right)\right] \quad (2.11)$$

$$\dot{x}_p = (1-s)\dot{x}H(\dot{x})H\left(z - 1 - \frac{sx_p}{1-s}\right) \quad (2.12)$$

$$\dot{x}_n = -(1-s)\dot{x}H(-\dot{x})H\left(-z - 1 - \frac{sx_n}{1-s}\right) \quad (2.13)$$

where x_p and x_n are the one-directional cumulative plastic deformation in the hysteretic component z, and s is the rigidity ratio of the hysteretic component z. Thus the description of Kato-Akiyama hysteretic model needs differential equations for the additional state variables

x_p and x_n controlling the stiffening and degrading of hysteresis in addition to the state variables x, $\dot{x}$, and z. The Kato-Akiyama model represents the stiffening or degrading characteristics according to $s > 0$ or $s < 0$, respectively. In a particular case when s vanishes, the Kato-Akiyama hysteresis is reduced to the bilinear hysteresis.

Origin-oriented Model: The origin-oriented model shown in Fig. 2.4 has zero-memory and origin-oriented features. The constitutive law of the normalized origin-oriented hysteretic

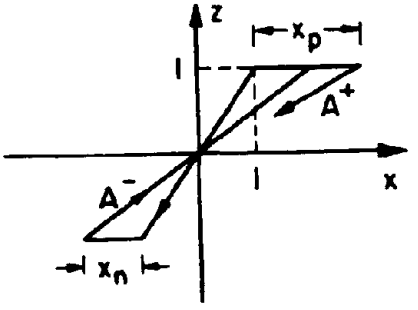

Figure 2.4: Origin-oriented Model

component is given by [207]

$$\dot{z} = \dot{x}\left[\{1 - H(\dot{x})H(z-1)\}\frac{H(z)}{1+x_p} - \{1 - H(-\dot{x})H(-z-1)\}\frac{H(-z)}{1+x_n}\right] \tag{2.14}$$

$$\dot{x}_p = \dot{x}H(\dot{x})H(z-1) \tag{2.15}$$

$$\dot{x}_n = -\dot{x}H(-\dot{x})H(-z-1) \tag{2.16}$$

where x_p and x_n are the absolute maximum and minimum inelastic displacements (total displacement minus unity), and are utilized to preserve the current positive and negative peak deformations.

Peak-oriented Model: The peak-oriented hysteretic model represents stiffness degrading characteristic which is closely related to the total cumulative plastic deformation. The model is shown in Fig. 2.5, and the normalized hysteretic component is given by [207]

$$\dot{z} = \frac{2\dot{x}}{2 + x_{pn}} [1 - H(\dot{x})H(z-1) - H(-\dot{x})H(-z-1)] \tag{2.17}$$

$$\dot{x}_{pn} = \dot{x}\,[H(\dot{x})H(z-1) - H(-\dot{x})H(-z-1)] \tag{2.18}$$

where x_{pn} is sum of x_p and x_n defined by Eqs. 2.15 and 2.16.

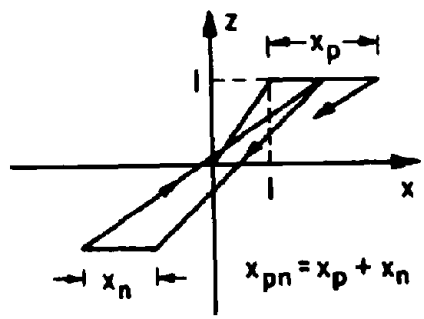

Figure 2.5: Peak-oriented Model

Slip Model: The normalized hysteretic component of slip model shown in Fig. 2.6 has the differential form [207]

$$\begin{aligned} \dot{z} \;=\; & \dot{x}\,[H(x - x_p)H(\dot{x})\{1 - H(z-1)\} + H(x)H(-\dot{x})\{1 - H(-z)\} + \\ & H(-x - x_n)H(-\dot{x})\{1 - H(-z-1)\} + H(-x)H(\dot{x})\{1 - H(z)\}] \end{aligned} \tag{2.19}$$

$$\dot{x}_p = \dot{x}H(\dot{x})H(z-1) \tag{2.20}$$

$$\dot{x}_n = -\dot{x}H(-\dot{x})H(-z-1) \tag{2.21}$$

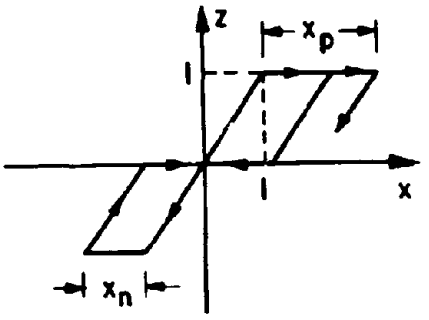

Figure 2.6: Slip Model

The idealized slip model proposed by Tanabashi and Kaneta [214] is given by Eqs. 2.19,2.20, and 2.21. In particular case when x_p and x_n in Eq. 2.19 are neglected, the slip model collapses to the double bilinear hysteretic model proposed by Iwan [108].

Clough Model: The stiffness degrading hysteretic model presented by Clough and Johnston [50] intended for use in reinforced concrete structures is shown in Fig. 2.7. In this model, the differential representation of the hysteretic component z becomes [208]

$$\begin{aligned} \dot{z} &= \dot{x}H(z)\left[\frac{1-z}{1+x_p-x}H(\dot{x})\{1-H(z-1)\}+H(-\dot{x})\right]+ \\ &\quad \dot{x}H(-z)\left[\frac{1+z}{1+x_p+x}H(-\dot{x})\{1-H(-z-1)\}+H(\dot{x})\right] \end{aligned} \tag{2.22}$$

$$\dot{x_p} = \dot{x}H(\dot{x})H(z-1) \tag{2.23}$$

$$\dot{x_n} = -\dot{x}H(-\dot{x})H(-z-1) \tag{2.24}$$

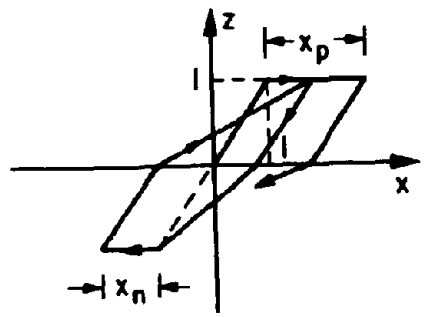

Figure 2.7: Clough Model

Other models such as those proposed by Takeda *et al.* [210], Fukada [70], Muto [142], and others extend the bilinear models to include various deterioration by using the similar set of empirical rules described earlier. Although these rules may be applied for a time history analysis of the response by means of a step-by-step numerical integration, they are difficult to put in mathematically convenient forms for analytical solution.

Smooth Hysteresis

The smooth hysteretic models are usually obtained from the constitutive equations of *endochronic theory* [220,225,143,25]. The endochronic concept is based on rate-dependent viscoplasticity without the existence of yield surface and was introduced in triaxial constitutive relations for metals by Valanis [220] who also coined the term "endochronic". The smooth hysteretic model is attractive mainly because it eliminates the sudden transition from elastic to inelastic states thus avoiding the attendant mathematical problems.

Bouc Model: A versatile smooth restoring force model capable of reproducing inelastic, hysteretic, but nondegrading behavior is proposed by Bouc [34] which has the following differential form of hysteretic component (Fig. 2.8)

$$\dot{z} = A\dot{x} - \beta|\dot{x}|z - \gamma\dot{x}|z| \tag{2.25}$$

in which β, γ, and A are parameters governing the amplitude and shape of hysteretic loops.

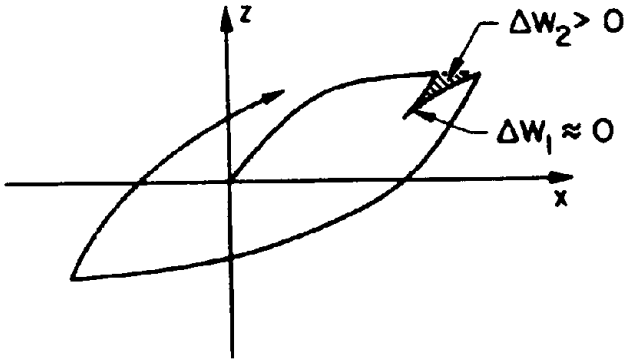

Figure 2.8: Bouc Model

A large variety of hysteresis are possible choosing appropriate values for the parameters of restoring force-deformation model. The main inconveniences of this constitutive relation are the lack of closure of hysteresis cycles and the anomalous behavior under cycles during unloading and loading phases without load reversal [25]. The first difficulty can be avoided by appropriate selection of model parameters. The second aspect, on the other hand, leads to violate a basic mechanical principle which in the rigid plastic case is known as the *normality rule* [45,46]. For an arbitrary hysteresis shown in Fig. 2.9, the work done ΔW on the material during unloading (AB) and reloading (BC) is equal to $\Delta W_1 - \Delta W_2$ which must be non-negative in accordance with Drucker's stability postulate [25,62]. When Bouc hysteresis is considered, $\Delta W_1 \approx 0$, $\Delta W_2 > 0$ (Fig. 2.8), and ΔW becomes largely negative thus violating Drucker's stability postulate.

Wen Model: Another parameter μ controlling the smoothness of transition from elastic to inelastic region in Bouc's hysteretic model has been incorporated by extending the model

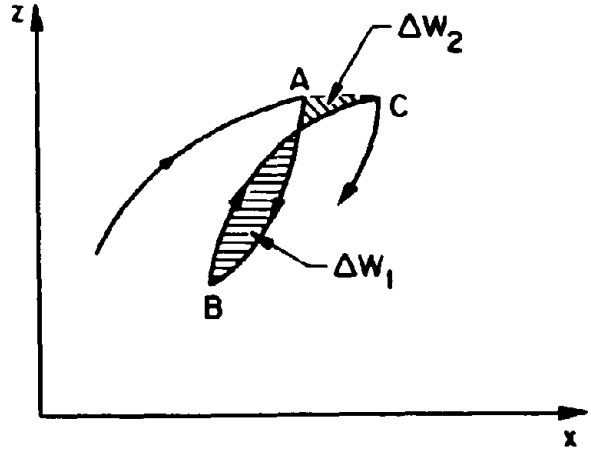

Figure 2.9: Unloading-Loading Cycle of a General Hysteresis

in Eq. 2.25 into the form [228]

$$\dot{z} = A\dot{x} - \beta|\dot{x}||z|^{\mu-1}z - \gamma\dot{x}|z|^{\mu}. \tag{2.26}$$

As shown in Fig. 2.10 when $\mu \nearrow \infty$, the Wen hysteresis reduces to that of bilinear model and when $\mu = 1$, the model collapses to original Bouc model as expected. In this model, the issue regarding violation of Drucker's stability postulate is still present. However, the degree to which this postulate is violated can be reduced by increasing the value of μ which was not possible for the original Bouc model. For example, when $\mu \nearrow \infty$, although $\Delta W_1 \simeq 0$, $\Delta W_2 \searrow 0$, and consequently $\Delta W = \Delta W_1 - \Delta W_2 \nearrow 0$. However, large values of μ (*i*) makes the step-by-step integration of nonlinear equations of motion more cumbersome, (*ii*) reduces the accuracy achievable by using equivalent linearization techniques, and (*iii*) more importantly, puts a serious limitation in the modeling capability as calibration with experimental results suggest the use of $\mu = 1$ for steel and $\mu = 2$ for reinforced concrete [204]. Nevertheless, this model has received a fair amount of attention in the seismic engineering community and will also be used here in this study.

Deterioration of the restoring force is achieved by prescribing the model parameters

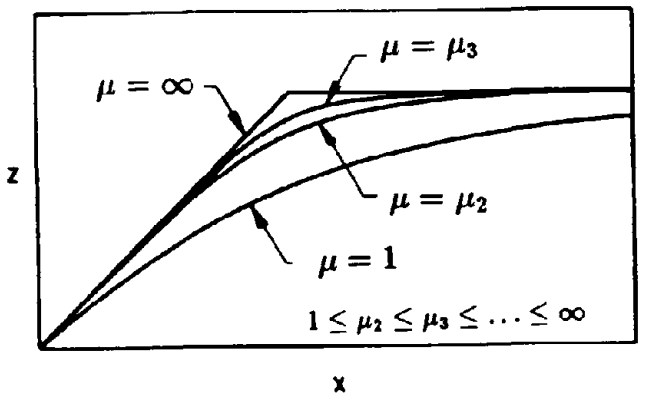

Figure 2.10: Effects of μ on Skeletal Curve of Wen Model

to be arbitrary functions of response severity such as total hysteretic energy dissipation or amplitude of response or both. Baber and Wen [20,21] used the energy based degradation in an extended Wen model

$$\dot{z} = \frac{1}{\eta}\left[A\dot{x} - \nu\left(\beta|\dot{x}||z|^{\mu-1}z - \gamma\dot{x}|z|^{\mu}\right)\right] \tag{2.27}$$

with additional parameters ν and η to incorporate strength and stiffness degradation by

$$A(t) = A_0 - \delta_A \varepsilon_T(t), \tag{2.28}$$

strength deterioration by

$$\nu(t) = \nu_0 + \delta_\nu \varepsilon_T(t), \tag{2.29}$$

and, stiffness degradation by

$$\eta(t) = \eta_0 - \delta_\eta \varepsilon_T(t) \tag{2.30}$$

in which δ_A, δ_ν δ_η are the constant rates of degradation, A_0, ν_0, η_0 are parameter values prior to loadings, and

$$\varepsilon_T(t) = (1-\alpha)k\int_0^t z(s)\dot{x}(s)ds \tag{2.31}$$

is the total hysteretic energy dissipated until time t. Sues *et al.* [205] used response amplitude based degradation given by

$$\eta = A\frac{x_{p_i} - x_{p_{i-1}}}{z_{p_i} - z_{p_{i-1}}} \tag{2.32}$$

in which x_{p_i} and z_{p_i} are the displacement and hysteretic amplitude in the ith half cycle. Baber and Noori [19] added a "slip-lock" element in tandem with the hysteretic force element which is able to reproduce the commonly observed pinching of the hysteretic loops exhibited by reinforced concrete. Although, the above degradation laws and pinching mechanism are arbitrarily chosen, they have been found useful in seismic analysis.

Casciati Model: In an attempt to avoid the limitations of previous models regarding violation of Drucker's stability postulate, an improved endochronic model is proposed by Casciati [45] by adding more terms in the Wen model giving

$$\dot{z} = A\dot{x} - \beta|\dot{x}||z|^{\mu-1}z - \gamma\dot{x}|z|^{\mu} + \beta_1|\dot{x}||z|^{\mu_1-1}z + \beta_1\dot{x}|z|^{\mu_1} \tag{2.33}$$

where β_1 and $\mu_1 < \mu$ are additional parameters of this model. The experience of Ref. [45] suggests that for endochronic models, the local violations of Drucker's stability postulate can not be avoided. However, with the model in Eq. 2.33 applied with appropriate parameters, the global results makes $\Delta W = \Delta W_1 - \Delta W_2$ a "small" quantity but not a positive one as the postulate would require.

Other hysteretic models such as Ramberg-Osgood model [112] describes the force-displacement skeleton curve by a three-parameter polynomial and allows a smooth transition from the elastic to plastic region and some freedom in the shape of the hysteresis. However, it is difficult to incorporate system degradation. A distributed element model which is an extension of the combined spring Coulomb damper concept has been proposed by Iwan [107] where the smooth transition can be properly reproduced.

Multivariate Hysteretic Law

Multivariate constitutive laws are essential for spatial extension of frames and the bidirectional nature of seismic excitation. For two-dimensional structures under biaxial excitation, the interaction of restoring forces in the two directions may significantly alter the response behavior. For example, the damage suffered from oscillation in one direction is likely to weaken the strength and/or stiffness in the other direction and vice versa. The endochronic restoring force model of Eq. 2.26 together with $\mu = 2$ has been extended quite arbitrarily to include such interaction by requiring that the hysteretic components in the two directions, i.e., z_x and z_y satisfy the following coupled differential equations [157]

$$\dot{z}_x = A\dot{u}_x - \beta|\dot{u}_x||z_x|z_x - \gamma\dot{u}_x z_x{}^2 - \beta|\dot{u}_y||z_y|z_x - \gamma\dot{u}_y z_x z_y \tag{2.34}$$

$$\dot{z}_y = A\dot{u}_y - \beta|\dot{u}_y||z_y|z_y - \gamma\dot{u}_y z_y{}^2 - \beta|\dot{u}_x||z_x|z_y - \gamma\dot{u}_x z_x z_y \tag{2.35}$$

where u_x and u_y are the displacements in the traditional x and y directions. A, β, and γ as in Eq. 2.26 are system parameters. Implicit in Eqs. 2.34 and 2.35 is the assumption that the hysteretic restoring forces are isotropic. For an orthotropic systems (implying stiffness and strength in the two directions are different) one can introduce a simple transformation of the response variables and still use the same equations [157]. As in the uniaxial model, deterioration can be introduced by letting parameters A, β, and γ be functions of time depending on the severity of response, *e.g.*, maximum response amplitude or hysteretic energy dissipation or both.

Endochronic theory was originally developed without the concept of yielding surface, but the identification of model parameters requires the availability of test results, which are presently scarce particularly for multivariate hysteresis. A multivariate endochronic model that at least considers the basic requirements of plasticity theory has thus been examined by Casciati [45,44]. The mathematical formulation of hysteresis is obtained in the tensorial form of three-dimensional analog of Bouc model and is given by [45]

$$\dot{\mathbf{Y}} = A\dot{\mathbf{E}} - \beta\| \mathbf{Y} \|^{\mu-2} \| \mathbf{Y} \otimes \dot{\mathbf{E}} \| \mathbf{Y} - \gamma\| \mathbf{Y} \|^{\mu-2}(\mathbf{Y} \otimes \dot{\mathbf{E}})\mathbf{Y} \tag{2.36}$$

in which A, β, γ and μ are model parameters, $\mathbf{E}$ is the deviatoric strain tensor, $\otimes$ is the symbol for tensor product, and $\| \mathbf{Y} \| \stackrel{\text{def}}{=} \sqrt{\mathbf{Y} \cdot \mathbf{Y}} \stackrel{\text{def}}{=} \sqrt{\text{Tr}(\mathbf{Y}^T \mathbf{Y})}$ is the norm of second-order tensor $\mathbf{Y}$ defined as

$$\mathbf{Y} = \mathbf{S} - \boldsymbol{\eta} \tag{2.37}$$

where $\mathbf{S}$ is the deviatoric stress tensor and $\boldsymbol{\eta}$ is the tensor of internal variables obtained from

$$\boldsymbol{\eta} = \kappa \dot{\boldsymbol{\epsilon}}^p \tag{2.38}$$

in which κ is some work hardening constant and $\dot{\boldsymbol{\epsilon}}^p$ is the plastic strain rate tensor given by

$$\dot{\boldsymbol{\epsilon}}^p = \frac{\partial \phi}{\partial \boldsymbol{\sigma}} \dot{\Lambda} \tag{2.39}$$

where $\phi = \phi(\boldsymbol{\sigma}, \boldsymbol{\eta})$ is the plastic potential, $\boldsymbol{\sigma}$ is the stress tensor, and $\dot{\Lambda}$ is the corresponding plastic multiplier. Details of derivation are available in the original reference [45].

Plasticity is governed by associated flow rule (plastic potential coincides elastic potential). Hardening is assumed to be kinematic (the subsequent yield surface is obtained from rigid body motion of initial yield surface), and also the motion is deemed to be linear during successive propagation of yield surfaces (Prager's Hardening). Comparisons of the model in Eq. 2.36 with the model in Eqs. 2.34 and 2.35 show that (*i*) the interaction of restoring forces does not include all the terms of $(\mathbf{Y} \otimes \dot{\mathbf{E}})$ and (*ii*) the yielding curve in Eqs. 2.34 and 2.35 is not convex thus violating a basic mechanical requirement of the theory of plasticity.

2.2.3 Evaluation of Hysteretic Models

Calibration of Model Parameters

In order to predict the restoring force behavior of an actual structure, it is necessary to determine appropriate values for the parameters of hysteretic models. A system identification technique based on a least square error minimization has been used by Sues *et al.* [204] for the smooth hysteretic model in Eq. 2.25. The values of model parameters from calibration with laboratory data suggest the use of (*i*) $A = 1$, $\mu = 1$, $\alpha = 0.04$, $\beta = \gamma$ for steel and (*ii*)

$A = 1, n = 2, \alpha = 0.02, \beta = -3\gamma$ $(\gamma < 0)$ for reinforced concrete in which γ is computed from $A/(\beta + \gamma)^{1/\mu} = F_y$, where F_y is the yield force usually known from material characteristics. Other methods such as those based on an extended Kalman filter method have been applied to the smooth hysteretic restoring forces. Methods for estimating the system parameter of the distributed element model and the Masing models have been proposed by Peng and Iwan [163] and Jayakumar and Beck [111]. Parameter calibration for biaxial models in Eqs. 2.34 and 2.35 has also been performed by Wen and Ang [227].

Comparisons with Experimental/Theoretical Results

The accuracy and capability of the hysteretic model are indicated by comparisons of the restoring force-displacement relations with those based on experimental and rigorous theoretical studies. The Wen hysteresis with the displacement dependent degradation law has been evaluated by Sues *et al.* [204,205]. Comparisons with the test results of Park and Paulay [155] and Gulkan and Sozen [81] shown in Figs. 2.11 and 2.12 exhibit overall satisfactory performance of the analytical model with the exception of pinching behavior exhibited by the corresponding laboratory data. In Ref. [226], the degrading and nondegrading biaxial hysteretic models based on Eqs. 2.34 and 2.35 are also compared with experimental studies of Takizawa and Aoyama [211] and classical plasticity solution by Powell and Chen [166]. Fig. 2.13 shows the force-displacement characteristics of a degrading endochronic model [157] and the corresponding test results of Takizawa and Aoyama [211] under nearly square displacement path. Figs. 2.14 and 2.15 show comparisons of results for nondegrading system based on rigorous plasticity theory [166] and endochronic model in Eqs. 2.34 and 2.35 under both diamond and square displacement paths. The agreements are found to be surprisingly good considering the generally complicated biaxial inelastic stress-strain relation and the simple and somewhat arbitrary nature of the endochronic models.

Effects of Uncertainty

The laboratory or field data for calibration of hysteretic model parameters are usually determined for certain structural systems and forcing functions such as sinusoidal waves and the *El Centro* earthquake in Refs. [204] and [205]. Hence, the applicability of calibrated model

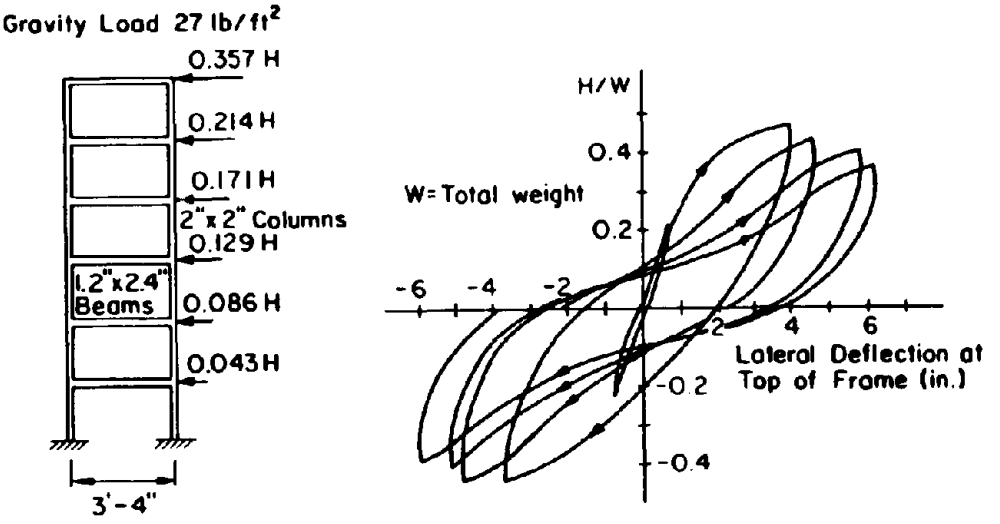

(a) Test Structure

(b) Experiment

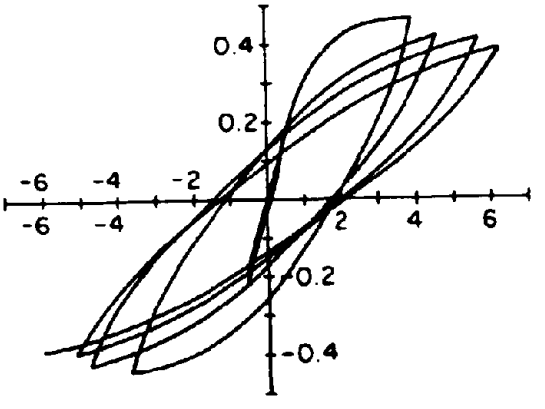

(c) Endochronic Model

Figure 2.11: Force-Displacement Characteristics of Uniaxial Hysteretic Model (Refs. 155 and 205)

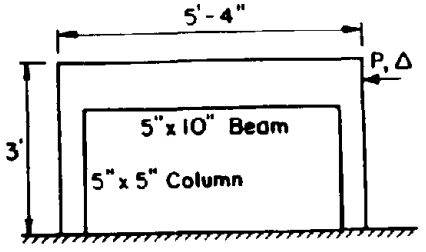

(a) Test Structure

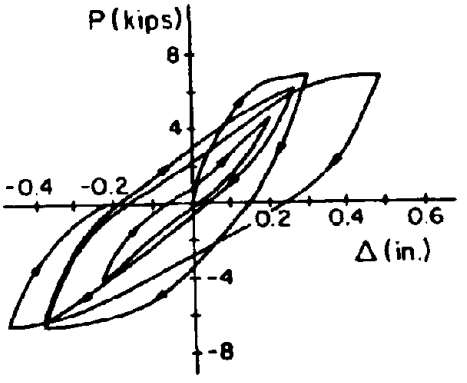

(b) Experiment

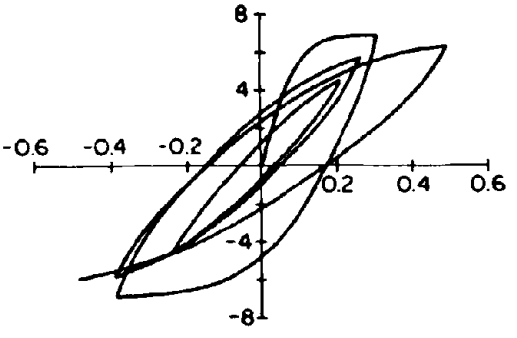

(c) Endochronic Model

Figure 2.12: Force-Displacement Characteristics of Uniaxial Hysteretic Model (Refs. 81 and 205)

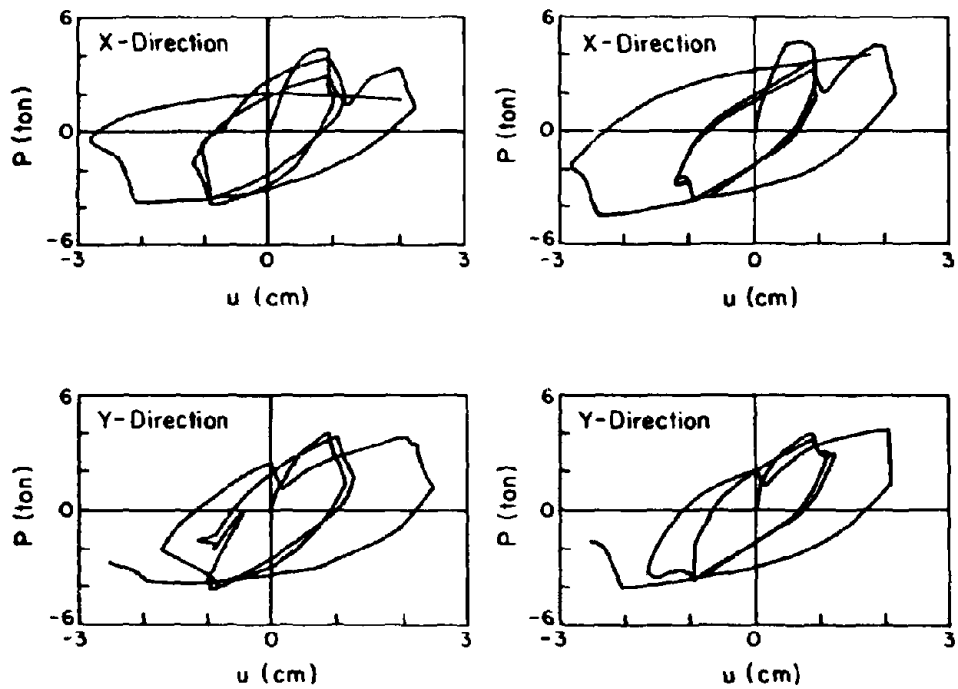

(a) Experiment (b) Endochronic Model

Figure 2.13: Force-Displacement Characteristics of Biaxial Hysteresis Based on Experimental and Endochronic Models (Refs. 211 and 226)

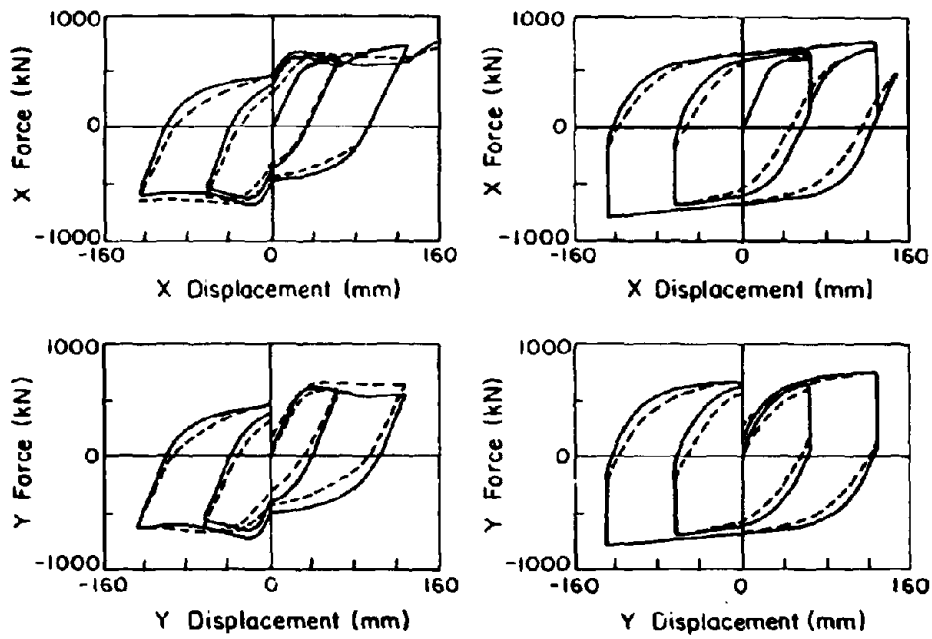

(a) Diamond Displacement Path (b) Square Displacement Path

——— Hinge Model ------ Fiber Model

Figure 2.14: Force-Displacement Characteristics of Biaxial Hysteresis Based on Plasticity Theory (Ref. 166)

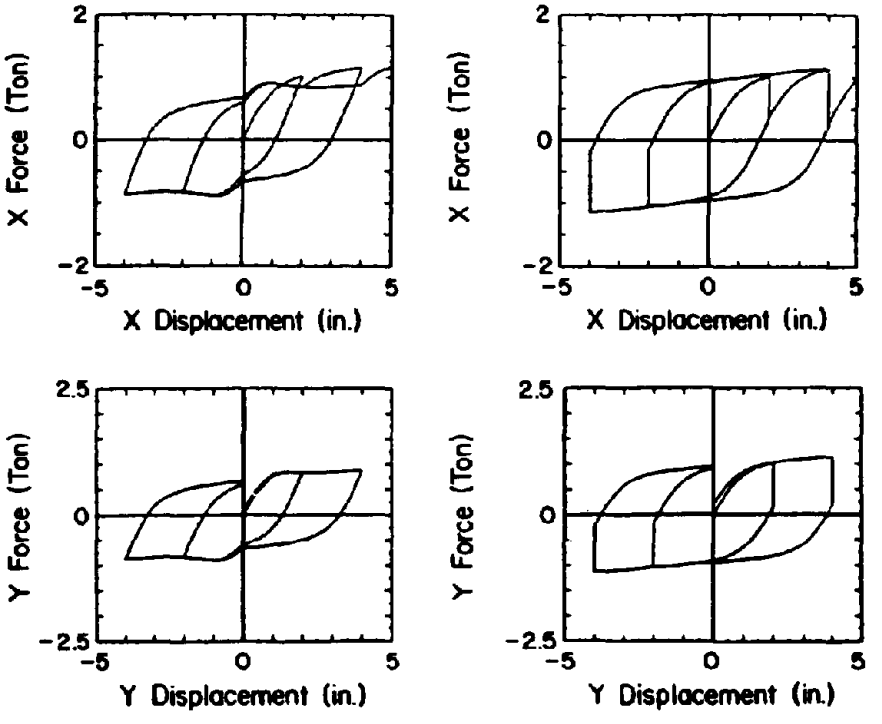

(a) Diamond Displacement Path

(b) Square Displacement Path

Figure 2.15: Force-Displacement Characteristics of Biaxial Hysteresis Based on Endochronic Model (Ref. 226)

parameters associated with a particular test setup may not be relevant for other structural systems and seismic events. Since there are inherent variabilities in system characteristics and load processes, the uncertainty in hysteretic models should also be taken into account.

Recently, a systematic investigation is conducted to study the sensitivity of seismic performance to the uncertainty in structural and material characteristics [174,175]. The method of analysis involves hysteretic constitutive laws commonly used in earthquake engineering and extensive simulation. Two distinct sources of variability are identified and they correspond to the uncertainty in (*i*) the mathematical idealization of hysteretic restoring force model and (*ii*) the parameters of restoring force characteristics given a hysteretic model [174,175].

Fig. 2.16 obtained from the original reference [175] shows the plots of exceedance probability of ductility ratio DR of a nonlinear oscillator relative to various thresholds μ_0 for three nondegrading models (elasto-plastic, bilinear, and Bouc). The ground acceleration is assumed to be stationary Gaussian band-limited white noise with varying one-sided spectral intensity G_0. For weak noise ($G_0 = 0.005\ in^2s^{-3}$), the exceedance probability for Bouc-Wen hysteresis is considerably smaller than that for either elasto-plastic or bilinear models which exhibit identical behavior due to mostly linear response. For strong noise ($G_0 = 0.5\ in^2s^{-3}$), the probabilities become similar for bilinear and Bouc Models both of which show smaller values of above probability than that for the elasto-plastic model. When the strength of the noise is somewhat intermediate ($G_0 = 0.05\ in^2s^{-3}$), all the hysteretic models exhibit practically similar behavior.

Also illustrated in Ref. [175], Table 2.1 provides the exceedance probability of a story level ductility ratio DR_k ($k = 1, 2, \cdots, 10$) of a 10-story steel frame relative to several thresholds $\mu_0 = 3, 4, 5, 6$ obtained for a specific hysteretic model (Bouc model) with both deterministic and uncertain parameters. The ground motion is assumed to be uniformly modulated stationary Gaussian colored noise with spectral parameters and modulation function defined in Ref. [175]. The tabulated results show that the uncertainty in the parameters of a specific hysteretic model can significantly increase the exceedance probability of story ductility. Clearly, both aspects of structural and material uncertainty discussed above can have significant effects on seismic performance of structural systems.

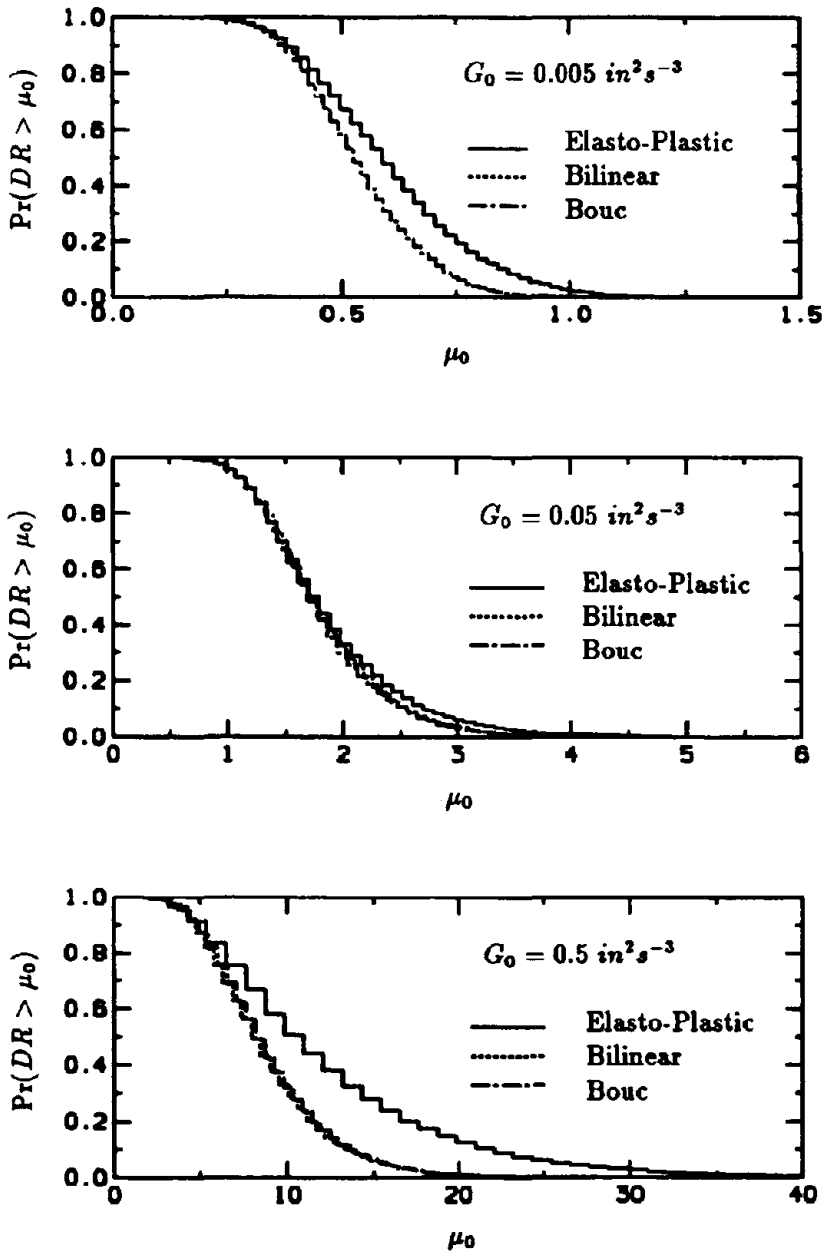

Figure 2.16: Effects of Modeling Uncertainty on the Exceedance Probability of Ductility Ratio (Ref. 175)

Table 2.1: Effects of Parameter Uncertainty on the Exceedance Probability of Ductility Ratio (Ref. 175)

Cases	story k	$\Pr(DR_k > \mu_0)$			
		$\mu_0 = 3$	$\mu_0 = 4$	$\mu_0 = 5$	$\mu_0 = 6$
Deterministic System	1	0.383000	0.151000	5.666×10^{-2}	2.233×10^{-2}
	2	0.201333	6.266×10^{-2}	1.566×10^{-2}	5.333×10^{-3}
	3	0.121000	2.400×10^{-2}	6.000×10^{-3}	1.666×10^{-3}
	4	7.633×10^{-2}	1.166×10^{-2}	2.000×10^{-3}	3.333×10^{-4}
	5	4.500×10^{-2}	5.666×10^{-3}	0.000	0.000
	6	4.400×10^{-2}	3.000×10^{-3}	0.000	0.000
	7	3.133×10^{-2}	9.999×10^{-4}	0.000	0.000
	8	0.000	0.000	0.000	0.000
	9	0.000	0.000	0.000	0.000
	10	0.000	0.000	0.000	0.000
Uncertain System	1	0.452666	0.269000	0.154333	9.099×10^{-2}
	2	0.312666	0.153000	7.733×10^{-2}	4.133×10^{-2}
	3	0.223000	9.200×10^{-2}	4.066×10^{-2}	2.200×10^{-2}
	4	0.161000	5.700×10^{-2}	2.433×10^{-2}	1.033×10^{-2}
	5	0.109333	3.466×10^{-2}	1.066×10^{-2}	5.000×10^{-3}
	6	0.114000	3.066×10^{-2}	7.333×10^{-3}	3.666×10^{-3}
	7	0.104605	2.133×10^{-2}	5.000×10^{-3}	1.333×10^{-3}
	8	1.333×10^{-3}	0.000	0.000	0.000
	9	9.999×10^{-4}	0.000	0.000	0.000
	10	0.000	0.000	0.000	0.000

2.3 Structural Models

In predicting the response and damage of actual structures, modeling of structural systems is an essential task. A model of a structure is defined as a mathematical representation of the behavior of the structure in its environment. The accuracy of response prediction depends on how well the models approximate the actual behavior of the structure. Hence, it is important to know the limitation of the mathematical models used to represent the structural systems.

The formulation of a mathematical model of a structure centers on the selection of parameters that define the configuration of the model. The configuration is characterized by the simultaneous locations of all material points. The number of independent parameters required to define the configuration represents the *degrees of freedom* of the model. These parameters are called the *generalized coordinates* [125] of the model. If a model has infinitely many degrees of freedom, it is called a *continuous model*; otherwise, it is called a *discrete model*.

2.3.1 Continuous Models

In continuum mechanics, the possibility of knowing the behavior of individual particles in the sense of modern physics is avoided. Instead, emphasis is provided on the gross or macroscopic behavior of material bodies. By no means, the model denies the existence of molecules, atoms, and subatomic particles, but simply sidesteps the issue by employing continuous representation of matter.

Consider a general three-dimensional body B defined as a *set* of uncountable infinity of points, called *material points*, that can be mapped homeomorphically into the closure of open, connected subsets of euclidean vector space $\mathcal{E}^3$. Each such homeomorphism defines a *configuration* of the body. Consider one particular configuration called *reference configuration* $\mathcal{B} \subset \mathcal{E}^3$ and identify material points of the body with their position vectors $\mathbf{X} \in \mathcal{B}$. Consider a *motion* of the body B from configuration $\mathcal{B}$ into other configuration $\chi_t : \mathcal{B} \mapsto \mathcal{E}^3$ (Fig. 2.17), i.e.,

$$\mathbf{x} = \chi_t(\mathbf{X}) = \chi(\mathbf{X}, t) \tag{2.40}$$

where t is the time variable and $\mathbf{x}$ is the position vector of the material point in the deformed

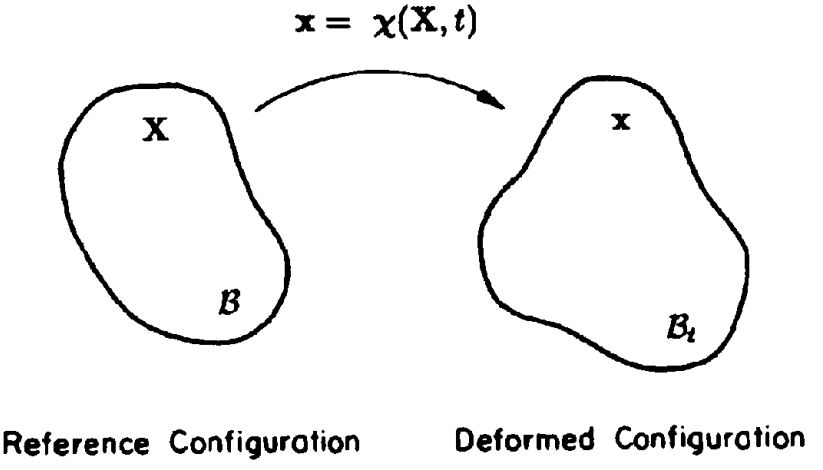

Figure 2.17: Kinematics of the Body B

configuration $\mathcal{B}_t = \chi(\mathcal{B}, t) = \{\chi(\mathbf{X}, t), \mathbf{X} \in \mathcal{B}\}$. From the Euler's (not Newton's) balance law of linear momentum, it can be shown [151,82,133] that the strong form of equations of motion of the body B is given by

$$\nabla \cdot \mathbf{T} + \rho \mathbf{b} = \rho \dot{\mathbf{v}} \tag{2.41}$$

in which, $\mathbf{T} \in \mathcal{L}(\mathcal{E}^3)$ is a second-order tensor known as Cauchy stress tensor, $\nabla \cdot \mathbf{T}$ is a vector field representing the divergence of tensor field $\mathbf{T}$, ρ is the scalar mass density of the material of the body B in the configuration $\mathcal{B}_t$, $\mathbf{b}$ is the vector field denoting the body force density in the configuration $\mathcal{B}_t$, $\mathbf{v} = \dot{\chi}(\mathbf{X}, t)$ is the velocity vector field in the configuration $\mathcal{B}_t$, and the overdot represents the derivative with respect to time t. In order for the motion $\mathbf{x} = \chi(\mathbf{X}, t)$ to be determined, the field equation (Eq. 2.41) must be supplemented by

appropriate boundary conditions and initial conditions. Finally, the set of equations are completed by specifying $\mathbf{T}$ as a function or functional of $t, \mathbf{x}, \mathbf{v}, \nabla\mathbf{x}$, and, in general, of higher derivatives of $\mathbf{x} = \chi(\mathbf{X}, t)$. The equation resulting from this specification is called the *constitutive equation* and its precise form depends on the nature of the material behavior being modeled.

While derivation of the governing field equations of continuous models is not unduly difficult, the attainment of general solution is a formidable task. To date, analytic solutions are known only for a few relatively simple continuous systems with linear elastic constitutive law, *e.g.*, uniform beams, strings, plates and shells with simple boundary conditions. For the dynamic analysis of skeletal structures like frames, the continuous model becomes extremely complex and have thus found limited use in practice.

2.3.2 Discrete Models

The discrete models are essentially based on discretization of a continuum to represent the configuration by a finite number of generalized coordinates. Among the discrete models, the finite element method and the finite difference method have received widespread use in the engineering community. Their versatility is reflected by a variety of characterizations and applications [23,24,52,73,92,150,236]. Once a continuum is discretized, say into finite elements, a step-by-step integration of equations of motion can be conducted. However, the inconvenience of such procedure is not of minor nature. The computational effort is still significant even with the recent developments of numerical techniques.

The development of discrete models for skeletal structural frames requires that compromises be made in deciding on the total number of degrees of freedom to be retained. A precise description of the structure may require many degrees of freedom than are acceptable from a computational viewpoint. Limitations of the degrees of freedom to be retained arise from both restrictions embedded in the available software and economic considerations of the expense in generating the numerical solutions.

Single-Degree-of-Freedom Systems

The single-degree-of-freedom (SDOF) models of multi-story structures are conceptually simple and have been considered by various researchers [21,1,213]. The model is applicable when the structural behavior is governed by a single generalized coordinate. A structural system represented by a SDOF model satisfies the equation of motion (Eq. 2.1)

$$m\ddot{X}_t + g\left(\{X_s, \dot{X}_s,\ 0 \le s \le t\}; t\right) = -mW_t \tag{2.42}$$

with the initial conditions

$$X_0 = 0 \quad \text{and} \quad \dot{X}_0 = 0 \tag{2.43}$$

in which X_t is the relative displacement response of the oscillator with respect to the ground motion, m is the constant mass, g is a functional representing the general nonlinear restoring force, and W_t is the seismic ground acceleration.

The SDOF model with linear elastic restoring force (*e.g.*, $g = c\dot{X}_t + kX_t$ with c and k representing damping coefficient and stiffness) associated with the fundamental mode of vibration is currently used in seismic design codes. The codes, however, account in an approximate way for the effects of second oscillatory mode.

Shear Beam Systems

Structures can not always be described by SDOF systems and, in general, have to be represented by more realistic multi-degree-of-freedom (MDOF) systems. A simplest such MDOF model is the shear beam systems [164,54,162] in which it is assumed that (*i*) total mass of the structure is concentrated at the levels of the floors, (*ii*) the girders on the floors are infinitely stiff as compared to the columns, and (*iii*) the deformation of the structures is independent of axial forces present in the columns. The first assumption transforms the problem from a structure with distributed mass to a structure which has only as many degrees of freedom as it has lumped masses at the floor level. The second assumption introduces the requirement that the joints between beams and columns are fixed against rotations. The third assumption leads to the condition that the rigid girders will remain horizontal during motion.

Consider a N-dimensional shear beam model of MDOF system shown in Fig. 2.18. The second order differential equation representing the equation of motion of kth mass (floor) exhibited in Fig. 2.18(b) is given by ($k = 1$ for the first floor and $k = N$ for the top floor)

$$\sum_{j=1}^{k} \ddot{U}_j(t) + W(t) + \frac{g_k}{m_k} - (1 - \delta_{kN})\frac{g_{k+1}}{m_k} = 0 \tag{2.44}$$

where $U_k(t)$ is the displacement of kth mass with respect to displacement of $(k-1)$th mass (except when $k = 1$), m_k is the kth mass, g_k is the kth general restoring force, $W(t)$ is the dynamic excitation representing ground acceleration due to earthquakes, N is the total number of masses (floors), and δ_{kN} is the *kronecker delta*, i.e., $\delta_{ij} = 1$ for $i = j$ or *zero* otherwise. When the $(k-1)$th equation is subtracted from the kth equation (except when $k = 1$), the resulting decoupled equation takes the form

$$\ddot{U}_k(t) - (1-\delta_{k1})\frac{g_{k-1}}{m_{k-1}} + \left[1 + (1-\delta_{k1})\frac{m_k}{m_{k-1}}\right]\frac{g_k}{m_k} - (1-\delta_{kN})\frac{m_{k+1}}{m_k}\frac{g_{k+1}}{m_{k+1}} = -\delta_{k1}W(t) \tag{2.45}$$

with the initial conditions

$$U_k(0) = 0 \quad \text{and} \quad \dot{U}_k(0) = 0 \tag{2.46}$$

in which once again δ_{k1},δ_{kN} are kronecker deltas introduced for the equation to be valid when $k = 1$ and $k = N$.

The shear beam model is applicable for weak-column and strong-beam type of structural systems. Although, design of such structures is not encouraged in earthquake engineering, the model has been used quite extensively due to its apparent simplicity [21,205]. When structural systems depart significantly from this type, a more detailed modeling is necessary. However, various techniques have been developed by researchers to obtain equivalent lateral stiffness and equivalent story strength [13,123,205] for their use in the shear beam idealization.

General Yielding Systems

Detailed discrete representations of structural systems are based on concentrated plasticity models at critical cross-sections and are widely used in the deterministic analysis of yielding

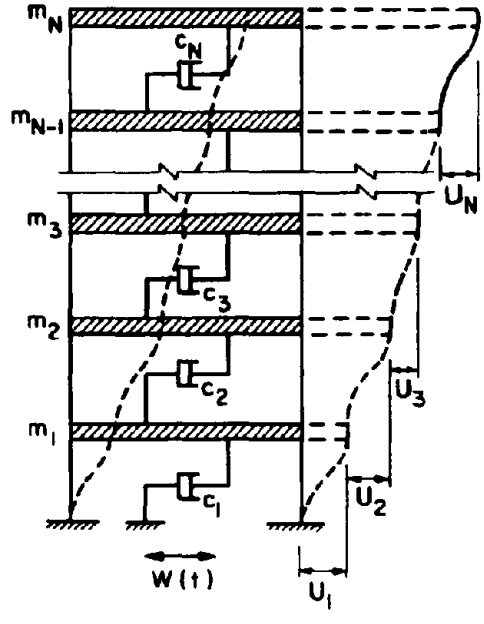

(a) Shear Beam Idealization

$$g_{k+1} = c_{k+1}\dot{U}_{k+1} + \alpha_{k+1}k_{k+1}U_{k+1} + (1-\alpha_{k+1})k_{k+1}Z_{k+1}$$

$$m_k\left[\sum_{j=1}^{k}\ddot{U}_j + W(t)\right]$$

$$g_k = c_k\dot{U}_k + \alpha_k k_k U_k + (1-\alpha_k)k_k Z_k$$

(b) Forces Acting on kth Mass

Figure 2.18: Shear Beam Systems

structures [26,27,51,75,206,212,154]. In general, the inelastic action may occur at arbitrary locations, however, it is the usual practice to restrict such action to regions immediately adjacent to the beam-column joints as shown in Fig. 2.19. The distributed masses are usually lumped at the floor level allowing only the translational inertia to be considered.

Consider again the framed structure shown in Fig. 2.19. The stochastic seismic modeling of this MDOF nonlinear system leads to the system of differential equations

$$\mathbf{m}\ddot{\mathbf{X}}_t + \mathbf{g}\left(\{\mathbf{X}_s, \dot{\mathbf{X}}_s,\ 0 \le s \le t\}; t\right) = -\mathbf{m}\mathbf{d}W_t \tag{2.47}$$

with the initial conditions

$$\mathbf{X}_0 = 0 \quad \text{and} \quad \dot{\mathbf{X}}_0 = 0 \tag{2.48}$$

in which $\mathbf{X}_t$ is the vector of generalized displacement, $\mathbf{g}$ is the vector functional representing general nonlinear hysteretic restoring forces, $\mathbf{m}$ is the mass matrix, $\mathbf{d}$ is the constant vector of proportionality indicating effects of the scalar base excitation on the different degrees of freedom, and W_t is the dynamic excitation representing seismic ground acceleration. Explicit solution of Eq. 2.47 usually requires step-by-step numerical integration for the time-history analysis.

2.3.3 Modeling Uncertainty

It is widely recognized that the variability in seismic performance evaluation is overwhelmingly dominated by the uncertainty in seismic load processes. However, in recent work of Rahman *et al.* [180] and Turkstra *et al.* [218], the modeling uncertainty of structural systems is found to contribute significant effects on seismic response of a real 24-story R/C flat slab building in Brooklyn, New York shown in Fig. 2.20.

The test structure is modeled as a two-dimensional frame-shear wall type building based on the assumption that the floors have perfect in-plane rigidity. Moment of inertia of all the columns are lumped into columns of a 3-bay planar frame (System-A). For the shear walls, the moment of inertia are lumped into two separate walls (System-B and -C) corresponding to contributions from small and large walls. Hinged links are then used to

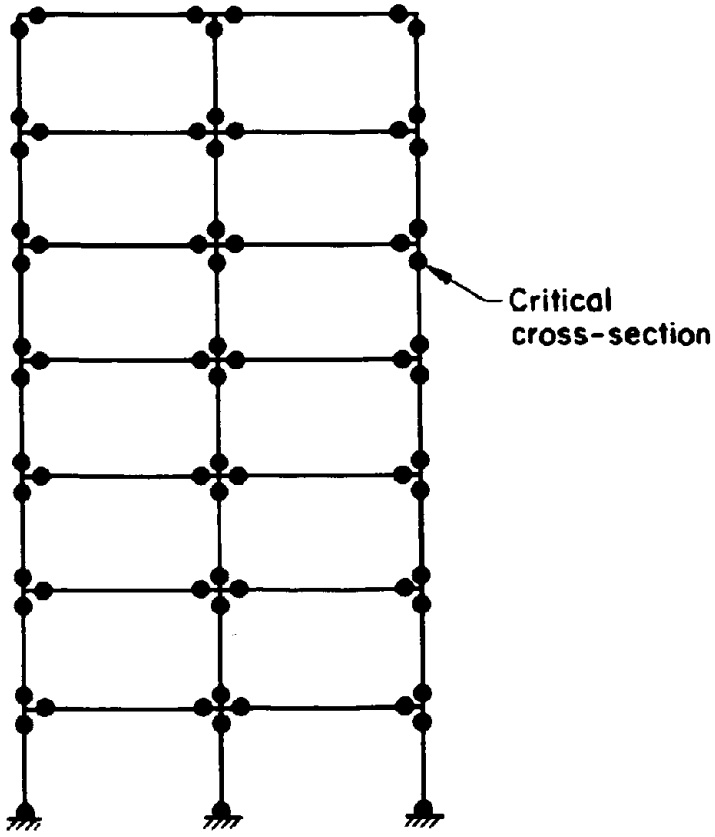

Figure 2.19: General Yielding Systems

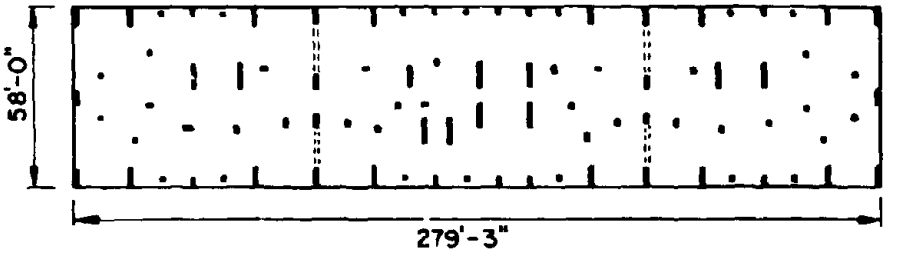

(a) Building Plan

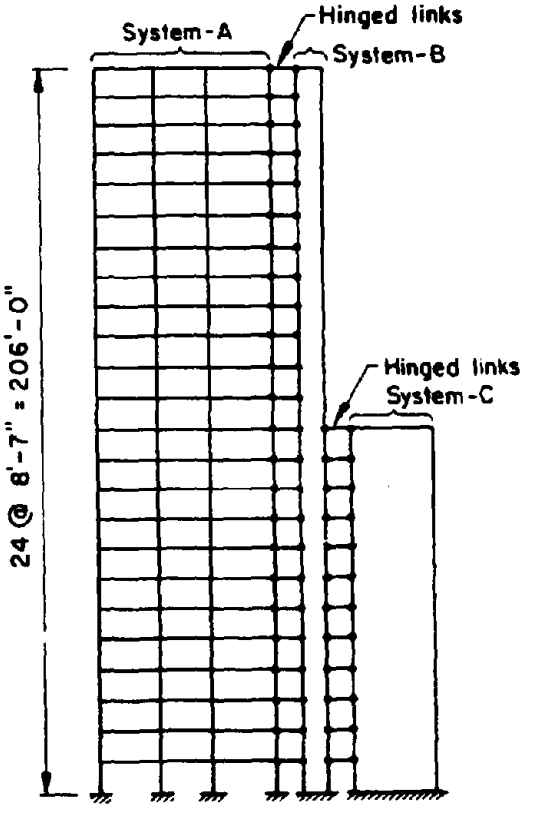

(b) Idealized Frame-Wall System

Figure 2.20: 24-story R/C Flat-Slab Building in Brooklyn, New York City (Ref. 180)

Table 2.2: Effects of λ_w on T_0 and Maximum Base Shear Coefficient (Ref. 180)

λ_w	T_0 (s)	Maximum Base Shear Coefficient
0.35	2.9	0.045
1.00	2.3	0.08

transfer the axial loads from System-A to System-B and then from System-B to System-C. The simplified idealized structure is shown in Fig. 2.20(b).

Out-of-plane bending of floor slabs is considered by idealizing slabs into equivalent beams [7,116] of same depth with effective width being some fraction λ_w (effective width coefficient) of slab panel width. Using the chart proposed by Khan [116] and Allen [7] with proper regard to the irregularity of plan, a lower bound of $\lambda_w = 0.35$ and an upper bound of $\lambda_w = 1.0$ were obtained. The variability of effective width coefficient λ_w may incorporate substantial amount of uncertainty in the response of structure due to earthquake loads. For example, the initial fundamental natural periods T_0 of the building are 2.9 seconds for $\lambda_w = 0.35$ and 2.3 seconds for $\lambda_w = 1.0$ [180].

Fig. 2.21 shows a plot of top displacement of the building versus seismic base shear coefficient obtained from nonlinear static analysis based on a bilinear force-deformation model [180]. Significant differences are noticed in the values of base shear coefficients when calculated for $\lambda_w = 0.35$ and $\lambda_w = 1.0$. Table 2.2 summarizes the results from the original reference [180] for $\lambda_w = 0.35$ and $\lambda_w = 1.0$.

2.4 Seismic Environment

In order to evaluate seismic performance of structure, it is necessary to determine the seismic hazard at a site for a specific exposure time. The estimation of earthquake hazard can take many forms and requires various levels of sophistication. Traditionally, seismic hazard is characterized by epicentral locations, maximum intensity of ground motion, and frequently by the peak ground acceleration (PGA), each of which provides partial information on earthquake loads. More accurate characterizations include mean earthquake arrival

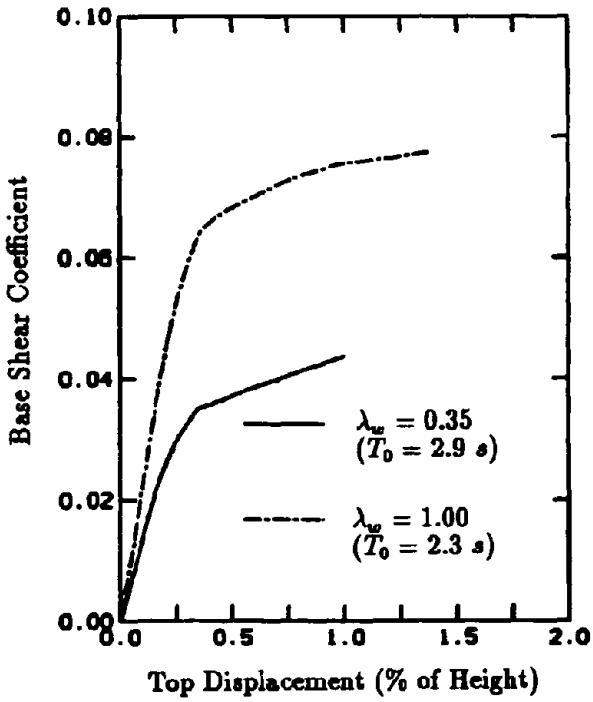

Figure 2.21: Base Shear Coefficient versus Top Displacement (Ref. 180)

rate, distribution of PGA, and duration and frequency content of ground motion.

This section briefly summarizes the state-of-the-art in seismic hazard estimation. The review will serve as the basis and the justification for seismic reliability analysis presented in the later sections of this report.

2.4.1 Seismic Hazard Map

Historically, a number of different methods have been used to develop seismic hazard maps in the United States. One early national zoning map along with a detailed zoning map of Boston has been discussed by Freeman [68]. Interest in the evaluation of seismic hazard has greatly increased in the past years, at least in part because of the realization of the importance of the hazard assessment of nuclear power plant sites and other critical facilities.

Extensive review of development of zoning maps are also given in Refs. [2] and [165]. Only an outline of the development of seismic zoning maps along with their relative merits and demerits on the application of building codes is attempted here. This will be done in the remainder of this section.

Ulrich Map

In 1948, a seismic map developed by Ulrich [186] was introduced which divided the conterminous United States into four zones numbered 0,1,2, and 3. Zone 3 was considered to have the greatest potential for earthquake damage. The map was adopted in 1949 by the International Conference of Building Officials (ICBO) for inclusion in the *Uniform Building Code* and became one of the first national zoning maps used for building code purposes in the United States. The numbered zones were used in the code in the development of the lateral force provisions considered appropriate for various parts of the country. Despite the fact that Ulrich map was developed with collaboration of leading seismologists in the country, the exact basis for the zones on the map was never explained clearly. The map displays epicenters of the larger earthquakes that occurred through 1946. The zones were apparently drawn on the basis of the maximum magnitude earthquake that had occurred in each zone. The zones are geometrical in outline and do not represent differences in ground motion. Thus, at some places on the map (*e.g.*, the western U.S.) zone 3 adjoins zone 1, etc. Within a few years, the map was withdrawn as misleading and subject to misinterpretation.

Richter Map

Another important seismic regionalization map was published by Richter [183,165] in 1958 containing several significant advances. For example, it depicted the estimated maximum ground motion rather than the distribution of earthquake epicenters. A notion of frequency of occurrence of earthquakes was also introduced, however, in a very qualitative way by coining the terms "occasional" and "frequent" for the region IX.

Algermissen Map

The 1970 edition [104] of the *Uniform Building Code* made use of a map developed by Algermissen [5]. The map has the same numbering scheme as in Ulrich map and is based

largely on the maximum Modified Mercalli intensity observed historically in each zone, but the spatial distribution of the intensities has been generalized to take into account some regional geological structures. The zoning map was adopted by the UBC in 1970, but the Code did not make use of the frequency of earthquake occurrence information that accompanied the map. Later, in the 1976 edition of UBC, this map was modified to introduce a zone 4 in some areas of California and Nevada, and in 1979 edition of UBC, additional modifications were introduced for Idaho [103].

Algermissen and Perkins Map

Due to a number of publications outlining feasibility of the application of probabilistic models on earthquake hazard estimation, a probabilistic acceleration map for the contiguous United States was developed by Algermissen and Perkins [4]. The quantity mapped in this hazard map is the 10% upper fractile of a random variable Y_{50} denoting largest peak ground acceleration for a lifetime period of 50 years. The concept of hazard mapping used in the construction of this map is that earthquakes are randomly distributed in magnitude, interarrival time, and space. Both the earthquake magnitude and interarrival time have exponential distributions. Independent and identically distributed exponential interoccurrence time has the implication that the seismic events occur as homogeneous Poisson process. The exponential magnitude distribution is an assumption based on empirical observation. The assumption of Poisson process for earthquakes in time is consistent with historical occurrence. Large shocks closely approximate a Poisson process, but as magnitude decreases, earthquakes may depart significantly from this fashion of arrival. However, ground motions associated with small earthquakes are of marginal interests in structural engineering applications, and consequently, the Poisson assumption may still serve as a useful and simple model [53].

The Applied Technology Council (ATC) report [16] contains two ground motion maps based on effective peak acceleration and effective peak velocity, which are used to compute lateral force coefficients for structural systems. For the conterminous United States, these two maps are based on the hazard map of Algermissen and Perkins. The Algermissen-Perkins map is also contained in the ATC report. The ATC effective peak acceleration map is very similar to the Algermissen-Perkins acceleration map with the exception that

the largest values of ground acceleration shown on the ATC map are $0.4g$ in California, while the Algermissen-Perkins map has accelerations as high as $0.8g$ in California. The ATC effective peak velocity map was derived from the Algermissen-Perkins acceleration map using principles and heuristic rules outlined in the report.

Although, the Algermissen and Perkins map introduced the probability into the description of ground motion, it is perceived to have three shortcomings. They include (*i*) characterization of seismic hazard in terms of only one ground motion parameter, peak ground acceleration, (*ii*) a focus on only one level of probability (*e.g.*, annual exceedance probability of 1/500), and (*iii*) lack of adequate geologic information in the generalization of the seismic history.

Algermissen, Perkins, Thenhaus, Hanson, and Bender Map

In 1982, Algermissen *et al.* [3] published an improved version of earlier map by including peak ground velocity in addition to peak ground acceleration which are mapped for the several reference periods of 10, 50, and 250 years at the 90% probability level of nonexceedance for the contiguous United States. The 50-year, 10% upper fractile map of Y_{50} for the contiguous United States is shown in Fig. 2.22. In many areas this new map differs from the 1976 Algermissen-Perkins map because of the increase in details resulting from greater emphasis on the geologic basis for seismic source zones. This new emphasis is possible because of extensive data recently acquired on Holocene and Quaternary faulting in the western United States and new interpretation of geologic structures controlling the seismicity pattern in the central and eastern United States. The most significant difference between the two maps is the delineation of specific fault zones such as Ramapo fault zone in New York-New Jersey and the Clarendon-Linden fault zone in northwestern New York as discrete seismic source zones.

Limitations of Seismic Hazard Maps

The earliest national earthquake hazard maps are primarily a geometric partitioning of the United States according to the maximum intensities experienced historically. Progress since then has featured an increased reliance on tectonic principles to generalize from the seismic

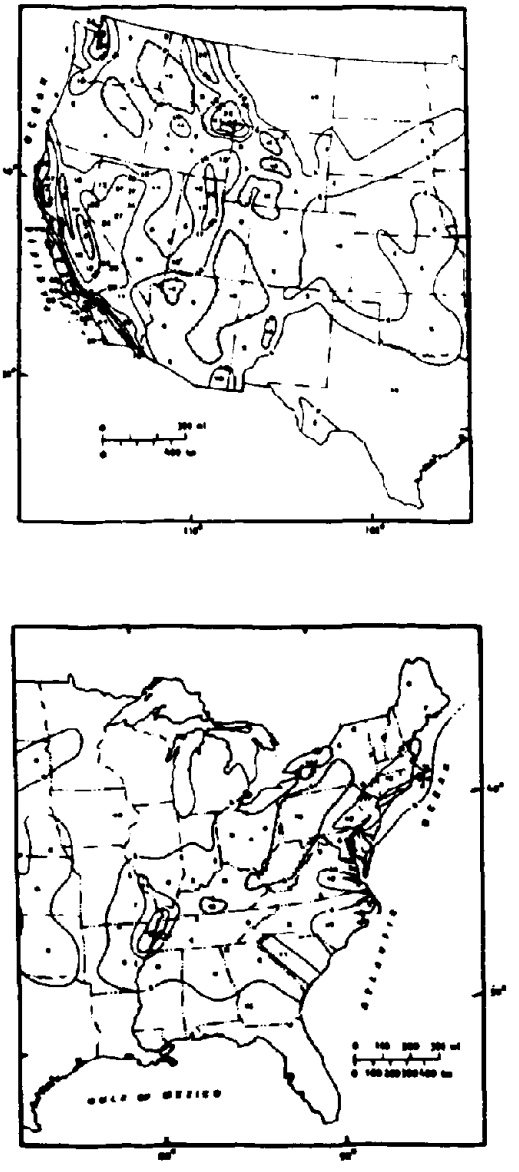

Figure 2.22: Probabilistic Ground Acceleration Map of U.S. (Ref. 3)

history to possible future earthquake locations, a focus on actual ground motion parameters (*e.g.*, peak ground acceleration, peak ground velocity, etc.) and the use of probability theory to incorporate seismic risk. However, all these maps provide only partial information, because they do not take into account duration and frequency content of ground motion and their inherent statistical variabilities.

The hazard maps of Algermissen and Perkins and Algermissen *et al.* are based on a single lifetime maximum ground motion parameter which are identified as a potential factor for the damageability of structures. However, conventional structures are usually designed to resist several seismic events during their lifetime (*e.g.*, 50 years). Hence, the lifetime peak ground acceleration or velocity may not be useful if damage accumulation between consecutive seismic events are permitted.

2.4.2 Stochastic Process

The seismic hazard maps express seismic input only in terms of peak ground acceleration or velocity which obviously does not provide all information necessary to describe the characteristics of a strong ground motion relevant to earthquake design. Frequency content and duration of motion can also play a significant role in the dynamic response and seismic performance of structures. The variabilities associated with these and other earthquake features suggest the use of random process models for characterizing seismic loads. Both stationary and nonstationary random processes have been proposed. However, due to transient nature of seismic ground acceleration, nonstationary models are more suitable than stationary models.

Stationary Random Process

A stationary random process is a fairly good approximation for earthquake excitation when the epicentral distance is large and the duration of strong motion is long compared with the fundamental period of structure. It may also provide valuable qualitative information about the nature of response even when these conditions are not met.

Gaussian White Noise

Perhaps the simplest stochastic model for seismic excitation is the stationary Gaussian white noise ξ_t. Bycroft [43] was one of the earliest to suggest the use of the model, which has the well-known properties

$$\mathrm{E}[\xi_t] = 0 \tag{2.49}$$

$$\text{and} \quad \mathrm{E}[\xi_t \xi_{t+s}] = \pi G_0 \delta(s) \tag{2.50}$$

where $\mathrm{E}[\cdot]$ denotes the expectation operator, $\delta(s)$ is the Dirac delta function, and G_0 is the one-sided mean spectral intensity of white noise ξ_t. It is well known that the assumption of constant spectral content of excitation is not realistic, nor even physically possible, since the mean square base acceleration is unbounded. Nevertheless, stationary white noise may be a satisfactory approximation for wide band excitation, when the excitation spectrum varies slowly in the vicinity of the structural system's natural frequency, and will be used as a first order approximation for seismic excitation in the current work.

Gaussian Colored Noise

Fourier analyses of existing strong-motion accelerograms reveal that the Fourier amplitude spectra are not constant with frequency even over a limited band. They are somewhat oscillatory in character, may have localized peak values at one or several frequencies, and usually damp out with increasing frequency. These suggest that a stationary filtered white noise of limited duration could be more representative of actual strong ground motion provided the filter transfer characteristics are properly selected.

Consider a system that can be described by a linear, time-invariant ordinary differential operator $\mathcal{L}\{\cdot\}$ such that the colored output $\widetilde{W}_t$ of the system due to the white input ξ_t is given by

$$\mathcal{L}\{\widetilde{W}_t\} = \xi_t. \tag{2.51}$$

The solution of above equation can be obtained as

$$\widetilde{W}_t = \int_{-\infty}^{+\infty} h_0(t-s)\xi_s ds \tag{2.52}$$

where $h_0(t)$ is a unit impulse response function. If $H_0(\omega)$ denotes the frequency response function of the same system, $H_0(\omega)$ and $h_0(t)$ are related by the following Fourier transform pair

$$H_0(\omega) = \int_{-\infty}^{+\infty} h_0(t)\exp(-i\omega t)\, dt \tag{2.53}$$

$$h_0(t) = \frac{1}{2\pi}\int_{-\infty}^{+\infty} H_0(\omega)\exp(i\omega t)\, d\omega \tag{2.54}$$

in which $i = \sqrt{-1}$ is an imaginary unit. It can be shown that the modulus of $H_0(\omega)$ can be related to the one-sided mean power spectral density $\tilde{G}(\omega)$ of the stationary colored process $\widetilde{W}_t$ by [203,128]

$$\tilde{G}(\omega) = G_0|H_0(\omega)|^2. \tag{2.55}$$

Several forms of $h_0(t)$ or $|H_0(\omega)|^2$ are available in the current literature. They have been used quite extensively in seismic analysis.

- **Kanai and Tajimi** [113,209,127,144]

$$\begin{aligned} h_0(t) &= H(t)\left[\omega_g^2\left(1-2\zeta_g^2\right)\exp(-\zeta_g\omega_g t)\frac{\sin\left(\omega_g\sqrt{1-\zeta_g^2}t\right)}{\omega_g\sqrt{1-\zeta_g^2}}\right] \\ &+ H(t)\left[2\zeta_g\omega_g\exp(-\zeta_g\omega_g t)\cos\left(\omega_g\sqrt{1-\zeta_g^2}t\right)\right] \end{aligned} \tag{2.56}$$

$$|H_0(\omega)|^2 = \frac{1+\left[2\zeta_g\left(\frac{\omega}{\omega_g}\right)\right]^2}{\left[1-\left(\frac{\omega}{\omega_g}\right)^2\right]^2+\left[2\zeta_g\left(\frac{\omega}{\omega_g}\right)\right]^2} \tag{2.57}$$

where $H(\cdot)$ is a unit step function, and ω_g and ζ_g are model parameters.

- **Bolotin** [32]

$$|H_0(\omega)|^2 = \frac{a}{2(\omega - \omega^*)^2 + a^2} + \frac{a}{2(\omega + \omega^*)^2 + a^2} \tag{2.58}$$

where a and ω^* are model parameters.

- **Shinozuka and Sato** [197]

$$h_0(t) = H(t)\exp(-\zeta_g \omega_g t)\frac{\sin\left(\omega_g\sqrt{1-\zeta_g^2}t\right)}{\omega_g\sqrt{1-\zeta_g^2}} \tag{2.59}$$

where ω_g and ζ_g are model parameters.

- **Iyengar and Iyengar** [109]

$$|H_0(\omega)|^2 = \exp(-a^2\omega^2) + b\omega^2\exp(-4a^2\omega^2) \tag{2.60}$$

where a and b are model parameters.

Nonstationary Random Process

In order to obtain an even more representative process for strong ground motion, the transient characteristics of actual accelerograms need to be considered. Generation of such artificial ground acceleration records usually resorts to stationary processes modulated by deterministic functions that specify the temporal variation of seismic intensity [32]. These nonstationary models, referred to as uniformly modulated processes [167], are characterized by time-invariant spectral shapes [12,129]. They have been generalized in several ways. For example, it has been proposed to generate accelerograms by passing a uniformly modulated stationary white noise through a shaping filter [197] or to represent consecutive nonoverlapping segments of a ground acceleration record by different uniformly modulated stationary processes [193]. Another type of representation proposed for the ground acceleration process is based on the response of a linear system to a modulated train of impulses with random magnitudes [161].

Oscillatory Process

Consider a class of oscillatory scalar random processes $V(t) \in C$ which admits a spectral representation of the form

$$V(t) = \int_{-\infty}^{+\infty} a(t;\omega)e^{i\omega t}dR(\omega) \tag{2.61}$$

in which $dR(\omega)$ is a process with orthogonal increments of variance

$$E[|dR(\omega)|^2] = dF(\omega) \tag{2.62}$$

and $\{a(t;\omega)\}$ is a family of slowly varying functions of time for all values of ω. The condition that the functions $a(t;\omega)$ vary slowly in time is essential to retain the frequency interpretation of the parameter ω. When this condition is met, $a(t;\omega)e^{i\omega t}$ can be interpreted as an amplitude modulated wave. From Eq. 2.61, $V(t)$ has mean *zero*, covariance function

$$B(t,t+u) \stackrel{\text{def}}{=} E[V(t)\overline{V}(t+u)] \tag{2.63}$$

$$= \int_{-\infty}^{+\infty} a(t;\omega)\overline{a}(t+u;\omega)e^{-i\omega u}dF(\omega) \tag{2.64}$$

where the overline denotes complex conjugate, and variance

$$\sigma_V(t)^2 = B(t,t) = \int_{-\infty}^{+\infty} |a(t;\omega)|^2 dF(\omega) \tag{2.65}$$

Let $F(\omega)$ be a differentiable function and $dF(\omega) = S(\omega)d\omega$. The evolutionary power spectral density of $V(t)$ at time t is [167]

$$S_t(\omega) = |a(t;\omega)|^2 S(\omega) \tag{2.66}$$

and represents the frequency content of the process in a small vicinity of t. Process $V(t)$ becomes stationary in the wide sense when the functions $a(t;\omega)$ are time-invariant.

Consider the special case in which $S(\omega)$ is a piecewise constant function with jumps of magnitude ${\sigma_q}^2/2$ at a finite number of frequencies ω_q, $q = -Q, \cdots, -1, 1, \cdots, Q$. In this case, the integral in Eq. 2.61 can be replaced with a finite sum that can be represented in terms of trigonometric functions in the form

$$V(t) = \sum_{q=1}^{Q} a_q(t)\sigma_q \left[A_q \cos(\omega_q t) + B_q \sin(\omega_q t)\right] \tag{2.67}$$

in which $a_q(t)$ is a slowly varying function of time, A_q and B_q are uncorrelated *zero* mean, unit variance Gaussian random variables. The one-sided mean power spectral density of the process $V(t)$ is

$$G_t(\omega) = \sum_{q=1}^{Q} |a_q(t)|^2 \sigma_q{}^2 \delta(\omega - \omega_q) \tag{2.68}$$

where $\delta(\cdot)$ is the Dirac's delta function. From Eqs. 2.67 and 2.68, the energy of an oscillatory process is associated with a fixed set of frequencies and fluctuates in time according to the modulation function $a(t;\omega)$ or $a_q(t)$. For example, the oscillatory process with evolutionary power spectrum in Eq. 2.68 has energy at frequency ω_q and the energy associated with this frequency is $|a_q(t)|^2\sigma_q{}^2$ at any instant of time t. Similarly, when $V(t)$ has a continuous spectrum the energy is distributed at any time within the range of frequencies where $G_t(\omega) > 0$.

An elementary example of an oscillatory process is [32]

$$W(t) = \psi(t)\widetilde{W}(t) \tag{2.69}$$

in which $\psi(t)$ = a slowly varying real-valued, non-negative deterministic function modulating the amplitude of $W(t)$, and $\widetilde{W}(t)$ = a real-valued zero mean wide sense stationary process with one-sided spectral density function $\tilde{G}(\omega)$. The family of oscillatory functions of the process is $\{\psi(t)\exp^{i\omega t}\}$ so that $W(t)$ has the following one-sided evolutionary spectral density $G_{W,t}(\omega)$

$$G_{W,t}(\omega) = \psi(t)^2 \tilde{G}(\omega) \tag{2.70}$$

of time-invariant shape. The process in Eq. 2.69 has been applied extensively to model and generate seismic accelerograms. Its samples generally have finite power at $\omega = 0$ even when $\tilde{G}(0) = 0$ [192]. Thus, the model predicts the existence of a static load that is meaningless in seismic analysis. Of course, this later observation does not create any practical problem as structure has always strength to withstand the above-mentioned static load.

In order to correct this undesirable sample property of the process in Eq. 2.69, it has been proposed to generate artificial accelerograms from a different process obtained by passing a uniformly modulated white noise through a linear filter [192]. This model belongs to the class of oscillatory processes since it can be regarded as the output of a time variant linear filter to stationary white noise. It has samples with no power at $\omega = 0$ but still has a time-invariant spectral shape. Generation of synthetic accelerograms based on this model involves some numerical difficulties. Besides, the design of the filters for shaping the white noise input is not straightforward when *e.g.*, $W(t)$ has a multi-modal spectral content. This is a common situation with seismic ground acceleration records.

Various forms of modulation function $\psi(t)$ (also known as intensity function, envelope function, etc.) are available in the literature. Some of them are described below.

- **Bolotin** [32]

$$\psi(t) = H(t)\exp(-\alpha t) \tag{2.71}$$

  where α is a model parameter.

- **Housner and Jennings** [91]

$$\psi(t) = H(t)H(t - t^*) \tag{2.72}$$

  where $t^* > 0$ is a model parameter.

- **Shinozuka and Sato** [197]

$$\psi(t) = H(t)c_\psi\left[\exp(-at) - \exp(-bt)\right] \tag{2.73}$$

  where a, b are model parameters and

$$c_\psi = \frac{1}{\left[\left(\frac{a}{b}\right)^{\frac{a}{b-a}} - \left(\frac{a}{b}\right)^{\frac{b}{b-a}}\right]} \tag{2.74}$$

is the normalizing constant.

- **Amin and Ang** [12,11]

$$\psi(t) = \begin{cases} 0 & t \le 0 \\ \left(\frac{t}{t_1}\right)^2, & 0 \le t \le t_1 \\ 1, & t_1 \le t \le t_2 \\ \exp[-c_\psi(t-t_2)], & t_2 \le t \end{cases} \tag{2.75}$$

in which c_ψ, t_1, and t_2 are model parameters.

- **Iyengar and Iyengar** [109]

$$\psi(t) = H(t)(a_1 + a_2 t)\exp(-a_3 t^{a_4}) \tag{2.76}$$

in which a_k, $k = 1, 2, 3, 4$ are model parameters.

Process with Modulated Amplitude and Frequency

An alternative nonstationary model for ground acceleration process has been developed by Grigoriu *et al.* [77,78]. It is obtained by modulating both the amplitude and the frequency of a stationary process. In this method, another frequency modulation function $\phi(t)$ in addition to amplitude modulation function $\psi(t)$ has been proposed to derive the nonstationary process $W(t)$ given by

$$W(t) = \psi(t)\widetilde{W}(\phi(t)). \tag{2.77}$$

It can be shown [77,78] that the time-dependent one-sided spectral density of $W(t)$ has the form

$$G_{W,t}(\omega) = \psi(t)^2 \tilde{G}\left(\omega \frac{t}{\phi(t)}\right) \tag{2.78}$$

When $\phi(t) = t$ (i.e., no frequency modulation), $G_{W,t}(\omega)$ coincides with the spectrum in Eq. 2.70 as expected, and $W(t)$ in Eq. 2.77 becomes a uniformly modulated process. The modulation function $\phi(t)$ determines the rate at which the spectrum of $W(t)$ changes with time. In contrast with oscillatory processes, that are defined for slowly varying spectra, $G_{W,t}(\omega)$ in Eq. 2.78 is valid for both slow and rapid changes in the frequency content.

Accelerograms recorded during the 1985 *Michoacan Earthquake* in Mexico have been used to calibrate the proposed process and an elementary oscillatory process [32]. Samples of these processes and actual accelerograms have been used to calculate extreme responses of linear and nonlinear single-degree-of-freedom systems. Figure 2.23 obtained from the original reference [77] shows the coefficient of variation (C.O.V.) of ductility demand of stiffness degrading systems for different natural periods. The plots are obtained for ground

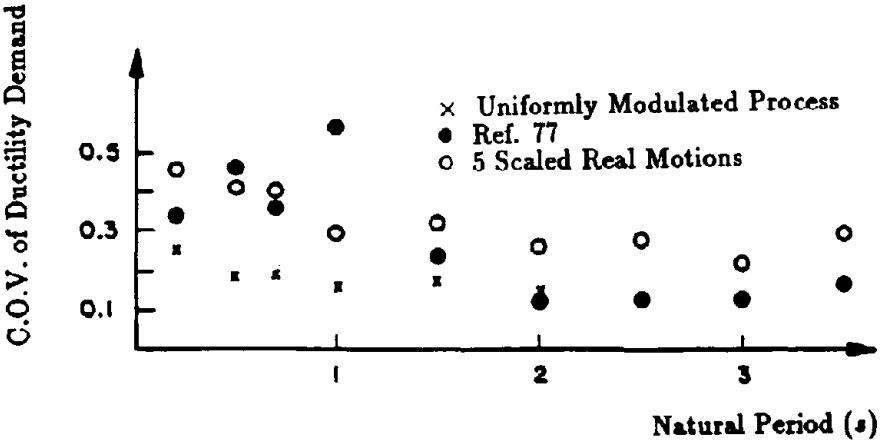

Figure 2.23: C.O.V. of Ductility Demand (Ref. 77)

accelerations based on currently used uniformly modulated process and the proposed model. Comparisons with corresponding coefficients of variation for actual ground motions show that the C.O.V. of ductility demand is systematically lower for systems excited with uniformly modulated process than those subjected to proposed model and actual ground accelerations.

On the other hand, ductility demands by the proposed model are consistent with those corresponding to actual ground motions. Further details on this subject can be obtained from the Ref. [77].

Digital Generation of Gaussian Processes

Considerable progress has been made in stochastic modeling of ground motion and in generating the corresponding sample functions for the purpose of nonlinear and parametric seismic response analysis. However, a large number of these analyses are performed under the assumption that the seismic ground motion consists of a single horizontal component. In this respect, the digital generation of univariate and one-dimensional stationary stochastic processes using spectral representation remains of critical importance in the seismic analysis.

A commonly used method [49] to generate the samples from a stationary Gaussian process $\widetilde{W}(t)$ with one-sided power spectral density $\tilde{G}(\omega)$ is obtained from

$$\widetilde{W}(t) = \sum_{k=1}^{N_\omega} C_k \sin(\omega_k t + \Phi_k) \tag{2.79}$$

in which ω_k is the discrete frequency, $C_k = \sqrt{2\tilde{G}(\omega_k)\Delta\omega_k}$ is the deterministic amplitude, N_ω is the number of discrete frequencies, and the phase angles Φ_k, $k = 1, 2, \cdots, N_\omega$ are independent and identical random variables uniformly distributed over $(0, 2\pi)$. Strictly, $\widetilde{W}(t)$ in Eq. 2.79 is not Gaussian when $N_\omega < \infty$. Asymptotically, however, as $N_\omega \to \infty$, $\widetilde{W}(t)$ approaches a Gaussian process according to the *Central Limit Theorem*. Moreover, a study [217] on simulating random sea waves showed that this method, which is based on deterministic amplitudes C_k may be unsatisfactory because of less variance of the simulated samples.

An alternative simulation scheme based on both random amplitudes and random phase angles have been proposed [203]. In this approach, the representation of $\widetilde{W}(t)$ has the form

$$\widetilde{W}(t) = \sum_{k=1}^{N_\omega} A_k \cos(\omega_k t) + B_k \sin(\omega_k t) \tag{2.80}$$

in which A_k and B_k ($k = 1, 2, \cdots, N_\omega$) are independent and identically distributed Gaussian

Table 2.3: Strong Motion Duration

	Moayyad and Mohraz (Ref. 140)			Vanmarcke and Lai (Ref. 221)	
	Soft Ground	Intermediate Ground	Hard Ground	Soil	Rock
Mean (s)	10.0	6.9	5.6	10.1	4.9
C.O.V	0.44	0.42	0.65	0.90	1.01
Sample Size	161	60	26	118	22

random variables with mean *zero* and variance $\tilde{G}(\omega_k)\Delta\omega_k$. Note that the representation of $\widetilde{W}(t)$ in Eq. 2.79 becomes equivalent to that in Eq. 2.80 if the amplitudes C_k are random and follow Rayleigh distributions.

Duration of Strong Motion

The duration of strong motion due to an earthquake may significantly effect nonlinear structural response and damage. A number of studies have been conducted to define and estimate the duration of strong motion for earthquakes [33,216,134,221,122,140]. Values of mean and coefficient of variation (C.O.V) of strong motion duration evaluated by Moayadd and Mohraz [140] and Vanmarcke and Lai [221] are summarized in Table 2.3. The differences in mean duration obtained from two sets of data do not appear to be significant. However, the coefficients of variation of strong motion duration show substantial differences. Based on the observation that strong motion duration is negatively correlated with peak ground acceleration, Lai [122] has suggested the following regression equation for design strong motion duration T_s

$$T_s = 30 \exp\left\{-3.254 a_{max}{}^{0.35}\right\} \tag{2.81}$$

for a design peak ground acceleration a_{max} (in g units) at a particular site.

Modeling Uncertainty

The variability in stochastic modeling of earthquakes constitutes one of the major causes affecting seismic response and reliability of structural systems. Following similar considerations to material models discussed previously, two sources can be identified. They correspond

Table 2.4: Statistical Data on ω_g and ζ_g

Probabilistic Characteristics	Soil (Sample Size = 118)		Rock (Sample Size = 22)	
	ω_g (rad/s)	ζ_g	ω_g (rad/s)	ζ_g
Mean	19.1	0.35	26.7	0.32
Coefficient of Variation	0.425	0.391	0.398	0.426

to the uncertainty in (i) the mathematical models of impulse response functions $h_0(t)$ (or $|H_0(\omega)|^2$) and modulation functions $\psi(t)$ and/or $\phi(t)$, and (ii) the corresponding parameters given a model.

A systematic study on the probabilistic characterization of parameters of ground accelerations is reported in Ref. [122]. Ground motions are characterized by the parameters of the Kanai-Tajimi spectral density function and by the strong motion duration. The spectral content and duration of 140 actual strong-motion accelerograms are studied with an aim of quantifying the uncertainty of ground motion representation. Parameters of Kanai-Tajimi spectrum and strong motion duration are estimated for each record based on the method of spectral moments. The statistics and dependence of the parameters are then evaluated from the data base used in the study. Means and coefficients of variation of ω_g and ζ_g obtained by Lai [122] for the two ground conditions classified as "rock" and "soil" are summarized in Table 2.4. They provide a rational basis for characterizing seismic input by considering uncertainty in the ground motion parameters. However, these information may not be useful if the nature of site spectrum departs significantly from Kanai-Tajimi spectrum.

2.5 Seismic Damage Assessment

A major objective of seismic design is the generation of structures that can survive earthquakes with a limited amount of damage. It has been proposed to evaluate structural performance by damage indices defined as scalar functions whose values can be related to particular structural (physical) damage states. In addition to the evaluation of the perfor-

mance of individual structures, damage indices can also be used to develop optimal strategies for codified seismic design.

Empirical and theoretical considerations have been applied to yield various estimates of structural damage [79,235]. The empirical damage models are based on statistics of structural damages observed at various sites during earthquakes [85,231]. Although, these observations of damage may be subjective, they sometimes provide useful qualitative information in overall seismic performance of structural systems. However, the empirical evaluation does not lend itself well to rationally predicting the strength reserve and response characteristics of a structure with a specified degree of damage because (*i*) it completely disregards the mechanics of materials that undergo large inelastic cyclic loads, (*ii*) future earthquakes may have different intensities, duration, and frequency content, (*iii*) recently built structures can differ significantly from the structures used to develop damage statistics, and (*iv*) the dynamic characteristics of the population of structures included in the statistical analysis may have altered due to repairs and damage accumulation in previous earthquakes.

The theoretical damage models account for characteristics of structure and seismic action and can have various degrees of complexity. They can be broadly divided into two classes [79,180] which are (*i*) strength-based damage indices, and (*ii*) response-based damage indices.

2.5.1 Strength-Based Damage Indices (SDI)

Damage index based on strength is simple and does not require response analysis. However, the index must be calibrated against observed damages and calibration usually requires a large data base.

Strength-based damage indices have first been proposed in China by Yang and Yang [233] and Japan by Shiga *et al.* [196] and Aoyama [14]. These indices depend on the geometry of structural elements and their general material properties. They have been extended by Meli [138] and used to relate them to observed damages resulting from the *1987 Mexico City Earthquake* [99]. The strength-based damage indices have been used in a Japanese code for evaluating existing buildings [15,152].

Shiga Index

Studies of reinforced concrete structures subjected to seismic ground motion indicate that the *Shiga* diagram [196] on the basis of column/wall area criteria can be used for damage assessment. The diagram consists of a plot of wall area index

$$WAI^i = \frac{\sum_{j=1}^{m_w{}^i} A_w{}^{ij}}{\sum_{k=i}^{N} A_f{}^k} \tag{2.82}$$

and average shear stress

$$\tau_{avg}{}^i = \frac{\sum_{k=i}^{N} W^k}{\sum_{j=1}^{m_w{}^i} A_w{}^{ij} + \sum_{j=1}^{m_c{}^i} A_c{}^{ij}} \tag{2.83}$$

for a lateral acceleration of $1g$, where WAI^i is the wall area index of i^{th} story, $\tau_{avg}{}^i$ is the average shear stress at i^{th} story, $A_w{}^{ij}$ is the area of j^{th} shear wall in i^{th} story, $A_c{}^{ij}$ is the area of j^{th} column in i^{th} story, $A_f{}^k$ is the total area of k^{th} floor, W^k is the weight of k^{th} floor, N is the total number of stories, $m_w{}^i$ is the total number of walls in i^{th} story, $m_c{}^i$ is the total number of columns in i^{th} story, i is the story coordinate. For a particular story level i, $\tau_{avg}{}^i$ indicates the intensity of seismic forces while WAI^i provides a measure of relative stiffness and hence the relative shear deformation capacity of the story compared with those of floors above.

Japanese Index

According to the Japanese code [15,152] for evaluating existing buildings, the damage due to potential seismic ground shaking can be estimated by a seismic damage index

$$I_S = E_0 G S_D T \tag{2.84}$$

where E_0 is the seismic sub-index of basic structural performance, G is the seismic sub-index of ground motion, S_D is the seismic sub-index of structural design, T is the seismic sub-index

of time-dependent deterioration. There are several levels of modeling for these sub-indices. The first level involves only shear capacities of each floor. The second level includes both shear and bending moment capacities of walls and columns. The data for seismic indices of actual structures which experienced several 1978 earthquakes in Japan suggest [15] that buildings with $I_S(first\ level) \geq 0.8$ and $I_S(second\ level) \geq 0.6$ are likely to have adequate seismic strength.

The SDI lacks rigor and must be based on a large set of observations. However, the method is very simple and does not necessitate any response analysis. Therefore, it is suitable for evaluating the seismic performance of large structural populations such as the low-rise buildings in the state of New York. Since field observations of damaged structures due to seismic loads are not readily available in New York State, the method can be calibrated from synthetic data obtained from the prediction of damage indices based on nonlinear dynamic analysis discussed in the next section of this review.

2.5.2 Response-Based Damage Indices (RDI)

Damage index based on response of nonlinear dynamic analysis is relatively complex but usually requires less data for calibration. It requires detailed information of structural and material models and description of ground motion(s) consistent with the site of structure.

The seismic performance of structures is commonly related to the capacity of undergoing inelastic deformations, defined as the ratio of a peak inelastic response to the corresponding yield response or ductility. This measure of structural performance can be unsatisfactory as demonstrated by experimental studies because it can not account for the duration and the frequency content of the seismic load. Experimental studies also show that alternative measures of seismic structural performance based solely on the low-cycle fatigue theory do not seem to provide either a satisfactory index for seismic damage [22]. These experimental results are consistent with the anticipated notion that failure of brittle systems is caused by excessive deformations while the failure of ideal ductile systems is initiated by repeated inelastic deformations [6]. Therefore, damage indices for actual structures, that are neither ideal brittle nor ideal ductile, should account for the damage effects of both excessive deformations and repeated inelastic deformations [158,235].

One of the most general damage indices proposed for seismic analysis is a bivariate random process $\mathbf{D}(t) \in \Re^2$ with components $D_m(t) \in \Re$ and $D_e(t) \in \Re$ denoting normalized values of maximum inelastic deformation and dissipated energy at any instant of time t [22]. The index attempts to account in a systematic way for the damage caused by both excessive inelastic deformations and cumulative damages caused by repeated inelastic load cycles. The use of bivariate process is also supported by experimental data on reinforced concrete beam-column assemblages subject to cyclic loads. These data show that current damage indices can be divided into two distinct sets, damage indices related to extreme deformations or stiffness degradation, and damage indices related to energy dissipation or structural deterioration. It is attractive from a theoretical point of view, but may have limited practical applications due to difficulties related to the estimation of the probability of failure that may depend on the entire history of $\mathbf{D}(t)$. An estimate of this probability, however, has been developed in Ref. [22] from experimental data in a transformed space of $\mathbf{D}(t)$ in which the damage index process is approximately isotropic.

Most of the existing damage indices used currently in seismic analysis focus on the maximum value of one of the two components of $\mathbf{D}(t)$ or related quantities. There have also been few attempts to develop damage indices that account in a simplified way on both components of $\mathbf{D}(t)$ or related quantities [47,159,160]. These damage indices are examined in the remainder of this section.

Maximum Deformation

Ductility Ratio (DR)

The ductility ratio DR defined as the ratio of the maximum deformation δ_m to the yield deformation δ_y given by

$$DR = \frac{\delta_m}{\delta_y} \tag{2.85}$$

has been applied extensively in seismic analysis to evaluate the capacity of structures undergoing inelastic deformation and develop inelastic response spectra [144]. It can be expressed in terms of various components of response, *e.g.*, displacement, rotation, and curvature [6,

149]. As a damage index, the ductility ratio may be unsatisfactory because it cannot account for both duration and frequency content of typical ground motions [22,235]. It is usually assumed that failure occurs when the ductility demand (response) in Eq. 2.85 exceeds structural ductility (capacity) that is equal to the ratio of the ultimate deformation under monotonic static load δ_u to δ_y [29,144].

Interstory Drift (ID)

The interstory drift ID has the expression

$$ID = \frac{\Delta_m}{h} \tag{2.86}$$

in which Δ_m = the maximum relative displacement between two stories and h = the story height [199,201]. From the analysis of test data on components and small scale structures, it was found that values of ID smaller than 1% correspond to damage of nonstructural components while values of ID larger than 4% may result in irreparable structural damage or collapse [199,215]. In another study, collapse is assumed to occur when ID exceed 6% [187]. As for ductility ratio, the interstory drift cannot account for effects of cumulative damage due to repeated inelastic deformation. Damage indices similar to those in Eqs. 2.85 and 2.86 have also been considered in Refs. [153] and [195].

Slope Ratio (SR)

Damage has also been related to stiffness degradation during seismic loading that can be measured by the slope ratio SR defined as

$$SR = \frac{K_r}{K_u} \tag{2.87}$$

where *e.g.*, K_r and K_u are slopes of loading and unloading branches of the force-displacement diagram. From tests of small scale structural systems, it has been determined that SR with values 1.0 and 0.2 correspond to safe structural behavior and critically damaged structures [215].

Flexural Damage Ratio (FDR)

Damage has also been correlated to the ratio of initial stiffness K_i to the reduced secant stiffness K_{rs} at the maximum displacement [22,187] given by

$$FDR = \frac{K_i}{K_{rs}} \tag{2.88}$$

where FDR represents the Flexural Damage Ratio.

Damage indices based in extreme inelastic deformations seem to be strongly correlated [22] so that their predictions are usually similar. For example, the correlation coefficient between rotational DR and FDR has been found to be 0.95 [22]. As previously mentioned, these indices can be unsatisfactory because they cannot account for effects of cumulative damage caused by repeated load reversals. Critical values of the damage indices considered in this section are determined from laboratory tests and/or field observations. Therefore, their use in the prediction of seismic damage for structures with mechanical characteristics significantly different from those used in the calibration process is questionable. Additional difficulties in the use of the damage indices relate to differences between features of future earthquakes and earthquakes considered in calibration, *e.g.*, duration and frequency content.

Cumulative Damage

Normalized Cumulative Rotation (NCR)

A simple measure of structural deterioration during a seismic event is the sum of all plastic excursions experienced by the structure. The value of this measure depends on the duration and intensity of the earthquake. For example, the damage index denoting normalized cumulative rotation [22] can be defined as

$$NCR = \frac{\sum |\theta_p|}{\theta_y} \tag{2.89}$$

where θ_p = inelastic rotation during half cycles, and θ_y = yield rotation. Statistical analyses of data on beam-column elements subject to cyclic loads show that the NCR is strongly related to the dissipated energy. These studies also show that damage indices based on only

cumulative inelastic deformation or dissipated energy may be inadequate to characterize the complex process of damage propagation and subsequent failure in concrete members [22]

Low Cycle Fatigue

The theory of low-cycle fatigue has been applied to the seismic analysis of structures subject to strong ground motion to estimate damage [149,201,202,234]. According to this theory, the total damage D_c is the sum of incremental damage ΔD_i in every load cycle i. i.e.,

$$D_c = \sum_i \Delta D_i \tag{2.90}$$

in which

$$\Delta D_i = \left\{ \left| \frac{\Delta \delta_t}{\Delta \delta_{tf}} \right|^{\frac{1}{m}} \right\}_i \tag{2.91}$$

$$\text{and} \qquad m = \frac{1}{1 - 0.86r}, \quad r = \frac{\Delta \delta_c}{\Delta \delta_t} \tag{2.92}$$

where $\Delta \delta_t$ and $\Delta \delta_c$ are the tensile and compressive change in the plastic deformation, and $\Delta \delta_{tf}$ is the tensile change in the plastic deformation in one cycle test to failure conducted at the relative ratio r. In applications, $\Delta \delta_{tf}$ can be approximately estimated by the deformation at failure under simple monotonic loads [201,202] with δ denoting strain [234] or deflection [149,201,202]. From the analysis of laboratory and field data it has been concluded that the exponent $1/m$ in Eq. 2.92 takes on values in the range $(1, 2)$ [201,202,234]. Since D_c in Eq. 2.90 is not sensitive to the value of this exponent [234], the damage index does not require any calibration. Therefore, it can be used directly to predict the damage state of any structural system for a postulated value of $1/m$ in the range $(1, 2)$. Failure is assumed to occur when $D_c = 1$. The determination of D_c in Eqs. 2.90 and 2.91 is somewhat complex and involves the entire response history. In addition, the index may be unsatisfactory since it cannot account, as the NCR index in Eq. 2.89, for the effect of maximum inelastic deformation.

Maximum Deformation and Cumulative Damage

Park *et al.*

A simplified failure criterion involving the components of the damage vector process $\mathbf{D}(t) \in \Re^2$ has been proposed in Refs. [159], [160] and [157]. It is based on scaled values of ductility and dissipated energy during the seismic ground shaking. The ductility, defined as the ratio of the maximum to the yield deformation δ_m/δ_y, is scaled by δ_y/δ_u in which δ_u is the ultimate deformation under monotonic static loads. The dissipated energy $\int dE$ is scaled by $\beta_e/(Q_y\delta_u)$ where Q_y is the yield force and β_e is a nonnegative constant usually obtained from experimental calibration. The failure is assumed to occur when the damage index DI representing a linear combination of the scaled components of $\mathbf{D}(t)$ given by

$$DI = \frac{\delta_m}{\delta_u} + \frac{\beta_e}{Q_y\delta_u}\int dE \tag{2.93}$$

exceeds unity. Under monotonically increasing loads, $\int dE = 0$ giving the damage index $DI = \delta_m/\delta_u$ so that failure is predicted to occur, as expected when $\delta_m = \delta_u$.

The assumptions in Eq. 2.93 that (*i*) the contributions to damage of the extreme deformation and dissipated energy can be superposed linearly, and (*ii*) the joint evolution in time of these components can be disregarded, do not seem to be in congruence with results obtained in Ref. [22]. In addition, the value of constant β_e is not specified and has to be obtained by calibration to laboratory and/or field data. Regression analysis of experimental data for reinforced concrete structures suggests [159]

$$\beta_e = \left(-0.447 + 0.073\frac{l}{d} + 0.24n_0 + 0.314P_t\right)0.7^{\rho_w} \tag{2.94}$$

where l/d is shear span ratio, n_0 is normalized axial stress, ρ_w is confinement ratio, and P_t is the longitudinal steel ratio. In evaluating the damage index in Eq. 2.93, it is apparent that a significant role is assigned to the parameter β_e which in turn depends on four completely unrelated variables.

Variability in mechanical properties of structural systems can be incorporated to generalize the aforementioned failure condition if the critical deterministic threshold of unity

is replaced by a random variable D_R. In this case, the failure condition is $DI > D_R$ [159]. Statistical analyses of tests in reinforced concrete members suggest that D_R follows a lognormal distribution with expected value equal to unity and standard deviation 0.54. First and second-moment descriptors of δ_m and $\int dE$ have been determined by approximate solutions of random vibration analyses based on stochastic equivalent linearization.

Maximum Softening Damage

A global damage index based on maximum softening of structure due to variation of its vibrational periods during a seismic event has been proposed by DiPasquale and Cakmak [59]. According to this model, the maximum softening damage δ_M is defined as [59]

$$\delta_M = 1 - \frac{(T_0)_{initial}}{(T_0)_{max}} \tag{2.95}$$

where $(T_0)_{initial}$ is the fundamental period of (undamaged) structure before it experiences the earthquake and $(T_0)_{max}$ is the maximum value of the fundamental period during a potential seismic event. This damage indicator, which measures the maximum relative stiffness reduction caused by the stiffness and strength deterioration of the actual structure, is calculated for an equivalent linear structure with slowly varying stiffness characteristics. Reference [59] presents some calibration results of this damage indicator using seismic simulations tests in the laboratory. Good correlation has been reported between predictions based on the maximum softening indicator and observed results from shaking table experiments and actual building structures. Recently, the Markov property of one- and two-dimensional maximum softening damage indicators has been investigated by Nielsen and Cakmak [146] and Nielsen, Köylüoğlu, and Cakmak [147].

Various other damage models such as those proposed by Krawinkler *et al.* [119], Gosain *et al.* [76], Hwang *et al.* [97], Darwin *et al.* [56], Bertero *et al.* [28], Blejwas *et al.* [31], Roufaiel *et al.* [189], Mizuhata *et al.* [139], Chung *et al.* [48], and Reinhorn *et al.* [182], have also been reported in the current literature. Details of these models can be obtained from Refs. [48] and [182].

Global Damage Evaluation from Local Damage Measures

Important decisions concerning the residual strength and safety of a damaged structure are currently based on a single structural or global damage index. This global damage index is usually obtained from heuristic combinations of local damage measures. The simplest technique in combining local damage indices is to use a weighting scheme giving the fundamental expression

$$DI_G = \frac{\sum_i w_i DI_{L,i}}{\sum_i w_i} \tag{2.96}$$

in which the subscripts L and G stands for local and global damage indices, and w_i is the weight assigned to each local index. The weighting factor can reflect the replacement cost and/or the relative importance of the substructure in maintaining the integrity of structure. For example, the lower story of a building might be assigned more importance than the upper stories. The weighting factor for any story could also depend on the magnitude of the damage index for that story, so that severely damaged stories are weighted more heavily. One approach used by Park *et al.* [157] is to make w_i proportional to $DI_{L,i}$. The equation for global damage index becomes

$$DI_G = \frac{\sum_i DI_{L,i}^2}{\sum_i DI_{L,i}}. \tag{2.97}$$

Due to the combination of detailed damage information of an entire structure into a single global estimator, too much information is lost thus allowing only a crude estimate of structural performance during seismic events. Since there is no one-to-one relation between local and global indices, a global measure of damage defined by Eq. 2.96 cannot characterize structural state uniquely and thus cannot be used to assess structural vulnerability to future loadings. Hence, evaluation of seismic reliability studies based on monitoring parameters of restoring force models at all critical structural components is more meaningful to simulate correctly the system degradation process.

Numerical Results for RDI

Available numerical studies on damage indices can be divided in three classes dealing with (*i*) calibration, (*ii*) performance evaluation, and (*iii*) effects of uncertainty in structural and ground motion characteristics.

Calibration of RDI

The calibration of most damage indices is usually based on laboratory experiments and involves various procedures for estimating the damage state. These procedures can be based on concepts of system identification, fuzzy sets, and expert systems [141,215]. The experimental results are determined for certain types of structures and earthquakes. Therefore, their applicability may not be relevant for other structural systems and seismic events. This is a significant limitation that may prevent the use of most of the damage indices in the prediction of seismic performance of structural systems and development of rational seismic codes.

Performance Evaluation of RDI

Damage indices are usually evaluated based on comparison between predicted and observed damages. A recent study [201] provides an extensive evaluation of the damage indices in Eqs. 2.90 and 2.93. Four structural systems are used in the evaluation: (*i*) interior reinforced concrete beams subject to cyclic and monotonic loads, (*ii*) a 1/10 size model of a 10 story reinforced concrete frame subjected to shaking table dynamic test, (*ii*) a full size 7 story reinforced concrete building subjected to 4 pseudo-dynamic tests simulating earthquakes at increasing intensity, and (*iv*) the Imperial County Services Building that was damaged during the October 15, 1979 Imperial Valley Earthquake. Details on available observations and calculations can be obtained from the original reference [201]. The calculations were performed under different assumptions regarding the ultimate displacement when this displacement was not available, *e.g.*, ultimate interstory displacement of 8 to 10 % are considered to be realistic. Values of constant β_e in Eq. 2.93 were assumed to be 0.25, 0.5, and 1.0. Results indicate that 0.25 is the optimal value of β_e in cases examined.

The analysis in Ref. [201] shows that the index in Eq. 2.93 overpredicts structural damage in some cases but available evidence is insufficient to determine whether the damage index in Eq. 2.90 is superior to the one in Eq. 2.93 or vice versa. Another study [158] shows a good agreement between the prediction of the index in Eq. 2.93 and damages observed in many structural systems. Unfortunately, this study does not give values of the parameters δ_u, Q_y, and β_e used in the analysis.

Effects of Uncertainty

A systematic investigation on effects of the uncertainty in the parameters of the seismic excitation and structural characteristics is reported in Ref. [149] for the ductility ratio in Eq. 2.85 and the damage index in Eq. 2.90. The analysis is based on a single degree of freedom model with elasto-plastic restoring force models and a set of 20 actual earthquakes scaled to the same peak ground acceleration. The structural damping, stiffness, and yield displacement are assumed to be deterministic or follow lognormal distributions. Results obtained by simulation based on Latin Hypercube Sampling indicate that the uncertainty in structural mechanical properties can increase significantly the variance of ductility ratio. It is also found that there is a little correlation between the damage indices in Eqs. 2.85 and 2.90. This is in agreement with other studies showing a weak correlation between damage indices based on the maximum deformation and cumulative effects of cyclic loads [22].

2.5.3 Evaluation of SDI

A recent study [180] based on both SDI and RDI is carried out for the assessment of seismic performance of existing buildings in New York City. Nonlinear dynamic analyses and statistical evidence from previous earthquakes are used to evaluate strength-based damage indices. Figure 2.24 shows the potential seismic damage for a 24-story R/C flat-slab building in Brooklyn obtained by a strength-based damage index defined by Eq. 2.84. Figure 2.25 shows the interstory drift (defined by Eq. 2.86) versus story coordinates for this 24-story structure subject to the actual and scaled versions of the *1986 San Salvador Earthquake*. Preliminary geological considerations suggest that the earthquake is adequate for the building site. The analysis accounts for the uncertainty in material characteristics. In all the cases,

the drift is found to exceed the allowable value (0.4 %) suggested by the *1988 Uniform Building Code*. Thus, comparisons with the results in Fig. 2.25 indicate that strength-based damage indices can provide a useful measure of seismic performance for buildings in New York City.

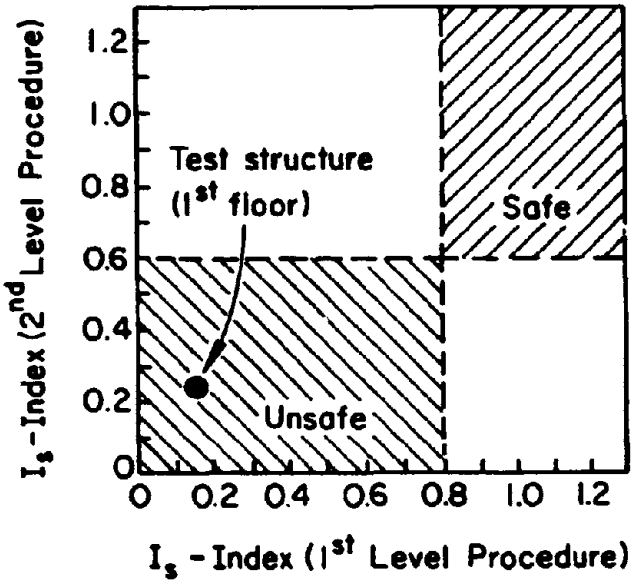

Figure 2.24: Strength-based Damage Index (Ref. 180)

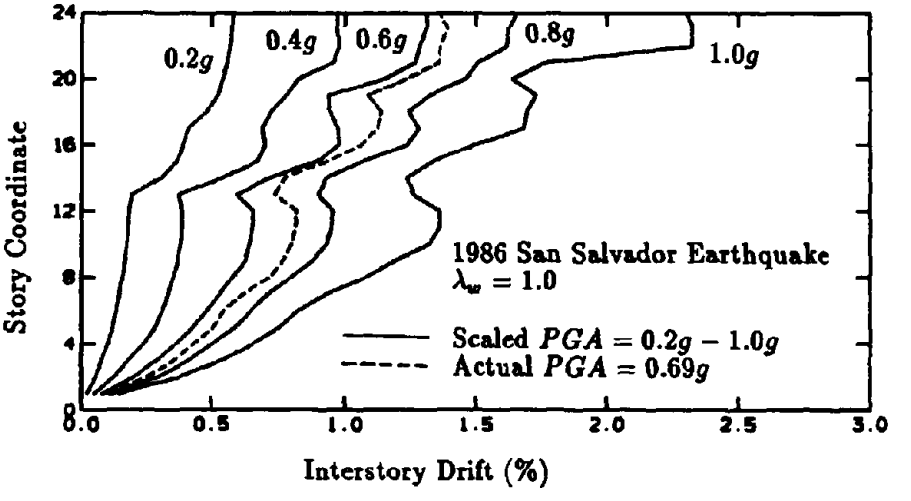

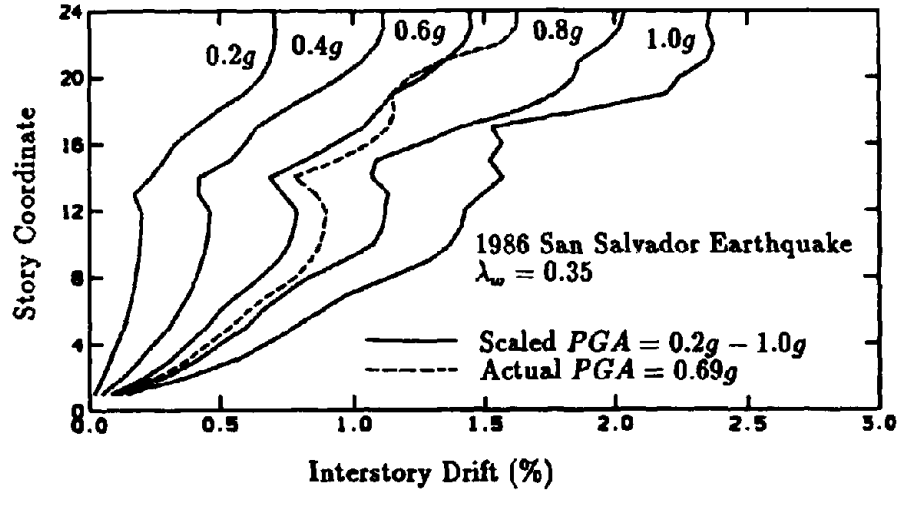

Figure 2.25: Response-based Damage Index (Ref. 180)

Page Intentionally Left Blank

SECTION 3
Static Reliability

3.1 Introduction

Current estimates of seismic reliability indices for building structures are obtained by static method. The static reliability analysis is based on (*i*) elementary models of seismic hazard, *e.g.* by the 50-yr maximum peak ground acceleration, (*ii*) stress analysis due to static loads applied laterally to structural systems, and (*iii*) limit states defined by strength-related elementary failure criteria at a particular structural component. Effects of structural redundancy, nonlinear dynamic response, and damage accumulation during consecutive seismic events are not explicitly considered in this simplified analysis.

The objective of this section is to assess seismic performance of code-designed structures by static reliability analysis. Several models of seismic hazard are also examined to evaluate sensitivity of seismic reliability estimates to particular hazard model.

3.2 Structural Strength

Building codes and standards used in structural design contain provisions for ensuring structural safety under extreme loads. The general form of equation from these provisions is obtained from the Load and Resistance Factor Design (LRFD) format [8,64,72,131] and is given by

$$\phi R_{ni} \geq C_i U \tag{3.1}$$

in which ϕ is the resistance factor, R_{ni} is the nominal code-specified resistance at ith structural component, C_i is the influence coefficient obtained from structural stress analysis due to factored ultimate load

$$U = \sum_j \gamma_j Q_{nj} \tag{3.2}$$

where Q_{nj} and γ_j are nominal load and corresponding load factor for the jth load component, respectively. Several load combinations are usually required to specify U in Eq. 3.2 which can be used in Eq. 3.1 to evaluate deterministic nominal strength R_{ni}. For example, when *the ACI Code 318-83* [9] is adopted, the explicit form of Eq. 3.2 becomes

$$U = \begin{cases} 1.4D_n + 1.7L_n \\ 0.75(1.4D_n + 1.7L_n \pm 1.87E_n) \\ 0.9D_n \pm 1.43E_n \end{cases} \tag{3.3}$$

where D_n, L_n, and E_n are code-specified nominal dead load, live load, and earthquake load respectively. Representative values of the nominal loads used in a wide variety of buildings can be obtained from the specification in *American National Standards Institute (ANSI) A58.1-82* [10], *Uniform Building Code* (UBC) [100,101,102] and many others. For example, the nominal seismic base shear E_n obtained from the *1988 Uniform Building Code* [100] is

$$E_n = \frac{ZICW}{R_w} \tag{3.4}$$

$$\text{where } C = \frac{1.25S}{T_0^{2/3}} \tag{3.5}$$

and from the *1985 Uniform Building Code* [101] is

$$E_n = ZIKCSW \tag{3.6}$$

$$\text{where } C = \frac{1}{15\sqrt{T_0}} \tag{3.7}$$

in which

Z = seismic zone factor

I = importance factor

K, R_w = building system factors

S = soil factor

T_0 = initial fundamental period of structure

W = weight of structure.

(3.8)

Data on structural resistance exhibit a distinct statistical scatter. Three major sources can be identified and they correspond to the uncertainty in (*i*) material properties (*e.g.*, yield strength of steel, compressive strength of concrete, etc.), (*ii*) geometry (*e.g.*, structural dimensions) and (*iii*) modeling accuracy (*e.g.*, the use of rectangular stress block in reinforced concrete design). Mean, coefficient of variation and probability distribution for structural strengths have been determined from test data on the strength of materials and laboratory experiments of full-scale members under idealized loading environments and in some cases, through simulation where a well-defined analytical model is available. A representative sampling of these data which summarizes results of numerous research programs are available in Ref. [65] and is shown in Table 3.1. The mean values are normalized with respect to the deterministic nominal resistance which is based on the model used to predict the strength in the appropriate material specification. The statistics include factors which reflect the effects of modeling and fabrication errors. Further studies may be found in Ref. [65].

3.3 Structural Loads

Most structural loads vary with time. If the structure is subjected to only one time-varying load (*e.g.*, live load) in addition to its time-invariant dead load, the total load effect may be determined by considering the combination of the dead load with the maximum time-varying load during some appropriate reference period of time τ (*e.g.*, 50 years). Frequently, however, more than one time-varying load act on a structure (*e.g.*, live load plus wind load or earthquake load). When more than one time-varying load acts, it is extremely unlikely that each load will reach its peak lifetime value at the same instant of time. Consequently, a structural component can be designed for a total load which is less than the sum of the peak loads. This is currently recognized in the *American National Standards Institute (ANSI) A58.1-82* [10].

Ideally, the load combinations should be dealt with applying the theory of random

Table 3.1: Statistical Data on Structural Resistance

Structural Member	Mean/Nominal	Coefficient of Variation	Probability Distribution
Structural Steel:			
Tension Members (Yielding)	1.05	0.11	Lognormal
Tension Members (Tensile Strength)	1.10	0.11	Lognormal
Compact Beam (Uniform Moment)	1.07	0.13	Lognormal
Beam-Column	1.07	0.15	Lognormal
Plate Girders, Flexure	1.08	0.12	Lognormal
A325 HS Bolts, Tension	1.20	0.09	Lognormal
Axially Loaded Column	1.08	0.14	Lognormal
Reinforced Concrete:			
Flexure, R/C, Grade 60	1.05	0.11	Normal
Flexure, R/C, Grade 40	1.14	0.14	Normal
Flexure, Pre-tensioned Beam	1.06	0.08	Normal
Flexure, Post-tensioned Beam	1.04	0.10	Normal
Short Columns (Compression Failure)	1.05	0.16	Normal
Short Columns (Tension Failure)	1.05	0.12	Normal

processes which accounts for the stochastic nature of the loads in both space and time. However, the probabilistic characterization of the maximum of a sum of stochastic load processes is not an easy task. A simple model for describing the maximum during period τ of a combination of loads follows from the assumption that the maximum total load occurs when one of the loads attains its maximum value during τ while the other loads assume their instantaneous or arbitrary-point-in-time values [219]. In other words, when the loads are assumed to be stationary, the maximum load effect S_i at the ith structural component is given by

$$S_i = \max_j \left[\max_\tau (C_{ij} Q_j) + \sum_{k \neq j} C_{ik} Q_k \right] \tag{3.9}$$

where Q_j is the jth load component and C_{ij} is the influence coefficient which transforms the jth load component into load effect at ith structural component. Eq. 3.9 enables a random variable rather than stochastic process characterization of the load combination. The arbitrary-point-in-time load is simply the value measured if the load processes were to be sampled at any instant of time and is typically much less than the associated nominal value. Recent research on load combinations [126,229] suggest that Eq. 3.9 is a good approximation in many practical cases, although it tends to be unconservative in instances where the probability of joint occurrence of more than one maximum load is not negligible.

Mean, coefficient of variation, and probability distributions of 50-yr maximum and arbitrary-point-in-time loads are available in Ref. [71] and is summarized in Table 3.2. The load subcommittees within the ANSI Committee A58 provided many of these estimates. By and large, these statistical studies are a synthesis of values reported in numerous previous studies on structural loads and load models, behavior of structural members, and reliability-based design. Insofar as possible, the load statistics are based on load surveys in situ, measurements of wind pressure on buildings, and probabilistic load modeling which converts a survey load to a maximum load used for the purpose of reliability analysis and design. In addition to the basic variability in the load, uncertainty also arises from the load model itself which transforms the actual spatially and temporally varying load into a statically equivalent uniformly distributed load (*e.g.*, dead load, live load, etc.) for the operational convenience of design process. These uncertainties are included in the coefficients of variation listed in

Table 3.2: Statistical Data on Structural Loads

Load Variable	Mean/Nominal	Coefficient of Variation	Probability Distribution
Dead, D	1.05	0.1	Normal
Live, L	Ref. 71	0.25	Type-I
Live, L_{apt}	Ref. 71	Ref. 65	Gamma
Wind, W	0.78	0.37	Type-I
Wind, W_{apt}	$(-0.021)^*$	$(18.7)^*$	Type-I
Snow, S	0.82	0.26	Type-II
Earthquake, E	(Site Dependent)*	$(2.3)^*$	Type-II
* Characteristic extreme and shape parameters			

Table 3.2. The probability distributions are obtained by the best fit to the upper percentiles of the distribution obtained from either Monte Carlo simulation or numerical integration. Detailed description of load modeling is available in Ref. [65]. In this study, an elaborate discussion on the probabilistic load characterization for seismic environment is presented.

3.3.1 Current Models of Seismic Hazard

Load effects due to seismic ground shaking are currently determined by the inverted triangular loads applied laterally to building structures. These loads are proportional to base shear E which can be obtained from [65,16]

$$E = \frac{1.2 Y_{50} S W}{R T_0^{2/3}} \tag{3.10}$$

where

$$\begin{aligned} Y_{50} &= \text{50-yr extreme peak ground acceleration (PGA)} \\ R &= \text{response modification factor} \\ S &= \text{soil factor} \\ T_0 &= \text{fundamental period of structure} \\ W &= \text{weight of structure.} \end{aligned} \tag{3.11}$$

According to Refs. [65] and [53], the cumulative distribution function of Y_{50} at a site can be modeled as *Extreme Type-II* distribution which is given by

$$\widetilde{F}_{50}(y) = \begin{cases} exp\left[-\left(\frac{y}{u}\right)^{-k}\right], & y \geq 0 \\ 0, & \text{otherwise} \end{cases} \tag{3.12}$$

in which the extreme and shape parameters u and k can be obtained from the Algermissen-Perkins map [2] giving the contour plots of 10% upper fractile of Y_{50}. The acceleration a_{10} has a return period of 475 years and is mapped for the entire continental United States. Assuming $k = 2.3$ as suggested in Refs. [65] and [149], u may be computed for any mapped value of a_{10} from $u = 0.38\ a_{10}$. This seismic hazard map of Algermissen-Perkins can not be related to the seismic zone map of *Uniform Building Code* [101], because the code map is based on largest historical event while the Algermissen-Perkins map accounts for the site seismicity and design lifetime. Moreover, it is also possible that different sites located at the same seismic zone of *Uniform Building Code* [100,101] are characterized by different values of a_{10}. Thus, the resultant reliability measures for structural systems can be very different due to the identical design base shear obtained from *Uniform Building Code* [100,101].

3.3.2 Alternative Models of Seismic Hazard

Consider a site affected by a single seismic source characterized by a mean rate of earthquake occurrence λ. It is assumed that (i) the earthquake arrivals follow a homogeneous Poisson process with mean rate λ, (ii) ground motions in different seismic events are independent and identically distributed stationary Gaussian processes $\widetilde{W}(t)$ with mean *zero*, one-sided mean power spectral density $\tilde{G}(\omega)$ for $\omega \in (0, +\infty)$ and (iii) seismic events have the same deterministic strong motion duration T_s. This representation of seismic hazard provides a very simplified model of seismic environment.

The distribution of the peak ground acceleration *during a seismic event* can be approximated by [203,179]

$$F(y) \stackrel{\text{def}}{=} \Pr\left(\max_{T_s} |\widetilde{W}(t)| < y\right) \simeq \exp\left[-\frac{T_s}{\pi}\sqrt{\frac{\lambda_2}{\lambda_0}}\exp\left\{-\frac{y^2}{2\lambda_0}\right\}\right] \tag{3.13}$$

where

$$\lambda_i \stackrel{\text{def}}{=} \int_0^\infty \omega^i \tilde{G}(\omega) d\omega \tag{3.14}$$

is the ith spectral moment of $\widetilde{W}(t)$. Therefore, the cumulative distribution function of the largest peak ground acceleration Y_τ *during a lifetime period* τ is [179]

$$\begin{aligned} F_\tau(y) &\stackrel{\text{def}}{=} \Pr\left(\max_\tau\{\widetilde{W}(t), 0 < t < \tau\} < y\right) \\ &= \sum_{n=0}^{\infty} [F(y)]^n \frac{(\lambda\tau)^n}{n!} \exp(-\lambda\tau) \\ &= \exp(-\lambda\tau) \sum_{n=0}^{\infty} \frac{[\lambda\tau F(y)]^n}{n!} \\ &= \exp[-\lambda\tau\{1 - F(y)\}] \end{aligned} \tag{3.15}$$

The peak ground acceleration a_{10}, defined as the 10% upper fractile of Y_{50}, can be obtained from the condition

$$F_{\tau=50yr}(y = a_{10}) \stackrel{\text{def}}{=} 0.9 \tag{3.16}$$

giving

$$\begin{aligned} a_{10} &= F^{-1}\left[1 + \frac{1}{50\lambda} \log\ 0.9\right] \\ &= F^{-1}\left[1 - \frac{1}{475\lambda}\right] \end{aligned} \tag{3.17}$$

Note that a_{10} depends on λ, T_s, and the spectral density $\tilde{G}(\omega)$ of ground motion. Different values of these parameters can yield the same peak ground acceleration a_{10}.

According to Eq. 3.12, the distribution of lifetime largest peak ground acceleration Y_{50} depends only on a_{10} without any explicit regard for other parameters of seismic hazard. It is possible that different sites characterized by same value of a_{10} may have very different values of λ, T_s, and other parameters. In all these cases, if the structural designs are identical due to same seismic zone of *Uniform Building Codes* [100,101], reliability estimates of these structures obtained from Eq. 3.12 will also be identical. Hence, a more realistic reliability analysis can be conducted by using Eqs. 3.15 and 3.13 which accounts for all site parameters of ground motion.

3.4 Structural Reliability Analysis

Structural reliability analysis requires a mathematical model derived from principles of mechanics and experimental data which relates the resistance and load variables for a specific performance criterion of interest. Let R_i and S_i denote two random variables representing structural strength and load effects at the ith structural component. The reliability of this component can be computed from the condition that the margin of safety $M_i = R_i - S_i > 0$. This condition can be expressed in the conventional form $M_i = g(\mathbf{X}) > 0$ where $\mathbf{X} \in \Re^n$ is a vector of basic random parameters characterizing uncertainty in both loads and resistances, and $g(\mathbf{x})$ is the performance function of the structural component. In the $\mathbf{x}$ space, this function $g(\mathbf{x})$ also known as limit state function separates the domain $\mathcal{D}$ of $\mathbf{X}$ into safe set $\mathcal{S} = \{\mathbf{x} : g(\mathbf{x}) > 0\}$ and failure set $\mathcal{F} = \{\mathbf{x} : g(\mathbf{x}) < 0\}$ and are shown in Fig. 3.1. The

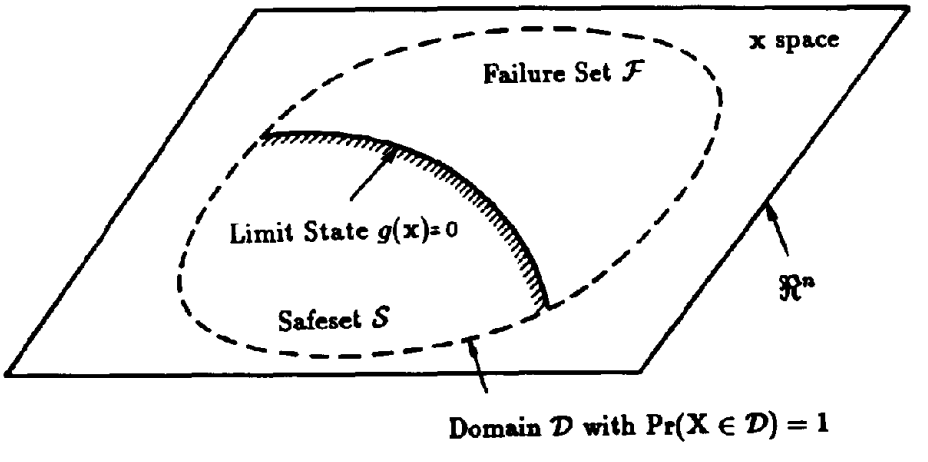

Figure 3.1: Definition of Limit State

lifetime reliability P_S is the complement of lifetime probability of failure P_F ($P_S = 1 - P_F$) which can be defined as

$$P_F \stackrel{\text{def}}{=} \Pr[g(\mathbf{X}) < 0] = \int_{g(\mathbf{x})<0} f_{\mathbf{X}}(\mathbf{x})d\mathbf{x} \tag{3.18}$$

in which $f_{\mathbf{X}}(\mathbf{x})$ is the joint probability density function of random vector $\mathbf{X} \in \Re^n$. The *generalized reliability index* β_G of the structural component can be obtained from [61]

$$\beta_G = \Phi^{-1}(-P_F) \tag{3.19}$$

in which $\Phi(\cdot)$ is the cumulative distribution function of standard univariate Gaussian random variable. In general, the n-fold integral in Eq. 3.18 cannot be calculated analytically. Alternatively, numerical integration can be performed, however, the computational effort becomes prohibitive when $n > 2$.

3.4.1 Approximate Methods for Reliability Analysis

Several approximate methods exist for performing the probability integration in Eq. 3.18. Among them, First- and Second-Order Reliability Methods [66,168,132,90,35], Variance Reduction [117], Importance Sampling [69,83,84,137,98], Directional Simulation [58,60,30], Monte Carlo Simulation [190], and many others can be applied to compute P_F and β_G in Eqs. 3.18 and 3.19, respectively. In this section, a few of them will be presented for their use in the approximate reliability analysis.

First- and Second-Order Reliability Methods (FORM/SORM)

First- and Second-Order Reliability Methods (FORM/SORM) are general state-of-the-art methods of structural reliability. The methods are based on linear (first-order) and quadratic (second-order) approximations of the limit state surface $g(\mathbf{x}) = 0$ tangent to the closest point of the surface to the origin of the space. The determination of this point involves nonlinear programming and is performed in the standard Gaussian image of the original space.

The FORM/SORM algorithms involve several steps. They will be described here briefly assuming a generic n-dimensional random vector $\mathbf{X}$. First, the space of uncertain parameters $\mathbf{x}$ is transformed into a new n-dimensional space $\mathbf{u}$ consisting of independent

standard Gaussian variables. The original limit state $g(\mathbf{x}) = 0$ then becomes mapped into the new limit state $g_U(\mathbf{u}) = 0$ in the u space. Second, the point on the limit state $g_U(\mathbf{u}) = 0$ having the shortest distance to the origin of the u space is determined by using an appropriate nonlinear optimization algorithm. This point, which has a distance β_{HL} to the origin of the u space, is referred to as the design point or β-point and is shown in Fig. 3.2. Third, the limit state $g_U(\mathbf{u}) = 0$ is approximated by a surface tangent to it at the

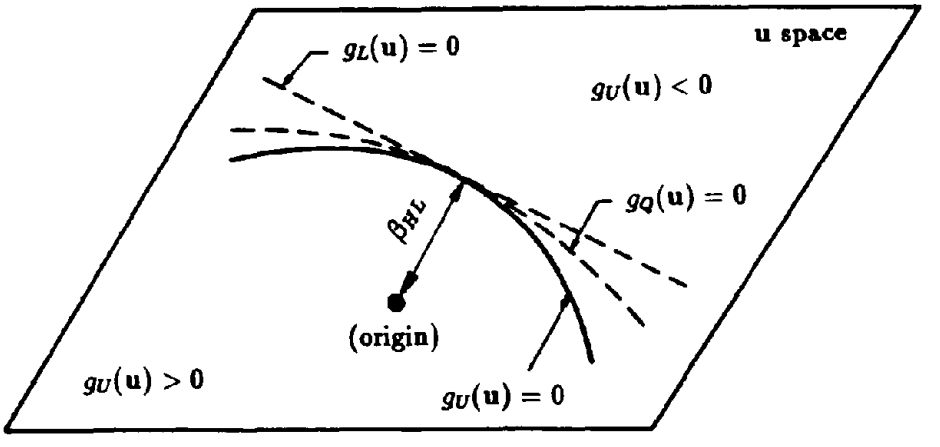

Figure 3.2: Linear and Quadratic Approximations to the Limit State

design point. Let such limit states be $g_L(\mathbf{u}) = 0$ and $g_Q(\mathbf{u}) = 0$, which correspond to the approximating surfaces as hyperplane (linear or first-order) and hyperparaboloid (quadratic or second-order), respectively (Fig. 3.2). The probability of failure P_F (Eq. 3.18) is thus approximated by $\Pr[g_L(\mathbf{U}) < 0]$ in FORM and $\Pr[g_Q(\mathbf{U}) < 0]$ in SORM. Let $P_{F,1}$ and $\beta_{G,1}$ be the first-order estimates and $P_{F,2}$ and $\beta_{G,2}$ be the second-order estimates of the actual failure probability P_F and the corresponding reliability index β_G. Analytical expressions can be developed to determine these probability estimates. Appendix A provides the derivation details of FORM/SORM equations. From Appendix A, the first-order estimates are

$$P_{F,1} = \Phi(-\beta_{HL}) \tag{3.20}$$

and

$$\beta_{G,1} = \beta_{HL} \tag{3.21}$$

and the second-order estimates are

$$P_{F,2} \simeq \Phi(-\beta_{HL}) \prod_{i=1}^{n-1} (1 - \kappa_i \beta_{HL})^{-\frac{1}{2}} \tag{3.22}$$

and

$$\beta_{G,2} = \Phi^{-1}\left(-P_{F,2}\right). \tag{3.23}$$

where

$$\Phi(u) = \frac{1}{\sqrt{2\pi}} \int_{-\infty}^{u} \exp\left(-\frac{1}{2}\xi^2\right) d\xi \tag{3.24}$$

is the cumulative distribution function of a standard Gaussian random variable, and κ_i are the principal curvatures of the limit state surface at the design point. FORM/SORM are analytical probability computation methods. Each input random variable and the performance function $g(\mathbf{x})$ must be continuous. Depending on the solver for nonlinear programming, additional requirement regarding smoothness i.e., differentiability of $g(\mathbf{x})$ may be required.

Monte Carlo Simulation and Importance Sampling

Consider a generic n-dimensional random vector $\mathbf{X}$ which characterizes uncertainty in all load and system parameters with the known joint distribution function $\mathbf{F}_{\mathbf{X}}(\mathbf{x})$. Suppose that $\mathbf{x}^{(1)}, \mathbf{x}^{(2)}, \cdots, \mathbf{x}^{(L)}$ are L realizations of input random vector $\mathbf{X}$ which can be generated independently. Let $g^{(1)}, g^{(2)}, \cdots, g^{(L)}$ be the output samples of $g(\mathbf{X})$ corresponding to the inputs $\mathbf{x}^{(1)}, \mathbf{x}^{(2)}, \cdots, \mathbf{x}^{(L)}$ that can be obtained by conducting repeated deterministic trials (analyses). Define L_F as the number of trials which are associated with negative values of $g(\mathbf{X})$. Then, the failure probability estimate by the direct Monte Carlo simulation is the ratio L_F/L which approaches the exact failure probability P_F when L approaches infinity. This

method is simple and relatively straightforward and should be used when each deterministic analysis does not require excessive computer time. When the analysis is computationally prohibitive or burdensome, alternative simulation method, known as Importance Sampling method, can be applied. In Importance Sampling, the random variables are sampled from a different probability density function, known as the sampling density. The purpose is to generate more outcomes from the region of interest, *e.g.*, the failure set $\mathcal{F} = \{\mathbf{x} : g(\mathbf{x}) < 0\}$. Using information from the FORM/SORM analyses, good sampling densities can be constructed. According to Hohenbichler [89], the failure probability estimate $P_{F,3}$ by importance sampling based on SORM improvement is

$$P_{F,3} \simeq \Phi(-\beta_{HL}) \prod_{k=1}^{n-1} \{1 - \kappa_k \Psi(\beta_{HL})\}^{-\frac{1}{2}} \frac{1}{N_{IS}} \sum_{j=1}^{N_{IS}} \frac{\Phi\left(h_Q(\hat{\mathbf{v}}_j)\right)}{\Phi(\beta_{HL})} \times \exp\left[-\frac{1}{2}\Psi(\beta_{HL}) \sum_{i=1}^{n-1} \kappa_i \hat{v}_{i,j}^2\right] \tag{3.25}$$

and the corresponding estimate of reliability index is

$$\beta_{G,3} = \Phi^{-1}(-P_{F,3}). \tag{3.26}$$

where $\Psi(-\beta_{HL}) = \phi(-\beta_{HL})/\Phi(-\beta_{HL})$, $\hat{\mathbf{v}}_j = \{\hat{v}_{1,j}, \hat{v}_{2,j}, \cdots, \hat{v}_{n-1,j}\}^T$ is the jth realization of the independent Gaussian random vector $\hat{\mathbf{V}} \in \Re^{n-1}$ with mean and variance of ith component being *zero* and $1/[1 - \Psi(\beta_{HL})]$, $h_Q(\hat{\mathbf{v}}_j)$ is the quadratic approximant in the form of rotational hyperparaboloid, and N_{IS} is the sample size for importance sampling. Details of this equation are also provided in Appendix A.

3.5 Numerical Examples

In this section, several numerical examples are illustrated to obtain seismic reliability indices by the static method. In the first example, a 5-story reinforced concrete (R/C) frame building designed by *1985 Uniform Building Code* is used to perform the reliability analysis based on current models of seismic hazard. In the second example, two 1-story special moment resisting frame structures designed by both *1985 Uniform Building Code* and *1988 Uniform*

Building Code are considered. Reliability analyses are carried out for each of the structures based on various models of seismic hazard discussed earlier.

3.5.1 Example 3.1

Structural Design

A 5-story, 3-bay R/C planar frame is analyzed and designed in accordance with the appropriate provisions of *1985 Uniform Building Code* and *ACI Code 318-83* for seismic zones-2 and -3. Thus, the static method and elementary failure criteria have been used in the analysis. Effects of structural redundancy and dynamic response are not included in this simplified analysis. Fig. 3.3(a) shows the typical plan of the building system. An interior frame is chosen to perform seismic analysis in the transverse direction and is shown in the Fig. 3.3(b).

Seismic design for the ith structural member of building frame by *ACI Code 318-83* requires

$$\phi R_{ni} \geq C_i U \tag{3.27}$$

where

$$U = \begin{cases} 1.4D_n + 1.7L_n \\ 0.75(1.4D_n + 1.7L_n \pm 1.87E_n) \\ 0.9D_n \pm 1.43E_n \end{cases} \tag{3.28}$$

is the ultimate factored load, R_{ni} is the nominal strength of ith structural component, C_i is the ith influence coefficient, and the resistance factor $\phi = 0.9$ for beams and $\phi = 0.7$ for columns. The nominal dead load D_n consists of mainly self-weight of structure and superimposed load of 30 psf for the floors and 10 psf for the roof. The nominal live load L_n is also assumed to be 30 psf for the floors and 10 psf for the roof. The nominal seismic base shear E_n can be obtained from Eq. 3.6 and are found to be 34 *kips* and 64 *kips* for seismic zones-2 and -3, respectively. The calculated base shears are based on $Z = 3/8$ for zone-2 and 3/4 for zone-3, $I = 1$, $K = 0.67$ for ductile moment resisting frame, C=0.10,

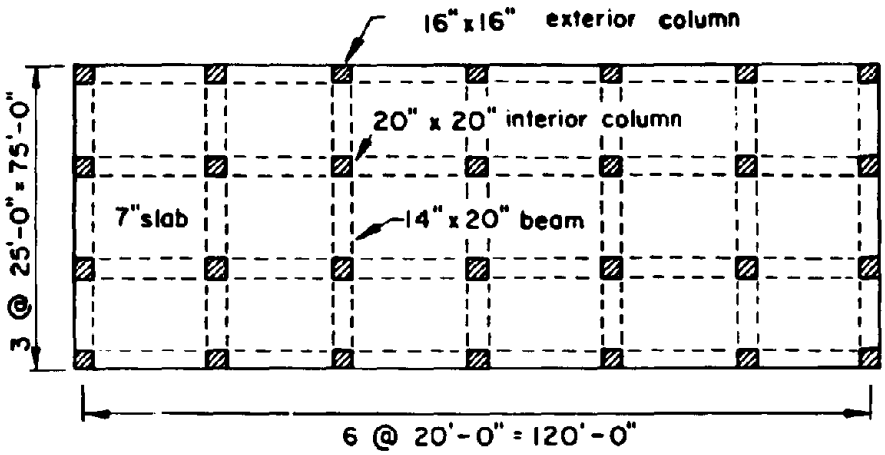

(a) Plan of Building System

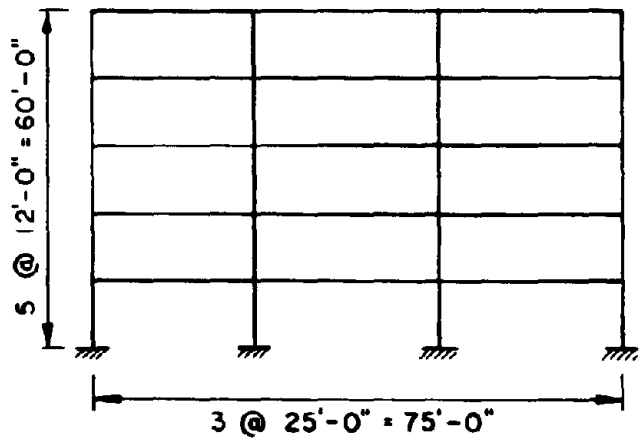

(b) Interior Frame of Building System

Figure 3.3: Plan and Interior Frame of Building Systems

Table 3.3: Distribution of Lateral Forces

Story	Lateral Forces (*kips*)	
	Zone-2	Zone-3
1	3	6
2	5	10
3	7	14
4	9	18
5	10	20

S=1.2 for stiff clay, and $W = 1043$ *kips*. For load combination involving earthquake, this nominal base shear is distributed along the height of building frame and is applied laterally to the structural systems. Since, the fundamental period of the frame is estimated to be less than 0.7 *s*, the concentrated lateral load F_t specified in the *1985 Uniform Building Code* is neglected. Tables 3.3 shows the distribution of lateral forces for seismic zones-2 and -3.

The size of the columns is 16 *in* $\times$ 16 *in* for exterior columns and 20 *in* $\times$ 20 *in* for interior columns. The size of the beams is assumed to be 14 *in* $\times$ 20 *in*. The columns have the same sizes throughout the height of the building. The beams also have the same dimension at all floor levels. The slab is assumed to be 7 *in* thick and is assumed to be constant throughout the structure. The dimensions of cross-sections of the above structural members are kept same for both zones-2 and -3. The amount of steel reinforcement, however, are obviously different due to differential design forces at the above zones and are exhibited in Fig. 3.4 and Tables 3.4 and 3.5. The dimensions of the top and bottom cover d and d' are assumed to be 2.5 *in*.

Normal weight concrete with the nominal values of compressive strength $f_c' = 4$ *ksi*, unit weight $w_c = 145$ *pcf*, and modulus of elasticity $E_c = 4000$ *ksi* are used. The reinforcing steel is obtained from *ASTM A615 Grade 60* with the nominal values of yield strength $F_y = 60$ *ksi*, modulus of elasticity $E_s = 29000$ *ksi*.

Reliability Analysis

FORM/SORM algorithms and importance sampling techniques are employed to determine the performance of above frames designed for seismic zones-2 and -3 of *1985 Uniform Building*

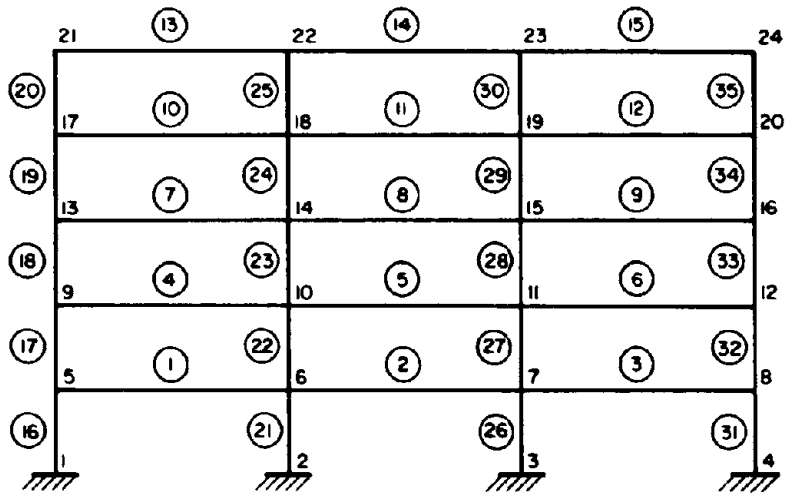

(a) Numbering of Members and Cross-Sections

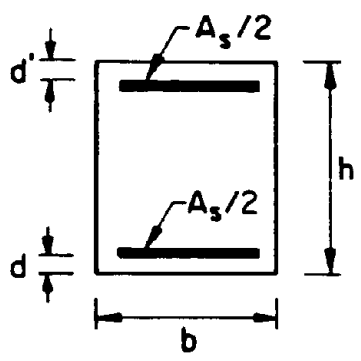

(b) Typical Column Cross-Section

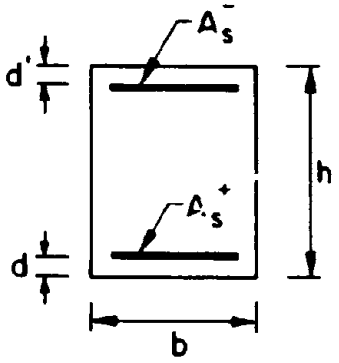

(c) Typical Beam Cross-Section

Figure 3.4: Cross-sectional Details of 5-story Frame

Table 3.4: Steel Reinforcement for Beams

Beam Cross-section*	Zone-2		Zone-3	
	A_s^- (in^2)	A_s^+ (in^2)	A_s^- (in^2)	A_s^+ (in^2)
5-6	3.16	3.14	4.54	3.33
6-5	4.37	3.14	6.08	3.33
6-7	4.37	2.65	6.08	2.85
9-10	3.38	3.14	4.79	3.33
10-9	4.37	3.14	6.08	3.33
10-11	4.37	2.65	6.08	2.85
13-14	3.16	3.14	4.37	3.33
14-13	4.00	3.14	5.39	3.33
14-15	4.00	2.65	5.39	2.85
17-18	3.00	3.14	3.58	3.33
18-17	4.00	3.14	4.54	3.33
18-19	4.00	2.65	4.54	2.85
21-22	1.80	2.40	2.18	3.00
22-21	3.16	2.40	4.16	3.00
22-23	3.16	2.08	4.16	2.51

* "$i - j$" implies cross-section i of member connected by nodes i and j

Table 3.5: Steel Reinforcement for Columns

Column	A_s (in^2)	
	Zone-2	Zone-3
16	2.64	3.60
17	2.64	4.74
18	2.64	4.74
19	2.64	4.74
20	3.98	6.00
21	4.00	5.08
22	4.00	5.08
23	4.00	5.08
24	4.00	5.08
25	4.00	5.08

Code. The reliability analysis is carried out for the load combination $D + L_{apt} + E$, where D, L_{apt} and E denote dead load, arbitrary-point-in-time live load, and earthquake load, respectively. The dead loads in all the floors and roof are assumed to be perfectly correlated requiring only one random variable to represent their uncertainty. The live loads, on the other hand, are modeled as five independent random variables. The load component in each type of the gravity loads is assumed to be uniformly distributed over the span of beams. The probabilistic characteristics of resistance and load variables are obtained from Table 3.1 and Table 3.2, respectively. For earthquake load, the cumulative distribution function of peak ground acceleration is based on seismic hazard in Eq. 3.12.

The seismic performance of this frame is evaluated by calculating component reliability indices at the critical cross-sections. The corresponding limit states are obtained from flexural action for beams and combined action of axial force and bending moment for columns. The explicit form of above limit state for beam (Flexure, R/C, Grade 60) is

$$g(\mathbf{X}) = R_n R' - \left[C_D D + \sum_{i=1}^{5} C_L{}^i L_{apt}{}^i + C_E E \right] \tag{3.29}$$

in which R_n is the deterministic nominal bending strength and R' is the Gaussian random variable with mean 1.05 and coefficient of variation 11% (Table 3.1). The limit state for column (Short Column, R/C, Tied) is

$$g(\mathbf{X}) = R_n R' - \left[\left(C_D D + \sum_{i=1}^{5} C_L{}^i L_{apt}{}^i + C_E E \right) \left(\sqrt{1 + e_n{}^2} \right) \right] \tag{3.30}$$

in which

$$R_n = P_n \sqrt{1 + e_n{}^2} \tag{3.31}$$

where P_n is the nominal axial force strength obtained from the interaction diagram of column cross-section for a nominal eccentricity ratio e_n and and R' is the Gaussian random variable with mean 1.05 and coefficient of variation 16% for compression failure and 12% for tension failure (Table 3.1). In both cases, C_D, $C_L{}^i$, and C_E are the influence coefficients representing either bending moments or axial forces at a specific cross-section due to relevant unit loads. They can be easily obtained following linear elastic static analysis of structural systems.

Note that in the above limit states $\mathbf{X} = \{D\ L_{apt}{}^1\ L_{apt}{}^2\ L_{apt}{}^3\ L_{apt}{}^4\ L_{apt}{}^5\ E\ R'\}^T$ is the 8-dimensional random vector characterizing uncertainty in the loads and resistances.

Discussions on Results

Tables 3.6 and 3.7 show the static reliability indices by FORM, SORM, and Importance Sampling technique obtained for columns and beams of the 5-story R/C frame structure designed for seismic zone-2 of *1985 Uniform Building Code* with $a_{10} = 0.1g$. The smallest reliability indices by FORM are found to be 2.19 for the beam and 2.25 for the column. Comparisons of these results with more accurate estimates by SORM and Importance Sampling confirm previous results with slight variation in the values of reliability indices. While the indices for most of the critical cross-sections of beams are quite low, the ones for the columns, however, are found to be comparatively large except for external columns at the top stories. The higher reliability of columns is expected due to the fact that most of the columns are designed with the minimum reinforcement ratio of 1% specified in the current *ACI code 318-83* in spite of considerably lower theoretical requirement. Since the value of a_{10} can vary within a same seismic zone (defined by code), similar reliability analyses are also carried for the same structure when $a_{10} = 0.15g$ and $a_{10} = 0.2g$. Results suggest that the indices based on FORM for zone-2 can be as low as 1.81 if $a_{10} = 0.15g$ and 1.5 if $a_{10} = 0.2g$.

The static reliability indices are also obtained by various estimates for the 5-story R/C frame structure designed for seismic zone-3 of *1985 Uniform Building Code* with several cases of $a_{10} = 0.2g$, $a_{10} = 0.3g$, and $a_{10} = 0.4g$. Based on FORM estimate, the smallest values of the above indices are 2.04 for $a_{10} = 0.2g$, 1.59 for $a_{10} = 0.3g$, and 1.30 for $a_{10} = 0.4g$. Comparisons of these results with those for zone-2 structure suggest that that current designs by *1985 Uniform Building Code* is less safe in areas of high seismicity.

It appears that the seismic reliability indices obtained by the static method can be very low for distribution of peak ground acceleration in Eq. 3.12. According to these results, (*i*) current design practice is unconservative when dealing with load combinations including earthquake because the reliability index is generally $3 - 4$ for gravity loads, and (*ii*) the seismic reliability estimate can be very different for code-designed structures due to large possible variation of a_{10} within a specific seismic zone.

Table 3.6: Static Reliability Indices for Columns (zone-2, $a_{10} = 0.1g$)

Cross-section* (Fig. 3.4)	FORM (Eq. 3.21)	SORM (Eq. 3.23)	Importance Sampling (Eq. 3.26)
1-5	4.29	4.34	3.97
5-1	4.29	4.25	4.25
5-9	3.42	3.36	3.34
9-5	3.63	3.58	3.52
9-13	3.71	3.71	3.71
13-9	3.34	3.34	3.34
13-17	2.99	2.96	2.94
17-13	2.56	2.52	2.48
17-21	3.16	3.13	3.13
21-17	2.25	2.22	2.20
2-6	4.25	4.24	4.24
6-2	4.70	4.97	4.68
6-10	4.84	5.02	5.02
10-6	4.90	4.92	4.92
10-14	5.33	5.32	5.32
14-10	5.23	5.22	5.22
14-18	5.78	5.78	5.78
18-14	5.64	5.64	5.64
18-22	6.22	6.22	6.22
22-18	5.92	6.09	5.96

* "$i - j$" implies cross-section i of member connected by nodes i and j

Table 3.7: Static Reliability Indices for Beams (zone-2, $a_{10} = 0.1g$)

Cross-section* (Fig. 3.4)	FORM (Eq. 3.21)	SORM (Eq. 3.23)	Importance Sampling (Eq. 3.26)
5-6	2.19	2.15	2.12
6-5	2.32	2.27	2.26
6-7	2.38	2.34	2.33
9-10	2.22	2.18	2.15
10-9	2.32	2.27	2.27
10-11	2.36	2.32	2.31
13-14	2.30	2.35	2.36
14-13	2.37	2.31	2.23
14-15	2.41	2.36	2.37
17-18	2.46	2.46	2.46
18-17	2.56	2.56	2.56
18-19	2.82	2.82	2.82
21-22	2.63	2.63	2.63
22-21	3.31	3.18	3.19
22-23	3.04	3.04	3.04

* "$i - j$" implies cross-section i of member connected by nodes i and j

3.5.2 Example 3.2

Structural Design

Consider two sites A and B in the western U.S. with mean earthquake arrival rates $\lambda_A = 0.92/yr$ and $\lambda_B = 0.024/yr$ [3] shown in Fig. 3.5. Geographically, site A is located in *River-*

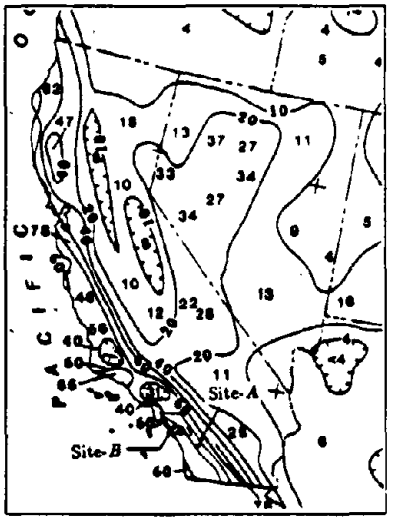

Figure 3.5: Probabilistic Map of a_{10} for Western U.S.

side and *San Diego* counties, while site B falls mostly into the *Orange* county of California. Both sites lie in the same seismic zone-4 of the *Uniform Building Code* [100,101] and have the same peak ground acceleration $a_{10} = 0.4g$. Consider a special moment resisting frame structure modeled as simple oscillator with damping ratio $\zeta = 0.05$, initial natural frequency $\omega_0 = 20.944\ rad/s$ (initial fundamental period $T_0 = 0.3\ s$), and weight W. The nominal base shear forces from the *1988 Uniform Building Code* and the *1985 Uniform Building Code* are $E_n = 0.09167W$ (Eq. 3.4) and $E_n = 0.08W$ (Eq. 3.6), respectively for zone-4. They are based on $S = 1$, $I = 1$, $R_w = 12$, $K = 0.67$, and $Z = 0.4$ (*1988 Uniform Building Code*) or $Z = 1$ (*1985 Uniform Building Code*).

The corresponding structural shear strength r and limit displacement x_l from the *1988 Uniform Building Code* are

$$r = \frac{\gamma E_n}{\phi} = \frac{1.4 \times 0.09167W}{0.9} = 0.1426W \tag{3.32}$$

and

$$x_l = \frac{\text{strength}}{\text{stiffness}} = \frac{0.1426W}{\omega_0{}^2 W/g} = 3.19\ mm \tag{3.33}$$

where $\gamma = 1.4$ and $\phi = 0.9$ are the load and resistance factors, respectively. Based on the *1985 Uniform Building Code*, $r = 0.1251W$ and $x_l = 2.8\ mm$.

Consider the alternative model of seismic hazard discussed in Section 3.3.2. Suppose, the ground motion in each seismic event can be represented by a *zero*-mean stationary Gaussian band-limited white noise $\xi(t)$ with one-sided mean power spectral density

$$G(\omega) = \begin{cases} G_0, & 0 < \omega < \bar{\omega} \\ 0, & \text{otherwise} \end{cases} \tag{3.34}$$

where G_0 is the spectral intensity of noise and $\bar{\omega}$ is the cutoff frequency for the band-limited white noise. Assuming $\bar{\omega} = 25\pi\ rad/s$ [179], the spectral moments can be obtained from Eq. 3.14 and are found to be $\lambda_0 = 78.54G_0$ and $\lambda_2 = 161492G_0$. From Eqs. 3.13 and 3.15 and the condition $F_{T=50\ yr}(y = a_{10}) = 0.9$, it can be shown that [179]

$$G_0 = \frac{{a_{10}}^2}{-157.1 \log\left[-\frac{1}{14.434T_s}\log\left\{1 + \frac{\log 0.9}{50\lambda}\right\}\right]}. \tag{3.35}$$

It is equal to 10026 mm^2s^{-3} when $\lambda = \lambda_A = 0.92\ /yr$ and 16090 mm^2s^{-3} when $\lambda = \lambda_B = 0.024\ /yr$ for a strong motion duration

$$T_s = 30\exp\left[-3.254\left(\frac{a_{10}}{g}\right)^{0.35}\right] = 2.83\ s \tag{3.36}$$

as proposed in Ref. [122]. Fig. 3.6 shows the variation of spectral intensity G_0 in Eq. 3.35 with mean rate λ. Sites A and B are characterized by frequent small seismic events and rare large earthquakes, respectively. However, designs at both sites are identical according to the *Uniform Building Code* [100,101].

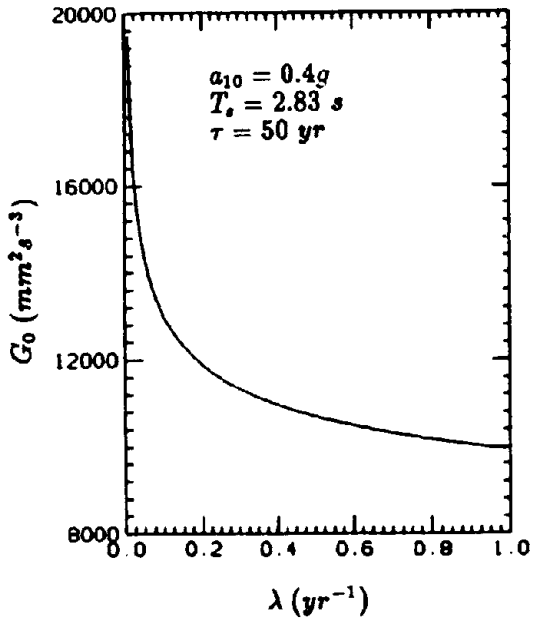

Figure 3.6: G_0 versus λ

Reliability Analysis

The seismic reliability P_S can be obtained from the probability that seismic load E does not exceed a deterministic base shear resistance r during the service lifetime τ. The assumption of deterministic structural characteristics is satisfactory at this level of analysis due to the large uncertainty in seismic load. Hence, the lifetime reliability

$$\begin{aligned} P_S &= \Pr(E < r) \\ &= \Pr\left(\frac{1.2Y_{50}SW}{RT_0^{\frac{2}{3}}} < r\right) \\ &= \Pr(Y_{50} < y_0) \end{aligned} \tag{3.37}$$

in which $y_0 = RT_0^{\frac{2}{3}}r/(1.2SW)$ is the design peak ground acceleration. Using $R = 7$ for special moment resisting frames, y_0 becomes $0.373g$ and $0.33g$ for *1988 Uniform Building Code* and *1985 Uniform Building Code*, respectively. From Eqs. 3.12 and 3.37, the seismic

reliability of the structure designed by the *1988 Uniform Building Code* is [100]

$$P_S = \exp\left[-\left\{\frac{0.373}{(0.38 \times 0.4)}\right\}^{-2.3}\right] = 0.88 \tag{3.38}$$

for both sites A and B. The corresponding reliability index is $\beta_G = \Phi^{-1}(0.88) = 1.175$. If the design is performed by the *1985 Uniform Building Code*, the reliability becomes $P_S = 0.845$ with $\beta_G = 1.015$.

Site seismicity can be accounted for in a more realistic way if reliability calculations are based on Eqs. 3.13 and 3.15. According to this method, reliabilities of structure designed by the *1988 Uniform Building Code* are $P_S = 0.68825$ ($\beta_G = 0.491$) for site A and $P_S = 0.8024$ ($\beta_G = 0.85$) for site B. The corresponding reliabilities of the structure designed by the *1985 Uniform Building Code* are $P_S = 0.098$ ($\beta_G = -1.29$) for site A and $P_S = 0.5664$ ($\beta_G = 0.167$) for site B.

Discussions on Results

Figure 3.7 shows the distribution $F(y)$ in Eq. 3.13 for sites A and B. Fig. 3.8 shows the lifetime probabilities $F_\tau(y)$ in Eq. 3.15 for $\tau = 50\ yr$ for sites A and B and corresponding lifetime distribution $\tilde{F}_{50}(y)$ in Eq. 3.12 used in Refs. [65] and [149].

Note that all these distributions take on the same values at $a_{10} = 0.4g$ but differ significantly for other values of peak ground acceleration. Thus designs by the *Uniform Building Code* [100,101] at sites with small values of λ are relatively safer than those with large values of λ, if the design peak ground acceleration y_0 is less than a_{10}. However, the above designs become relatively unsafe when y_0 is greater than a_{10}.

Designs by the *1988 Uniform Building Code* have higher reliability than those by the *1985 Uniform Building Code*. However, in designs by both codes (*i*) the reliability indices are lower than those for gravity loads consistent with findings in Refs. [65] and [149], and (*ii*) reliability of structure depends strongly on mean arrival rate λ.

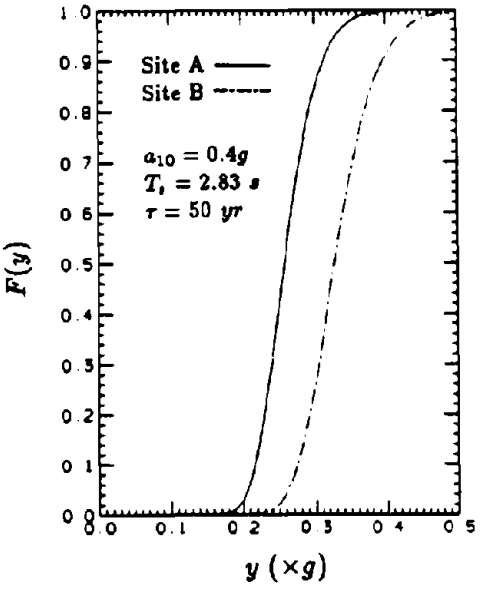

Figure 3.7: $F(y)$ at sites A and B

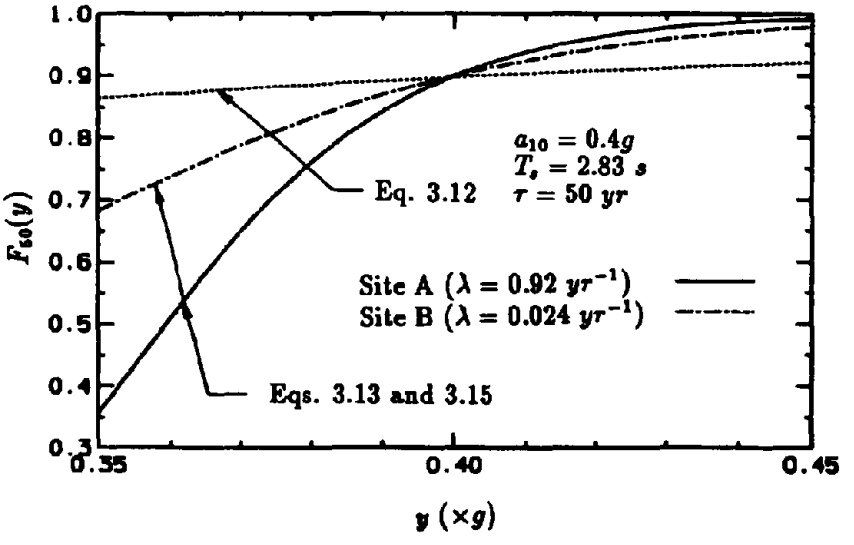

Figure 3.8: $F_\tau(y)$ at sites A and B

SECTION 4
Dynamic Reliability Of Nondegrading Systems

4.1 Introduction

There is a growing consensus in the earthquake engineering community that a single ground motion parameter such as peak ground acceleration and the static analysis may not reliably predict the actual behavior of structure. In addition to earthquake intensity, the evaluation of seismic performance must account for the details of ground acceleration and the dynamic structural characteristics. It is thus essential to conduct a parallel dynamic reliability analysis for an assessment of static reliability measures obtained earlier.

In this section, dynamic reliability analyses are performed to evaluate the adequacy of static reliability indices obtained in the previous phase of the work. The analysis involves (*i*) stochastic models of seismic ground acceleration, (*ii*) simple nondegrading models of structural systems, and (*iii*) damage-related failure criteria. Both linear and nondegrading nonlinear systems are considered and the reliability estimates are made by using several failure criteria. The following sections will continue to focus on this evaluation procedure by including various types of nonlinearity and system degradation process.

4.2 Linear Systems

4.2.1 Equations of Motion

Consider a system of differential equations representing the motion of discrete, linear elastic multi-degree-of- freedom structures

$$\mathbf{m}\ddot{\mathbf{X}}_t + \mathbf{c}\dot{\mathbf{X}}_t + \mathbf{k}\mathbf{X}_t = -\mathbf{m}\mathbf{d}W_t \tag{4.1}$$

in which $\mathbf{m}$ is the mass matrix, $\mathbf{c}$ is the damping matrix, $\mathbf{k}$ is the stiffness matrix, $\mathbf{X}_t \in \Re^n$ is the generalized displacement vector at time t, $\mathbf{d} \in \Re^n$ is a influence coefficient or direction vector which contains unity for all degrees of freedom in the same direction of ground motion(*e.g.*, translations) and *zeros* for all other degrees of freedom (*e.g.*, rotations),

and W_t is a general real-valued *zero* mean nonstationary colored process. It is assumed that the system mechanical properties are deterministic.

Mechanical linear systems can be divided into two classes: systems with proportional and nonproportional damping. Damping matrix of systems with proportional damping can be expressed as a linear combination of mass and stiffness matrices. As a result, classical modes of vibration exist and response characteristics can be obtained from the joint statistics of the pairs of modal coordinates [80]. This section examines systems with more general nonproportional damping.

Following the state vector approach [67,94,136] with the designation of $\boldsymbol{\theta}_{1,t} = \mathbf{X}_t$ and $\boldsymbol{\theta}_{2,t} = \dot{\mathbf{X}}_t$, the equivalent $2n$ first order linear differential equations in state variables become

$$\dot{\boldsymbol{\theta}}_t = \mathbf{A}\boldsymbol{\theta}_t + \mathbf{G}W_t \tag{4.2}$$

where

$$\boldsymbol{\theta}_t = \begin{Bmatrix} \boldsymbol{\theta}_{1,t} \\ \boldsymbol{\theta}_{2,t} \end{Bmatrix}, \tag{4.3}$$

$$\mathbf{G} = \begin{Bmatrix} \mathbf{0} \\ -\mathbf{d} \end{Bmatrix}, \tag{4.4}$$

and

$$\mathbf{A} = \begin{bmatrix} \mathbf{0} & \mathbf{I} \\ -\mathbf{m}^{-1}\mathbf{k} & -\mathbf{m}^{-1}\mathbf{c} \end{bmatrix}. \tag{4.5}$$

with $\mathbf{I}$ representing the n-dimensional identity matrix.

4.2.2 Coordinate Transformation

Consider a general change of physical variables $\boldsymbol{\theta}_t \in \Re^{2n}$ into canonical variables $\mathbf{V}_t \in C^{2n}$ via the transformation

$$\boldsymbol{\theta}_t = \boldsymbol{\Phi}\mathbf{V}_t \tag{4.6}$$

which uncouples the real system in Eq. 4.2 into the following complex modal coordinates given by

$$\dot{\mathbf{V}} = \mathbf{\Xi}\mathbf{V}_t + \mathbf{\Phi}^{-1}\mathbf{G}W_t \tag{4.7}$$

where $\mathbf{\Phi}$ is a complex matrix comprising eigenvectors of $\mathbf{A}$ and $\mathbf{\Xi} = \mathbf{\Phi}^{-1}\mathbf{A}\mathbf{\Phi}$ is a complex diagonal matrix with diagonal elements $\varphi_k \in \mathcal{C}, k = 1, 2, \cdots, 2n$ as the eigenvalues of $\mathbf{A}$. Assume that the eigenvalues φ_k and eigenvectors $\mathbf{\Phi}_k$ of $\mathbf{A}$ are distinct so that the matrix $\mathbf{\Phi} = [\mathbf{\Phi}_1, \mathbf{\Phi}_2, \cdots, \mathbf{\Phi}_{2n}]$ has an inverse. From Eq. 4.7, the kth uncoupled equation

$$\dot{V}_{k,t} = \varphi_k V_{k,t} + f_k W_t \tag{4.8}$$

with the initial condition $V_{k,t} = 0$ has the solution

$$V_{k,t} = f_k \int_0^t \exp[\varphi_k(t-u)] W_u du \tag{4.9}$$

where $V_{k,t} \in \mathcal{C}$ and $f_k \in \mathcal{C}$ are the kth components of $\mathbf{V}_t \in \mathcal{C}^{2n}$ and $\mathbf{\Phi}^{-1}\mathbf{G} \in \mathcal{C}^{2n}$, respectively.

4.2.3 Second Moment Descriptors of Response

Expectation, variances and covariances of pairs of modal coordinates $\mathbf{V}_t \in \mathcal{C}^{2n}$ can be evaluated using Eq. 4.9 and are given by

$$\mathrm{E}[V_{k,t}] = 0 \tag{4.10}$$

$$\mathrm{E}[V_{k,t}\overline{V}_{l,s}] = f_k \overline{f}_l \int_0^t du\ \exp(\varphi_k[t-u]) \int_0^s dv\ \overline{\exp(\varphi_l[s-v])}\mathrm{E}[W_u W_v]] \tag{4.11}$$

where the overline denotes the complex conjugate. These results simplify significantly when the excitation W_t is stationary and/or white. The above moments (i.e., means, variances and covariances) can be assembled into the complex modal mean vector

$$\boldsymbol{\mu}_V \stackrel{\text{def}}{=} \mathrm{E}[\mathbf{V}_t] = \mathbf{0} \tag{4.12}$$

and complex modal covariance matrix

$$\boldsymbol{\Sigma}_V(t,s) \stackrel{\text{def}}{=} \mathrm{E}\left[\mathbf{V}_t \overline{\mathbf{V}}_s^T\right] \tag{4.13}$$

where E[·] is the expectation operator. Using Eq. 4.6, the second-moment statistics of response $\boldsymbol{\theta}_t \in \Re^{2n}$ can be found as

$$\boldsymbol{\mu}_\theta \stackrel{\text{def}}{=} \mathrm{E}[\mathbf{X}_t] = \boldsymbol{\Phi}\mathrm{E}[\mathbf{V}_t] = \mathbf{0} \tag{4.14}$$

and

$$\boldsymbol{\Sigma}_\theta(t,s) \stackrel{\text{def}}{=} \mathrm{E}\left[\boldsymbol{\theta}_t \boldsymbol{\theta}_s^T\right] = \mathrm{E}\left[\boldsymbol{\Phi}\mathbf{V}_t \overline{\mathbf{V}}_s^T \boldsymbol{\Phi}^T\right] = \boldsymbol{\Phi}\boldsymbol{\Sigma}_V(t,s)\boldsymbol{\Phi}^T \tag{4.15}$$

where $\boldsymbol{\mu}_\theta$ and $\boldsymbol{\Sigma}_\theta(t,s)$ are real mean vector and real covariance matrix of $\boldsymbol{\theta}_t \in \Re^{2n}$. Suppose, a response vector process of interest $\mathbf{Y}_t$ can be related to the physical state vector $\boldsymbol{\theta}_t$ through the linear transformation

$$\mathbf{Y}_t = \mathbf{B}\boldsymbol{\theta}_t \tag{4.16}$$

where $\mathbf{B}$ is an appropriate deterministic matrix of influence coefficients. Then, the second-moment characteristics of $\mathbf{Y}_t$ becomes

$$\boldsymbol{\mu}_Y \stackrel{\text{def}}{=} \mathrm{E}[\mathbf{Y}_t] = \mathbf{B}\mathrm{E}[\boldsymbol{\theta}_t] = \mathbf{0} \tag{4.17}$$

and

$$\boldsymbol{\Sigma}_Y(t,s) \stackrel{\text{def}}{=} \mathrm{E}\left[\mathbf{Y}_t \mathbf{Y}_s^T\right] = \mathrm{E}\left[\mathbf{B}\boldsymbol{\theta}_t \boldsymbol{\theta}_s^T \mathbf{B}^T\right] = \mathbf{B}\boldsymbol{\Sigma}_\theta(t,s)\mathbf{B}^T \tag{4.18}$$

where $\boldsymbol{\mu}_Y$ and $\boldsymbol{\Sigma}_Y(t,s)$ are real mean vector and real covariance matrix of $\mathbf{Y}_t$.

4.2.4 Seismic Reliability Analysis

Consider a discrete linear system with the state vector $\boldsymbol{\theta}_t$ satisfying Eq. 4.2 where $\mathbf{A}$ and $\mathbf{G}$ are assumed to be time-invariant and deterministic. Consider the model of seismic hazard discussed in Section 3.3.2. Suppose, the ground motion in each seismic event is modeled as a *zero* mean stationary Gaussian white noise ξ_t with one-sided spectral intensity G_0.

The seismic performance of structural systems can be evaluated from the condition that the maximum interstory displacement at the ith story level exceeds an admissible value. For a N story structure, there are N such failure modes. These failure criteria are usually relevant when the limit states associated with the serviceability of building systems are considered.

Consider now the ith interstory response vector process $\mathbf{\Delta}_{i,t} = \{\delta_{i,t}, \dot{\delta}_{i,t}\}^T$ where

$$\delta_{i,t} = Y_{i,t} - Y_{i-1,t} \tag{4.19}$$

$$\dot{\delta}_{i,t} = \dot{Y}_{i,t} - \dot{Y}_{i-1,t} \tag{4.20}$$

in which the ith component $Y_{i,t}$ of $\mathbf{Y}_t \in \Re^N$ denotes the ith story displacement. The mean μ_Δ and covariance $\mathbf{\Sigma}_\Delta(t,s)$ of the interstory response vector $\mathbf{\Delta}_{i,t} \in \Re^2$ becomes

$$\mu_\Delta \stackrel{\text{def}}{=} \mathrm{E}[\mathbf{\Delta}_{i,t}] = \mathbf{0} \tag{4.21}$$

and

$$\begin{aligned} \mathbf{\Sigma}_\Delta(t,s) &\stackrel{\text{def}}{=} \mathrm{E}\left[\mathbf{\Delta}_{i,t}\mathbf{\Delta}_{i,s}^T\right] \\ &= \begin{bmatrix} \mathrm{E}(Y_{i,t} - Y_{i-1,t})(Y_{i,s} - Y_{i-1,s}) & \mathrm{E}(Y_{i,t} - Y_{i-1,t})(\dot{Y}_{i,s} - \dot{Y}_{i-1,s}) \\ (\mathrm{sym}) & \mathrm{E}(\dot{Y}_{i,t} - \dot{Y}_{i-1,t})(\dot{Y}_{i,s} - \dot{Y}_{i-1,s}) \end{bmatrix} \end{aligned} \tag{4.22}$$

which can be easily obtained from the known covariance matrix $\mathbf{\Sigma}_Y(t,s)$ in Eq. 4.18. Since the input excitation is Gaussian process, the state vector $\boldsymbol{\theta}_t$ is Gaussian and so are the responses $\mathbf{Y}_t$ and $\mathbf{\Delta}_{i,t}$.

Event Reliability

The event reliability $P_{S,i}(T_s)$ represents the probability that the maximum ith interstory displacement $\delta_{i,t}$ does not exceed a critical threshold $\delta_{i,cr}$ during an earthquake of deterministic strong motion duration T_s. Thus, the reliability is

$$P_{S,i}(T_s) \stackrel{\text{def}}{=} \Pr\left(\max_{0<t<T_s} |\delta_{i,t}| < \delta_{i,cr}\right) \tag{4.23}$$

which cannot be generally determined exactly. However, it can be approximated by [203, 128]

$$P_{S,i}(T_s) \simeq \exp\left[-2\int_0^{T_s} \nu(\delta_{i,cr};t)\,dt\right] \tag{4.24}$$

in which $\nu(\delta_{i,cr};t)$ is the transient mean $\delta_{i,cr}$-upcrossing rate of nonstationary Gaussian random process $\delta_{i,t}$ at time t. Exact and approximate methods for calculating mean upcrossing rates of Gaussian processes can be found in the current literature and is given by [184,185]

$$\nu(\delta_{i,cr};t) = \frac{1}{\sqrt{\Sigma_{11}(t,t)}}\phi\left(\frac{\delta_{i,cr}}{\sqrt{\Sigma_{11}(t,t)}}\right)\left[\sigma_{i,t}{}^*\phi\left(\frac{\mu_{i,t}{}^*}{\sigma_{i,t}{}^*}\right)+\mu_{i,t}{}^*\Phi\left(\frac{\mu_{i,t}{}^*}{\sigma_{i,t}{}^*}\right)\right] \tag{4.25}$$

where

$$\mu_{i,t}{}^* = \frac{\delta_{i,cr}\Sigma_{12}(t,t)}{\Sigma_{11}(t,t)}, \tag{4.26}$$

$$\sigma_{i,t}{}^{*2} = \Sigma_{22}(t,t) - \frac{\{\Sigma_{12}(t,t)\}^2}{\Sigma_{11}(t,t)}, \tag{4.27}$$

and $\Sigma_{ij}(t,t)$, $i,j = 1,2$ is the ijth element of $\mathbf{\Sigma}_\Delta(t,t)$ in Eq. 4.23. When $\delta_{i,t}$ attains stationarity, $\mathbf{\Sigma}_\Delta(t,t)$ becomes time-invariant with its constant elements $\Sigma_{11}(t,t) = \Sigma_{11}$, $\Sigma_{12}(t,t) = 0$, and $\Sigma_{22}(t,t) = \Sigma_{22}$. Consequently, the steady-state mean $\delta_{i,cr}$-upcrossing rate $\nu_{ss}(\delta_{i,cr})$ simplifies to

$$\nu_{ss}(\delta_{i,cr}) = \frac{1}{2\pi}\sqrt{\frac{\Sigma_{22}}{\Sigma_{11}}}\exp\left(-\frac{\delta_{i,cr}{}^2}{2\Sigma_{11}}\right). \tag{4.28}$$

Eqs. 4.25 and 4.28 can be used to substitute $\nu(\delta_{i,cr};t)$ in Eq. 4.24 to obtain event reliability in Eq. 4.23 when $\delta_{i,t}$ is assumed to be nonstationary and stationary, respectively.

Lifetime Reliability

The lifetime reliability $P_{S,i}(\tau)$ can be defined by the probability that the ith interstory displacement $\delta_{i,t}$ does not exceed $\delta_{i,cr}$ during the lifetime τ of structural system. This can be obtained following similar considerations as in Eqs. 3.13 and 3.15. Accordingly, the reliability is

$$P_{S,i}(\tau) = \exp\left[-\lambda\tau\{1 - P_{S,i}(T_s)\}\right] \tag{4.29}$$

where λ is mean arrival rate of earthquakes discussed in the previous section.

4.2.5 Numerical Example

Example 4.1

Consider the special moment resisting frames in Example 3.2 designed by both *1988 Uniform Building Code* and *1985 Uniform Building Code*. The seismic reliability indices of these frames are already computed by the static method for the two sites A and B which are characterized by the same value of $a_{10} = 0.4g$ but different mean earthquake arrival rates $\lambda_A = 0.92/yr$ and $\lambda_B = 0.024/yr$, respectively. In this example, these reliability measures are evaluated by the dynamic method with linear elastic restoring force.

Consider the model of seismic hazard discussed in Section 3.3.2. Suppose, the ground motion W_t in each seismic event is modeled as stationary Gaussian band-limited white noise with one-sided mean power spectral density $G(\omega) = G_0$ for $\omega \leq \bar{\omega}$ and *zero* otherwise. The spectral intensity G_0 is equal to 10026 $mm^2\ s^{-3}$ when $\lambda = \lambda_A = 0.92\ yr^{-1}$ and 16090 $mm^2\ s^{-3}$ when $\lambda = \lambda_B = 0.024\ yr^{-1}$ for a strong motion duration $T_s = 2.83\ s$ as obtained earlier. Assume that the frames can be represented by linear oscillator with initial natural frequency $\omega_0 = 20.944\ rad/s$ and damping ratio $\zeta = 0.05$.

The event reliability $P_S(T_s)$ of the linear oscillator can be obtained from the probability that the largest value of displacement response δ_t of the oscillator with respect to ground motion does not exceed a critical threshold δ_{cr} during strong motion duration T_s. Note that the description of such failure criterion does not uniquely characterize seismic performance. When δ_t is stationary and the structural characteristics and strong motion duration T_s are assumed to be deterministic, the event reliability $P_S(T_s)$ obtained from Eq. 4.23 becomes

$$\begin{aligned} P_S(T_s) &= \Pr\left(\max_{0<t<T_s} |\delta_t| < \delta_{cr}\right) \\ &\simeq \exp\left[-2\nu_{ss}(\delta_{cr})T_s\right] \end{aligned} \tag{4.30}$$

Table 4.1: Reliability of Linear Systems

Design Code (δ_{cr})	Site (λ)	G_0 (mm^2s^{-3})	$\nu_{ss}(\delta_{cr})$	$P_S(T_s)$ (β_E)	$P_S(\tau)$ (β_L)
UBC(85) (19.6 mm)	A (0.92/yr)	10026	8.81×10^{-5}	0.9998 (3.54)	0.991 (2.366)
	B (0.024/yr)	16090	6.36×10^{-3}	0.9821 (2.1)	0.9787 (2.028)
UBC(88) (22.3 mm)	A (0.92/yr)	10026	3.1×10^{-6}	0.999991 (4.3)	0.9996 (3.35)
	B (0.024/yr)	16090	7.98×10^{-4}	0.997744 (2.84)	0.9973 (2.78)

where the stationary mean δ_{cr}-upcrossing rate $\nu_{ss}(\delta_{cr})$ of δ_t can be obtained from Eq. 4.28 as

$$\nu_{ss}(\delta_{cr}) = \frac{1}{2\pi}\sqrt{\frac{\Sigma_{22}}{\Sigma_{11}}}\exp\left(-\frac{{\delta_{cr}}^2}{2\Sigma_{11}}\right) \tag{4.31}$$

with $\Sigma_{11} \simeq \pi G_0/4\zeta{\omega_0}^3$ and $\Sigma_{22} \simeq \pi G_0/4\zeta\omega_0$ for a sufficiently large bandwidth $\bar{\omega} = 25\pi$, as obtained earlier. Correspondingly, the event reliability index β_E can be defined as

$$\beta_E = \Phi^{-1}\left(P_S(T_s)\right) \tag{4.32}$$

where $\Phi(\cdot)$ is the standard Gaussian cumulative distribution function. From Eq. 4.29, the lifetime reliability $P_S(\tau)$ of the oscillator becomes

$$P_S(\tau) = \exp\left[-\lambda\tau\{1 - P_S(T_s)\}\right]. \tag{4.33}$$

with the corresponding lifetime reliability index β_L defined as

$$\beta_L = \Phi^{-1}\left(P_S(\tau)\right). \tag{4.34}$$

Table 4.1 shows both event and lifetime reliabilities of the special moment resisting frames for the sites A and B calculated from the Eqs. 4.30 and 4.33 for a strong motion duration $T_s = 2.83\ s$, respectively. Also included in the table are the corresponding

reliability indices which are calculated by using Eqs. 4.32 and 4.34. These reliability measures by the linear elastic dynamic method are obtained when the design is modified to $r^* = 7r$ in Eq. 3.52 to account for the use of $R = 7$ in designing the special moment resisting frame structures [100,101].

Results show that (*i*) the reliability indices by static and dynamic methods have significantly different values, (*ii*) designs by two editions of *Uniform Building Code* [100, 101] have different reliabilities at sites with frequent small earthquakes and infrequent large earthquakes, although the sites are characterized by the same value of a_{10}, (*iii*) designs by *1988 Uniform Building Code* is safer than those by *1985 Uniform Building Code*, and (*iv*) *event* and *lifetime* reliabilities of these designs can differ significantly particularly at sites with frequent small earthquakes.

4.3 Nonlinear Nondegrading Systems

When studying the effects of yielding on structural response an ideal nondegrading elasto-plastic (EP) material behavior is often assumed to be the first choice. This simple and idealized hysteretic restoring force with its vanishing stiffness during yielding is attractive at least for two reasons. One follows the observation that many materials roughly exhibit this behavior, at least near ultimate loads. The other reason lies in the mathematical simplicity of the model which allows analytical treatment feasible for nonlinear random vibration of hysteretic systems.

4.3.1 Ideal Elasto-Plastic Oscillator

Consider a single-degree-of-freedom (SDOF) lightly damped nonlinear oscillator with mass m subjected to stationary Gaussian random excitation $\widetilde{W}_t$ with the relative displacement response X_t satisfying the differential equation

$$\ddot{X}_t + 2\zeta\omega_0\dot{X}_t + {\omega_0}^2 Z_t = -\widetilde{W}_t \tag{4.35}$$

In Eq. 4.35, ω_0 is the initial natural frequency, ζ is the viscous damping ratio, and Z_t is the ideal elasto-plastic hysteretic variable which can be modeled as

$$\dot{Z}_t = \dot{X}_t \left[1 - H(\dot{X}_t/x_y)H(Z_t/x_y - 1) - H(-\dot{X}_t/x_y)H(-Z_t/x_y - 1)\right] \tag{4.36}$$

where x_y is the yield displacement of the oscillator, and $H(\xi)$ is a unit step function, i.e., $H(\xi) = 1$ for $\xi \geq 0$ and 0 for $\xi < 0$. Fig. 4.1(a) shows the restoring force characteristics of the ideal elasto-plastic oscillator. At the start of the motion and until $|X_t|$ crosses the yield level x_y for the first time, the solution of Eq. 4.36 becomes $Z_t = X_t$ with the corresponding restoring force $F = \omega_0{}^2 X_t$. Thus, the response of this EP system is identical to that of an associated linear system with constant stiffness $k = \omega_0{}^2 m$ and is shown in Fig. 4.1(b). Behavior surrounding the onset of the inelastic deformation is equivalent to a first-crossing problem for the associated linear oscillator [222,224,232,223].

In between yield level crossings, the EP system also behaves like a linear oscillator. Suppose that at some known time t, the most recent yield level crossing brought the total plastic deformation up to a value $X_t{}^p = d$. The total displacement at time t will then consist of a permanent set d and a linear elastic component $X_t{}^e$, i.e., $X_t = d + X_t{}^e$. The process $X_t{}^p$ changes rather abruptly whenever inelastic action occurs. For $d = 0$, i.e., before any plastic deformation, $X_t = X_t{}^e$. A realization of this process $X_t{}^e$ is shown in Fig. 4.2(a). It is obtained by subtracting the plastic deformation process $X_t{}^p$ in Fig. 4.2(b) from the total displacement process X_t in Fig. 4.2(c). The permanent set $X_t{}^p$ remains invariant as long as the absolute value of $X_t{}^e$ is smaller than the yield threshold x_y. Each time $|X_t{}^e|$ exceeds x_y, however, inelastic action is known to occur.

4.3.2 Seismic Performance Evaluation

Consider the seismic hazard model discussed in Section 3.3.2. Suppose, the ground motion in each seismic event can be modeled as stationary Gaussian random process $\widetilde{W}_t$ with one-sided mean power spectral density $\tilde{G}(\omega)$. The structural and material characteristics are assumed to be deterministic.

Seismic performance of structural systems can be evaluated in terms of the condition that a specific response or damage level is not exceeded during ground motion. In this section, several response quantities of interest along with their stationary probabilistic characteristics are discussed.

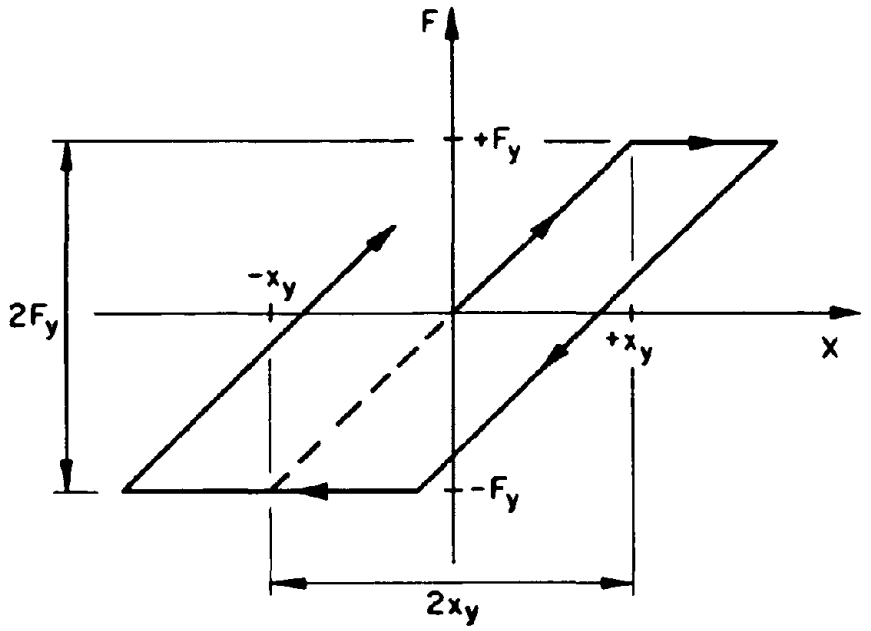

(a) Nondegrading Elasto-Plastic Hysteresis

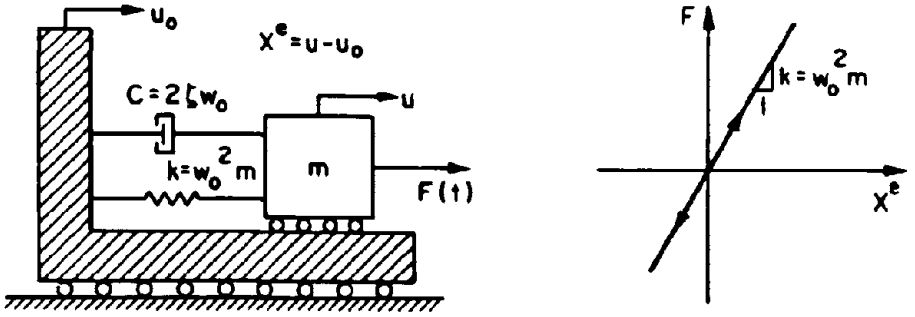

(b) Associated Linear System

Figure 4.1: Ideal Elasto-Plastic Oscillator

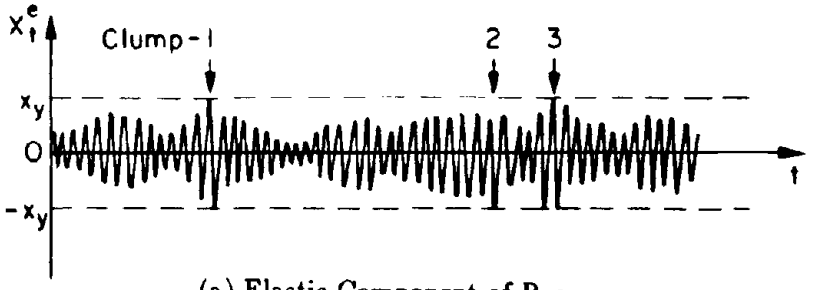

(a) Elastic Component of Response

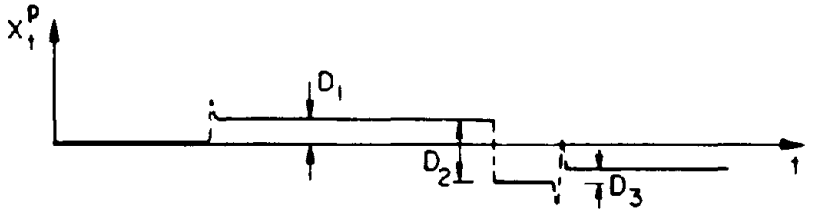

(b) Plastic Component of Response

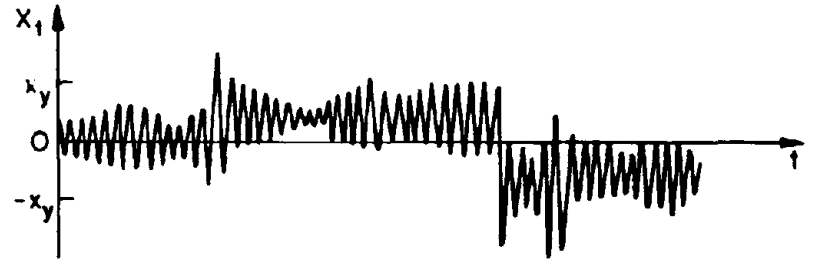

(c) Total Response

Figure 4.2: Elasto-Plastic Response Characteristics

Event Reliability

Ductility Factor

One of the most extensively used damage index in seismic analysis is the ductility factor. If the plastic action occurs during deterministic strong motion duration T_s associated with a seismic event $\widetilde{W}_t$, the ductility factor can be expressed as

$$\begin{aligned} \text{Ductility Factor} &\stackrel{\text{def}}{=} 1 + \frac{\max\limits_{0 \le t \le T_s} |X_t^p|}{x_y} \\ &= 1 + \frac{M_s}{x_y} \end{aligned} \tag{4.37}$$

where M_s represents peak inelastic deformation during strong motion duration T_s. The event reliability $P_S(T_s)$ of the nonlinear oscillator can be obtained from the probability that the ductility factor does not exceed a threshold μ_0 during a time interval $(0, T_s)$. Thus, reliability becomes

$$\begin{aligned} P_S(T_s) &\stackrel{\text{def}}{=} \Pr\left[\text{Ductility Factor} < \mu_0\right] \\ &= \Pr\left[M_s < x_y(\mu_0 - 1)\right] \\ &= F_{M_s}\left(x_y(\mu_0 - 1)\right) \end{aligned} \tag{4.38}$$

in which $F_{M_s}(\xi)$ is the cumulative probability distribution of M_s. This probability can be approximated by viewing the upcrossings of the process $|X_t^p|$ of a fixed threshold d as a nonhomogeneous Poisson process with transient mean rate $\nu_{M_s}(d;t)$. The mean rate $\nu_{M_s}(d;t)$ is proportional to the stationary mean rate $\nu_c(x_y)$ of jump occurrence in X_t^p and can be obtained from

$$\nu_{M_s}(d;t) = \nu_c(x_y)p(d;t) \tag{4.39}$$

where $p(d;t)$ is the probability that a plastic set contribution at time t results in an upcrossing of the level d. The net result which can be obtained from the original reference [222] is the following approximate expression for $F_{M_s}(\xi)$

$$F_M(\xi) = \exp\left[-\{\exp[\nu_c(x_y)T_s] - 1\}\exp\left(-\frac{\xi}{\delta}\right)\right] \tag{4.40}$$

where

$$\delta = \frac{{\sigma_{X^e}}^2}{2x_y}. \tag{4.41}$$

and

$$\nu_c(x_y) = \frac{1}{2\pi}\sqrt{\frac{\Lambda_2}{\Lambda_0}}\exp\left[-\frac{{x_y}^2}{2\Lambda_0}\right]\left(1 - \exp\left[-\sqrt{\frac{\pi}{2}}\frac{qx_y}{\sigma_{X^e}}\right]\right) \tag{4.42}$$

in which

$$\Lambda_i = \int_0^\infty \omega^i G_{X^e}(\omega)d\omega \tag{4.43}$$

is the ith spectral moment of $X_t{}^e$ with one-sided mean power spectral density $G_{X^e}(\omega)$, and q is a factor determining the degree of correlation among successive peaks given by

$$q = \left[1 - \frac{{\Lambda_1}^2}{\Lambda_0\Lambda_2}\right]^{\frac{1}{2}}. \tag{4.44}$$

Since $X_t{}^e$ represents response of the associated linear oscillator, $G_{X^e}(\omega)$ can be readily determined from the input spectrum $\tilde{G}(\omega)$.

Cumulative Plastic Deformation

Another useful indicator of seismic damage assessment of structural systems is the energy dissipated during strong motion duration T_s of a seismic event [148]. This dissipated energy is proportional to accumulated absolute plastic deformation Δ_t which is defined as

$$\Delta_t = \sum_{i=1}^{N_t} |\Delta_i| \tag{4.45}$$

where $|\Delta_i|$ is the absolute plastic set during ith isolated $(-x_y, +x_y)$-outcrossing of the displacement response $X_t{}^e$ of the associated linear system. Assuming that the damping force $2\zeta\omega_0\dot{X}_t^e$ is very small compared with the yield force $F_y = {\omega_0}^2 m x_y$ in spring (a consequence of small ζ), Karnopp and Scharton [114] derived a simple approximate expression

$$|\Delta| = \frac{\dot{X}_t^{e^2}}{2\omega_0{}^2 x_y} \tag{4.46}$$

which follows from the argument that all the kinetic energy $m\dot{X}_t^{e^2}/2$ of the oscillator is released into work done $F_y|\Delta| = \omega_0{}^2 m x_y|\Delta|$ due to plastic deformation. The event reliability $P_S(T_s)$ of the oscillator can be similarly obtained from the probability that Δ_{T_s} does not exceed a threshold d during a time interval $(0, T_s)$ and is given by

$$P_S(T_s) \stackrel{\text{def}}{=} \Pr\left[\Delta_{T_s} < d\right] \tag{4.47}$$

In spite of correlated outcrossings, an estimate of above reliability can be obtained by assuming statistical independence of homogeneous Poisson x_y-upcrossings of $X_t{}^e$ with steady-state mean rate $\nu(x_y) = 1/2\pi\ \sqrt{\Lambda_2/\Lambda_0}\ \exp(-x_y{}^2/2\Lambda_0)$. Thus, the reliability becomes

$$\begin{aligned}
P_S(T_s) &= \Pr\left[\Delta_{T_s} < d\right] \\
&= \Pr\left(\sum_{i=1}^{N_{T_s}} \frac{\dot{X}_{t_i}^{e^2}}{2\omega_0{}^2 x_y} < d\right) \\
&= \sum_{k=0}^{\infty} \Pr\left(\sum_{i=1}^{k} \frac{\dot{X}_{t_i}^{e^2}}{2\omega_0{}^2 x_y} < d \,|N_{T_s} = k\right) \Pr(N_{T_s} = k) \\
&= \sum_{k=0}^{\infty} \Pr\left(\sum_{i=1}^{k} \widetilde{\dot{X}_{t_i}^{e}}^2 < \frac{2x_y d}{\sigma_{X^e}{}^2} \,|N_{T_s} = k\right) \frac{[2\nu(x_y)T_s]^k}{k!} \exp[-2\nu(x_y)T_s] \\
&= \exp[-2\nu(x_y)T_s] + \sum_{k=1}^{\infty} \int_0^{\frac{2x_y d}{\sigma_{X^e}{}^2}} \frac{\left(\frac{2x_y d}{\sigma_{X^e}{}^2}\right)^{\frac{k}{2}-1}}{2^{k/2}\Gamma(k/2)} \times \\
&\quad \exp\left(-\frac{x_y \xi}{\sigma_{X^e}{}^2}\right) \frac{[2\nu(x_y)T_s]^k}{k!} \exp[-2\nu(x_y)T_s]\, d\xi
\end{aligned} \tag{4.48}$$

where

$$\Gamma(v) \stackrel{\text{def}}{=} \int_0^{\infty} \eta^{v-1} \exp(-\eta) d\eta \tag{4.49}$$

is the gamma function, $\widetilde{\dot{X}_{t_i}^{e}}$, $i = 1, 2, \cdots, k$ is independent and identically distributed standard Gaussian random variable, and $\sum_{i=1}^{k} \widetilde{\dot{X}_{t_i}^{e}}^2 = \sum_{i=1}^{k} \left(\dot{X}_{t_i}^{e}/\omega_0 \sigma_{X^e}\right)^2$ is the chi-squared random variable with k degrees of freedom.

The event reliability index β_E can be defined as

$$\beta_E = \Phi^{-1}(P_S(T_s)) \tag{4.50}$$

where $P_S(T_s)$ is the event reliability which can be obtained from either of the Eqs. 4.38 and 4.47 associated with the failure criteria based on ductility and cumulative plastic deformation, respectively.

Lifetime Reliability

The *lifetime* reliability $P_S(\tau)$ of the oscillator can be obtained following similar considerations as in Eqs. 3.13 and 3.15. Accordingly, the reliability is

$$P_S(\tau) = \exp\left[-\lambda\tau\{1 - P_S(T_s)\}\right] \tag{4.51}$$

with the corresponding lifetime reliability index β_L defined as

$$\beta_L = \Phi^{-1}(P_S(\tau)). \tag{4.52}$$

Note that Eqs. 4.51 and 4.52 can not be applied when the analysis accounts for structural degradation.

4.3.3 Numerical Example

Example 4.2

Consider again the special moment resisting frames at sites A and B in Examples 3.2 and 4.1 which are designed by both *1988 Uniform Building Code* and *1985 Uniform Building Code*. Dynamic method with linear elastic restoring forces are already applied to assess the adequacy of the static reliability indices for these simple structures. This example continues to focus on the evaluation of above reliability estimates by considering nondegrading elasto-plastic hysteresis for the nonlinear oscillator representing the special moment resisting frames.

Assume as before that the ground motion W_t in each seismic event is a stationary Gaussian band-limited white noise with one-sided mean power spectral density $G(\omega) = G_0$

for $\omega \leq \bar{\omega}$ and *zero* otherwise. The spectral intensity G_0 is equal to 10026 $mm^2\ s^{-3}$ when $\lambda = \lambda_A = 0.92\ yr^{-1}$ and 16090 $mm^2\ s^{-3}$ when $\lambda = \lambda_B = 0.024\ yr^{-1}$ for a strong motion duration $T_s = 2.83\ s$ as obtained earlier. Assume that the frames can be represented by an ideal nondegrading elasto-plastic oscillator with initial natural frequency $\omega_0 = 20.944\ rad/s$ and damping ratio $\zeta = 0.05$. The yield displacement x_y of the EP oscillator is assumed to be the limit displacement x_l (Eq. 3.33) obtained from the *Uniform Building Code*.

Two different failure criteria depending on ductility factor and cumulative plastic deformation are employed to obtain the seismic reliability of the EP oscillator representing the above frames at sites A and B. Fig. 4.3 shows the plots of ductility-based event and lifetime reliabilities in Eqs. 4.38 and 4.51 of the structures designed by *1988 Uniform Building Code* for different values of μ_0 at the sites A and B. They indicate significant differences in the above reliability measures for the two sites A and B although they are characterized by the same value of $a_{10} = 0.4g$. This observation is also exhibited when the reliabilities shown in Fig. 4.4 are computed from Eqs. 4.48 and 4.51 for a different failure criteria associated with the cumulative plastic deformation in Eq. 4.45. Figs. 4.5-4.6 provide the similar sets of plots of event and lifetime reliabilities associated with above failure criteria (ductility and cumulative plastic deformation) for the structures designed by *1985 Uniform Building Code* at the sites A and B. The above probabilities depend essentially on earthquake intensity and duration and on structural dynamic characteristics. Thus, designs at sites with the same a_{10} can have different reliabilities because such sites may correspond to earthquakes of different occurrence rate λ and spectral intensity G_0.

The system factors R and K in the *Uniform Building Code* depends essentially on the ductility characteristics of structural systems. However, there is no reliable way of obtaining corresponding ductility capacity for a code-specific system factors. Therefore, for several ductility thresholds $\mu_0 = 6, 8, 10$, the event and lifetime reliabilities along with the associated reliability indices of above designs are shown in Table 4.2. Significant differences are exhibited when these reliability measures are compared with those obtained by the static method in Section 3.

Results show that (*i*) the reliability indices by static and dynamic methods have very different values, (*ii*) designs by two editions of *Uniform Building Code* [100,101] have differ-

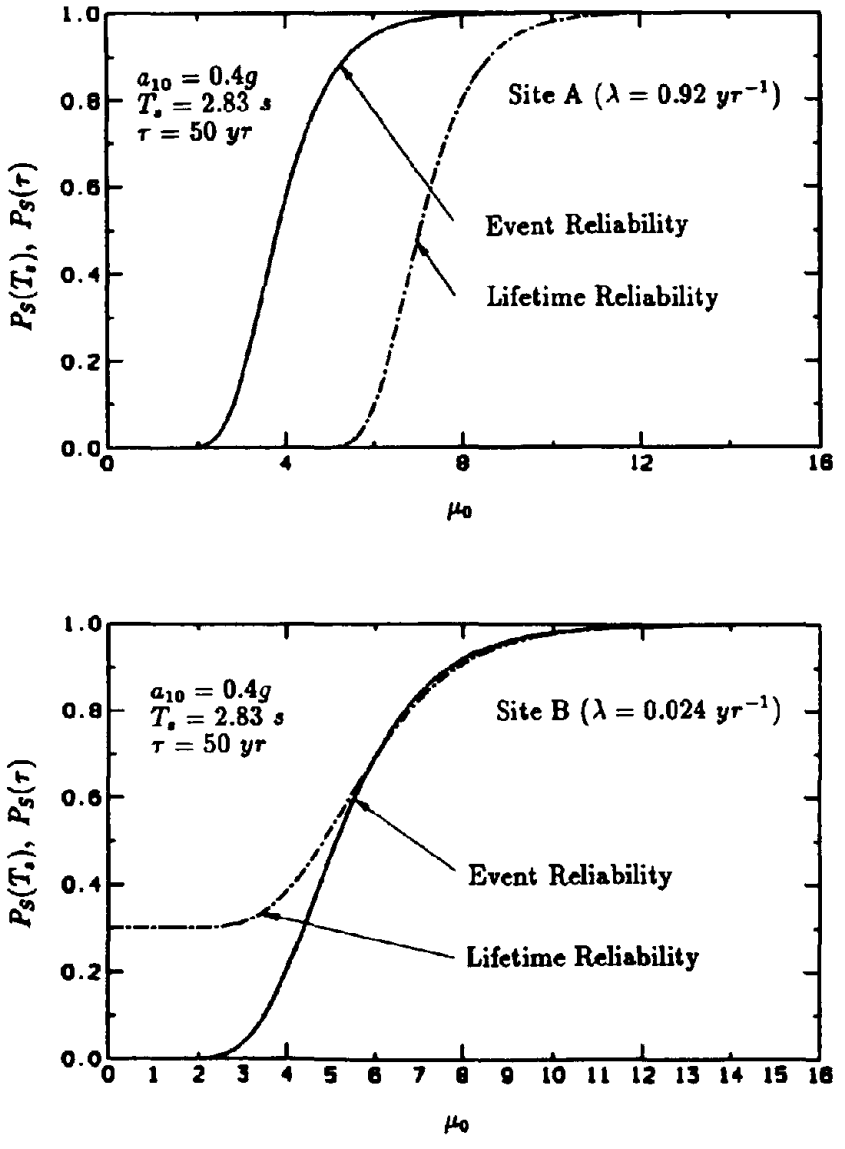

Figure 4.3: Event and Lifetime Reliabilities of Elasto-Plastic Oscillator Designed by UBC(88) for Failure Criteria Based on Ductility

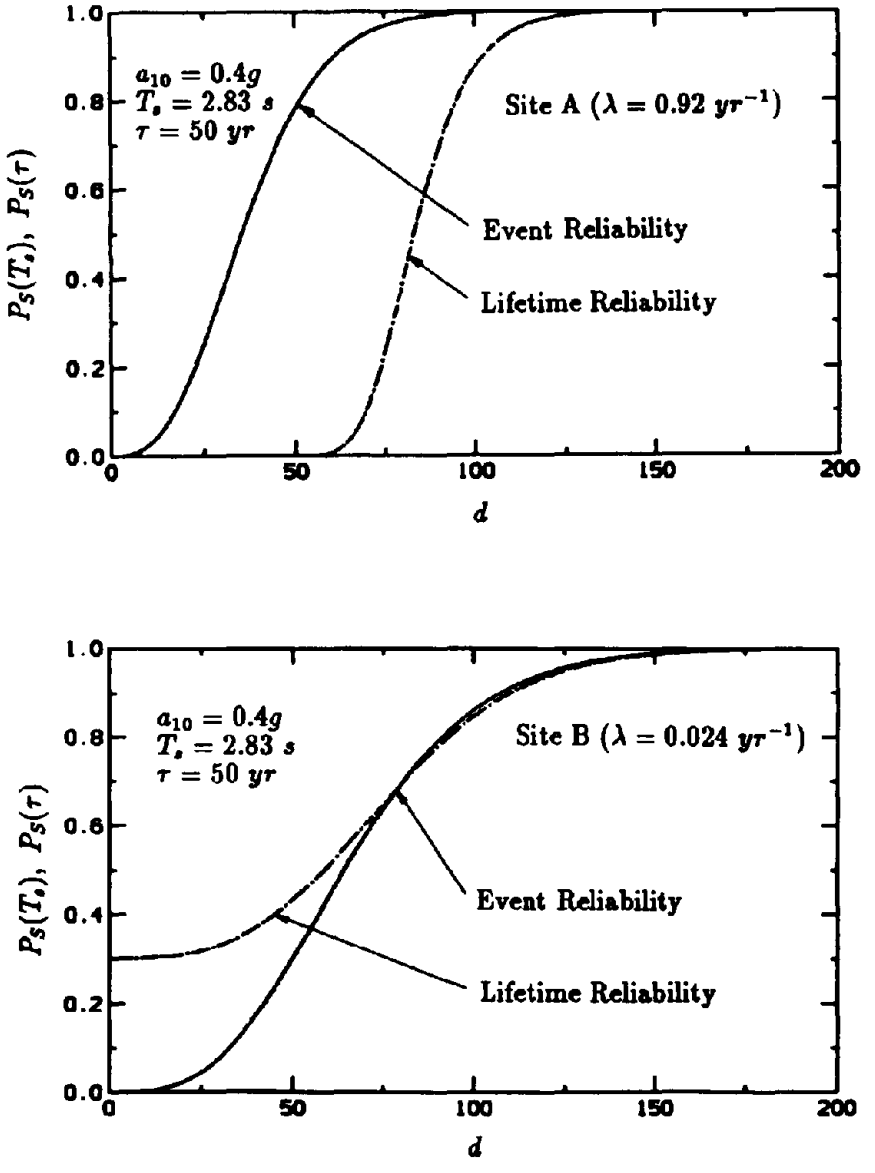

Figure 4.4: Event and Lifetime Reliabilities of Elasto-Plastic Oscillator Designed by UBC(88) for Failure Criteria Based on Cumulative Plastic Deformation

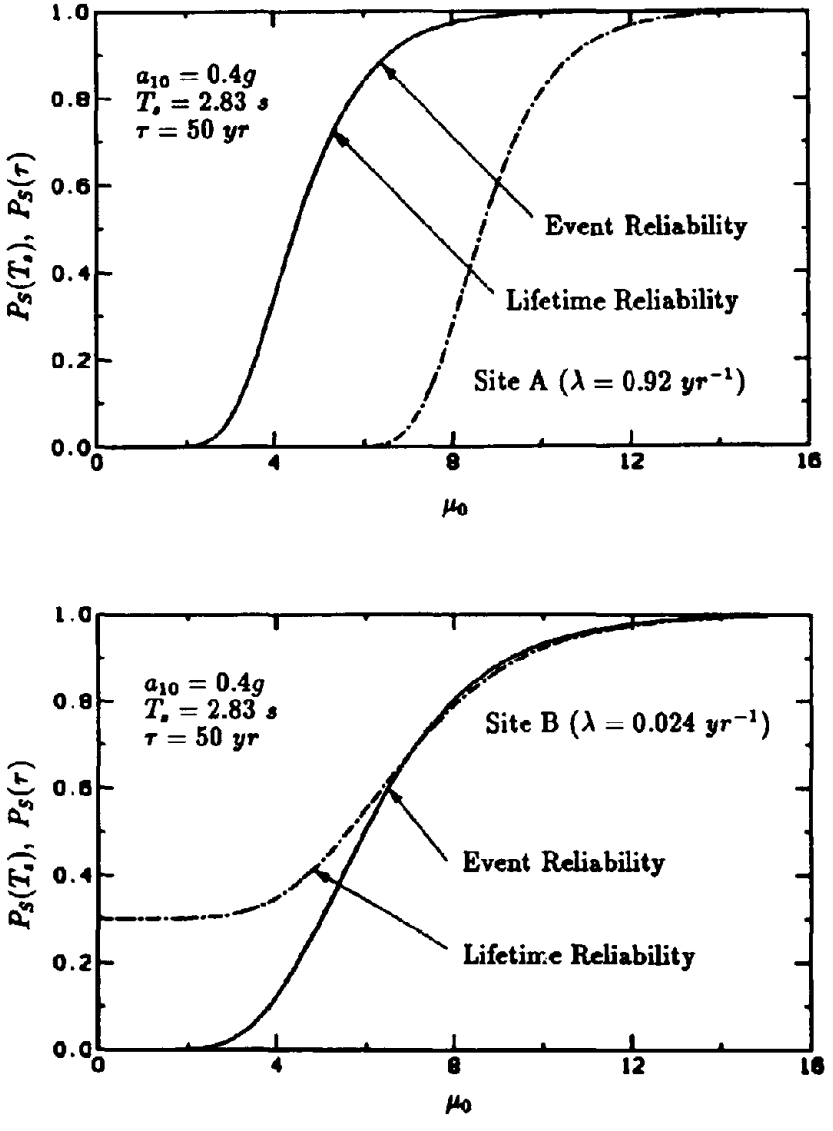

Figure 4.5: Event and Lifetime Reliabilities of Elasto-Plastic Oscillator Designed by UBC(85) for Failure Criteria Based on Ductility

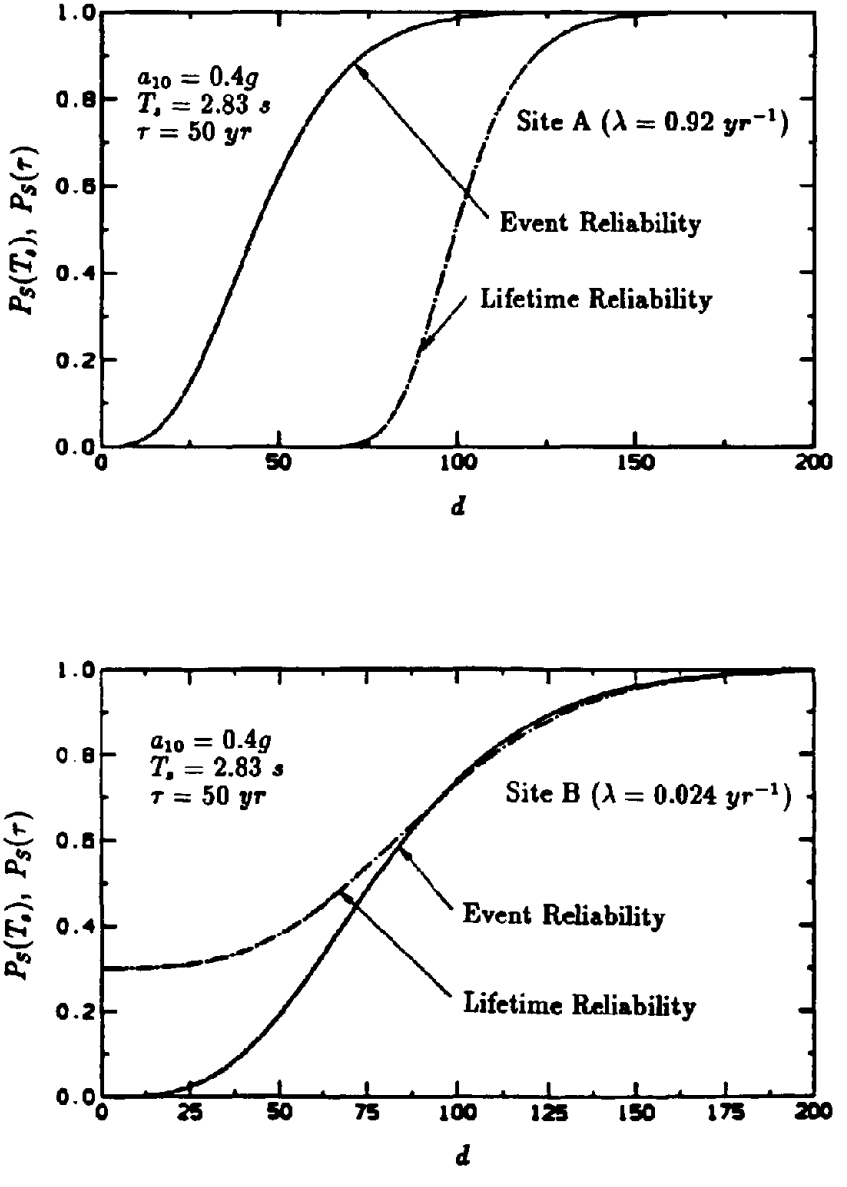

Figure 4.6: Event and Lifetime Reliabilities of Elasto-Plastic Oscillator Designed by UBC(85) for Failure Criteria Based on Cumulative Plastic Deformation

Table 4.2: Event and Lifetime Reliabilities of Elasto-Plastic Oscillator for Failure Criteria Based on Ductility

Design Code (x_y)	Site (λ)	$\mu_0 = 6$		$\mu_0 = 8$		$\mu_0 = 10$	
		$P_S(T_s)$ (β_E)	$P_S(\tau)$ (β_L)	$P_S(T_s)$ (β_E)	$P_s(\tau)$ (β_L)	$P_S(T_s)$ (β_E)	$P_S(\tau)$ (β_L)
UBC(85) (2.8 mm)	A (0.92/yr)	0.8399 (0.99)	0.0063 (−2.49)	0.9724 (1.92)	0.281 (−0.58)	0.9955 (2.62)	0.8143 (0.89)
	B (0.024/yr)	0.5072 (0.02)	0.5536 (0.14)	0.8043 (0.86)	0.7907 (0.81)	0.9326 (1.50)	0.9223 (1.42)
UBC(88) (3.19 mm)	A (0.92/yr)	0.9496 (1.64)	0.0982 (−1.29)	0.9952 (2.59)	0.8019 (0.85)	0.9996 (3.32)	0.9797 (2.05)
	B (0.024/yr)	0.6965 (0.52)	0.6948 (0.51)	0.9207 (1.41)	0.9092 (1.34)	0.9813 (2.08)	0.9778 (2.01)

ent reliabilities at sites with frequent small earthquakes and infrequent large earthquakes, although the sites are characterized by the same value of a_{10}, (*iii*) designs by *1988 Uniform Building Code* is safer than those by *1985 Uniform Building Code.* and (*iv*) *event* and *lifetime* reliabilities of these designs can differ significantly particularly at sites with frequent small earthquakes. Similar observations were noted when the nondegrading linear systems were considered.

SECTION 5
Dynamic Reliability Of Degrading Systems

5.1 Introduction

A proper selection of restoring force models for the constituent components of specific structural systems is one of the major factors governing accurate prediction of seismic response and reliability [175]. For example, when the reinforced concrete structures are considered, it is desirable that the hysteretic loops of various components exhibit several significant aspects such as stiffness degradation, strength deterioration, and pinching behavior, which have all been observed in the laboratory tests. The system of ordinary differential equations which represents the motion of these degrading systems due to earthquake ground acceleration are usually nonlinear with time-dependent coefficients. Generally, no exact analytic method exists to obtain the solutions of these nonlinear time-varying systems. For large systems, the only feasible approach to the deterministic stress analysis is the numerical step-by-step integration of equation of motion.

This section continues to examine the validity of static reliability indices by conducting seismic analysis of nonlinear degrading systems. The method of analysis is based on (*i*) stochastic models of seismic ground acceleration, (*ii*) nonlinear dynamic analysis of degrading structural systems, and (*iii*) damage-related limit states. Various failure criteria based on maximum deformation combined with cumulative load effects and interstory drift are employed to obtain seismic reliability measures of reinforced concrete frame structures designed by *1985 Uniform Building Code*. Results from these analyses provide a means to evaluate the adequacy of static reliability indices for the above frames, which were presented in a previous section of this report.

5.2 Seismic Load Process

The characterization of seismic load process at a site during the lifetime of structure requires description of all seismic events including pre-shocks, main events, and after shocks. It

is expected that a code-designed structure will withstand all these earthquakes during its exposure time. A very simple model of seismic hazard based on a filtered Poisson process was discussed in Section 3.3.2. This model was applied to obtain dynamic reliability measures of linear and nonlinear nondegrading systems in Section 4. However, when the structures are modeled as nonlinear degrading systems, the equation (*e.g.*, Eq. 4.51) used previously to obtain lifetime reliability from event reliability cannot be applied. Thus, the reliability analysis becomes much more difficult as it requires to account for the cumulative damage during consecutive events.

Alternatively, it has been proposed to evaluate seismic performance due to the lifetime largest load effect. This largest load effect is not physically realizable and it characterizes only an artificial seismic environment. Nevertheless, such description of hazard is abundant in the current deterministic and probabilistic seismic analysis. It will be used here in this section for the initial study to obtain dynamic reliability measures for degrading systems. The issues related to more realistic hazard model (Section 3.3.2.) and damage accumulation between consecutive seismic events will be addressed in the following sections.

Consider a site where the lifetime largest load effect during exposure time τ of seismic environment can be represented by a nonstationary colored process $W_\tau(t)$ with strong motion duration T_s. Suppose, the ground acceleration process $W_\tau(t)$ can be modeled as a uniformly modulated random process

$$W_\tau(t) = \psi(t)\widetilde{W}_\tau(t) \tag{5.1}$$

where $\psi(t)$ is a modulation function and $\widetilde{W}_\tau(t)$ is a *zero* mean stationary Gaussian colored noise with one-sided mean power spectral density [113,209,127,144]

$$\tilde{G}(\omega) = \begin{cases} G_0 \dfrac{1+\left[2\zeta_g(\frac{\omega}{\omega_g})\right]^2}{\left[1-(\frac{\omega}{\omega_g})^2\right]^2+\left[2\zeta_g(\frac{\omega}{\omega_g})\right]^2}, & \omega \in (0,\infty) \\ 0, & \text{otherwise.} \end{cases} \tag{5.2}$$

The spectrum in Eq. 5.2 is obtained when a stationary Gaussian white noise with one-sided spectral intensity G_0 is passed through a time-invariant linear filter with the frequency response function in Eq. 2.56 with the spectral parameters ζ_g and ω_g. Fig. 5.1 shows the

plots of one-sided Kanai-Tajimi spectrum of $\widetilde{W}_t$.

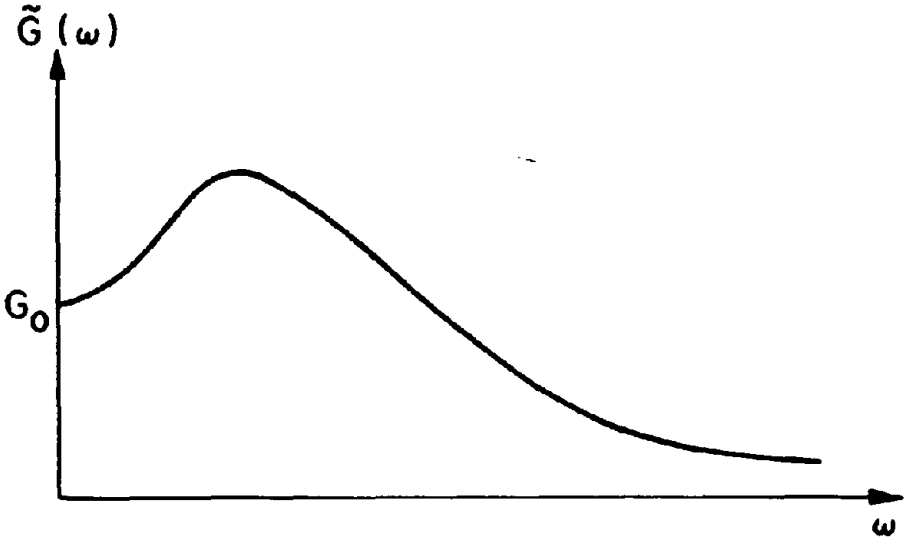

Figure 5.1: One-sided Kanai-Tajimi Spectra

During the stationary strong motion phase of $W_\tau(t)$, the distribution of lifetime peak ground acceleration Y_{50} can be obtained from spectral characteristics of $\widetilde{W}_\tau(t)$ as

$$\begin{aligned} \bar{F}_{50}(y) &\stackrel{\text{def}}{=} \Pr\left(\max_{0<t<T_s} |W_\tau(t)| < y\right) \\ &\simeq \exp\left[-2\tilde{\nu}(y)T_s\right] \end{aligned} \tag{5.3}$$

in which $\bar{F}_{50}(y)$ is the cumulative distribution function of Y_{50},

$$\begin{aligned} \tilde{\nu}(y) &\simeq \frac{1}{2\pi}\sqrt{\frac{\tilde{\lambda}_2}{\tilde{\lambda}_0}}\exp\left(-\frac{y^2}{2\tilde{\lambda}_0}\right) \\ &= \tilde{\nu}(0)\exp\left(-\frac{y^2}{2\tilde{\lambda}_0}\right) \end{aligned} \tag{5.4}$$

is the stationary mean y-upcrossing rate of $\widetilde{W}_\tau(t)$ with

$$\tilde{\nu}(0) = \frac{1}{2\pi}\sqrt{\frac{\tilde{\lambda}_2}{\tilde{\lambda}_0}} \tag{5.5}$$

as the stationary mean *zero*-upcrossing rate of $\widetilde{W}_\tau(t)$, and $\tilde{\lambda}_i$ is ith spectral moment of $\widetilde{W}_\tau(t)$ given by

$$\tilde{\lambda}_i = \int_0^\infty \omega^i \tilde{G}(\omega) d\omega. \tag{5.6}$$

When the expression for $\tilde{G}(\omega)$ in Eq. 5.2 is substituted in Eq. 5.6, the spectral moments $\tilde{\lambda}_0$ and $\tilde{\lambda}_2$ can be obtained as

$$\tilde{\lambda}_0 = \rho_0 G_0 \tag{5.7}$$

$$\tilde{\lambda}_2 = \rho_2 G_0 \tag{5.8}$$

in which

$$\rho_0 = \frac{\pi\omega_g}{4\zeta_g}\left[J_0(\Omega^*)\left(1+4{\zeta_g}^2\right)\right] \tag{5.9}$$

$$\rho_2 = \frac{\pi{\omega_g}^3}{4\zeta_g}\left[J_2(\Omega^*)+4{\zeta_g}^2 J_4(\Omega^*)\right] \tag{5.10}$$

$$J_i(\Omega^*) = \frac{4\zeta_g}{\pi}\int_0^{\Omega^*} \frac{\Omega^i d\Omega}{(1-\Omega^2)^2+4{\zeta_g}^2\Omega^2}, \tag{5.11}$$

$\Omega^* = \omega^*/\omega_g$, ω^* is the cutoff frequency which replaces the upper integration limit of infinity in Eq. 5.6 [122].

5.2.1 Site Consistent Spectral Intensity

Consider the lifetime peak ground acceleration Y_{50} at a site which has the cumulative distribution function shown in Eq. 5.3. From this distribution function, it can be shown that the approximate expected value of Y_{50} is [57]

$$\mathrm{E}\left[Y_{50}\right] \simeq \left(\sqrt{2\log[2\tilde{\nu}(0)T_s]}+\frac{\gamma}{\sqrt{2\log[2\tilde{\nu}(0)T_s]}}\right)\tilde{\lambda}_0^{\frac{1}{2}} \tag{5.12}$$

where $\gamma \simeq 0.5772$ is the Euler's constant. Consider now the alternative description of the distribution function of Y_{50} given by [53,65]

$$\tilde{F}_{50}(y) = \exp\left[-\left(\frac{y}{u}\right)^{-k}\right] \tag{5.13}$$

with the parameters $k \simeq 2.3$, and $u = 0.38a_{10}$ where a_{10} is the 10% upper fractile of Y_{50}. The expected value of Y_{50} from this Extreme Type-II distribution function in Eq. 5.13 is

$$\mathrm{E}[Y_{50}] = u\Gamma\left(1 - \frac{1}{k}\right) = 1.58u = 0.60a_{10}. \tag{5.14}$$

When the two expected values in Eqs. 5.12 and 5.14 are equated, they give rise to an expression for the site specific spectral intensity

$$G_0 = \frac{1}{\rho_0}\left[\frac{0.6a_{10}}{\sqrt{2\log[2\tilde{\nu}(0)T_s]} + \frac{\gamma}{\sqrt{2\log[2\tilde{\nu}(0)T_s]}}}\right]^2 \tag{5.15}$$

which is consistent with the site specific value of a_{10} obtained from the Algermissen-Perkins map (Fig. 2.22) [3]. For a given T_s and spectral parameters ω_g and ζ_g, ρ_0 and ρ_2 can be calculated by using Eqs. 5.9 and 5.10. Using these values, $\tilde{\nu}(0)$ can be obtained from Eq. 5.5. Finally, for any site specified value of a_{10}, the corresponding spectral intensity G_0 can be computed from Eq. 5.15. Note that when the quantities T_s, ω_g, ζ_g are treated as random variables, G_0 also becomes random. However, the same algorithm can be applied by using their relevant realizations.

5.2.2 Generation of Synthetic Seismograms

An elementary example of the oscillatory process is the uniformly modulated random process which can represent seismic ground acceleration [32]

$$W_\tau(t) = \psi(t)\widetilde{W}_\tau(t) \tag{5.16}$$

in which $\psi(t)$ is a slowly varying real-valued deterministic function modulating the amplitude of $W_\tau(t)$, and $\widetilde{W}_\tau(t)$ is real-valued, *zero* mean stationary Gaussian process with one-sided

mean power spectral density $\tilde{G}(\omega)$. The family of oscillatory functions of the process is $\{\psi(t)e^{i\omega t}\}$ so that $W_\tau(t)$ has the following one-sided evolutionary power spectral density

$$G_t(\omega) = \psi(t)^2 \tilde{G}(\omega). \tag{5.17}$$

Consider a discrete approximation of $\tilde{G}(\omega)$ in Fig. 5.1 consisting of N_ω spikes each of which has magnitude $\tilde{G}(\omega_k)$ at the frequency ω_k and is shown in Fig. 5.2. The associated

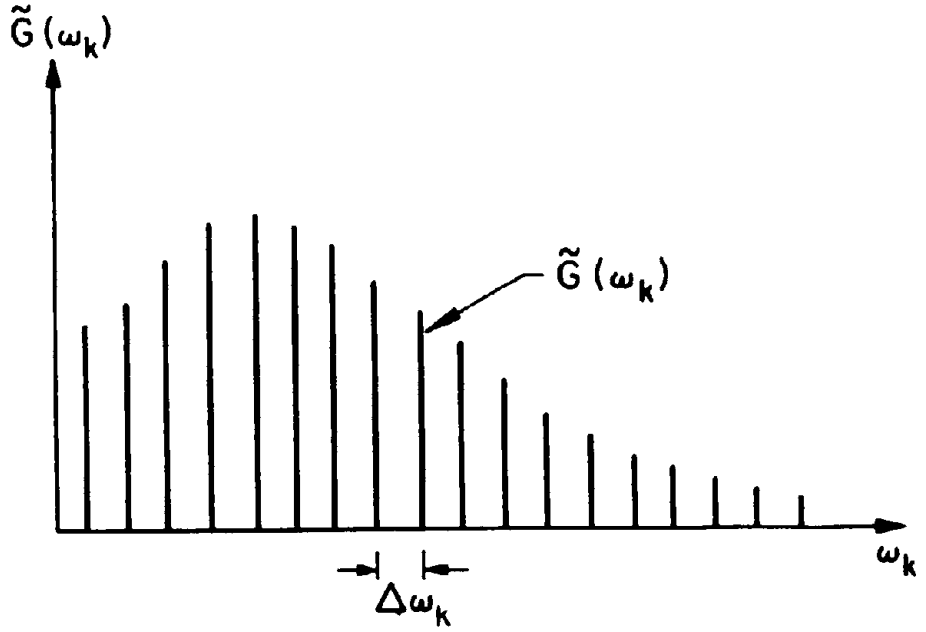

Figure 5.2: Discretization of Kanai-Tajimi Spectra

stationary process $\widetilde{W}_\tau(t)$ can thus be represented by a superposition of harmonic components giving the discrete spectral decomposition of $W_\tau(t)$ as

$$W_\tau(t) = \psi(t) \sum_{k=1}^{N_\omega} \sigma_k \left[A_k \cos(\omega_k t) + B_k \sin(\omega_k t)\right] \tag{5.18}$$

where $\sigma_k = \sqrt{\tilde{G}(\omega_k)\Delta\omega_k}$, A_k and B_k are independent and identically distributed standard Gaussian random variables.

Algorithm for Artificial Accelerograms

The following list provides a procedure for generating artificial seismograms. The input time series is consistent with site specific spectral parameters and the 10% upper fractile a_{10} of lifetime peak ground acceleration.

- Input values of filter parameters ω_g and ζ_g suitable for the soil condition of site or generate their samples, if random;
- Calculate the quantities ρ_0 and ρ_2 from Eqs. 5.9 and 5.10.
- Calculate the $\tilde{\nu}(0)$ of $\widetilde{W}_\tau(t)$ from Eq. 5.5.
- Input strong motion duration T_s or generate its sample, if random. Specify the site consistent value of a_{10} and hence calculate the corresponding one-sided mean power spectral intensity G_0 from Eq. 5.15.
- Discretize the mean power spectral density $\tilde{G}(\omega)$ into N_ω spikes
- Generate $2N_\omega$ samples of independent standard Gaussian random variable to obtain a realization of stationary Gaussian random process $\widetilde{W}_\tau(t)$.
- Multiply with the modulation function $\psi(t)$ to obtain a realization of nonstationary random process $W_\tau(t)$.

5.3 Nonlinear Degrading Systems

5.3.1 Equation of Motion

Consider a discrete, nonlinear structural system subjected to seismic ground acceleration. The equation of motion satisfies the following governing system of ordinary differential equation

$$\mathbf{m}\ddot{\mathbf{X}}_t + \mathbf{c}\dot{\mathbf{X}}_t + \mathbf{g}\left(\{\mathbf{X}_s, 0 < s < t\}; \boldsymbol{\alpha}\right) = -\mathbf{m}\mathbf{d}W_\tau(t) \tag{5.19}$$

with the initial conditions

$$\mathbf{X}_0 = \mathbf{0} \text{ and } \dot{\mathbf{X}}_0 = \mathbf{0} \tag{5.20}$$

in which $\mathbf{X}_t \in \Re^n$ is the vector of generalized displacement, $\mathbf{m}$ is the constant mass matrix, $\mathbf{c}$ is the linear time-invariant viscous damping matrix, $\mathbf{g}$ is a vector functional representing general nonlinear hysteretic degrading restoring forces, $\boldsymbol{\alpha}$ is a constant vector of hysteretic parameters determining rules for structural degradation, $\mathbf{d}$ is an influence coefficient vector, and $W_\tau(t)$ is a real-valued scalar stochastic process representation of ground acceleration.

5.3.2 Constitutive Law for Reinforced Concrete Structures

The univariate restoring force used to describe the hysteretic behavior of reinforced concrete structures due to seismic ground shaking depends on the type of structural component to be modeled. A three parameter hysteretic model developed by Park *et al.* [156] is used for the nonlinear dynamic analysis conducted in this study. This model consists of piecewise linear segments in the hysteretic loops and is capable of representing various types of reinforced concrete members with appropriate choice of parameters.

Fig. 5.3 shows a nonsymmetric trilinear backbone curve consisting of generalized force versus displacement plot to describe the monotonic loading behavior of individual components of reinforced concrete structures. The discontinuities in each direction (positive and negative) correspond to the cracking and yielding points of a critical cross-section and may occur at different magnitudes due to differential quantities of reinforcing steel at top and bottom of cross-section (*e.g.*, beams with dissimilar positive and negative steel reinforcements). A wide variety of restoring forces can be achieved through the combination of this general nonsymmetric trilinear skeleton curve and a general hysteretic rule governed by a vector $\boldsymbol{\alpha} = \{\alpha_1, \alpha_2, \alpha_3\}^T$ of hysteretic parameters. The values of the three components of $\boldsymbol{\alpha}$ determine the properties of (*i*) stiffness degradation, (*ii*) strength deterioration, and (*iii*) pinching behavior of the material model.

During repeated load reversals due to seismic ground acceleration, the stiffness of a reinforced concrete component experiences a progressive reduction as the magnitude of the deformation process increases. The decay in stiffness is usually caused by cracking of the concrete and bond deterioration of the reinforcing steel-concrete interface [189]. The

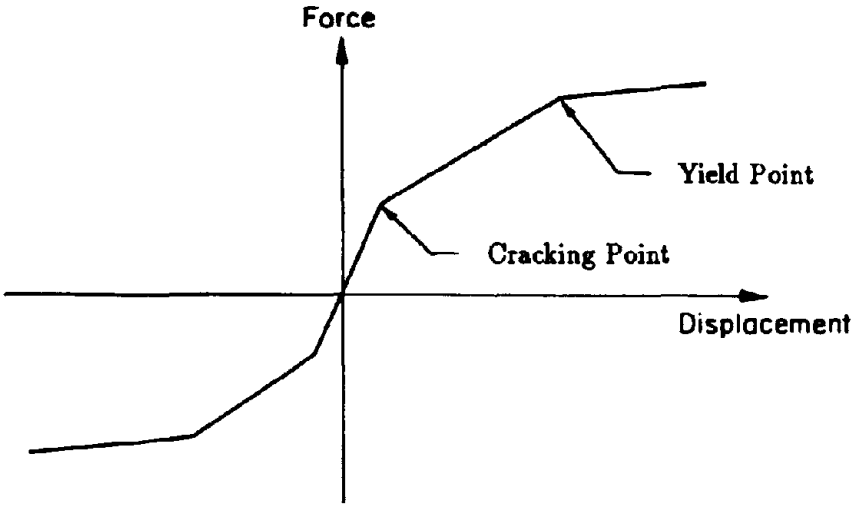

Figure 5.3: Trilinear Backbone Curve

parameter α_1 specifies the degree of the stiffness degradation.

In addition to stiffness degradation, reinforced concrete members also undergo strength deterioration under cyclic loading. The strength degradation reduces maximum load capacity of a member and depends essentially on the amount of hysteretic energy dissipated [76, 106,159] and many other structural factors such as the confinement ratio, magnitude of axial force, and concrete strength. Correlation between commencement of strength decay and the spalling of concrete cover has also been observed [17]. In the three parameter model, the rate at which the strength deterioration occurs is determined by the parameter α_2.

The restoring force model also accounts for the pinching phenomena of reinforced concrete members by the third parameter α_3. This is mainly caused by the slippage of the reinforcing steel when there is a sudden stress reversal. This behavior is usually pronounced and become biased for T-beams in reinforced concrete structures where there is substantial difference in the longitudinal steel ratios between the top and bottom reinforcing bars. The introduction of pinching leads to a general reduction of hysteretic loop areas and indirectly to the amount of energy dissipation. An elaborate study of the effects of all the components

of α can be obtained from the original reference [156].

5.4 Seismic Response and Reliability

5.4.1 Computer Code IDARC

IDARC, which is an acronym for Inelastic Damage Analysis of Reinforced Concrete Structures, is a deterministic code for structural dynamic analysis and was developed by Park *el.* [156]. The program, based on a "three-parameter" hysteretic model described earlier, can perform both static and dynamic response analyses of reinforced concrete structures under seismic excitations. A wide variety of structural models are available that include beam elements, column elements, shear-wall elements, edge-column elements, and transverse-beam elements. The combination of these five element types allows for a wide variety of structural configurations that can be analyzed by *IDARC*. Details of these element types can be obtained from Ref. [156].

The response and damage analysis in *IDARC* are conducted by performing direct step-by-step numerical integration of the equations of motion (Eq. 5.19). The basic operation in the step-by-step numerical integration of a system of differential equations is the approximate conversion to a set of simultaneous algebraic equations. This is accomplished by introducing a simple relation between displacement, velocity, and acceleration vectors which may be assumed to be valid for a small time increment. Appendix B provides a numerical procedure for the incremental dynamic analysis that was coded in *IDARC* [23, 145] to compute the nonlinear response characteristics of structural systems. This numerical scheme with the parameters $\gamma_1 = 1/2$ and $\gamma_2 = 1/4$ (see Appendix B) is unconditionally stable. Thus, the determination of the time step Δt depends only on the accuracy desired in the numerical integration. In this study, *IDARC* is used for the structural dynamic analysis.

5.4.2 Seismic Performance Evaluation

Seismic performance of structural systems can be evaluated in terms of the condition that a specific response or damage level is not exceeded during ground motion $W_r(t)$. Both ground acceleration and structural and material characteristics are assumed to be random. Hence, a realistic assessment requires computation of the non-exceedance probability of a response

quantity of interest. In this section, several damage indices based on maximum deformation and cumulative load effects are considered.

Maximum Deformation

The simplest damage index based on maximum deformation is the interstory drift ID which can be defined as [199,201]

$$ID = \frac{\Delta_m}{h} \tag{5.21}$$

in which Δ_m is the maximum relative displacement between two stories and h is the story height [199,201]. The lifetime seismic reliability $P_S(\tau)$ can be evaluated by the probability

$$P_S(\tau) \stackrel{\text{def}}{=} \Pr(ID < \delta_0) \tag{5.22}$$

where δ_0 is the allowable threshold of interstory drift. Hence, the corresponding reliability index becomes

$$\beta_L = \Phi^{-1}(P_S(\tau)). \tag{5.23}$$

Maximum Deformation and Cumulative Damage

Structural damage during earthquake depends primarily on maximum deformation and the hysteretic energy dissipated during repeated load cycles [22,47,159,160,157]. The damage of any structural members can be measured by the index [159,160,157]

$$DI = \frac{\delta_m}{\delta_u} + \frac{\beta_e}{Q_y \delta_u} \int dE \tag{5.24}$$

where δ_m is the maximum deformation, δ_u is the ultimate deformation under monotonic loading, Q_y is the calculated yield strength, dE is the incremental absorbed hysteretic energy, and β_e is a non-negative parameter which can be estimated from the experimental data. The probabilistic evaluation of seismic performance based on this damage index requires the computation of lifetime seismic reliability $P_S(\tau)$ given by

$$P_S(\tau) \stackrel{\text{def}}{=} \Pr(DI < d_0) \tag{5.25}$$

where d_0 is the allowable value of structural damage. Accordingly, the reliability index becomes

$$\beta_L = \Phi^{-1}(P_S(\tau)). \tag{5.26}$$

5.5 Numerical Example

Consider the 5-story, 3-bay R/C planar frames in Example 3.1 which is designed by appropriate provisions of *1985 Uniform Building Code* and *ACI Code 318-83* for seismic zones-2 and -3. Design details of these frames and the seismic reliability estimates by static method are already provided in Section 3. In this example, a dynamic reliability analysis is performed to obtain benchmark results against which the static reliability indices can be compared.

5.5.1 Structural System

The structural modeling of the frames are done by using beams and columns with critical cross-sections at their ends. The stiffness matrix of an element is derived from the inverse of the flexibility matrix with the flexibility distribution assumed to be linearly varying between the critical cross-section and the point of contraflexure. Details of this model can be obtained from the original reference [156].

The trilinear backbone curve of a structural component is defined by various component properties, such as cracking moments, cracking curvature, yield moment, and yield curvature. These quantities are calculated from a number of empirical relations developed from experimental results of reinforced concrete structures available in the current literature [156]. The post-yielding stiffness is taken as 1.5% of the initial elastic stiffness of the member.

The uniaxial constitutive law for each individual critical cross-section of the frame can be described by the trilinear backbone curve and the model parameters α_1, α_2, and α_3 that determine the properties of hysteretic loops. The stiffness degradation parameter α_1 is taken as 2.0 for both beams and columns which is found to be fairly representative for reinforced concrete structures [156]. The strength deterioration parameter α_2 of an individual member is calculated from the empirically developed expression in Ref. [156]. No slippage of the reinforcement is allowed either in beam or in column and the pinching parameter α_3 is set

to one extreme value which does not account for pinching effect in the restoring force. A typical hysteretic rule for beam or column element is shown in Fig. 5.4.

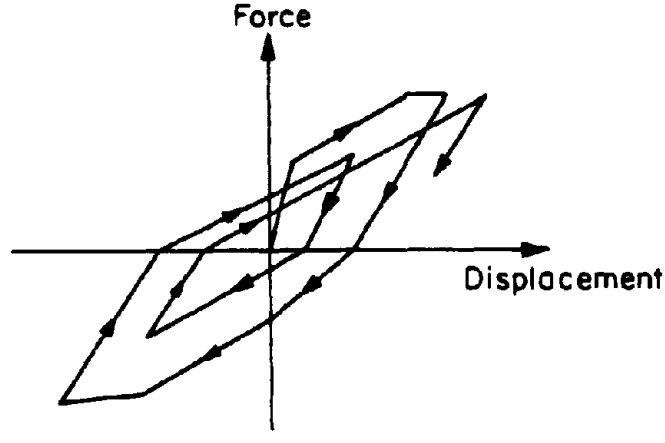

Figure 5.4: A Typical Three Parameter Model with Degrading Hysteresis

The concrete strength f_c' and yield strength F_y of steel reinforcement are treated as independent random variables with mean 3.39 *ksi* and 67.5 *ksi*, and coefficients of variation 18% and 9.8%, respectively [105,130]. The probability distribution of f_c' and F_y are modeled as Gaussian and lognormal variables, respectively [65].

Mass is assumed to be lognormal random variable with mean value equal to the nominal value and coefficient of variation 11% [121,205,175]. The damping property is specified by damping ratio in the first mode with mean 0.02, coefficient of variation 65% [121,205,175], and lognormal distribution function. The uncertainty in the stiffness property will be determined by the variabilities in the basic parameters such as concrete strength, and yield strength of steel. Due to common construction and workmanship, each of the random variables accounting for the masses of system are assumed to be perfectly correlated among all the stories.

5.5.2 Seismic Load Process

Consider the seismic hazard discussed in Section 5.2. It is assumed that the ground acceleration can be represented by an elementary Gaussian oscillatory process $W_\tau(t)$ which admits a multiplicative decomposition of a *zero* mean stationary Gaussian random process $\widetilde{W}_\tau(t)$ with one-sided mean power spectral density $\tilde{G}(\omega)$ in Eq. 5.2 and a modulation function $\psi(t)$ in Eq. 2.75. The Kanai-Tajimi spectral parameters ω_g and ζ_g are assumed to be independent random variables with their mean values 16.5 rad/s and 0.8 and coefficients of variation 42.5% and 42.6%, respectively [140,205]. These values are consistent with the intermediate soil condition for which the frames are originally designed. The probability distribution functions of ω_g and ζ_g are modeled as gamma and lognormal, respectively [122]. The strong motion duration T_s is also treated as a random variable with mean 6.9 s, coefficient of variation 42% [140,205], and lognormal cumulative distribution function. The modulation function $\psi(t)$ in Eq. 2.75 is chosen with $t_1 = 0.15T_s$, $t_2 = 1.15T_s$, and $c_\psi = 2.0/T_s$. The total duration T_d of ground motion is assumed to be 1.5 times the strong motion duration T_s. The artificial earthquakes are generated in accordance with the algorithm described in Section 5.2.2.

5.5.3 Seismic Performance Evaluation

Seismic performance of 5-story, 3-bay reinforced concrete frame structures are evaluated by calculating the lifetime reliabilities in Eqs. 5.22 and 5.25 depending on two damage-based failure criteria discussed in Section 5.4.3. In principle, these probabilities can be calculated by using statistical linearization method [228,230,20,21,18,172]. This method is based on the linearization of a system of nonlinear differential equations (Eq. 5.19) via minimization of the expected value of some error measure. In earthquake engineering, the linearization method has been applied quite extensively mainly for response and reliability analysis of nondegrading systems. Recent investigations on the accuracy of statistical linearization for nonlinear degrading systems, however, reveal that the method may significantly underestimate the probabilistic characteristics of seismic response [172].

In this study, the reliabilities are estimated by direct Monte Carlo simulation. The associated deterministic nonlinear dynamic analysis for a particular sample of simulation is

performed by the computer code *IDARC* [156] described earlier. This program computes the deterministic structural response by direct step-by-step numerical integration using the Newmark algorithm. In brief, the effort in simulation consists of the following steps. First, the samples of random variables representing mechanical models of structural systems are generated which are consistent with their probability distribution functions. Second, realizations of site-specific seismic ground motions are generated from the algorithm described in the Section 5.2.2. Third, nonlinear dynamic analyses are conducted by *IDARC* for each of these sample structures and earthquake ground motions to obtain samples of several response variables of interest. Fourth, standard statistical analyses are performed to determine probabilistic characteristics of these response or damage variables.

Maximum Deformation

Consider the interstory drift ID in Eq. 5.21 which represents one of many damage indices based on maximum deformation of structural response. Fig. 5.5 shows the associated lifetime reliabilities in Eq. 5.22 for the 2nd story of the 5-story frame structure designed for seismic zone-2. These probabilities are plotted for different values of deterministic threshold δ_0. The different plots in each figure correspond to several possible values of $a_{10} = 0.10g$, $0.15g$, and $0.20g$ within the same seismic zone-2. Fig. 5.6 exhibit the similar results for seismic zone-3 for several cases of $a_{10} = 0.20g$, $0.30g$, and $0.40g$. The rightward shift of the plots in these figures confirm the anticipation that the structural reliability decreases with increasing values of a_{10} within a same seismic zone. Reliabilities for other stories, which are not shown here, can be obtained from the Ref. [171].

Maximum Deformation and Cumulative Damage

Consider the damage index DI in Eq. 5.24 which is based on combined effects of maximum deformation and cumulative load effects due to seismic ground motion. Figs. 5.7 and 5.8 show the corresponding lifetime reliabilities in Eq. 5.25 of the beam component 2 and the column component 21 or 26 of the 5-story frame designed for seismic zone-2 (see Section 3). These probabilities are plotted for different values of deterministic allowable damage threshold d_0. The different plots in each figure are associated with several representative

values of $a_{10} = 0.10g$, $0.15g$, and $0.20g$ within the seismic zone-2.

Figs. 5.9 and 5.10 show the similar sets of above plots for the same frame structure designed for seismic zone-3 for several cases of of $a_{10} = 0.20g$, $0.30g$, and $0.40g$. Similar trend of decreasing seismic reliability is observed due to increase in the value of a_{10}. The reliability plots for other structural members of the frame designed for both zone-2 and zone-3, which are not shown here, are also available in Ref. [171].

5.5.4 Comparison with Static Reliability Indices

One major objective of this numerical example is the evaluation of static reliability estimates obtained in the previous phase of the study. This can be accomplished by comparing the static reliability indices with the reliability measures obtained from nonlinear dynamic analyses. The dynamic reliability is estimated both at the member (Eq. 5.25) and story levels (Eq. 5.22).

Table 5.1 shows the smallest reliability index β_L in Eq. 5.23 based on interstory drift ID (Eq. 5.21) which is obtained for the 5-story frame designed for seismic zone-2. These values are tabulated for several cases of $a_{10} = 0.10g$, $0.15g$, and $0.20g$ and critical thresholds $\delta_0 = 0.5\%$, 1.0%, 2.0%, 3.0%, and 4.0%. Table 5.1 also provides the similar information for designs in seismic zone-3 for several cases of $a_{10} = 0.20g$, $0.30g$, and $0.40g$. Results show that the conclusions regarding seismic reliability estimates depend significantly on the critical thresholds for the interstory drift and specific values of a_{10} within a same seismic zone.

Table 5.2 shows the smallest reliability index β_L in Eq. 5.26 based on the damage index DI (Eq. 5.24) which is obtained for the 5-story frame designed for seismic zone-2. The critical threshold of $d_0 = 0.4$ proposed in Ref. [156] is used here to calculate the above quantities in the table. Table 5.2 also produces similar information when the frame is designed for seismic zone-3. Although the failure criteria (in static and dynamic reliability analyses) are different, these member level reliability indices can be compared with corresponding static reliability measures obtained previously and is summarized in Table 5.3. Comparisons of minimum reliability indices for the 5-story frame obtained for various combinations of seismic zone and a_{10} exhibit significant differences due to the static

Table 5.1: Dynamic Reliability Indices of 5-story Frame with Failure Criteria Based on Damage Index ID (Eq. 5.23)

δ_0	Minimum β_L based on ID (Eq. 5.23)					
	Zone-2			Zone-3		
	$a_{10}=0.1g$	$a_{10}=0.15g$	$a_{10}=0.2g$	$a_{10}=0.2g$	$a_{10}=0.3g$	$a_{10}=0.4g$
0.5%	2.55	1.51	0.79	0.90	-0.21	-0.85
1.0%	4.31	3.29	2.59	2.72	1.38	0.67
2.0%	6.07	5.07	4.38	4.53	2.98	2.19
3.0%	7.10	6.10	5.42	5.59	3.91	3.09
4.0%	7.83	6.84	6.17	6.35	4.57	3.72

and the dynamic methods. Similar results were also found when the nondegrading systems were considered (Section 4). However, note that the comparisons are valid only when the component reliabilities are considered. Concepts of system reliability are not explored in this study.

In a recent work by O'Connor and Ellingwood [149], a similar study regarding adequacy of static reliability indices for simple structural systems was performed. Their findings suggest that the static method provides satisfactory seismic structural performance when compared with the dynamic method. However, in Ref. [149], the analysis was based on elementary stochastic modeling of ground motion in which the peak ground acceleration is assumed to be random with the cumulative distribution function defined be Eq. 3.12 and the frequency contents are obtained from an ensemble of actual seismograms. Also their study involved simple 1-story portal frame and ideal elasto-plastic material model without any degrading characteristics. It is interesting to note that in this study, static reliability indices are found to significantly underestimate structural reliability particularly at sites with low seismicity.

Table 5.2: Dynamic Reliability Indices of 5-story Frame with Failure Criteria Based on Damage Index DI (Eq. 5.26)

Zone	a_{10}	Minimum β_L based on DI (Eq. 5.26)
Zone-2	0.1g	7.69
	0.15g	6.57
	0.2g	5.13
Zone-3	0.2g	5.12
	0.3g	3.60
	0.4g	2.91

Table 5.3: Static Reliability Indices of 5-story Frame

Zone	a_{10}	Minimum $\beta_{G,1}$ (Eq. 3.21)
Zone-2	0.1g	2.19
	0.15g	1.81
	0.2g	1.50
Zone-3	0.2g	2.04
	0.3g	1.59
	0.4g	1.30

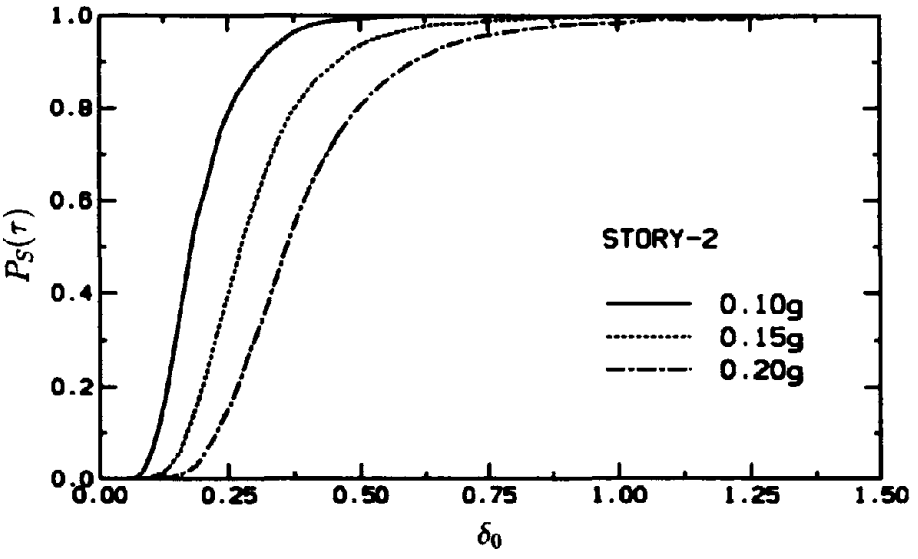

Figure 5.5: Dynamic Reliability of 5-story Frame at zone-2 with Failure Criteria Based on Interstory Drift

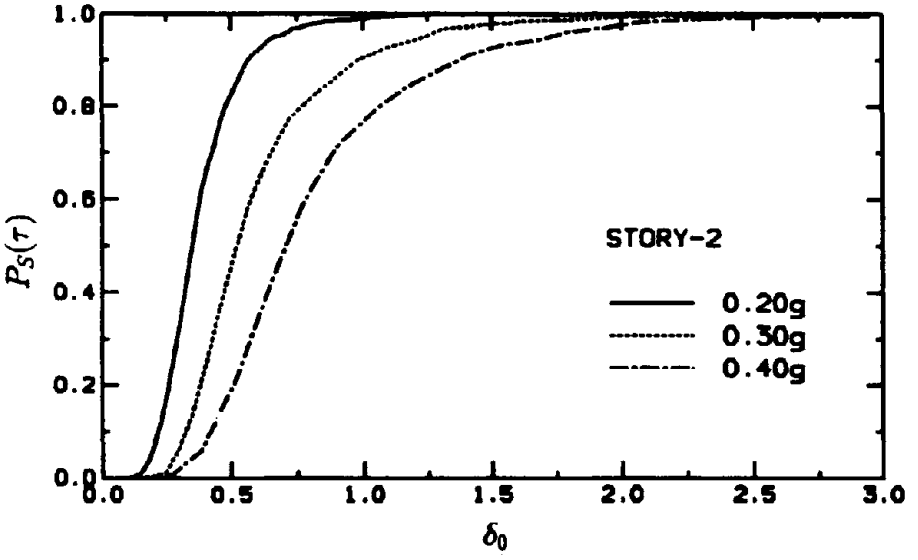

Figure 5.6: Dynamic Reliability of 5-story Frame at zone-3 with Failure Criteria Based on Interstory Drift

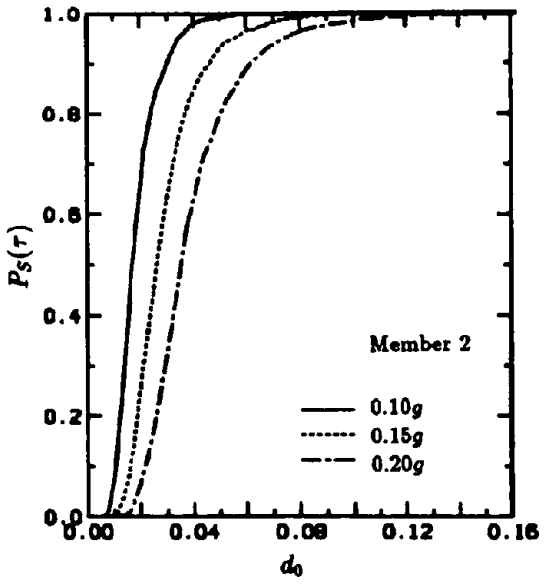

Figure 5.7: Dynamic Reliability of 5-story Frame at zone-2 with Failure Criteria Based on Damage Index DI (Beam Member 2)

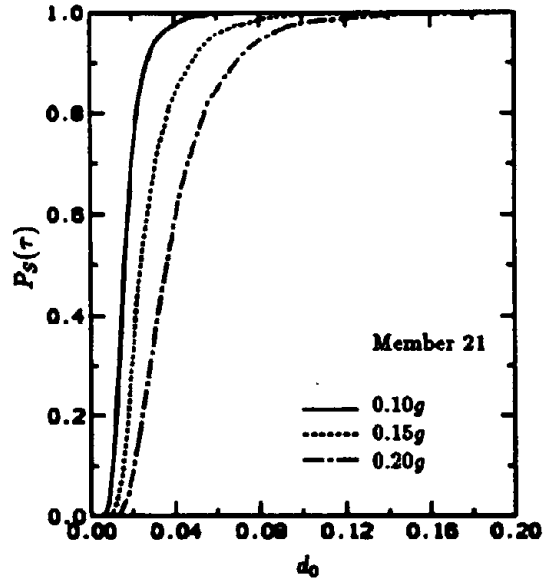

Figure 5.8: Dynamic Reliability of 5-story Frame at zone-2 with Failure Criteria Based on Damage Index DI (Column Member 21 or 26)

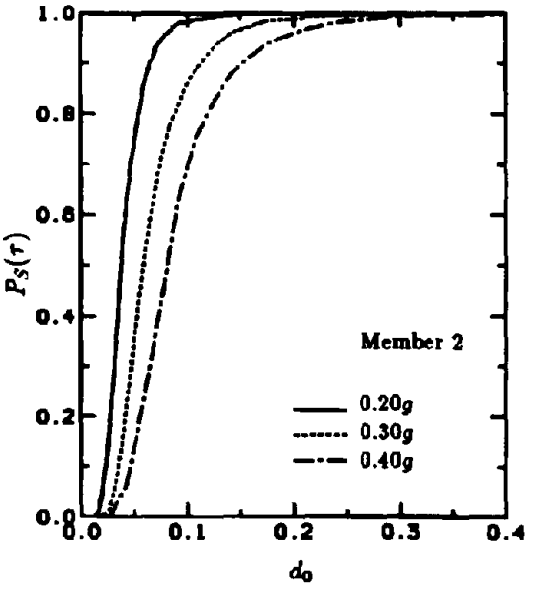

Figure 5.9: Dynamic Reliability of 5-story Frame at zone-3 with Failure Criteria Based on Damage Index DI (Beam Member 2)

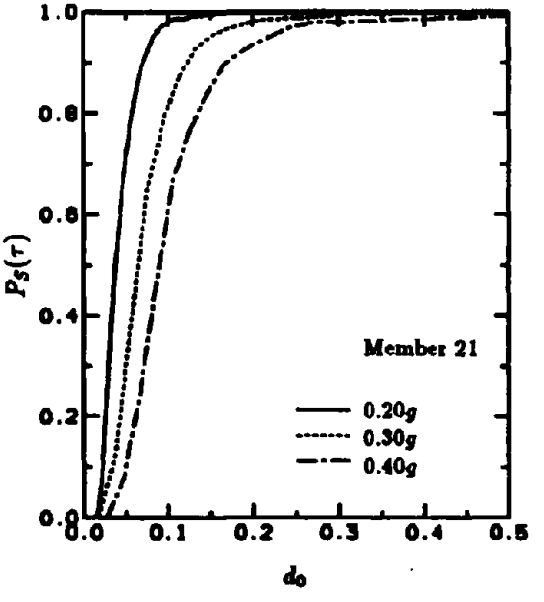

Figure 5.10: Dynamic Reliability of 5-story Frame at zone-3 with Failure Criteria Based on Damage Index DI (Column Member 21 or 26)

SECTION 6
A Markov Model For Seismic Reliability Analysis

6.1 Introduction

Current methods for evaluating the overall seismic performance of structural systems are based on *global damage indices* and *lifetime maximum seismic hazard*. The global indices are obtained by heuristic combinations of local damage measures, and the seismic hazard is modeled without any consideration for cumulative damage during consecutive seismic events. Such a global measure of damage can not characterize structural state uniquely, provides only a crude estimate of structural performance during seismic events, and cannot be used to assess structural vulnerability to future loadings. Since most structures are designed to resist several earthquakes during their exposure time, the lifetime largest ground motion may not be meaningful as a design load parameter due to accumulation of damage between consecutive seismic events. This is particularly true and unavoidable for a series of earthquakes including pre-shocks, main events, and after-shocks during which repairs of structural systems can not be performed.

Another important issue in the evaluation of seismic performance is the lack of exact knowledge in the initial state of structural systems. This uncertainty is primarily caused by manufacturing processes, errors in design, inadequate construction, unsatisfactory quality control for new structures, and lack of information concerning damage caused by previous seismic events for existing buildings. Reliability analysis solely based on current definitions of global damage indices can not be applied to determine sensitivity to initial state of structural systems. Hence, any rational assessment of structural performance should simultaneously account for the mechanical degradation process of all critical cross-sections and components.

The objectives of this section are to evaluate the seismic performance and sensitivity to initial state of structural systems and determine the vulnerability of structures exposed to one or more earthquakes. A new methodology based on a Markov model is proposed for seismic reliability analysis. The method of analysis is based on (*i*) simple but realistic characterization of seismic hazard, (*ii*) nonlinear dynamic analysis for estimating structural

response to earthquakes, (*iii*) uncertainty in initial state of structural systems, and (*iv*) failure conditions incorporating damage accumulation during consecutive seismic events. Simple structures designed by the *Uniform Building Code* are used to illustrate the proposed method. Effects of uncertainty in the initial state of these systems on seismic reliability are also investigated.

6.2 Seismic and Mechanical Models

6.2.1 Seismic Hazard

Consider a site which is affected by a single seismic source characterized by a mean rate of earthquake occurrence λ. It is assumed that (*i*) the earthquake arrivals follow a homogeneous Poisson process with mean rate λ, (*ii*) ground motions in different seismic events are independent stochastic processes $W^i(t)$, $i = 1, 2, \cdots, N(\tau)$ where $N(\tau)$ represents the random number of seismic events during lifetime period τ, and (*iii*) seismic event i has random duration t^i. The supposition of stationary Poisson process has the implication that the inter-arrival times are independent and follow the same exponential distribution. Although this representation provides an elementary model of the seismic environment, it has been found to be consistent with historical occurrences for ground motions associated with earthquakes that are of engineering interest in structural applications [2]. Consequently, the Poisson assumption may still serve as a useful but simple model of seismic hazard [53]. A similar but simplified version of this filtered Poisson process model was also adopted in Sections 3 and 4 of this report. Fig. 6.1 shows the schematics of seismic environment at a site.

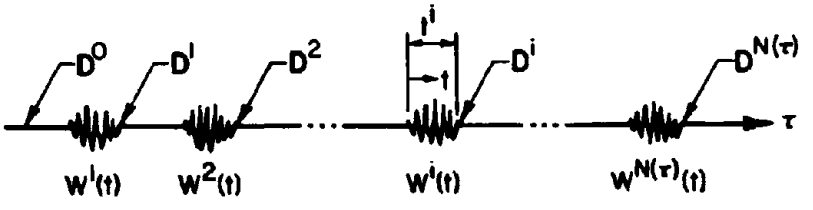

Figure 6.1: Seismic Hazard at a Site

6.2.2 Nonlinear Degrading Systems

Consider a general multistory framed structure with n_c critical cross-sections each of which has n_p parameters to describe the restoring force model. The stochastic seismic modeling of this multi-degree-of-freedom, hysteretic, and degrading system leads to the matrix differential equations of the form (Eq. 2.47)

$$\mathbf{m}\ddot{\mathbf{X}}^i(t) + \mathbf{g}^i\left(\{\mathbf{X}^i(s), \dot{\mathbf{X}}^i(s), 0 \le s \le t\}; t\right) = -\mathbf{m}\mathbf{d}W^i(t) \tag{6.1}$$

with the initial conditions

$$\mathbf{X}^i(0) = \mathbf{0}, \quad \text{and} \quad \dot{\mathbf{X}}^i(0) = \mathbf{0} \tag{6.2}$$

where t is the local time coordinate originating at the beginning of seismic event i, $\mathbf{X}^i(t)$ is a vector of generalized displacements, $\mathbf{g}^i$ is the vector functional representing general nonlinear hysteretic restoring forces, $\mathbf{m}$ is the constant mass matrix, $\mathbf{d}$ is a vector of influence coefficients, and $W^i(t)$ is the stochastic process representation of ith seismic event. In earthquake engineering, the total restoring force $\mathbf{g}^i$ is usually modeled by the superposition of a nonhysteretic component

$$\mathbf{g}^i_{nh} = \mathbf{c}\,\dot{\mathbf{X}}^i(t) + \mathbf{k}^i_{nh}\left(\mathbf{X}^i(t)\right)\mathbf{X}^i(t) \tag{6.3}$$

and a hysteretic component

$$\mathbf{g}^i_h = \mathbf{k}^i_h\left(\mathbf{Z}^i(t)\right)\mathbf{X}^i(t) \tag{6.4}$$

where $\mathbf{c}$ is the constant viscous damping matrix, $\mathbf{k}^i_{nh}$ is the nonhysteretic part of stiffness matrix, $\mathbf{k}^i_h$ is the hysteretic part of stiffness matrix, and $\mathbf{Z}^i(t)$ is the vector of additional hysteretic variables the time evolution of which can be modeled by a set of general nonlinear ordinary differential equations

$$\dot{\mathbf{Z}}^i(t) = \mathbf{F}^i\left(\mathbf{X}^i(t), \dot{\mathbf{X}}^i(t), \mathbf{Z}^i(t), t; \mathbf{A}^i(t)\right) \tag{6.5}$$

in which $\mathbf{F}^i$ is a general nonlinear vector function the explicit expression of which depends on the hysteretic rule governed by a particular constitutive law, and $\mathbf{A}^i(t) \in \Re^n$ is a damage state vector which has $n = n_c n_p$ components equal to the parameters of restoring forces at all critical cross-section of a structural system at time t during seismic event i and $\Re^n$ is the n-dimensional real vector space. Following the state vector approach [67,94,136] with the designation of

$$\begin{aligned} \boldsymbol{\theta}_1{}^i(t) &= \mathbf{X}^i(t) \\ \boldsymbol{\theta}_2{}^i(t) &= \dot{\mathbf{X}}^i(t) \\ \boldsymbol{\theta}_3{}^i(t) &= \mathbf{Z}^i(t), \end{aligned} \tag{6.6}$$

the equivalent system of first-order nonlinear differential equations in state variables become

$$\begin{aligned} \dot{\boldsymbol{\theta}}_1^i(t) &= \boldsymbol{\theta}_2{}^i(t) \\ \dot{\boldsymbol{\theta}}_2^i(t) &= -\mathbf{m}^{-1}\left[\mathbf{c}\,\boldsymbol{\theta}_2{}^i(t) + \mathbf{k}^i{}_{sh}\left(\boldsymbol{\theta}_1{}^i(t)\right)\boldsymbol{\theta}_1{}^i(t) + \mathbf{k}^i{}_h\left(\boldsymbol{\theta}_3{}^i(t)\right)\boldsymbol{\theta}_1{}^i(t)\right] - \mathbf{d}\,W^i(t) \\ \dot{\boldsymbol{\theta}}_3^i(t) &= \mathbf{F}^i\left(\boldsymbol{\theta}_1{}^i(t), \boldsymbol{\theta}_2{}^i(t), \boldsymbol{\theta}_3{}^i(t), t; \mathbf{A}^i(t)\right) \end{aligned} \tag{6.7}$$

which can be recast in a more compact form

$$\dot{\boldsymbol{\theta}}^i(t) = \mathbf{h}^i\left(\boldsymbol{\theta}^i(t), t; \mathbf{A}^i(t)\right) \tag{6.8}$$

with the initial conditions

$$\boldsymbol{\theta}^i(0) = \mathbf{0} \tag{6.9}$$

where $\mathbf{h}^i(\cdot)$ is a vector function, $\boldsymbol{\theta}^i(t)$ is the response state vector, $\mathbf{A}^i(t) \in \Re^n$ is the damage state vector representing state of parameters in the restoring force, and are given by

$$\boldsymbol{\theta}^i(t) = \left\{ \begin{array}{c} \boldsymbol{\theta}_1{}^i(t) \\ \boldsymbol{\theta}_2{}^i(t) \\ \boldsymbol{\theta}_3{}^i(t) \end{array} \right\}, \tag{6.10}$$

and

$$\mathbf{A}^i(t) = \begin{Bmatrix} A^i{}_1(t) \\ A^i{}_2(t) \\ \cdot \\ \cdot \\ \cdot \\ A^i{}_n(t) \end{Bmatrix}. \tag{6.11}$$

When the excitation is random, $\mathbf{A}^i(t)$ is a vector stochastic process and it characterizes structural state uniquely.

6.3 Markov Model

6.3.1 Damage State Vector

Consider a damage state vector $\mathbf{A}^i$ which has $n = n_c n_p$ components equal to parameters of restoring forces at all critical cross-sections of a structural system at the end of seismic event i. It can be obtained from

$$\mathbf{A}^i = \mathbf{A}^i(t^i) \tag{6.12}$$

where $\mathbf{A}^i(t)$ is defined earlier in Eq. 6.5. State vector $\mathbf{A}^i$ can be conveniently mapped into a normalized damage state vector $\mathbf{D}^i$ by the relation

$$D_j{}^i = 1 - \frac{A_j{}^i}{A_j{}^0} \tag{6.13}$$

where $j = 1, 2, \cdots, n$ represents the index for the component of vectors $\mathbf{A}^i \in \Re^n$ and $\mathbf{D}^i \in \Re^n$. This simple transformation permits the domain of each component of $\mathbf{D}^i$ to lie between 0 and 1. Note that the state vector $\mathbf{D}^i$ provides complete characterization of structural state at the end of earthquake i. Hence, one needs only $\mathbf{D}^i$ to perform dynamic analysis and determine structural performance through a new seismic event.

A duty cycle (DC) is a repetitive period of operation in the life of a structure that causes an increase in damage. For earthquake resistant structure, each seismic event corre-

sponds to a DC. If the earthquake is modeled as a filtered Poisson process with each seismic event assumed to be an independent random process, damage state vector $\mathbf{D}^i$ at the end of an ith DC depends only on initial state $\mathbf{D}^{i-1}$ at the start of the DC, and on that DC itself. It is independent of damage and loading history up to the start of that DC. In other words, the propagation of damage state vector $\mathbf{D}^i$ can be treated as Markov process evolving on a discrete time scale [169,171,176,177]. The evolution of a discrete version of $\mathbf{D}^i$ can be described by *one-step transition matrix* $\mathbf{T}(i)$ with the element $T_{pq}(i)$ representing the probability that damage changes from state p to state q due to seismic event i. This is explained in the forthcoming section.

6.3.2 Transition Matrix

Consider a domain $\mathcal{D} \subseteq \Re^n$ as shown in Fig. 6.2 having $\Pr(\mathbf{D}^i \in \mathcal{D}) \simeq 1$ with $K = \prod_{j=1}^{n} l_j$ cells (states) $\{C_p\}$ such that $\mathcal{D} = \cup_{p=1}^{K} C_p$, $C_p \cap C_q = \emptyset \quad (p \neq q)$, and l_j represents the number of discretized states of jth component of $\mathbf{D}^i \in \Re^n$. Consider the change in stochastic vector process $\mathbf{D}^i, i = 0, 1, 2, \cdots, N(\tau)$, taking values in a finite or countable number of cells $C_1, C_2, \cdots, C_K$. Let $\Pr(\mathbf{D}^i \in C_p)$ be the probability that damage state vector $\mathbf{D}^i$ is in cell C_p after i seismic events. Then row vector $\mathbf{P}(i) = \{\Pr(\mathbf{D}^i \in C_1), \Pr(\mathbf{D}^i \in C_2), \cdots, \Pr(\mathbf{D}^i \in C_K)\}$ gives the probability that $\mathbf{D}^i$ belongs to any of the cells $C_1, C_2, \cdots, C_K$ after i seismic events.

Suppose the seismic events constitute a sequence of independent random processes. Then the probability $\Pr(\mathbf{D}^i \in C_q | \mathbf{D}^{i-1} \in C_p$, past history of structural loading and damage) is equal to $T_{pq}(i) = \Pr(\mathbf{D}^i \in C_q | \mathbf{D}^{i-1} \in C_p)$ because system performance is completely specified by the value of damage state vector $\mathbf{D}^{i-1}$ at the application of earthquake i. Denote $\mathbf{T}(i) = \{T_{pq}(i)\}, \ p, q = 1, 2, \cdots, K$ as one-step transition matrix from time $i-1$ to time i associated with the ith DC. Hence, $\{\mathbf{D}^i, i = 0, 1, 2, ..., N(\tau)\}$ is a discrete-state (DS), discrete-time (DT) *Markov Vector Process*, where $N(\tau)$ designates the total (random) number of seismic events at a site. Fig. 6.3 shows the schematic diagram of transition probabilities for Markov process $\mathbf{D}^i$.

The estimation of transition probability $T_{pq}(i)$ involves computation of conditional probability density of the random vector $\mathbf{D}^i | \mathbf{D}^{i-1} \in C_p$ for all the cells C_p, $p = 1, 2, \cdots, K$. The method of *Monte Carlo Simulation* can be used for this purpose due to unavailability of

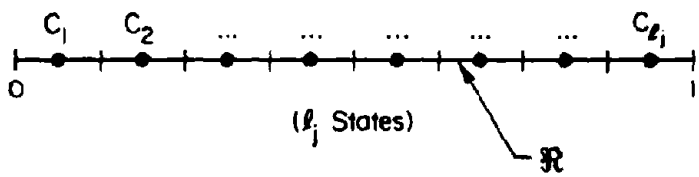

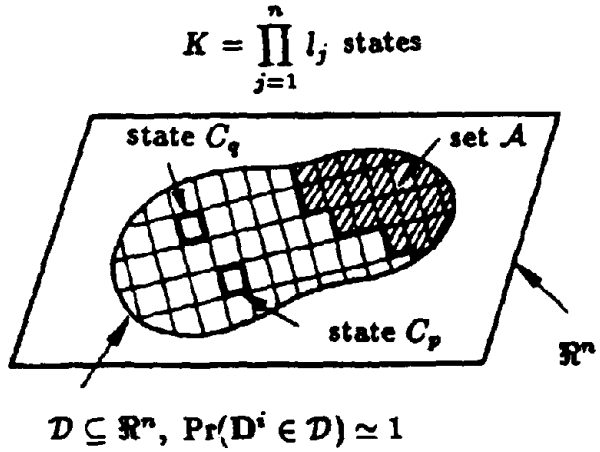

Figure 6.2: Discretization of Sample Space

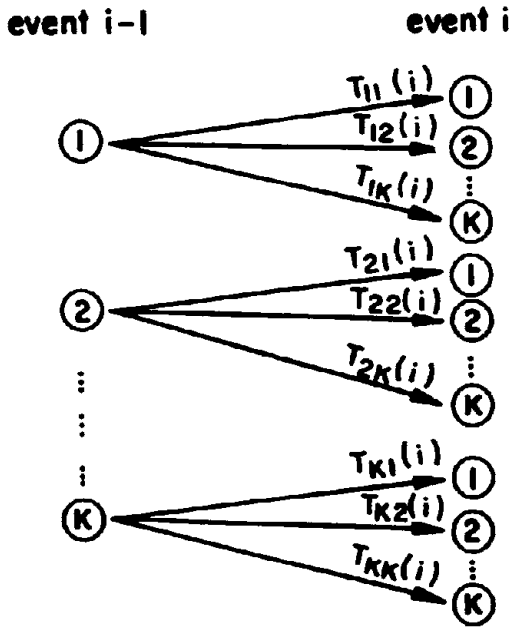

Figure 6.3: Schematic Diagram for Transition Probabilities

analytic solutions. Each deterministic trial in the simulation method requires nonlinear dynamic analysis. Mathematically, this corresponds to the computational effort for solving the deterministic initial-value problem in Eqs. 6.8 and 6.9. Various numerical integrators such as Runge-Kutta method [191,120,87,93,110], Adam's or Gear's method [74,194,88], Bulirsch-Stoer Extrapolation method [38], and several others can be applied to obtain the solution. The selection of a particular method depends on its computational efficiency, numerical accuracy and stability, and "stiffness" of the nonlinear system of differential equations. In this study, several numerical schemes are tested and finally the fifth- and sixth-order Runge-Kutta integrators are determined to be satisfactory and used for structural analysis. Appendix C summarizes the Runge-Kutta method for step-by-step numerical integration.

It is worth noting that for a small increase in the dimension of damage state vector, there is a correspondingly large increase in the order of transition matrix. For example, when the dimension n of $\mathbf{D}^i$ is increased to $n+1$, the order of $\mathbf{T}(i)$ increases from $\prod_{j=1}^{n} l_j = K$ to $\prod_{j=1}^{n+1} l_j = l_{n+1}K$. This observation regarding rapid increase in computational involvement suggest the initial use of Markov model for shear beam idealization of framed structures.

6.3.3 Evolution of Distribution of $\mathbf{D}^i$

Consider a K-dimensional row vector which prescribes the joint probability mass function of the random vector $\mathbf{D}^i$ denoting damage after ith seismic event. The probability of $\mathbf{D}^i$ following i seismic events is [161,169,171,176,177,178],

$$\mathbf{P}(i) = \mathbf{P}(i-1)\mathbf{T}(i) \ , \ i = 1, 2, ..., N(\tau) \tag{6.14}$$

When this equation is used recursively, the distribution of probability of being in state C_p, $p = 1, 2, 3, \cdots, K$ after i seismic events becomes

$$\mathbf{P}(i) = \mathbf{P}(0) \prod_{j=1}^{i} \mathbf{T}(j) \tag{6.15}$$

where $\mathbf{P}(0)$ denotes the initial vector representing probability distribution of $\mathbf{D}^0$. In general, Eq. 6.15 defines a nonstationary Markov Process due to differential severities of DCs.

However, if one assumes independent and identically distributed random processes for earthquakes with same deterministic duration, the Markov process becomes stationary and Eq. 6.15 takes the form

$$\mathbf{P}(i) = \mathbf{P}(0)\mathbf{T}^i \tag{6.16}$$

where the index i has been dropped because of the invariance of transition matrix to severities of DCs.

6.3.4 Lifetime Distribution

The lifetime probability distribution $\mathbf{P}(\tau)$ defined as the distribution of damage index vector $\mathbf{D}^{N(\tau)}$ in lifetime τ can be obtained from the theorem of total probability

$$\begin{aligned}
\mathbf{P}(\tau) &= \sum_{i=0}^{\infty} \mathbf{P}(i) \Pr\{N(\tau) = i\} \\
&= \sum_{i=0}^{\infty} \mathbf{P}(i) \frac{(\lambda\tau)^i}{i!} \exp(-\lambda\tau) \\
&\simeq \sum_{i=0}^{i^*} \mathbf{P}(i) \frac{(\lambda\tau)^i}{i!} \exp(-\lambda\tau)
\end{aligned} \tag{6.17}$$

in which i^* is a finite real integer to be determined from the observation that the i^*th component of above summation in Eq. 6.17 is negligibly small. For stationary Markov process, a more compact form of lifetime distribution can be obtained as

$$\begin{aligned}
\mathbf{P}(\tau) &= \sum_{i=0}^{\infty} \mathbf{P}(0)\mathbf{T}^i \frac{(\lambda\tau)^i}{i!} \exp(-\lambda\tau) \\
&= \mathbf{P}(0) \exp(-\lambda\tau) \sum_{i=0}^{\infty} \frac{(\lambda\tau\mathbf{T})^i}{i!} \\
&= \mathbf{P}(0) \exp(-\lambda\tau[\mathbf{I} - \mathbf{T}])
\end{aligned} \tag{6.18}$$

where $\mathbf{I} \in \mathcal{L}\left(\Re^K\right)$ is the identity matrix. Determination of above probability requires computation of $e^{\mathbf{A}}$ where $\mathbf{A} = -\lambda\tau[\mathbf{I} - \mathbf{T}]$. Appendix D describes the evaluation procedures of linear algebra to calculate $e^{\mathbf{A}}$ for a general square matrix $\mathbf{A} \in \mathcal{L}\left(\Re^K \times \Re^K\right)$, where $\mathcal{L}\left(\Re^K \times \Re^K\right)$ denotes a set of linear mapping from $\Re^K$ to $\Re^K$.

6.3.5 Mean First Passage Time

Another quantity of engineering interest in seismic performance evaluation is the mean number of earthquakes before absorption to any undesirable damage state(s). Considering homogeneous Markov process with stationary transition probabilities, let $\mu_{\mathcal{A}}(p)$ denote the mean number of seismic events before the system enters a damage set $\mathcal{A} \subseteq \mathcal{D}$ with $\mathcal{A} \cup \mathcal{A}^c = \mathcal{D} \subseteq \Re^n$ (Fig. 6.2) if the initial damage state is $C_p \subseteq \mathcal{A}^c$. Then, the mean first passage time is given by [169,171,176,177,178]

$$\begin{aligned}
\mu_{\mathcal{A}}(p) &= \mathrm{E}\left[\text{Absorption time}|\mathbf{D}^0 \in C_p\right] \\
&= \sum_{C_q \in \mathcal{A}^c} \mathrm{E}\left[\text{Absorption time}|\mathbf{D}^0 \in C_p, \mathbf{D}^1 \in C_q\right] \Pr\left(\mathbf{D}^1 \in C_q | \mathbf{D}^0 \in C_p\right) \\
&= 1 + \sum_{C_q \in \mathcal{A}^c} \mathrm{E}\left[\text{Absorption time}|\text{initial state is } C_q\right] T_{pq} \\
&= 1 + \sum_{C_q \in \mathcal{A}^c} \mu_{\mathcal{A}}(q) T_{pq}
\end{aligned} \tag{6.19}$$

When the initial states are uncertain, the mean first passage time can still be obtained from $\mu_{\mathcal{A}}(p)$ by averaging relative to the probability of $\mathbf{D}^0$. Let $\mu_{\mathcal{A}}$ represent the mean number of events the system starting at initial state $C_p \subseteq \mathcal{A}^c$ with probability $\Pr(\mathbf{D}^0 \in C_p)$ has to wait before absorption to damage set $\mathcal{A} \subseteq \mathcal{D}$. It is given by [169,171,177]

$$\mu_{\mathcal{A}} = \sum_{C_p \in \mathcal{A}^c} \mu_{\mathcal{A}}(p) \Pr\left(\mathbf{D}^0 \in C_p\right). \tag{6.20}$$

6.4 Numerical Example

6.4.1 Seismic Hazard

Consider two sites A and B in the western U.S. with mean earthquake arrival rates $\lambda_A = 0.92/yr$ and $\lambda_B = 0.024/yr$ [3,179]. These sites were also considered in Sections 3 and 4. Both sites lie in the same seismic zone-4 of the *1988 Uniform Building Code* [100] and have the same peak ground acceleration $a_{10} = 0.4g$. The ground motions in different seismic events are assumed to be independent and identically distributed *zero*-mean stationary Gaussian processes $W(t)$ with band-limited *white* power spectral density $G(\omega)$ given by

$$G(\omega) = \begin{cases} G_0, & 0 < \omega < \bar{\omega} \\ 0, & \text{otherwise} \end{cases} \tag{6.21}$$

where the spectral intensity G_0 is equal to 10026 mm^2s^{-3} when $\lambda = \lambda_A = 0.92$ $/yr$ and 16090 mm^2s^{-3} when $\lambda = \lambda_B = 0.024$ $/yr$ for a deterministic strong motion duration $T_s = 2.83$ s and bandwidth $\bar{\omega} = 25\pi$ rad/s as proposed in Ref. [122]. Sites A and B are characterized by frequent small seismic events and rare large earthquakes, respectively. However, designs at both sites are identical according to the *1988 Uniform Building Code.*

6.4.2 Structural System

Consider a special moment resisting framed structure [100] illustrated in Sections 3 and 4 which is modeled here as a hysteretic, degrading Bouc-Wen oscillator [34,228,230] with linear damping ratio $\zeta = 0.05$, initial natural frequency $\omega_0 = 20.944$ rad/s, mass m, and is subjected to the ith seismic event $W^i(t) = W(t)$ giving the equation of motion

$$m\ddot{X}^i(t) + g^i\left(\{X^i(s), \dot{X}^i(s), 0 \le s \le t\}; t\right) = -mW(t) \tag{6.22}$$

where $X^i(t)$ is the relative displacement of oscillator with respect to ground motion at time t during seismic event i. The total restoring force g^i is assumed to admit an additive decomposition of nonhysteretic component

$$g^i{}_{nh}\left(X^i(t), \dot{X}^i(t)\right) = 2\zeta\omega_0 m\dot{X}^i(t) + \alpha\omega_0{}^2 mX^i(t) \tag{6.23}$$

and hysteretic component

$$g^i{}_h\left(\{X^i(s), \dot{X}^i(s), 0 \le s \le t\}; t\right) = (1-\alpha)\omega_0{}^2 mZ^i(t) \tag{6.24}$$

where the hysteretic variable $Z^i(t)$ satisfies the ordinary nonlinear differential equation [34, 228,230]

$$\dot{Z}^i(t) = A^i(t)\dot{X}^i(t) - \beta\left|\dot{X}^i(t)\right|\left|Z^i(t)\right|^{\mu-1} Z^i(t) - \gamma\dot{X}^i(t)\left|Z^i(t)\right|^{\mu} \tag{6.25}$$

in which α quantifies the participation of linear restoring force. The model parameters μ, β, γ are assumed to be constants while the parameter $A^i(t)$ which controls system degradation has the following implicit time dependency through the dissipated hysteretic energy ε_t at local time t [21]

$$A^i(t) = A^{i-1}(T_s) - \delta_A \varepsilon_t \tag{6.26}$$

where δ_A signifies constant rate of system deterioration with ε_t satisfying the differential equation

$$\dot{\varepsilon}_t = (1-\alpha)\omega_0{}^2 m Z^i(t)\dot{X}^i(t) \tag{6.27}$$

Note that the degradation law in Eqs. 6.26 and 6.27 is defined here quite arbitrarily. It is obtained from one of the main choices available in the current literature. Further study with more realistic buildings needs to be undertaken to make decisions regarding the proper selection of structural deterioration. The time-invariant parameters governing hysteresis are chosen as $\alpha = 0.04$, $\mu = 1$, $\beta = 0.1505$, and $\gamma = 0.1505$ consistent with the initial stiffness and strength values of the oscillator [204]. Structural deterioration is permitted by assigning a small value of $\delta_A = 1.0 \times 10^{-6}$ in Eq. 6.26. The structural characteristics are assumed to be deterministic.

The state of structure is represented by $A^i = A^i(T_s) \in \Re$ denoting the value of parameter $A^i(t)$ of restoring force model at the end of ith seismic event. The corresponding normalized damage index $D^i = 1 - A^i/A^0$ which varies from 0 to 1 is discretized into $K = l_1 = 16$ distinct cells (states) of equal length 0.0625 and is shown in Fig. 6.4. When this index is calibrated to the observed seismic damage in actual structures, each or group of these cells can be correlated with common engineering measures such as minor, medium, severe, reparable, nonreparable, and collapse damage states. Regardless, the discretized cells $C_1, C_2, \cdots, C_{16}$ in succession denote progressive states of structural damage. Since the damage is an irreversible process, after each seismic event without any subsequent repair, the structural state advances only to any of the higher numbered damage states, or it may remain in the same state. In other words, once $D^{i-1} \in C_p$, there is a *zero* probability that $D^i \in C_q$ when $q < p$ for all $p = 1, 2, \cdots, 16$. Specially for $p = 16$, i.e., for the cell C_{16} which

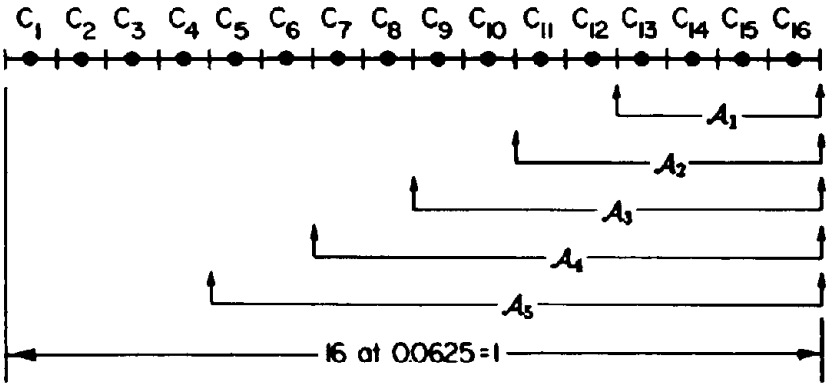

Figure 6.4: Discretization of Sample Space of $D^i \in \Re$

represent state of largest possible damage, if the damage process ever enters that state, the probability of remaining in that state becomes unity. This state is known as the "absorbing" or "trapping" state since once entered the process is never left.

6.4.3 Structural Response and Reliability

As mentioned previously, Eqs. 6.22 to 6.27 can be rewritten as a system of first-order ordinary differential equations analogous to Eqs. 6.8 and 6.9. This nonlinear system of equations for the initial value problem is then solved by using step-by-step numerical integration. Fifth- and sixth-order explicit Runge-Kutta integrators are used to obtain such solutions.

The transition matrix $\mathbf{T}$ is constructed by performing several conditional Monte Carlo simulations each with 1000 samples. In brief, the effort in the simulation consists of the following three steps. First, the oscillator is pre-assigned a damage index (before seismic event i) which is associated with the damage state C_p. A representative value, such as the midpoint of the cell C_p, can be used to define this deterministic damage index. This also defines the initial value $A^i(0)$ of the degrading parameter $A^i(t)$ of the hysteretic model

during the ith seismic event. Second, with the condition $D^{i-1} \in C_p$, 1000 samples of random excitation representing the ith seismic event $W(t)$ are artificially generated. Third, 1000 deterministic nonlinear dynamic analyses are carried out with the oscillator subjected to each of these realizations of $W(t)$. This generates 1000 samples of conditional damage index $D^i|D^{i-1} \in C_p$ following seismic event i from which its histogram can be developed. Fig. 6.5 shows the histograms of $D^i|D^{i-1} \in C_p$ for the cells C_p, $p = 1, 2, \cdots, 15$ obtained for both the sites A and B. Due to larger spectral intensity G_0, the shapes of above histograms for site B exhibit more spread than those for site A. These histograms which estimates the conditional probability densities are used to construct the first 15 rows of corresponding transition matrix $\mathbf{T}$. Since the cell C_{16} is absorbing state, the last row of the transition matrix is calculated by setting $T_{16,q} = 1$ for $q = 16$ and *zero* otherwise. Here, no repairs of structural systems are considered following each seismic event. This has the implication that $\mathbf{T}$ is an upper triangular matrix. In case there is a systematic maintenance program after each seismic event, the transition matrix will need to be modified based on inspection and repair methodologies.

The *event* distribution of damage, starting from any damaged state of system, can be obtained from the transition matrices described earlier. Fig. 6.6 shows the evolution of this distribution of D^i, with respect to seismic event i, according to Eq. 6.16 for both sites A and B starting with deterministic initial state $C_p = C_1$ of structural system, [i.e., when $P_p(0)$ representing the pth component of $\mathbf{P}(0)$ is 1 for $p = 1$ and *zero* otherwise]. However, if the initial state is uncertain and particularly if it has uniform distribution with $P_p(0) = 1/16$ for all $p = 1, 2, \cdots, 16$, the same equation can be used to obtain above evolution of damage probability $\mathbf{P}(i)$. Fig. 6.7 exhibits such probabilities for both sites A and B.

The *lifetime* probability distribution of damage after $N(\tau)$ seismic events are computed using Eq. 6.18 with the assumption of initially undamaged deterministic state of system, i.e., when $P_p(0) = 1$ for $p = 1$ and *zero* otherwise. Fig. 6.8 shows the lifetime probability mass function of $D^{N(\tau)}$ with $\tau = 50$ years for both the sites A and B. Based on these case-specific studies, buildings at sites with infrequent large earthquakes appear to sustain less damage than those at sites with frequent small seismic events. Similar results were found in Sections 3 and 4 of this report. However, more studies need to be undertaken

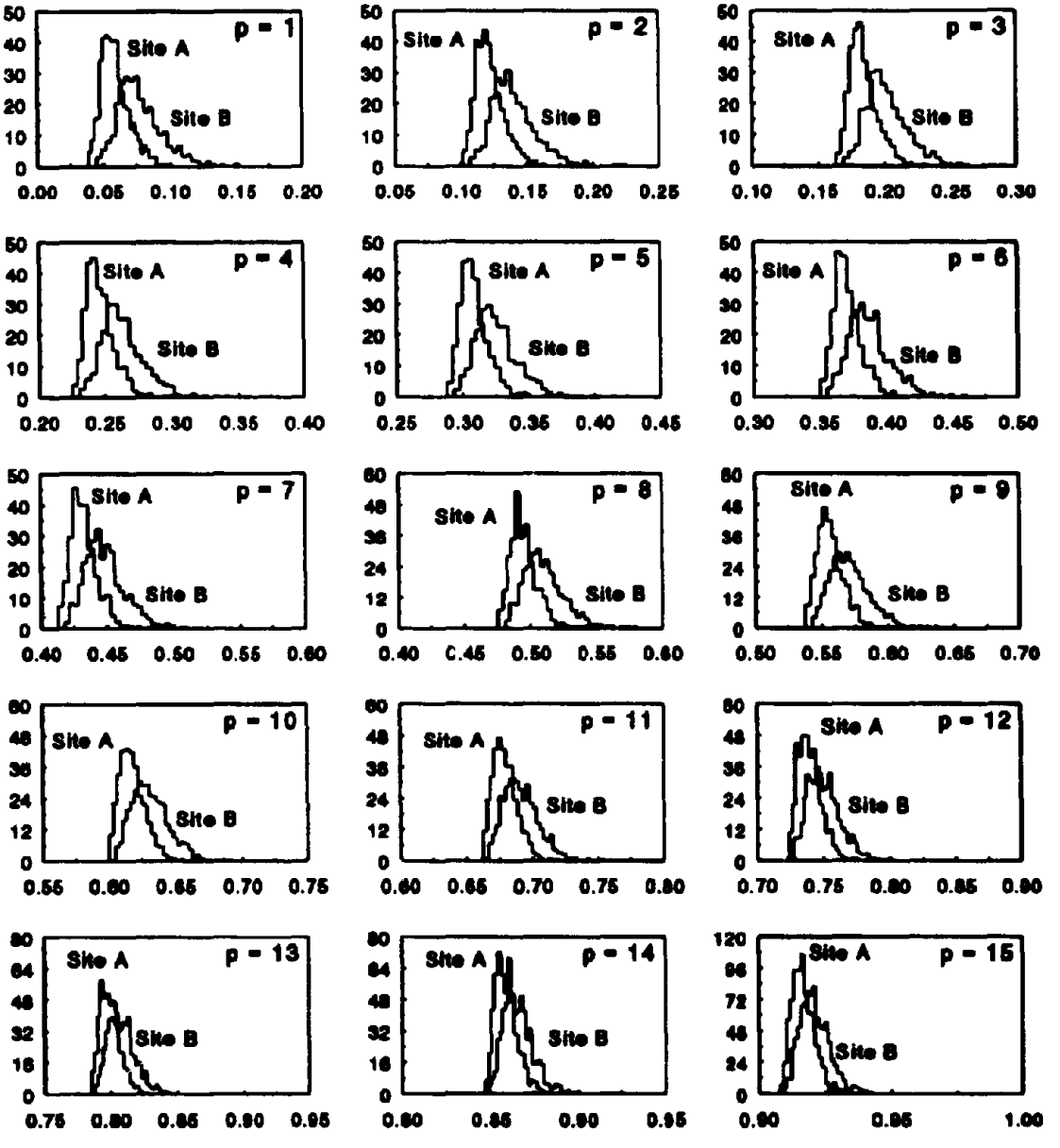

Figure 6.5: Histogram of $D^i|D^{i-1} \in C_p$, $p = 1 - 15$

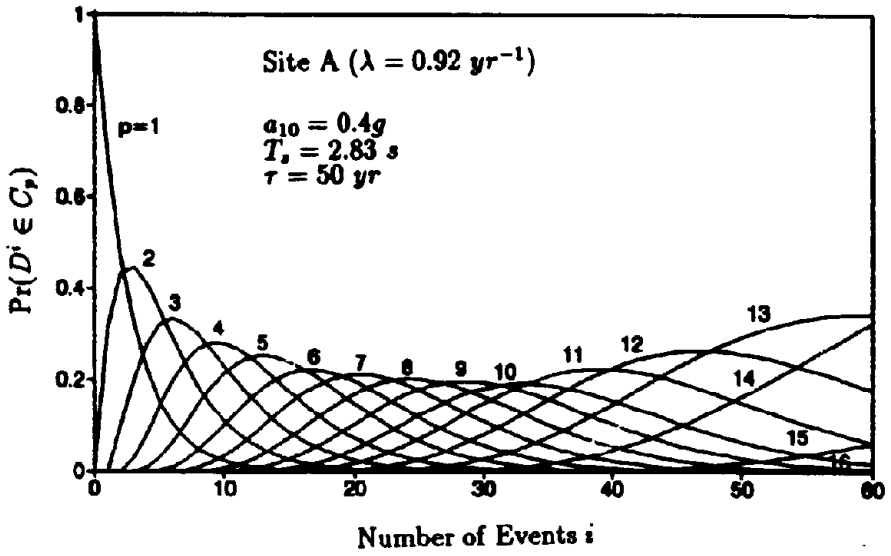

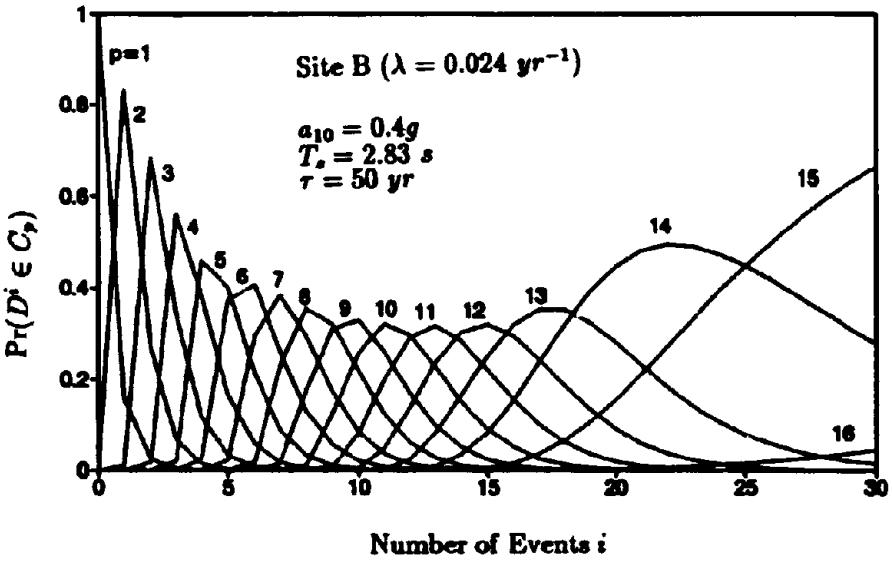

Figure 6.6: Evolution of Damage Probability Belonging to State C_p for Site A and Site B with Deterministic Initial State

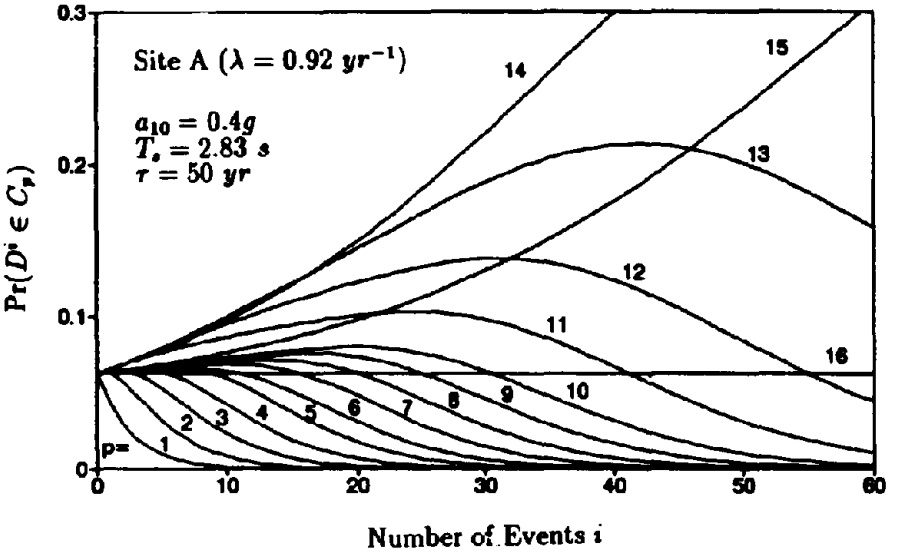

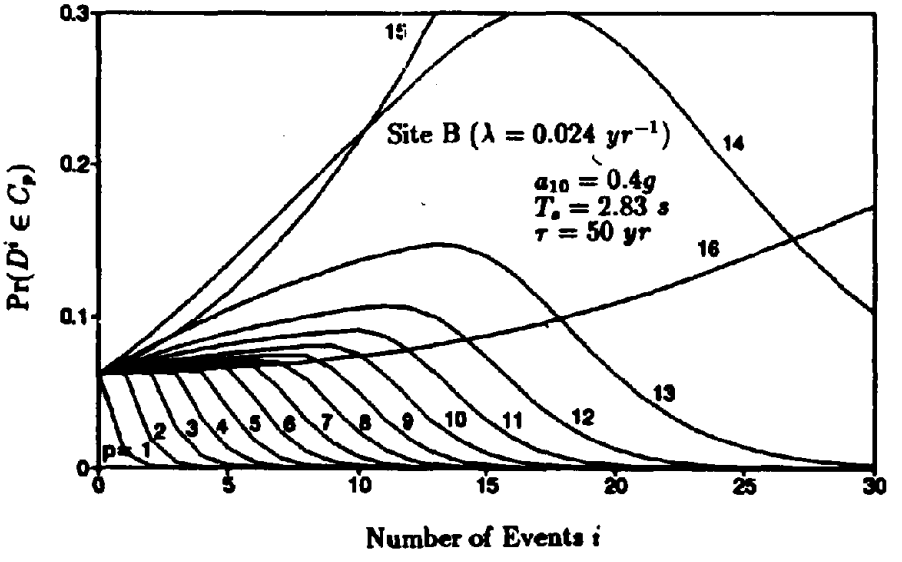

Figure 6.7: Evolution of Damage Probability Belonging to State C_p for Site A and Site B with Uncertain Initial State

Table 6.1: Mean First Passage Times with Uncertain Initial States

Damage Set $\mathcal{A}$	$\mu_{\mathcal{A}}$	
	Site-A	Site-B
$\mathcal{A}_1$	24.89	7.53
$\mathcal{A}_2$	13.78	4.69
$\mathcal{A}_3$	8.34	2.88
$\mathcal{A}_4$	4.59	1.62
$\mathcal{A}_5$	2.09	0.75

to make a generic conclusion.

Figure 6.9 shows the lifetime probabilities for $\tau = 50$ years starting from a uniform distribution of initial damage state for the sites A and B. Due to change in initial condition, the reliabilities can still be obtained directly from Eq. 6.18 and previous transition matrices. Results show that the uncertainty regarding initial condition can yield significant variation on seismic reliability estimates.

Consider several damage sets $\mathcal{A}_1$, $\mathcal{A}_2$, $\mathcal{A}_3$, $\mathcal{A}_4$, and $\mathcal{A}_5$ which are defined in Fig. 6.4. These damage sets may represent collections of undesirable damage states, which may be prescribed for a specific design condition. The mean first passage time providing the number of seismic events before absorption to these several sets of undesirable damage state(s) starting from any deterministic initial damage state is exhibited in Fig. 6.10 for both sites A and B. For example, when the site B is considered, if the deterministic initial state is C_4 (i.e., $p = 4$), the structure will require 13.4, 9.46, 6.42, 3.74, and 1.23 number of earthquakes on the average to enter the damage sets $\mathcal{A}_1$, $\mathcal{A}_2$, $\mathcal{A}_3$, $\mathcal{A}_4$, and $\mathcal{A}_5$, respectively. They are computed from Eq. 6.19 and are obtained for both Site-A and Site-B. Due to large difference in the mean arrival times of the two sites, the mean first passage time for Site-A is found to be considerably higher than that for Site-B. When the initial state is uncertain and the probability of D^0 is uniformly distributed among all states, the corresponding mean absorption times for the sites A and B can still be calculated from Eqs. 6.19 and 6.20. They are given in Table 6.1. All these results provide useful information to make decisions for optimal inspection and repair of structural systems.

The Markov model, developed in this section, can also be applied to evaluate seis-

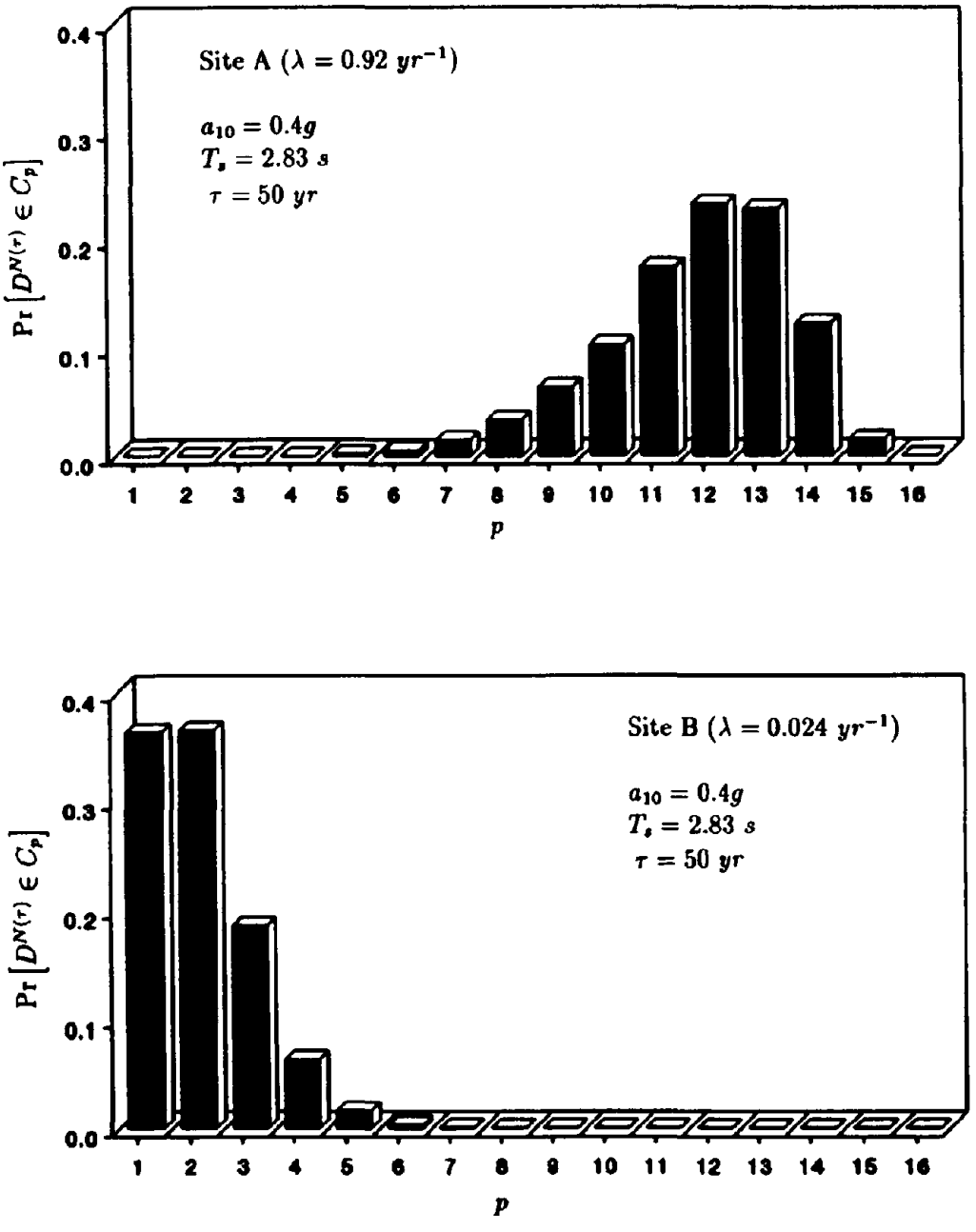

Figure 6.8: Lifetime Probabilities with Deterministic Initial State

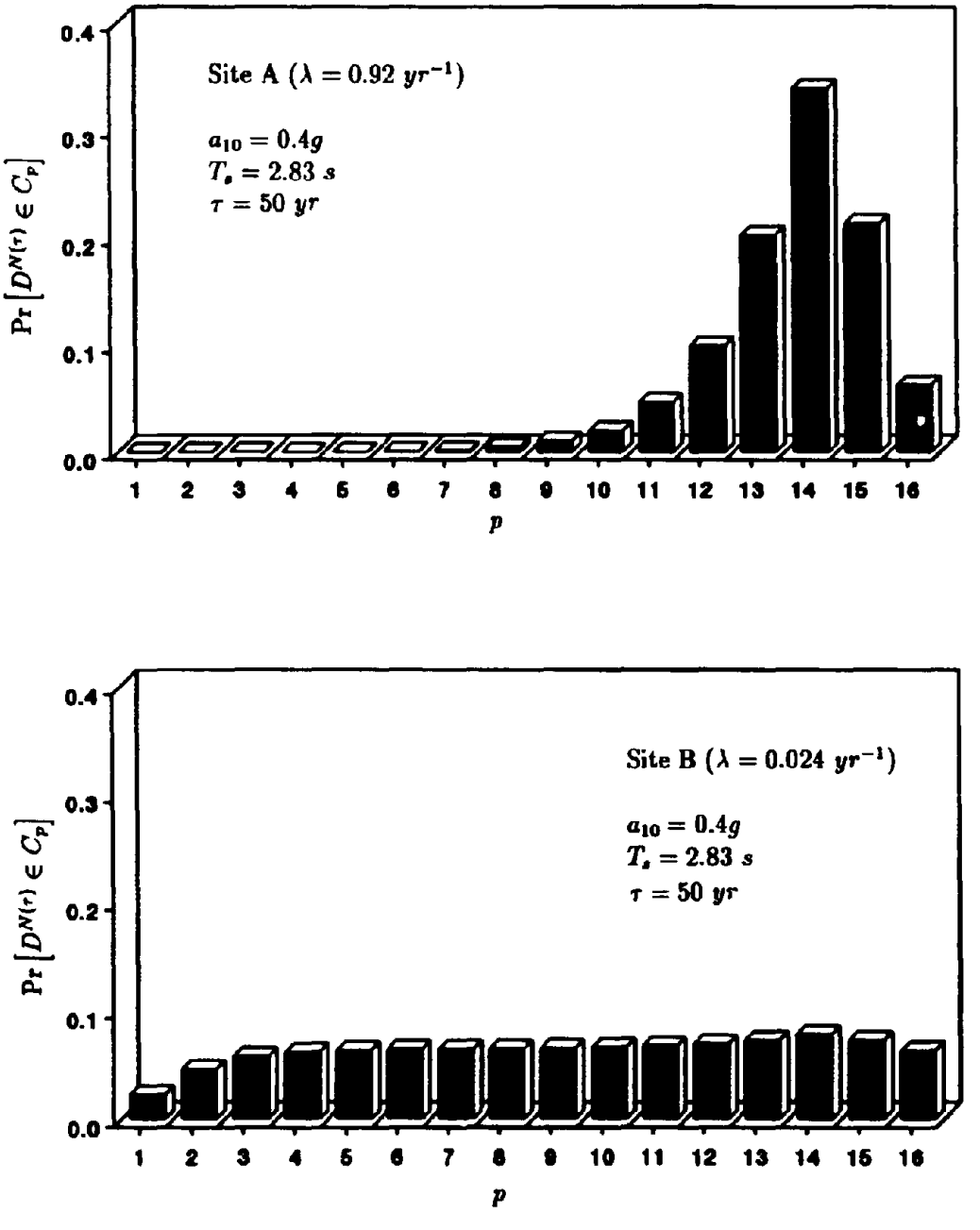

Figure 6.9: Lifetime Probabilities with Uncertain Initial State

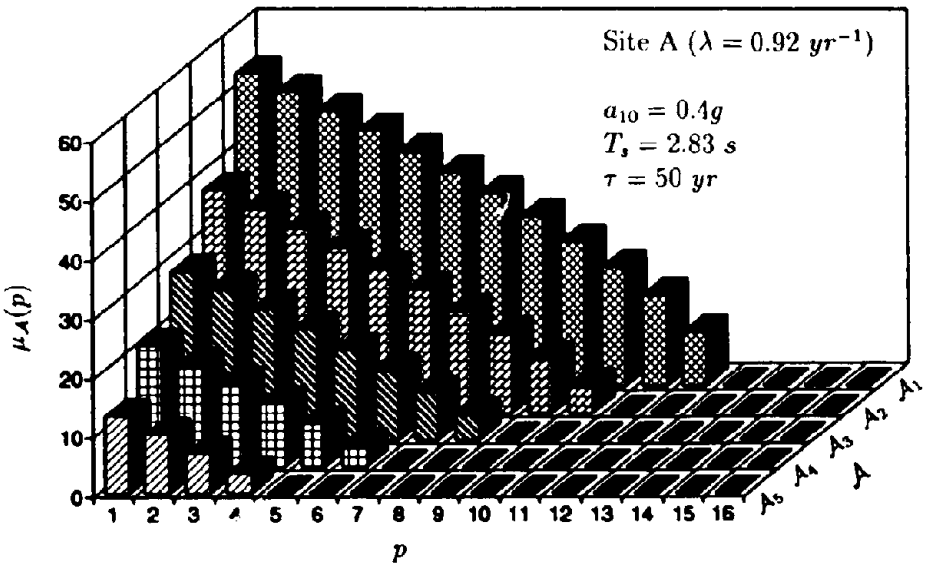

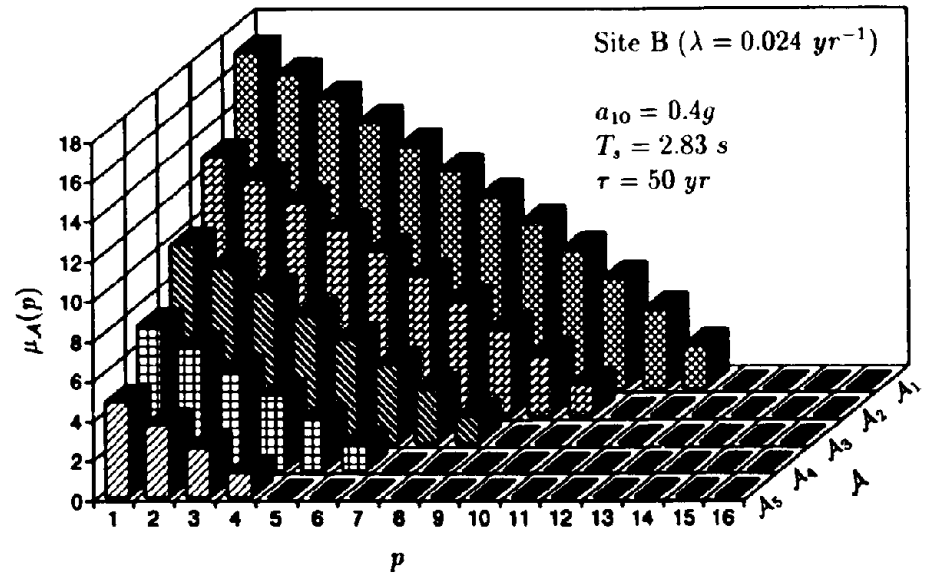

Figure 6.10: Mean First Passage Times with Deterministic Initial States

mic performance of existing structures that have been exposed to past earthquakes. The analysis, however, requires calculation of transition matrix which can be performed by two approaches. In the first approach, the transition probabilities can be computed by carrying out stochastic dynamic analysis of new structures, as done here. One can then use the same transition matrix with an appropriate initial state characterizing damage state of the existing structures. In the second approach, an estimation procedure can be developed by obtaining the preceding probabilities from a suitable database involving observed performance of existing structures.

6.4.4 Conclusions

A new methodology based on a Markov model is proposed to evaluate seismic performance and sensitivity to initial state of structural systems and determine the vulnerability of structures exposed to one or more earthquakes. The analysis accounts for simple but realistic characterization of seismic hazard, nonlinear dynamic analysis for estimating structural response, uncertainty in the initial state of structural systems, and failure conditions incorporating damage accumulation during consecutive seismic events.

The method is based on theoretical development using general hysteretic restoring force characteristics which can be applied to both reinforced concrete and steel structures. It estimates both *event* and *lifetime* reliabilities thus providing a designer more control in seismic performance evaluation. It can be used to determine the damage probability evolution during several earthquakes allowing investigation on seismic vulnerability of new and existing structures. The model facilitates computation of mean first passage time determining average number of seismic events before the structure will suffer potential damage. It also evaluates sensitivity of seismic reliability due to variability in the initial state of structural systems.

The Markov model developed in this report has been applied to evaluate seismic reliability measures of simple code-designed structures. Results suggest that designs by the *Uniform Building Code* have different reliabilities at sites with frequent small earthquakes and infrequent large earthquakes, although the sites are characterized by the same value of a_{10}. Similar findings were also obtained in the previous sections of this report when the

reliabilities were calculated for nondegrading systems.

The uncertainty regarding initial condition can yield significant variation on seismic reliability. Since, variability regarding initial conditions can play a significant role in seismic reliability estimate, it is essential that any reliability scheme has provisions of uncertain initial condition(s). Using the Markov structure, this is accomplished here with little effort.

A small increase in the dimension of damage state vector representing state of structural systems is associated with comparatively large increase in the order of transition matrix. Correspondingly, the computational involvement in obtaining transition probabilities may become significant.

SECTION 7
Local and Global Damage Indices

7.1 Introduction

Conventional seismic analysis of discrete, nonlinear structural systems is based on concentrated plasticity model, which describes the local restoring force characteristics at the critical components of interest. For building frames, these restoring force-deformation relations are defined locally at the member level for shear type buildings (*e.g.*, column shear force versus relative column end displacement) or at the cross-section level for general yielding frames, (*e.g.*, bending moment versus curvature or rotation at the end joints of beam-column). Given a hysteretic model, the parameters of such local restoring forces are usually estimated from experimental calibration. Using this local model with the restoring forces adequately defined at all critical components, the equations of motion can be directly integrated to yield various structural response characteristics. However, the inconvenience with regard to the applicability of local model as a practical analysis tool for large structural systems is not of minor nature. This is obviously because of the large dimension in which the stress analysis has to be performed. The computational effort is still significant and time-consuming even with the recent development of numerical techniques and computational facilities. These issues become more significant when numerous deterministic analyses are required in a full probabilistic analysis. It is thus desirable to perform structural dynamic analysis on some reduced dimension to lessen computational burden without any serious loss of accuracy in the results. In principle, this can be achieved by using a global model, which describes restoring force-deformation characteristics at a global level (*e.g.*, story shear force versus relative story displacements for shear type buildings). But, when such a model is to be used, it is required to know *apriori* the parameters which govern the global hysteretic characteristics of structural systems. Currently, there are no rational methodologies available for determining these global parameters.

In addition, some of the parameters of local restoring forces are usually related to known physical properties such as strength and stiffness of structural components. Any

change in the values of these time-variant parameters due to a potential seismic event is thus indicative of induced damage due to possible structural degradation. This suggests that conceptual models of *local damage indices* can be developed from the known state of local parameters. During a seismic event, such local indices not only describe progression of structural damage for seismic performance evaluation, but also provide a unique characterization of structural state due to one-to-one correspondence with the parameters of local restoring forces. Unless the mechanistic relations between local and global damage indices are established, the usefulness of seismic performance evaluation based on global damage indices are very much limited.

This section proposes a global hysteretic model and establishes analytical relations between the parameters of local and global hysteretic models for seismic analysis of multi-story shear type buildings. In both models, the analyses involve hysteretic constitutive laws commonly used in earthquake engineering to represent restoring forces and nonlinear dynamic analysis to estimate seismic response and reliability of structural systems. However, when the global model is used, the dimension of dynamic structural analysis becomes much smaller, and hence, the computational effort can be reduced significantly. From the proposed relation between these models, the local hysteretic behavior and damage can be recovered from analysis based on global models. Several numerical examples based on nondegrading and degrading characteristics of both single- and multi-degree-of-freedom systems are presented to illustrate and validate the proposed methodology.

Once the correlations between local and global damage indices are established, they are applied to implement the Markov model developed in the earlier phase of this study for estimating stochastic seismic performance of degrading multi-story structures. Such a model facilitates a systematic investigation on the validity of current seismic reliability practice which are based on lifetime largest seismic hazard without any consideration of cumulative damage during consecutive seismic events. A numerical example of a 5-story building structure designed by the *1988 Uniform Building Code* is presented. Effects of uncertainty in the initial state of system on the seismic performance are also investigated.

7.2 Local and Global Models

Consider a shear beam model of N-degree-of-freedom systems shown in Fig. 7.1(a). The second order differential equation representing the equation of motion of kth mass (floor) exhibited in Fig. 7.1(b) can be obtained from Eqs. 2.44 and 2.45.

7.2.1 Local Restoring Force

Suppose that the kth story of building consists of n_k number of individual columns (Fig. 7.1(c)) each of which may be associated with different stiffness and strength characteristics. The total restoring force g_k at the kth story can be modeled by the superposition of the nonhysteretic component $g_k^{nh}\left(U_k(t), \dot{U}_k(t)\right) = c_k\dot{U}_k(t) + \sum_{l=1}^{n_k} \alpha_{kl} k_{kl} U_k(t)$ and the hysteretic component $g_k^{h}\left(\{U_k(s), \dot{U}_k(s), 0 \le s \le t\}; t\right) = \sum_{l=1}^{n_k}(1-\alpha_{kl})k_{kl}Z_{kl}(t)$ and is thus given by

$$g_k = c_k\dot{U}_k(t) + \sum_{l=1}^{n_k}\alpha_{kl}k_{kl}U_k(t) + \sum_{l=1}^{n_k}(1-\alpha_{kl})k_{kl}Z_{kl}(t) \tag{7.1}$$

in which c_k is the kth constant damping (viscous) coefficient, α_{kl} is the parameter defining participation of the linear restoring force, k_{kl} is the stiffness, and $Z_{kl}(t)$ is the hysteretic variable all of which are associated with the lth column of kth story. It is assumed here that the evolution of $Z_{kl}(t)$ can be modeled by a first-order nonlinear ordinary differential equation [34,228,230]

$$\dot{Z}_{kl}(t) = A_{kl}(t)\dot{U}_k(t) - \beta_{kl}|\dot{U}_k(t)||Z_{kl}(t)|^{\mu_k - 1}Z_{kl}(t) - \gamma_{kl}\dot{U}_k(t)|Z_{kl}(t)|^{\mu_k} \tag{7.2}$$

where β_{kl}, γ_{kl}, μ_k are the time-invariant parameters and $A_{kl}(t)$ is the time-varying parameter of local hysteretic restoring force model. The parameter $A_{kl}(t)$, which controls stiffness and strength degradation, has the following time dependency through the dissipated hysteretic energy at time t [21]

$$A_{kl}(t) = A_{kl}(0) - \delta_{A_{kl}}\int(1-\alpha_{kl})k_{kl}Z_{kl}(t)dU_k(t) \tag{7.3}$$

in which $\delta_{A_{kl}}$ represents constant rate of local deterioration. As mentioned previously, the degradation law in Eqs. 7.3 is defined here quite arbitrarily. It is obtained from one of the

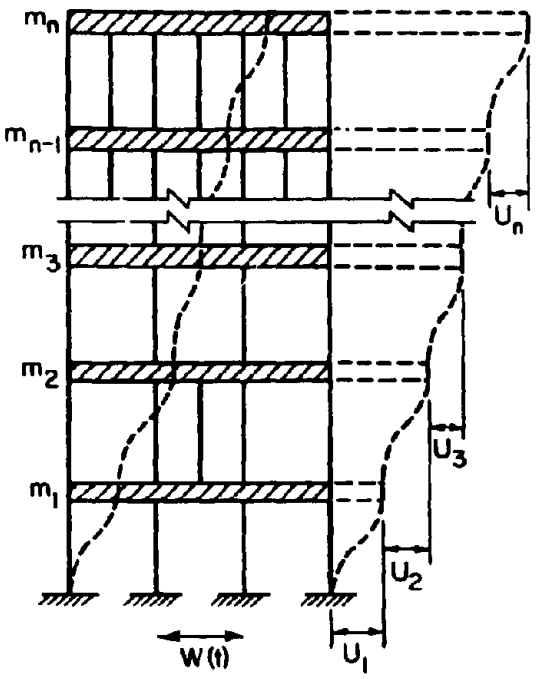

(a) Shear Beam Idealization

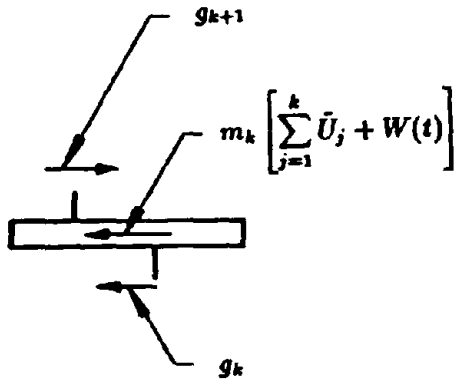

(b) Forces Acting on kth Mass

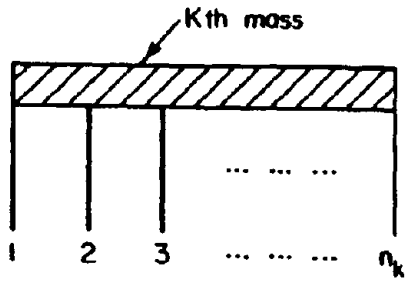

(c) Columns at kth Story

Figure 7.1: Shear Beam Idealization of Framed Structures

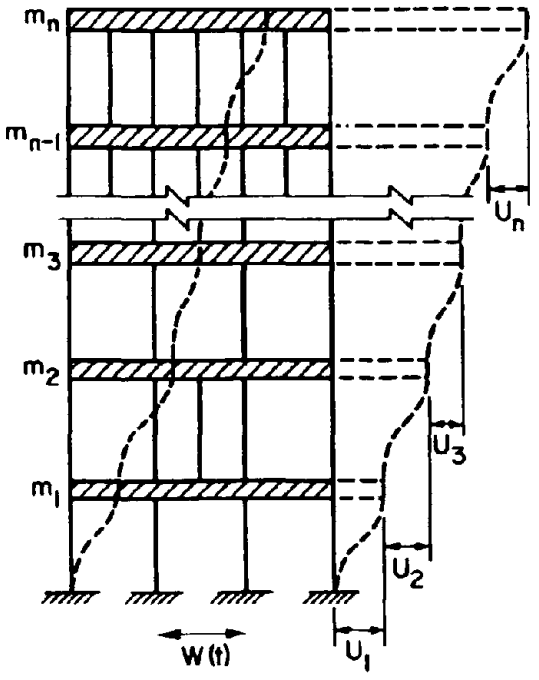

(a) Shear Beam Idealization

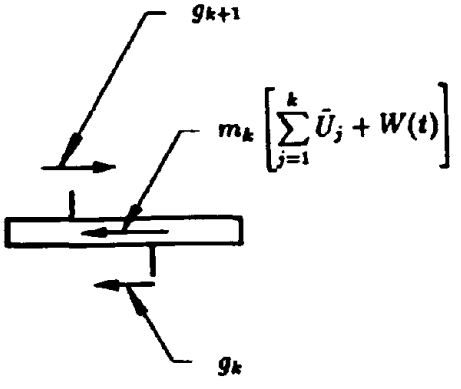

(b) Forces Acting on kth Mass

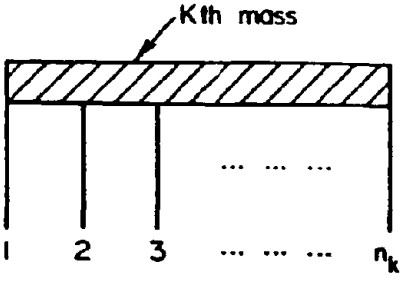

(c) Columns at kth Story

Figure 7.1: Shear Beam Idealization of Framed Structures

many choices available in the current literature. Following the state vector approach with the designation of state variables $\theta_{k1}(t) = U_k(t)$, $\theta_{k2}(t) = \dot{U}_k(t)$, and $\theta_{k3}(t) = Z_{k1}(t), \cdots, \theta_{k,2+n_k}(t) = Z_{k,n_k}(t)$ at the kth story, the equivalent system of first order differential equations corresponding to Eqs. 2.45 and 7.2 becomes

$$\begin{aligned}
\dot{\theta}_{k1}(t) &= \theta_{k2}(t) \\
\dot{\theta}_{k2}(t) &= (1-\delta_{k1})\frac{g_{k-1}}{m_{k-1}} - \left[1 + (1-\delta_{k1})\frac{m_k}{m_{k-1}}\right]\frac{g_k}{m_k} + (1-\delta_{kn})\frac{m_{k+1}}{m_k}\frac{g_{k+1}}{m_{k+1}} - \delta_{k1}W(t) \\
\dot{\theta}_{k3}(t) &= A_{k1}(t)\theta_{k2}(t) - \beta_{k1}|\theta_{k2}(t)||\theta_{k3}(t)|^{\mu_k - 1}\theta_{k3}(t) - \gamma_{k1}\theta_{k2}(t)|\theta_{k3}(t)|^{\mu_k} \\
&\vdots \\
\dot{\theta}_{k,2+n_k}(t) &= A_{k,n_k}(t)\theta_{k2}(t) - \beta_{k,n_k}|\theta_{k2}(t)||\theta_{k,2+n_k}|^{\mu_k - 1}\theta_{k,2+n_k} - \gamma_{k,n_k}\theta_{k2}(t)|\theta_{k,2+n_k}|^{\mu_k}
\end{aligned} \tag{7.4}$$

which can be recast in a compact form

$$\dot{\boldsymbol{\theta}}(t) = \mathbf{h}\left(\boldsymbol{\theta}(t), t; \mathbf{A}(t)\right) \tag{7.5}$$

with the initial conditions $\boldsymbol{\theta}(0) = \mathbf{0}$, where $\boldsymbol{\theta}(t) = \{\cdots, \theta_{k1}(t), \theta_{k2}(t), \theta_{k3}(t), \cdots, \theta_{k,2+n_k}(t), \cdots\}^T$ is a real $(2n + \sum_{k=1}^{n} n_k)$-dimensional response state vector, $\mathbf{A}(t) = \{\cdots, A_{k1}(t), A_{k2}(t), \cdots, A_{k,n_k}(t), \cdots\}^T$ is a real $(\sum_{k=1}^{n} n_k)$-dimensional damage state vector representing state of time-variant parameters in the local restoring force, $\mathbf{h}(\cdot)$ is a vector function, $\mathbf{0}$ is a null vector, and the superscript T is a symbol for transpose of a general vector. At any time t during a potentially damaging seismic event, $\mathbf{A}(t)$ characterizes uniquely state of structural damage due to any stiffness degradation or strength deterioration.

7.2.2 Global Restoring Force

Suppose that the total restoring force g_k at the kth story can be modeled globally by the superposition of the nonhysteretic component $g_k^{nh}\left(U_k(t), \dot{U}_k(t)\right) = c_k\dot{U}_k(t) + \alpha^*{}_k k^*{}_k U_k(t)$ and the hysteretic component $g_k^{h}\left(\{U_k(s), \dot{U}_k(s), 0 \le s \le t\}; t\right) = (1-\alpha_k)k^*{}_k Z^*{}_k(t)$. It is given by

$$g_k = c_k\dot{U}_k(t) + \alpha^*{}_k k^*{}_k U_k(t) + (1-\alpha^*{}_k)k^*{}_k Z^*{}_k(t) \tag{7.6}$$

in which α^*_k is the global parameter defining participation of kth linear restoring force, k^*_k is the kth story stiffness, and $Z^*_k(t)$ is the single kth global hysteretic variable the evolution of which can be modeled by a similar first-order nonlinear ordinary differential equation

$$\dot{Z}^*_k(t) = A^*_k(t)\dot{U}_k(t) - \beta^*_k|\dot{U}_k(t)||Z^*_k(t)|^{\mu^*_k-1}Z^*_k(t) - \gamma^*_k\dot{U}_k(t)|Z^*_k(t)|^{\mu^*_k} \tag{7.7}$$

where β^*_k, γ^*_k, μ^*_k are the time-invariant parameters and $A^*_k(t)$ is the time-varying parameter of the global hysteretic restoring force model. The parameter $A^*_k(t)$ which now controls story stiffness and strength degradation is expected to follow a similar degradation rule

$$A^*_k(t) = A^*_k(0) - \delta^*_{A_k}\int(1-\alpha^*_k)k^*_k Z^*_k(t)\,dU_k(t) \tag{7.8}$$

in which $\delta^*_{A_k}$ represents a constant rate of global deterioration. Following designation of state variables $\theta^*_{k1}(t) = U_k(t)$, $\theta^*_{k2}(t) = \dot{U}_k(t)$, and $\theta^*_{k3}(t) = Z^*_k(t)$, the equivalent system of first order differential equations corresponding to Eqs. 2.45 and 7.7 becomes

$$\begin{aligned}
\dot{\theta}^*_{k1}(t) &= \theta^*_{k2}(t) \\
\dot{\theta}^*_{k2}(t) &= (1-\delta_{k1})\frac{g_{k-1}}{m_{k-1}} - \left[1+(1-\delta_{k1})\frac{m_k}{m_{k-1}}\right]\frac{g_k}{m_k} + (1-\delta_{kn})\frac{m_{k+1}}{m_k}\frac{g_{k+1}}{m_{k+1}} - \delta_{k1}W(t) \\
\dot{\theta}^*_{k3}(t) &= A^*_k(t)\theta^*_{k2}(t) - \beta^*_k|\theta^*_{k2}(t)||\theta^*_{k3}(t)|^{\mu^*_k-1}\theta^*_{k3}(t) - \gamma^*_k\theta^*_{k2}(t)|\theta^*_{k3}(t)|^{\mu^*_k}
\end{aligned} \tag{7.9}$$

which can be recast in a compact form

$$\dot{\boldsymbol{\theta}}^*(t) = \mathbf{h}^*\left(\boldsymbol{\theta}^*(t), t; \mathbf{A}^*(t)\right) \tag{7.10}$$

with the initial conditions $\boldsymbol{\theta}^*(0) = \mathbf{0}$, where $\boldsymbol{\theta}^*(t) = \{\cdots, \theta^*_{k1}(t), \theta^*_{k2}(t), \theta^*_{k3}(t), \cdots\}^T$ is the $3n$-dimensional response state vector, $\mathbf{A}^*(t) = \{A^*_1(t), A^*_2(t), \cdots, A^*_n(t)\}^T$ is the n-dimensional damage state vector representing state of time-variant parameters in the global restoring force, and $\mathbf{h}^*(\cdot)$ is a vector function. Note that in both local and global models, the dynamic structural analysis can be viewed as a nonlinear initial-value problem with the system of the differential equations described above. But, the dimension of $\boldsymbol{\theta}^*(t)$ is much smaller than that of $\boldsymbol{\theta}(t)$, particularly when the total number of columns n_k for all the

stories $k = 1, 2, \cdots, n$ is very large. Hence, when the global model is used, the computational effort in solving the initial value problem can be reduced significantly. Application of the global model, however, will require estimation of its parameters from the known calibrated parameters of local model. They are discussed in the forthcoming section.

7.2.3 Relation between Local and Global Parameters

Structural analyses are usually based on local constitutive law. The parameters of these local models can be calibrated from experimental data. For large structures with many components, it is however, desirable to perform stress analysis based on global constitutive law to facilitate practical design [170,176]. This requires estimation of the parameters of global models. Hence, it is important to establish relations between the parameters of local and global models.

Consider the kth total restoring force g_k in Eq. 7.1 obtained from the local restoring forces. Following simple algebra, it can be shown that

$$\begin{aligned} g_k &= c_k \dot{U}_k(t) + \sum_{l=1}^{n_k} w_{kl}\alpha_{kl} \sum_{l=1}^{n_k} k_{kl}\, U_k(t) \\ &+ \left(1 - \sum_{l=1}^{n_k} w_{kl}\alpha_{kl} \times \frac{\sum_{l=1}^{n_k} w_{kl}\alpha_{kl} Z_{kl}(t)}{\sum_{l=1}^{n_k} w_{kl} Z_{kl}(t) \sum_{l=1}^{n_k} w_{kl}\alpha_{kl}} \right) \sum_{l=1}^{n_k} k_{kl} \sum_{l=1}^{n_k} w_{kl} Z_{kl}(t) \end{aligned} \tag{7.11}$$

in which

$$w_{kl} = \frac{k_{kl}}{\sum_{l=1}^{n_k} k_{kl}} \tag{7.12}$$

is the stiffness-based weighting coefficient. Further simplification of above equation can be accomplished by noting that

$$\frac{\sum_{l=1}^{n_k} w_{kl}\alpha_{kl} Z_{kl}(t)}{\sum_{l=1}^{n_k} w_{kl} Z_{kl}(t) \sum_{l=1}^{n_k} w_{kl}\alpha_{kl}} \to 1 \tag{7.13}$$

when $\alpha_{kl} \to 0$. In earthquake engineering, this is not a significant limitation as the quantity α_{kl} which also represents the ratio of post- to pre-yield stiffnesses is indeed small for realistic material models. Recent calibration with laboratory data reported in Ref. [205] suggests that $\alpha_{kl} = 0.04$ for steel and $\alpha_{kl} = 0.02$ for reinforced concrete. Thus, with this approximation, Eq. 7.11 takes the form

$$g_k = c_k \dot{U}_k(t) + \sum_{l=1}^{n_k} w_{kl}\alpha_{kl} \sum_{l=1}^{n_k} k_{kl}\, U_k(t) + \left(1 - \sum_{l=1}^{n_k} w_{kl}\alpha_{kl}\right) \sum_{l=1}^{n_k} k_{kl} \sum_{l=1}^{n_k} w_{kl} Z_{kl}(t) \qquad (7.14)$$

which when compared with the kth total restoring force g_k in Eq. 7.6 obtained from the global restoring force gives

$$\alpha^*{}_k = \sum_{l=1}^{n_k} w_{kl}\alpha_{kl}, \quad k^*{}_k = \sum_{l=1}^{n_k} k_{kl} \quad \text{and} \quad Z^*{}_k(t) = \sum_{l=1}^{n_k} w_{kl} Z_{kl}(t). \qquad (7.15)$$

Time-Invariant Parameters

Consider the rate equation of global hysteretic variable $Z^*{}_k(t)$ in Eq. 7.15 which can be expanded as following:

$$\begin{aligned}
\dot{Z}^*_k(t) &= \sum_{l=1}^{n_k} w_{kl} \dot{Z}_{kl}(t) \\
&= \sum_{l=1}^{n_k} w_{kl} \left[A_{kl}(t)\dot{U}_k(t) - \beta_{kl}|\dot{U}_k(t)||Z_{kl}(t)|^{\mu_k - 1} Z_{kl}(t) - \gamma_{kl}\dot{U}_k(t)|Z_{kl}(t)|^{\mu_k} \right] \\
&= \sum_{l=1}^{n_k} w_{kl} A_{kl}(t)\dot{U}_k(t) - \frac{\sum_{l=1}^{n_k} w_{kl}\beta_{kl}|Z_{kl}(t)|^{\mu_k - 1} Z_{kl}(t)}{\left|\sum_{l=1}^{n_k} w_{kl} Z_{kl}(t)\right|^{\mu_k - 1} \sum_{l=1}^{n_k} w_{kl} Z_{kl}(t)} |\dot{U}_k(t)| \left|\sum_{l=1}^{n_k} w_{kl} Z_{kl}(t)\right|^{\mu_k - 1} \times \\
&\quad \sum_{l=1}^{n_k} w_{kl} Z_{kl}(t) - \frac{\sum_{l=1}^{n_k} w_{kl}\gamma_{kl}|Z_{kl}(t)|^{\mu_k}}{\left|\sum_{l=1}^{n_k} w_{kl} Z_{kl}(t)\right|^{\mu_k}} \dot{U}_k(t) \left|\sum_{l=1}^{n_k} w_{kl} Z_{kl}(t)\right|^{\mu_k}. \qquad (7.16)
\end{aligned}$$

Comparison of above equation with Eq. 7.7 suggests

$$\mu^*{}_k = \mu_k, \quad A^*{}_k(t) = \sum_{l=1}^{n_k} w_{kl} A_{kl}(t) \quad \text{and} \tag{7.17}$$

$$\beta^*{}_k = \frac{\sum_{l=1}^{n_k} w_{kl}\beta_{kl}|Z_{kl}(t)|^{\mu_k-1}Z_{kl}(t)}{\left|\sum_{l=1}^{n_k} w_{kl}Z_{kl}(t)\right|^{\mu_k-1}\sum_{l=1}^{n_k} w_{kl}Z_{kl}(t)}, \quad \gamma^*{}_k = \frac{\sum_{l=1}^{n_k} w_{kl}\gamma_{kl}|Z_{kl}(t)|^{\mu_k}}{\left|\sum_{l=1}^{n_k} w_{kl}Z_{kl}(t)\right|^{\mu_k}}. \tag{7.18}$$

Note that the expressions for the global parameters in Eq. 7.18 involve local hysteretic variables $Z_{kl}(t)$ at both numerator and denominator which in turn may be dependent on external load parameters. This has the immediate bearing that the global parameters $\beta^*{}_k$ and $\gamma^*{}_k$ are no longer time-invariant as their counterparts are in the local level. Thus, when a global modeling is adopted, exact determination of these parameters is not possible due to lack of *apriori* knowledge regarding evolution of local hysteretic variables.

For earthquake type of loading, it is however, feasible to search for approximate evaluation of above global parameters and still treat them as time-invariant hysteretic parameters. Two extreme cases based on the magnitude of seismic intensity can be perceived. When the intensity of seismic noise is not extremely large, the time span during which large differences in the values of $Z_{kl}(t)$ may occur can be neglected. This will allow approximation of $Z_{kl}(t)$ to be a common time function (say, $\hat{Z}_k(t)$) thus simplifying Eq. 7.18 into

$$\beta^*{}_k \simeq \sum_{l=1}^{n_k} w_{kl}\beta_{kl} \quad \text{and} \quad \gamma^*{}_k \simeq \sum_{l=1}^{n_k} w_{kl}\gamma_{kl}. \tag{7.19}$$

On the contrary, when the intensity of seismic noise is very large, it can be argued that $Z_{kl}(t)$ assumes its maximum value $Z_{kl,max}(0)$ most of the time during ground motion. The largest value $Z_{kl,max}(0)$ can be easily obtained by substituting the expression for $\dot{Z}_{kl}(t)$ in Eq. 7.2 into the following equation of maximization

$$\frac{d}{dU_k(t)}Z_{kl}(t) = \frac{\dot{Z}_{kl}(t)}{\dot{U}_{kl}(t)} = 0 \tag{7.20}$$

giving [21]

$$Z_{kl,max}(t) = \left[\frac{A_{kl}(t)}{\beta_{kl}+\gamma_{kl}}\right]^{\frac{1}{\mu_k}}. \tag{7.21}$$

Following replacement of $Z_{kl}(t)$ in Eq. 7.18 by $Z_{kl,max}(0)$ in Eq. 7.21 at $t = 0$ along with the observation that at any time t the signs of $Z_{kl}(t)$ are the same, another estimate of above parameters can be obtained as

$$\beta^*{}_k \simeq \frac{\sum_{l=1}^{n_k} w_{kl}\beta_{kl}\left[\frac{A_{kl}(0)}{\beta_{kl}+\gamma_{kl}}\right]}{\left(\sum_{l=1}^{n_k} w_{kl}\left[\frac{A_{kl}(0)}{\beta_{kl}+\gamma_{kl}}\right]^{\frac{1}{\mu_k}}\right)^{\mu_k}} \quad \text{and} \quad \gamma^*{}_k \simeq \frac{\sum_{l=1}^{n_k} w_{kl}\gamma_{kl}\left[\frac{A_{kl}(0)}{\beta_{kl}+\gamma_{kl}}\right]}{\left(\sum_{l=1}^{n_k} w_{kl}\left[\frac{A_{kl}(0)}{\beta_{kl}+\gamma_{kl}}\right]^{\frac{1}{\mu_k}}\right)^{\mu_k}}. \tag{7.22}$$

The two sets of estimates of $\beta^*{}_k$ and $\gamma^*{}_k$ given above apply to two extreme cases of load intensity and can be used as some sort of bounds for the determination of above parameters. When the strength of noise is somewhat intermediate, the appropriate values of these parameters can be interpolated from these bounds.

Time-Variant Parameter

Consider the infinitesimal total hysteretic energy dissipated at the kth story from the local model (Eq. 7.3) which can be expanded as

$$\begin{aligned}
&\sum_{l=1}^{n_k}(1-\alpha_{kl})k_{kl}Z_{kl}(t)\,dU_k(t) \\
&= \left(1-\sum_{l=1}^{n_k} w_{kl}\alpha_{kl} \times \frac{\sum_{l=1}^{n_k} w_{kl}\alpha_{kl}Z_{kl}(t)}{\sum_{l=1}^{n_k} w_{kl}Z_{kl}(t)\sum_{l=1}^{n_k} w_{kl}\alpha_{kl}}\right) \times \sum_{l=1}^{n_k} k_{kl}\sum_{l=1}^{n_k} w_{kl}Z_{kl}(t)\,dU_k(t) \\
&= \left(1-\sum_{l=1}^{n_k} w_{kl}\alpha_{kl}\right)\sum_{l=1}^{n_k} k_{kl}\sum_{l=1}^{n_k} w_{kl}Z_{kl}(t)\,dU_k(t) \\
&= (1-\alpha^*{}_k)k^*{}_kZ^*{}_k(t)\,dU_k(t)
\end{aligned} \tag{7.23}$$

due to similar consideration as in Eq. 7.13. From Eq. 7.17 with $A_{kl}(t)$ in Eq. 7.3,

$$\begin{aligned}
A^*{}_k(t) &= \sum_{l=1}^{n_k} w_{kl}\left[A_{kl}(0) - \delta_{A_{kl}}\int(1-\alpha_{kl})k_{kl}Z_{kl}(t)\,dU_k(t)\right] \\
&= A^*{}_k(0) - \sum_{l=1}^{n_k} w_{kl}\delta_{A_{kl}}\int(1-\alpha_{kl})k_{kl}Z_{kl}(t)\,dU_k(t)
\end{aligned} \tag{7.24}$$

which can be compared with Eq. 7.8 and the dissipated energy in Eq. 7.23 to yield

$$\delta^*{}_{A_k} = \frac{\sum_{l=1}^{n_k} w_{kl}\delta_{A_{kl}}(1-\alpha_{kl})k_{kl}\int Z_{kl}(t)\dot{U}_k(t)dt}{\sum_{l=1}^{n_k}(1-\alpha_{kl})k_{kl}\int Z_{kl}(t)\dot{U}_k(t)dt} \tag{7.25}$$

in which the order of integral and summation operators is interchanged in the denominator, and $dU_k(t) = \dot{U}_k(t)\,dt$. Again, the exact evaluation of $\delta^*{}_{A_k}$ requires information regarding time evolution of local hysteretic variables. Following similar consideration as in Eq. 7.19 with small seismic intensity, the above equation reduces to

$$\delta^*{}_{A_k} \simeq \frac{\sum_{l=1}^{n_k} w_{kl}\delta_{A_{kl}}(1-\alpha_{kl})k_{kl}}{\sum_{l=1}^{n_k}(1-\alpha_{kl})k_{kl}}. \tag{7.26}$$

When α_{kl} is small or if it does not vary within the columns at a particular story, Eq. 7.26 simplifies to

$$\delta^*{}_{A_k} = \sum_{l=1}^{n_k} {w_{kl}}^2\delta_{A_{kl}}. \tag{7.27}$$

When the intensity of noise is large, similar arguments given earlier for time-invariant parameters may be applied to obtain another equation for $\delta^*{}_{A_k}$. However, such estimate may not be reliable in degrading systems with large seismic intensity. This is because as time advances, $A_{kl}(t) \to 0$, and $Z_{kl,max}(t) = [A_{kl}(t)/(\beta_{kl}+\gamma_{kl})]^{1/\mu_k} \to 0$ at a much faster rate due to the rapid loss of stiffness and/or strength. At any time during ground motion, it is difficult to anticipate variation of $Z_{kl}(t)$ among various columns.

Recovery of Local Hysteresis

Once the global parameters are estimated from the known values of local parameters, practical seismic analysis can be performed based on global restoring force model. It is however, desirable to recover the local hysteretic behavior of structural systems. This will allow determination of local damage distribution which is uniquely related to the global model.

Consider the partitions of local and global response state vectors $\boldsymbol{\theta}(t) = \{\boldsymbol{\theta}_1(t), \boldsymbol{\theta}_2(t)\}^T$ and $\boldsymbol{\theta}^*(t) = \{\boldsymbol{\theta}^*{}_1(t), \boldsymbol{\theta}^*{}_2(t)\}^T$ in which $\boldsymbol{\theta}_1(t) = \boldsymbol{\theta}^*{}_1(t) = \{\cdots, U_k(t), \dot{U}_k(t), \cdots\}^T$ is the $2n$-dimensional traditional state vector (in both local and global models) comprising relative displacement and velocity of each story mass, and $\boldsymbol{\theta}_2(t) = \{\cdots, Z_{k1}(t), \cdots, Z_{k,n_k}(t), \cdots\}^T$ and $\boldsymbol{\theta}^*{}_2(t) = \{\cdots, Z^*{}_k(t), \cdots\}^T$ are $(\sum_{k=1}^{n} n_k)$- and n-dimensional state vectors consisting of additional hysteretic variables corresponding to local and global models, respectively. Suppose, at any time t, the state vector $\boldsymbol{\theta}^*(t)$ can be obtained by solving the global initial value problem in Eq. 7.10. Following extraction of the component state vector $\boldsymbol{\theta}^*{}_1(t)$ from the global solution $\boldsymbol{\theta}^*(t)$, it can be substituted for $\boldsymbol{\theta}_1(t)$ in the local initial value problem of Eq. 7.5 to yield solution for the state vector $\boldsymbol{\theta}_2(t)$ of local hysteretic variables. This way, the local hysteretic characteristics and damage of a building frame can be recovered following structural analysis based on the global model.

7.2.4 Numerical Example

Example 7.1

In this example, a single-degree-of-freedom system with both nondegrading and degrading restoring forces is investigated to evaluate the adequacy of global hysteretic model in predicting various seismic response characteristics. The nonlinear systems of first-order ordinary differential equations in the initial value problems of both local (Eq. 7.5) and global (Eq. 7.10) models are solved by the fifth- and sixth-order Runge-Kutta integrators (see Appendix C)

Consider a 1-story ($n = 1$) shear building with mass $m_1 = 1$, damping coefficient $c_1 = 0$ which consists of 4 different columns with the stiffness $k_{11} = 100$, $k_{12} = 200$, $k_{13} = 300$, $k_{14} = 400$, and the strength $F_{11} = 960$, $F_{12} = 2400$, $F_{13} = 4800$, $F_{14} = 9600$. From the above physical properties with the parameter identification procedures proposed in Ref. [205], the time-invariant parameters of local model are: $\mu_1 = 1$, $\beta_{11} = \gamma_{11} = 0.05$, $\beta_{12} = \gamma_{12} = 0.04$, $\beta_{13} = \gamma_{13} = 0.03$, $\beta_{14} = \gamma_{14} = 0.02$, and $A_{1l}(0) = 1$, $\alpha_{1l} = 0.04$, for all $l = 1, 2, 3, 4$. Note that the stiffness and strength characteristics are assumed to be widely different among the columns. Both nondegrading ($\delta_{A_{kl}} = 0$) and degrading ($\delta_{A_{kl}} \neq 0$)

systems are considered. The above structural and material properties provide complete local characterization of nondegrading system. When the degrading system is considered, it is assumed to follow the deterioration rule in Eq. 7.3, and the values of additional time-variant parameters $\delta_{A_{kl}}$ for all the columns are taken as 5.0×10^{-6} in this study.

Suppose that the nonlinear behavior of the building system can be approximated by a single hysteretic variable describing the restoring force for building system itself. The time-invariant parameters corresponding to this global model can be calculated from Eqs. 7.15 and 7.17 as $k^*_1 = 1000$, $A^*_1(0) = 1$, $\alpha^*_1 = 0.04$, and $\mu^*_1 = 1$, respectively. Two different estimates of β^*_1 and γ^*_1 are obtained following Eq. 7.19 and Eq. 7.22. They are found to be $\beta^*_1 = \gamma^*_1 = 0.03$ and $\beta^*_1 = \gamma^*_1 = 0.027$, respectively. Obviously when the system is nondegrading ($\delta_{A_{kl}} = 0$), the global time-variant parameter $\delta^*_{A_1} = 0$ (Eq. 7.25 or 7.26). For degrading system, the global rate of degradation $\delta^*_{A_1}$ is computed to be 1.5×10^{-6} by using Eq. 7.26 or 7.27.

A sample of modulated Gaussian white noise of duration 6 s with one-sided power spectral intensity G_0 scaled to unity is shown in Fig. 7.2. This simulated time-series multi-

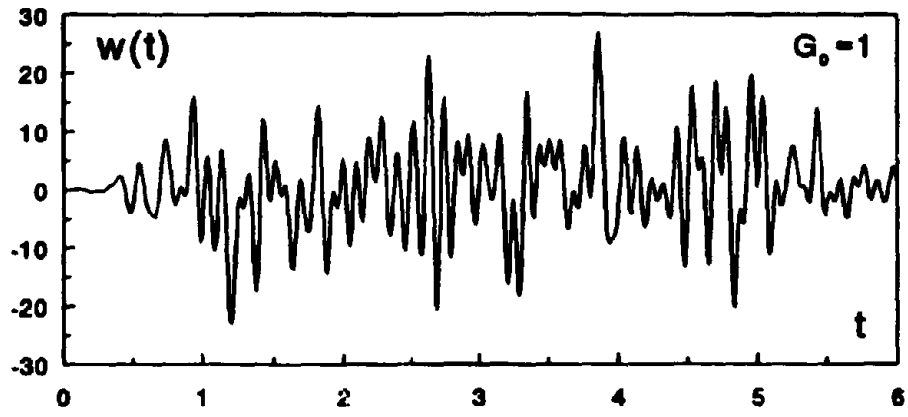

Figure 7.2: A Sample of Modulated Gaussian White Noise ($G_0 = 1$)

plied with varying levels of intensity $G_0 = 1.0 \times 10^5$ and 1.0×10^7 are used as deterministic inputs to the single-degree-of-freedom nonlinear oscillator.

Nondegrading System

Figure 7.3(a) shows the time evolution of relative displacement and velocity of the oscillator due to deterministic forcing function in Fig. 7.2 with $G_0 = 1.0 \times 10^5$. Results of both local and global hysteretic models with two different estimates of β^*_1 and γ^*_1 are shown in the figure. Excellent agreement between these models are obtained irrespective of the approximations in Eqs. 7.19 and 7.22. No meaningful difference in response is noted due to closeness of bounds of estimated global parameters. Also shown in Fig. 7.3(b) are the exact time variations of β^*_1 and γ^*_1 in Eq. 7.18 in which the local hysteretic variables $Z_{1l}(t)$ are obtained following dynamic analysis based on local model. It clearly indicates the accuracy of estimated global parameters β^*_1 and γ^*_1 from the proposed equations. The evolution of $Z_{1l}(t)$ mentioned above is shown in Fig. 7.3(c) which confirms previous anticipation of negligible time interval during which $Z_{1l}(t)$ are different. Accordingly, Eq. 7.19 provides simpler but useful approximation for global parameters. Fig. 7.3(c) also shows the evolution of displacement dependent story restoring forces $Q_1(t) = \sum_{l=1}^{4} q_{1l}(t)$ with $q_{1l}(t) = \alpha_{1l} k_{1l} U_1(t) + (1 - \alpha_{1l}) k_{1l} Z_{1l}(t)$ and $Q^*_1(t) = \alpha^*_1 k^*_1 U_1(t) + (1 - \alpha^*_1) k^*_1 Z^*_1(t)$, which are obtained from local and global models, respectively. Again, very good agreement between the results of both models is obtained.

Figure 7.4(a) exhibits the plots of restoring forces $q_{1l}(t)$ and $Q_1(t)$ versus displacement $U_1(t)$ which are obtained from local model thus providing hysteretic loops for individual columns and system itself. For comparison with the results of global model, Figs. 7.4(b) and 7.4(c) show similar kind of plots of restoring force $Q^*_1(t)$ and the recovered column restoring forces $q^*_{1l}(t) = \alpha_{1l} k_{1l} U_1(t) + (1 - \alpha_{1l}) k_{1l} Z^*_{1l}(t)$ in which the conventional state variables $U_1(t)$ and $\dot{U}_1(t)$ are calculated from the global model (Eq. 7.10) and the recovered local hysteretic variables $Z^*_{1l}(t)$ are obtained by directly integrating Eq. 7.2. They all indicate that the global model with both estimates of parameters β^*_1 and γ^*_1 can accurately predict both local and global hysteretic characteristics of structural systems.

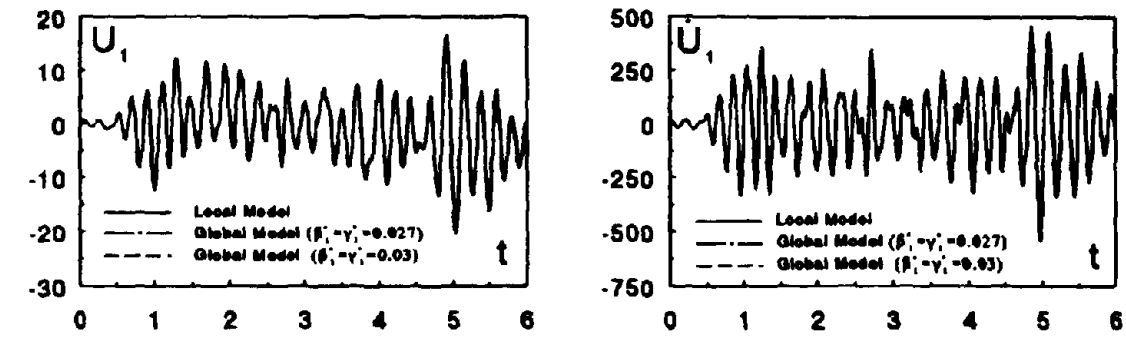

(a) Displacement and Velocity Response

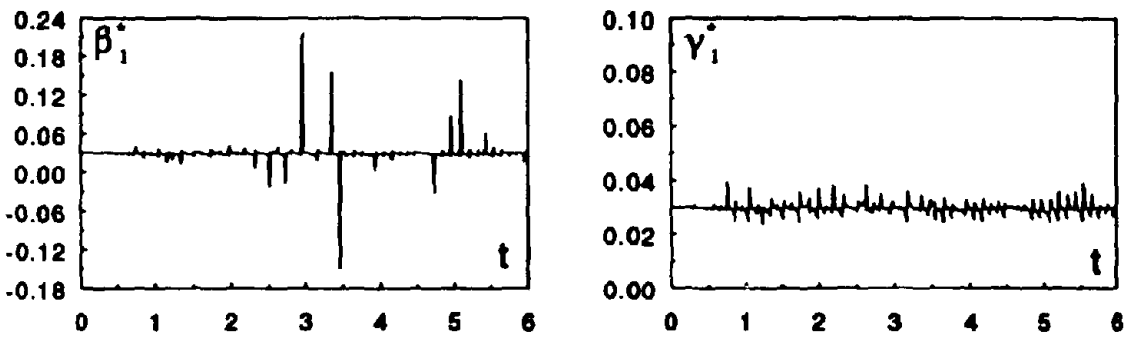

(b) Exact Global Parameters from Local Model

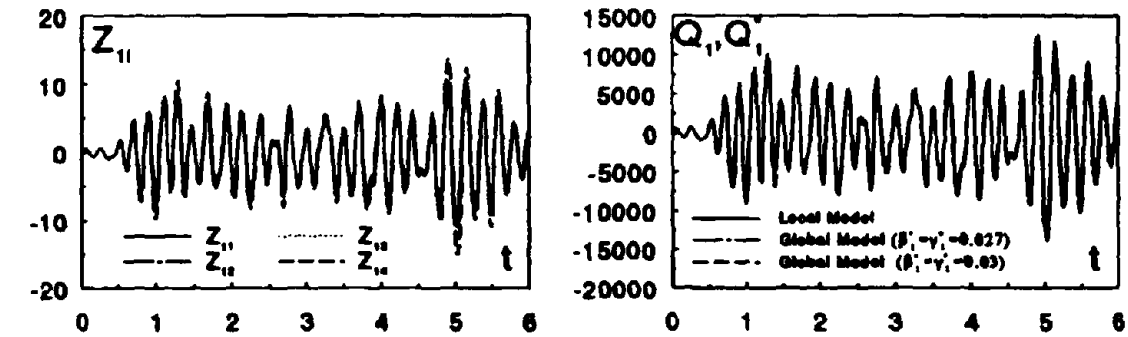

(c) Hysteretic Variables and Total Restoring Forces

Figure 7.3: Time History of Various Responses for Nondegrading System with $G_0 = 1.0 \times 10^5$

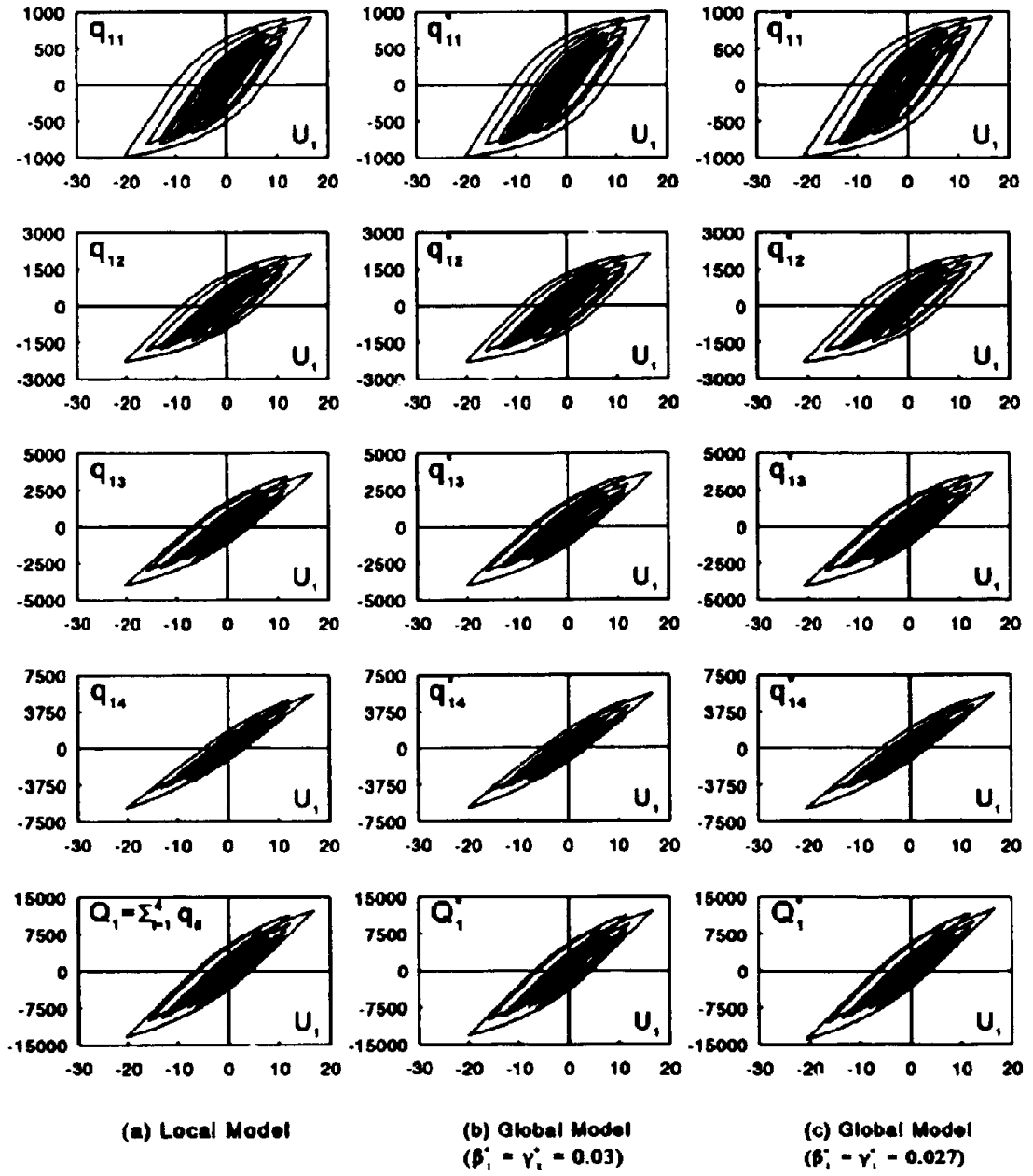

Figure 7.4: Hysteretic Loops for Nondegrading System with $G_0 = 1.0 \times 10^5$

Figures 7.5 and 7.6 show similar sets of plots of various responses for a seismic input in Fig. 7.2 with a larger intensity $G_0 = 1.0 \times 10^7$. Results of global model with both estimates of parameters β^*_1 and γ^*_1 are found to be quite satisfactory when compared with those obtained from local model. However, when the intensity is very large ($G_0 = 1.0 \times 10^7$), the response characteristics due to global models with estimated parameters $\beta^*_1 = \gamma^*_1 = 0.027$ are found to be superior than those obtained with $\beta^*_1 = \gamma^*_1 = 0.03$. This is due to the fact that the significant amount of time the values of $Z_{1l}(t)$ as obtained from local model and exhibited in Fig. 7.5(c) are equal to $Z_{1l,max}(0) = [A_{1l}(0)/(\beta_{1l} + \gamma_{1l})]^{1/\mu_1}$. Due to the close proximity of bounds, however, the results based on $\beta^*_1 = \gamma^*_1 = 0.03$ are still found to be reasonably good.

Degrading System

Figure 7.7(a) exhibits the time evolution of displacement and velocity responses of the degrading oscillator for the deterministic input in Fig. 7.2 with intensity $G_0 = 1.0 \times 10^5$. The results are compared again with those obtained from global models with two different estimates of β^*_1 and γ^*_1 as discussed earlier. As noted in nondegrading systems, excellent agreement between results of local and global models are also obtained here for degrading systems. The exact time evolution of β^*_1, γ^*_1, and $\delta^*_{A_1}$ in Eqs. 7.18 and 7.25 and the hysteretic variables $Z_{1l}(t)$ obtained from local model are also shown in Figs. 7.7(b) and 7.7(c), respectively.

Figure 7.7(c) also shows the time evolution of restoring forces $Q_1(t)$ and $Q^*_1(t)$ obtained from local and global hysteretic models. These story level restoring forces along with the column restoring forces $q_{1l}(t)$ and $q^*_{1l}(t)$ are also plotted against the displacement $U_1(t)$ in Fig. 7.8 providing various hysteretic loops. Results suggest that the global model with appropriate parameters can predict hysteretic structural response with very good accuracy.

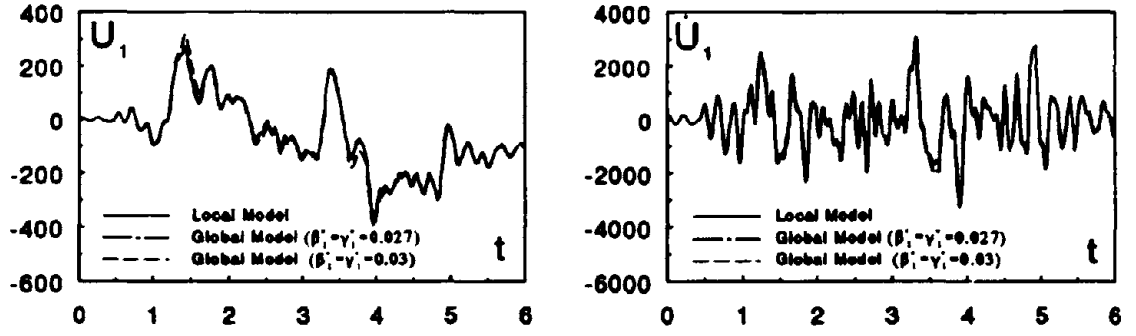

(a) Displacement and Velocity Response

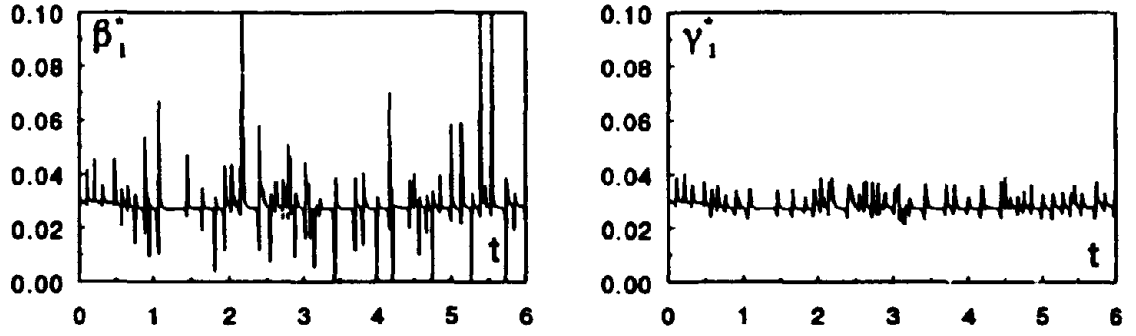

(b) Exact Global Parameters from Local Model

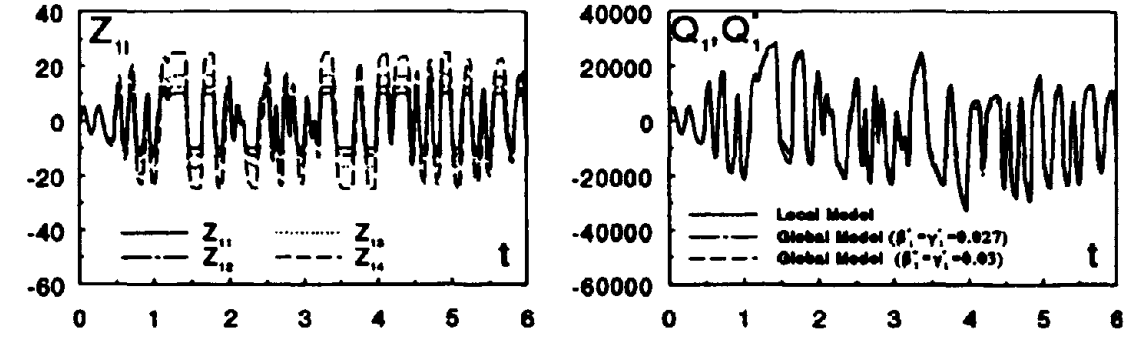

(c) Hysteretic Variables and Total Restoring Forces

Figure 7.5: Time History of Various Responses for Nondegrading System with $G_0 = 1.0 \times 10^7$

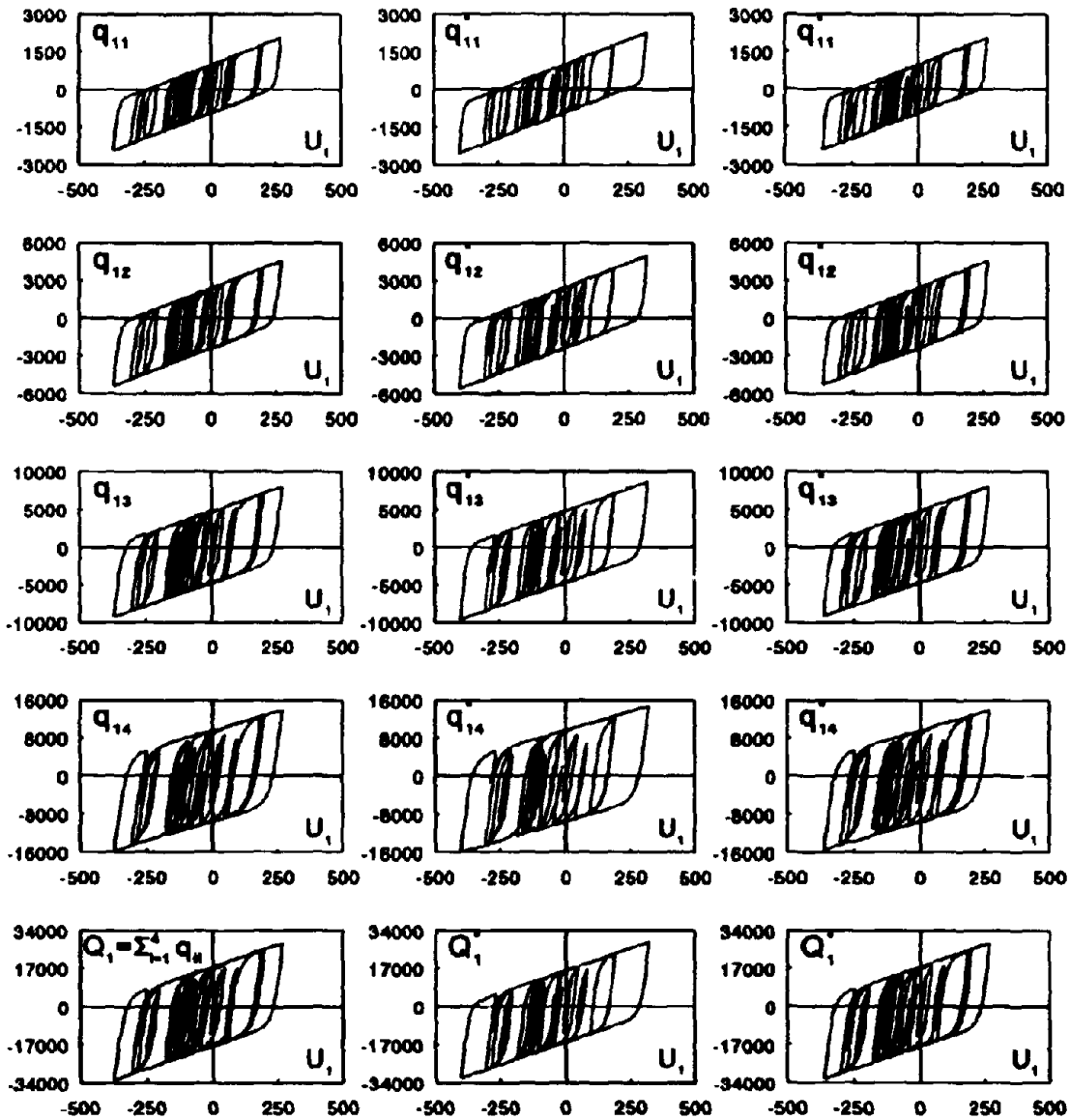

Figure 7.6: Hysteretic Loops for Nondegrading System with $G_0 = 1.0 \times 10^7$

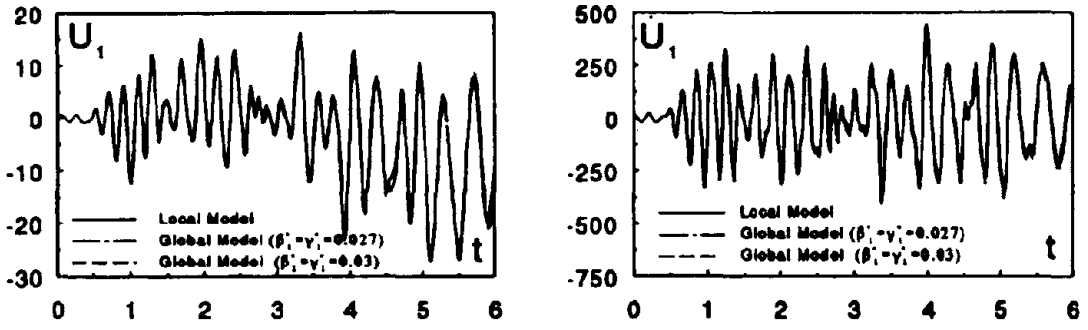

(a) Displacement and Velocity Response

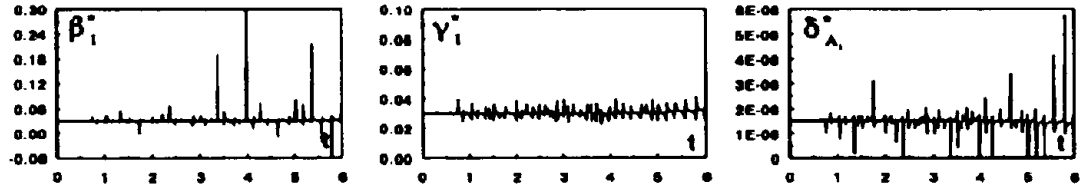

(b) Exact Global Parameters from Local Model

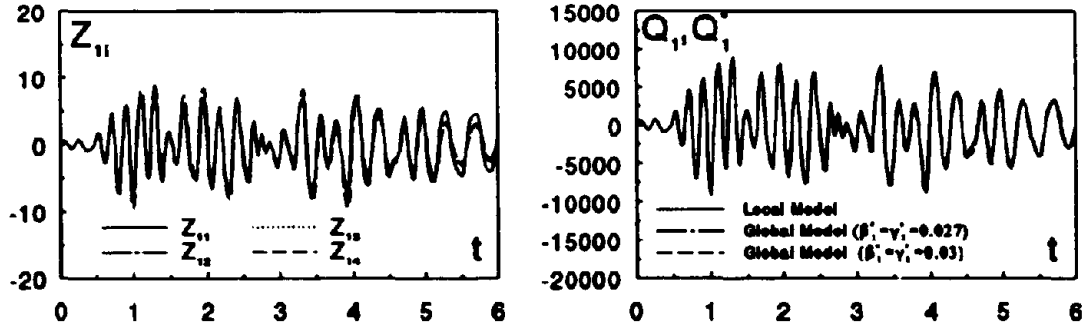

(c) Hysteretic Variables and Total Restoring Forces

Figure 7.7: Time History of Various Responses for Degrading System with $G_0 = 1.0 \times 10^5$

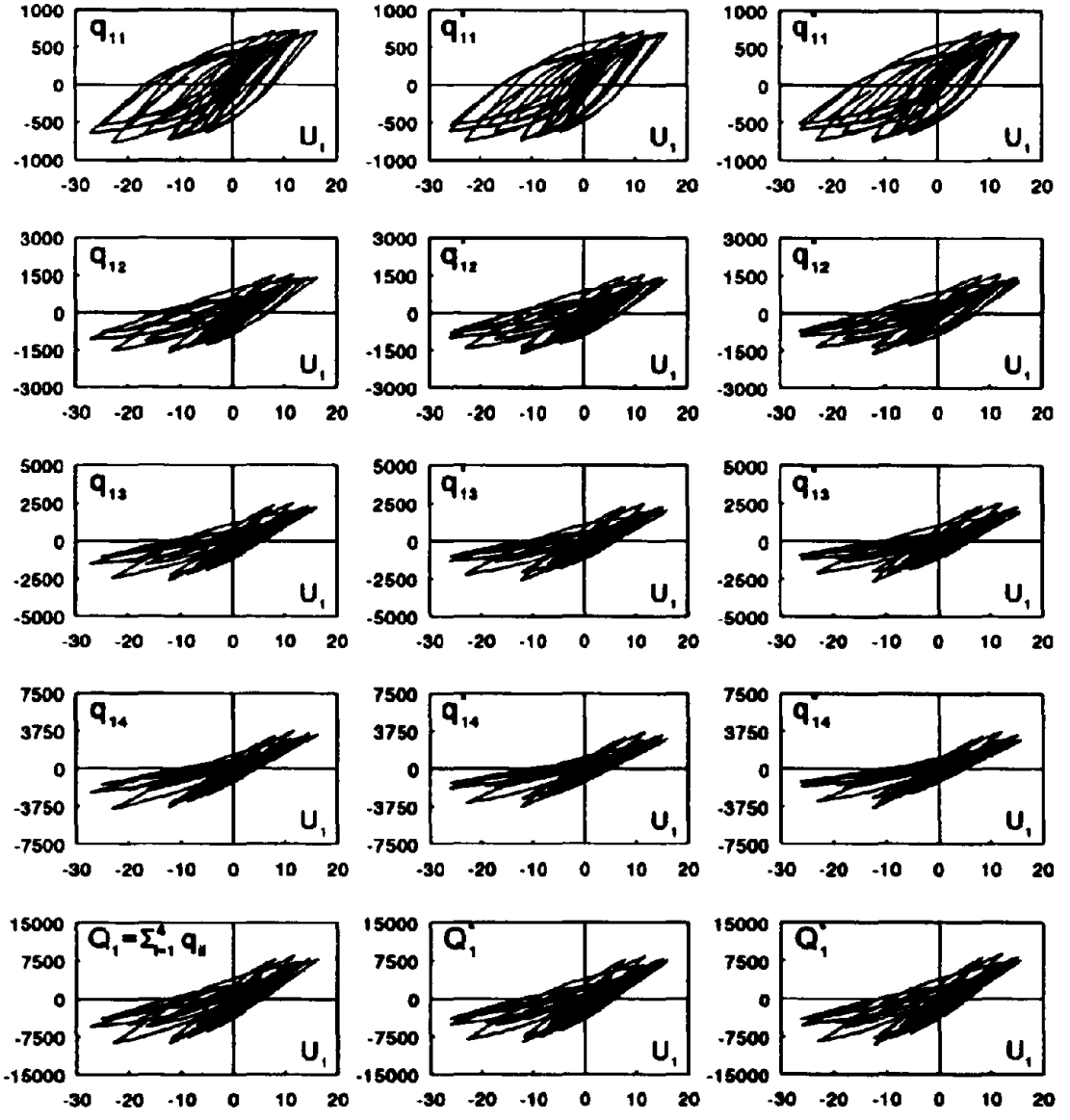

Figure 7.8: Hysteretic Loops for Degrading System with $G_0 = 1.0 \times 10^5$

7.3 Applications to Seismic Reliability Analysis

Current methods for evaluating seismic performance of structural systems are based on *lifetime maximum seismic hazard* without any provisions for cumulative damage among all seismic events during lifetime [169,171,177]. This single largest load effect is not physically realizable and it characterizes only an artificial seismic environment. Nevertheless, such hazard description is abundant in both deterministic and probabilistic seismic analysis. Since most structures are designed to resist several seismic events during their exposure time, the lifetime maximum ground motion may not be meaningful load process due to damage accumulation between consecutive seismic events. This is particularly true and unavoidable for a series of earthquakes including pre-shocks, main events, and after-shocks during which repairs of structural systems can not be performed. In this section, seismic reliability of degrading multi-story structures obtained from the lifetime maximum seismic hazard is evaluated by a new methodology based on a Markov model proposed in Section 6.

7.3.1 Seismic Hazard

Consider a site affected by a single seismic source characterized by a mean rate of earthquake occurrence λ. It is assumed that (i) the earthquake arrivals follow a homogeneous Poisson process with mean rate λ, (ii) ground motions in different seismic events are independent and identical stochastic processes $W^i(t)$, $i = 1, 2, \cdots, N(\tau)$ where $N(\tau)$ represents the random number of seismic events during lifetime period τ, and (iii) seismic event i has the same deterministic duration t_0.

Consider an elementary representation $W^i(t) = Y^i w(t)$ where $w(t)$ is a deterministic function of time representing either a synthetic or an actual ground acceleration with peak ground acceleration scaled to unity and Y^i is the random peak ground acceleration during ith seismic event with the independent and identical cumulative distribution function $F(y)$. Therefore, the cumulative distribution function of the largest peak ground acceleration Y_τ *during a lifetime period* τ is

$$F_\tau(y) \stackrel{\text{def}}{=} \Pr\left(\max_{1 \le i \le N(\tau)} \{Y^i\} \le y\right) = \exp\left[-\lambda\tau\{1 - F(y)\}\right]. \tag{7.28}$$

According to a study by Ellingwood *et al.* [65], $F_\tau(y)$ for $\tau = 50$ years can also be approximated by the *Extreme Type*-II distribution (see also Cornell [53])

$$\tilde{F}_{50}(y) = exp\left[-\left(\frac{y}{u}\right)^{-k}\right] \; ; \; y \geq 0 \tag{7.29}$$

with the parameters $k \simeq 2.3$ and $u = 0.38a_{10}$, where a_{10} is defined as the 10% upper fractile of Y_{50}. The peak ground acceleration a_{10} has been used by Algermissen *et al.* [3] to develop hazard maps of the entire continental United States. The distribution in Eq. 7.29 depends only on a_{10} without any explicit regard for the mean arrival rate of earthquakes. These issues are discussed in the previous sections of this report. Nevertheless, Eq. 7.29 will be used here as an approximation to the cumulative distribution function of Y_{50}. When Eq. 7.29 is substituted in Eq. 7.28 (with $\tau = 50\ yr$), the event distribution $F(y)$ can be obtained as

$$F(y) = 1 - \frac{1}{50\lambda}\left(\frac{y}{u}\right)^{-k} \tag{7.30}$$

for $y \geq u(50\lambda)^{-1/k}$ and *zero* otherwise.

Note that the stochastic model of ground acceleration considered here is quite elementary. The random nature of excitation is only due to the random variable description of peak ground acceleration (PGA) without any regard to the variability of its frequency content. Moreover, the probabilistic characteristics of PGA are also based on approximate equations. However, these simplified assumptions can be justified on the light of the objective of this study, *i.e.* to determine adequacy of current seismic reliability analysis based on lifetime largest load effect.

7.3.2 Nonlinear Degrading Systems

Consider the shear beam model of building systems in Fig. 7.1. The equation of motion for these structural systems and the associated hysteretic models are discussed in previous sections. Assume that all the parameters describing local restoring forces for the columns are available. Using the proposed equations, the parameters of global hysteretic model (at the story level) for these nonlinear systems can be readily calculated.

7.3.3 Current Performance Evaluation

Current estimates of seismic reliability analysis are based on a simplified representation of seismic hazard obtained from the largest load effect during the exposure time τ. Damage accumulation between consecutive seismic events is not considered in the analysis.

Consider a damage state vector $\mathbf{A}^{*,max} \in \Re^n$ obtained at the end of an earthquake $W_\tau(t) = Y_\tau w(t)$ of duration t_0, where Y_τ is the maximum peak ground acceleration (random) in time τ and $\Re^n$ is the n-dimensional real vector space. The state vector $\mathbf{A}^{*,max}$ can be mapped into a normalized damage state vector $\mathbf{D}^{max}$ with components

$$D_j^{max} = 1 - \frac{A^{*,max}{}_j}{A^{*,0}{}_j} \tag{7.31}$$

where $j = 1, 2, \cdots, n$ represents an index for the component of vectors $\mathbf{A}^{*,max} \in \Re^n$ and $\mathbf{D}^{max} \in \Re^n$ and $A^{*,0}{}_j$ is the initial value *i.e.* the jth component of $\mathbf{A}^*(0)$. Consider a domain $\mathcal{D} \subseteq \Re^n$ having $\Pr(\mathbf{D}^{max} \in \mathcal{D}) \simeq 1$ with $K = M^n$ cells (states) $\{C_p\}$ such that $\mathcal{D} = \cup_{p=1}^{K} C_p$, $C_p \cap C_q = \emptyset$ $(p \neq q)$, and M represents the number of discretized states of each component of $\mathbf{D}^{max} \in \Re^n$. Define a norm $\| \mathbf{D}^{max} \| \stackrel{\text{def}}{=} \max_{j=1}^{n} D_j^{max}$ of $\mathbf{D}^{max}$ representing lifetime largest story damage with its state space discretized into M distinct states $d_1, d_2, \cdots, d_M$. Let $\mathcal{C}_m \subseteq \mathcal{D} \subseteq \Re^n$ define a potential damage set of $\mathbf{D}^{max} \in \Re^n$ which comprises all the cells $C_j \in \mathcal{C}_m$ such that the largest component of $\mathbf{D}^{max}$ is in state d_m. Denote $\mathcal{Q}_m(\tau)$ as the lifetime probability that $\| \mathbf{D}^{max} \| \in d_m$ or $\mathbf{D}^{max} \in \mathcal{C}_m$. By successive conditioning and deconditioning, this lifetime probability can be obtained from the equation

$$\mathcal{Q}_m(\tau) \stackrel{\text{def}}{=} \Pr(\mathbf{D}^{max} \in \mathcal{C}_m) = \int_0^\infty I(\mathcal{C}; y) f_\tau(y) dy \simeq \sum_{k=1}^{\infty} I(\mathcal{C}; y_k) f_\tau(y_k) \Delta y_k \tag{7.32}$$

where $f_\tau(y) = dF_\tau(y)/dy$ is the probability density function of Y_τ and $I(\mathcal{C}; y_k)$ is an indicator variable which is equal to *one* if the sample of $\mathbf{D}^{max}$ due to a realization $y_k w(t)$ of ground motion $Y_\tau w(t)$ is such that $\mathbf{D}^{max} \in \mathcal{C}_m$ and *zero* otherwise.

7.3.4 Proposed Performance Evaluation

Damage State Vector

Consider a damage state vector $\mathbf{A}^{*,i} \in \Re^n$ obtained at the end of ith earthquake $W^i(t) = Y^i w(t)$ with the deterministic duration t_0. Similar to Eq. 7.31, the state vector $\mathbf{A}^{*,i}$ can also be mapped into a normalized damage state vector $\mathbf{D}^i$ by the relation

$$D_j^i = 1 - \frac{A^{*,i}{}_j}{A^{*,0}{}_j} \tag{7.33}$$

where $j = 1, 2, \cdots, n$ represents an index for the component of vectors $\mathbf{A}^i \in \Re^n$ and $\mathbf{D}^i \in \Re^n$. Note that the state vector $\mathbf{D}^i$ provides complete characterization of structural state at the end of earthquake i. Hence, one needs only $\mathbf{D}^i$ to perform dynamic analysis and determine structural performance through a new seismic event, because the vector defines the structural state uniquely.

When the earthquake is modeled as a filtered Poisson process with each seismic event assumed to be an independent random process, damage state vector $\mathbf{D}^i$ at the end of an ith event depends only on initial state $\mathbf{D}^{i-1}$ at the start of the event, and on that event itself. It is independent of damage and loading history up to the start of that event. In other words, the propagation of damage state vector $\mathbf{D}^i$ can be treated as Markov process evolving on a discrete time scale.

Transition Matrix

Consider a domain $\mathcal{D} \subseteq \Re^n$ having $\Pr(\mathbf{D}^i \in \mathcal{D}) \simeq 1$ with $K = M^n$ cells (states) $\{C_p\}$ such that $\mathcal{D} = \cup_{p=1}^{K} C_p$, $C_p \cap C_q = \emptyset$ $(p \neq q)$, and M represents the number of discretized states of each component of $\mathbf{D}^i \in \Re^n$. Consider the change in stochastic vector process $\mathbf{D}^i, i = 0, 1, 2, \cdots, N(\tau)$, taking values in a finite or countable number of cells $C_1, C_2, \cdots, C_K$. Let $\Pr(\mathbf{D}^i \in C_p)$ be the probability that damage state vector $\mathbf{D}^i$ is in cell C_p after i seismic events. Then row vector $\mathbf{P}(i) = \{\Pr(\mathbf{D}^i \in C_1), \Pr(\mathbf{D}^i \in C_2), \cdots, \Pr(\mathbf{D}^i \in C_K)\}$ gives the probability that $\mathbf{D}^i$ belongs to any of the cells $C_1, C_2, \cdots, C_K$.

The evolution of a discrete version of $\mathbf{D}^i$ can be described by *one-step transition matrix* $\mathbf{T} \in \mathcal{L}(\Re^K \times \Re^K)$ with the element T_{pq} representing the probability that damage changes from state p to state q due to a single seismic event where $\mathcal{L}(\Re^K \times \Re^K)$ symbolizes

a set of linear mapping from $\Re^K$ to $\Re^K$. This transition probability T_{pq} can be obtained following similar considerations as in Eq. 7.32 and is given by

$$T_{pq} \stackrel{\text{def}}{=} \Pr\left(\mathbf{D}^i \in C_q | \mathbf{D}^{i-1} \in C_p\right) = \int_0^\infty I(C_p, C_q; y) f(y) dy \simeq \sum_{k=1}^{\infty} I(C_p, C_q; y_k) f(y_k) \Delta y_k \tag{7.34}$$

where $f(y) = dF(y)/dy$ is the probability density function of Y^i and $I(C_p, C_q; y_k)$ is another indicator variable which is equal to *one* if the samples of $\mathbf{D}^i$ and $\mathbf{D}^{i-1}$ due to a realization $y_k w(t)$ of ground motion $Y^i w(t)$ are such that $\mathbf{D}^i \in C_q | \mathbf{D}^{i-1} \in C_p$ and *zero* otherwise.

Evolution of Distribution of $\mathbf{D}^i$

Consider a K-dimensional row vector which prescribes the joint probability mass function of the random vector $\mathbf{D}^i$ denoting damage after ith seismic event. The probability of $\mathbf{D}^i$ following i seismic events is

$$\mathbf{P}(i) = \mathbf{P}(i-1)\mathbf{T} \ , \ i = 1, 2, ..., N(\tau) \tag{7.35}$$

which can be used recursively to reach

$$\mathbf{P}(i) = \mathbf{P}(0)\mathbf{T}^i. \tag{7.36}$$

Consider again a norm $\| \mathbf{D}^i \| \stackrel{\text{def}}{=} \max_{j=1}^{n} D_j{}^i$ of $\mathbf{D}^i$ representing largest story damage after ith seismic event. As before, suppose that the state space of $\| \mathbf{D}^i \|$ can be discretized into M distinct states $d_1, d_2, \cdots, d_M$. Let $C_m \subseteq \mathcal{D} \subseteq \Re^n$ define a potential damage set of $\mathbf{D}^i \in \Re^n$ which comprises all the cells $C_j \in C_m$ such that the largest component of $\mathbf{D}^i$ is in state d_m. This time, denote $Q_m(i)$ as the event probability that $\| \mathbf{D}^i \| \in d_m$ or $\mathbf{D}^i \in C_m$ which can be obtained from

$$Q_m(i) = \sum_{C_j \in C_m} P_j(i) \tag{7.37}$$

in which $P_j(i)$ is the jth component of $\mathbf{P}(i)$ representing the probability that $\mathbf{D}^i$ belongs to the cell C_j.

Lifetime Distribution

The lifetime probability distribution $\mathbf{P}(\tau)$ defined as the distribution of damage index vector $\mathbf{D}^{N(\tau)}$ in lifetime τ can be obtained as

$$\mathbf{P}(\tau) = \mathbf{P}(0)\exp(-\lambda\tau[\mathbf{I} - \mathbf{T}]) \tag{7.38}$$

where $\mathbf{I}$ is the K-dimensional identity matrix.

Consider the damage set $\mathcal{C}_m \subseteq \mathcal{D}$ with the largest component of damage state vector in state d_m. Denote $\mathcal{Q}_m(\tau)$ as the lifetime probability that $\| \mathbf{D}^{N(\tau)} \| \in d_m$ or $\mathbf{D}^{N(\tau)} \in \mathcal{C}_m$. This probability can be obtained from

$$\mathcal{Q}_m(\tau) = \sum_{C_j \in \mathcal{C}_m} P_j(\tau) \tag{7.39}$$

in which $P_j(\tau)$ is the jth component of $\mathbf{P}(\tau)$ representing the lifetime probability that $\mathbf{D}^{N(\tau)}$ belongs to the cell C_j.

7.3.5 Numerical Example

Example 7.2

Structural System

Consider a 5-story building frame designed according to the *Uniform Building Code* [100] for seismic zone-4. The building has 4 columns ($n_k = 4$) at each story and is idealized as a 5-degree-of-freedom shear beam system (stick model) with one degree of freedom per story. The lumped masses are $m_1 = m_2 = m_3 = m_4 = 0.0898\ kN\ s^2\ mm^{-1}$ for the first (bottom) to fourth stories and $m_5 = 0.0762\ kN\ s^2\ mm^{-1}$ for the fifth (top) story. The viscous damping coefficients are $c_1 = 0.844\ kN\ s\ mm^{-1}$, $c_2 = 0.638\ kN\ s\ mm^{-1}$, $c_3 = 0.491\ kN\ s\ mm^{-1}$, $c_4 = 0.390\ kN\ s\ mm^{-1}$, and $c_5 = 0.288\ kN\ s\ mm^{-1}$ for the bottom to top stories. The damping is assumed to be proportional to the initial stiffness matrix and the values of above damping coefficients correspond to 3% of critical for the first mode. Table 7.1 provides the lateral stiffness and strength properties of columns along with the parameters of local

Table 7.1: Column Properties and Hysteretic Parameters of Local Model

Story (k)	Column (l)	Stiffness k_{kl} (kN/mm)	Strength (kN)	$A_{kl}(0)$	β_{kl}	γ_{kl}	μ_k	$\delta_{A_{kl}}$	α_{kl}
1	1	19.22	91.23	1	0.064	-0.021	2	3.00E-5	0.02
	2	46.89	272.53	1	0.043	-0.014	2	3.00E-5	0.02
	3	46.89	272.53	1	0.043	-0.014	2	3.00E-5	0.02
	4	19.22	91.23	1	0.064	-0.021	2	3.00E-5	0.02
2	1	19.22	114.45	1	0.041	-0.014	2	3.36E-5	0.02
	2	30.78	224.36	1	0.027	-0.009	2	3.36E-5	0.02
	3	30.78	224.36	1	0.027	-0.009	2	3.36E-5	0.02
	4	19.22	114.45	1	0.041	-0.014	2	3.36E-5	0.02
3	1	19.22	129.44	1	0.032	-0.011	2	3.54E-5	0.02
	2	19.22	161.82	1	0.021	-0.007	2	3.54E-5	0.02
	3	19.22	161.82	1	0.021	-0.007	2	3.54E-5	0.02
	4	19.22	129.44	1	0.032	-0.011	2	3.54E-5	0.02
4	1	11.34	68.63	1	0.039	-0.013	2	3.36E-5	0.02
	2	19.22	142.42	1	0.026	-0.009	2	3.36E-5	0.02
	3	19.22	142.42	1	0.026	-0.009	2	3.36E-5	0.02
	4	11.34	68.63	1	0.039	-0.013	2	3.36E-5	0.02
5	1	11.34	48.17	1	0.080	-0.027	2	3.54E-5	0.02
	2	11.34	58.94	1	0.053	-0.018	2	3.54E-5	0.02
	3	11.34	58.94	1	0.053	-0.018	2	3.54E-5	0.02
	4	11.34	48.17	1	0.080	-0.027	2	3.54E-5	0.02

hysteretic model for the columns at each story. All the structural characteristics are assumed to be deterministic.

Evaluation of Global Hysteretic Model

The information regarding the parameters of local constitutive law for the columns at each story is used to compute the parameters of the global hysteretic model. The global model describes the restoring force at each story and its parameters are determined from the Eqs. 7.15, 7.17, 7.19, and 7.26 proposed earlier. Table 7.2 provides the estimated values of these global parameters for each story.

In order to evaluate the global parameters, a numerical investigation is carried out for this 5-story building structure regarding deterministic structural behavior due to both local

Table 7.2: Hysteretic Parameters of Global Model

Story (k)	k^*_k (kN/mm)	β^*_k	γ^*_k	μ^*_k	A^*_k	$\delta^*_{A_k}$	α^*_k
1	132.22	0.049	-0.016	2	1	8.85E-6	0.02
2	100.00	0.032	-0.011	2	1	8.85E-6	0.02
3	76.88	0.026	-0.009	2	1	8.85E-6	0.02
4	61.12	0.031	-0.010	2	1	8.85E-6	0.02
5	45.36	0.067	-0.022	2	1	8.85E-6	0.02

and global models. A classical seismogram of *1940 El Centro* (NS Component) earthquake with varying peak ground accelerations (PGA) is used as deterministic input to this system. The above ground acceleration with scaled PGA equal to $1.0g$ ($1.0g = 9.81\ m/s^2$) is shown in Fig. 7.9(a).

Consider the normalized damage indices $\hat{A}^*_k(t)$ and $\hat{A}_k(t)$ defined as

$$\hat{A}^*_k(t) = 1 - \frac{A^*_k(t)}{A^*_k(0)} \quad \text{and} \quad \hat{A}_k(t) = 1 - \frac{\sum_{l=1}^{4} w_{kl} A_{kl}(t)}{\sum_{l=1}^{4} w_{kl} A_{kl}(0)} \tag{7.40}$$

in which $A^*_k(t)$ and $A_{kl}(t)$ are the time-variant degrading parameters of local and global restoring forces. In both cases, $\hat{A}^*_k(t)$ and $\hat{A}_k(t)$ represent the damage indices at the kth story obtained from local and global models, respectively.

Figures 7.9(b)-(f) show the time evolution of the damage indices $\hat{A}^*_k(t)$ and $\hat{A}_k(t)$ at the kth story ($k = 1, 2, \cdots, 5$) which is obtained for deterministic seismic ground acceleration in Fig. 7.9(a) with various PGA = $0.2g$, $0.4g$, and $1.0g$. It is assumed that $A_{kl}(0) = 1$, and hence, $A^*_k(0) = 1$ from Eq. 7.17. Comparisons of results associated with local and global constitutive law suggest that the global hysteretic model with its parameters estimated from proposed equations can predict structural damage with very good accuracy.

From the above numerical verification, it is now possible to perform seismic analysis based on global model. Thus, the story level damage state vector $\mathbf{A}^{*,i}$ or its normalized version $\mathbf{D}^i$ (Eq. 7.33) can be assumed to be Markovian thus allowing significant reduction in the computational involvement for the construction of transition matrices.

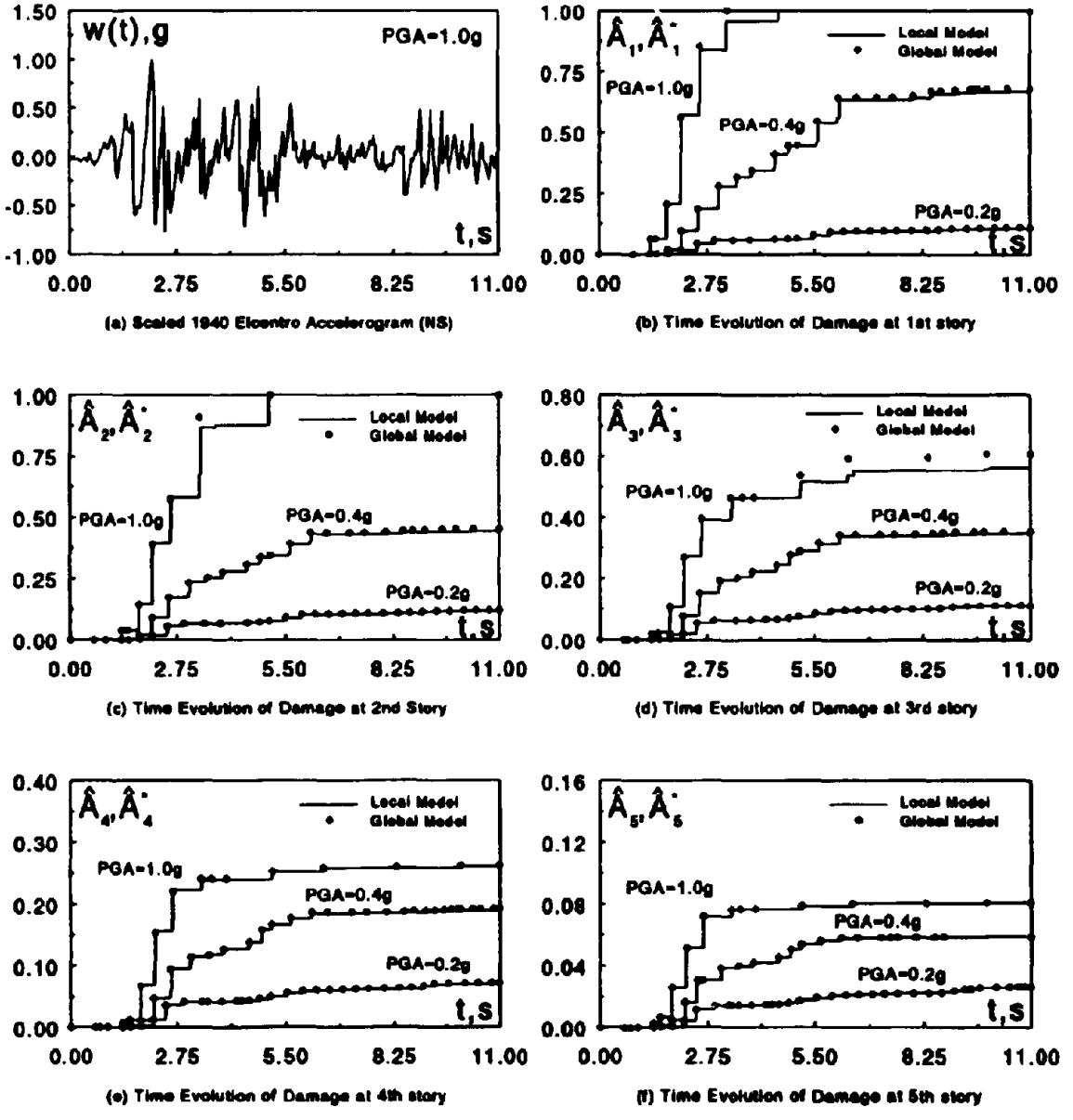

Figure 7.9: Damage Indices due to Deterministic Analysis of a 5-story Building Frame

Seismic Environment

Consider two sites C and D in the western United States with $\lambda = 0.36\ yr^{-1}$, $a_{10} = 0.40g$, and $\lambda = 0.67\ yr^{-1}$, $a_{10} = 0.46g$, respectively. Several counties of California can be identified with the seismic parameters close to above sites such as *Mendocino* and *Sonoma* ($\lambda = 0.3581\ yr^{-1}$ $a_{10} = 0.4g$), *Orange* ($\lambda = 0.3584\ yr^{-1}$ $a_{10} \simeq 0.4g$), *San Diego* ($\lambda = 0.32\ yr^{-1}$ $a_{10} = 0.41g$), *Monterey* ($\lambda = 0.67\ yr^{-1}$ $a_{10} = 0.46g$), and others [3]. They all fall in the same seismic zone-4 of *Uniform Building Code* [100] resulting in identical structural designs for buildings. The ground motion in each seismic event is represented by a deterministic time function multiplied by a random peak ground acceleration. The function $w(t)$ is assumed to be the scaled *1940 El Centro* (NS component) accelerogram truncated at 11 seconds and is shown in Fig. 7.9(a). The probabilistic characteristics of peak ground accelerations are obtained from the Eqs. 7.29 and 7.30.

Structural Response and Reliability

Consider a normalized damage state vector $\mathbf{D}^i \in \Re^5$ with the components describing story damages after ith seismic event. Suppose, a component $D_j{}^i$ ($j = 1,2,3,4,5$) of $\mathbf{D}^i$ representing damage at the jth story is discretized into 4 ($M = 4$) non-overlapping states $d_1 = (0.0, 0.2)$, $d_2 = (0.2, 0.4)$, $d_3 = (0.4, 0.6)$, and $d_4 = (0.6, 1.0)$ as shown in Fig. 7.10. Hence, $\mathbf{D}^i$ can take on $K = 4^5 = 1024$ number of distinct states (cells) in the domain $\mathcal{D} \in \Re^5$. Thus, the transition matrix $\mathbf{T}$ has dimension 1024×1024. However, if all the cells associated with the largest component of $\mathbf{D}^i$ (i.e., the largest story damage) being greater than 0.6 are assumed to be *absorbing* states (i.e., states once entered they are never left), the dimension of $\mathbf{T}$ dramatically reduces to 244×244 ($3^5 + 1 = 244$). In this example, the transition matrix $\mathbf{T}$ is constructed based on the reduced dimension 244×244 and its elements are obtained by using Eq. 7.34. The nonlinear dynamic analysis is carried out by explicit numerical scheme such as fifth- and sixth-order Runge-Kutta integrators.

Consider the state space of largest story damage $\| \mathbf{D}^i \| \stackrel{\text{def}}{=} \max_{j=1}^{5} D_j{}^i$ which is discretized into 4 ($M = 4$) distinct states d_1, d_2, d_3, and d_4 defined earlier. Fig. 7.11 shows the evolution of event probability $Q_m(i) = \Pr(\| \mathbf{D}^i \| \in d_m)$, $m = 1$, 2, 3, and 4 of the largest

story damage $\| \mathbf{D}^i \|$ in Eq. 7.37 starting with an initially undamaged state for both sites C and D. The plots provide useful information regarding rates of probability flow among different damage sets which cannot be obtained unless damage accumulation is permitted between seismic events. It is assumed that the undamaged state mentioned above can be characterized by an initial state with ${D_j}^0 \in d_1$ for $j = 1, 2, \cdots, 5$. This defines the initial probability vector $\mathbf{P}(0)$ in Eqs. 7.36 and 7.38 to compute event and lifetime probabilities.

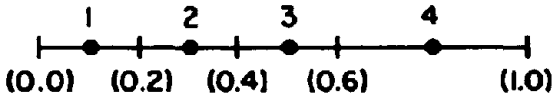

Figure 7.10: Discretization of Sample Space of ${D_j}^i$

Consider several cases of deterministic initial states of structural system. They are as follows: ${D_j}^0 \in d_1$, $j = 1, 2, \cdots, 5$ (Case-1); ${D_1}^0 \in d_2$, ${D_j}^0 \in d_1$, $j = 2, 3, \cdots, 5$ (Case-2); and ${D_1}^0 \in d_3$, ${D_j}^0 \in d_1$, $j = 2, 3, \cdots, 5$ (Case-3). In all three cases, the first story is assigned unabsorbing states of progressive damage (*i.e.*, d_1, d_2, and d_3) while all the top stories are assigned lowest possible damage state (*i.e.*, d_1). Table 7.3 shows the lifetime probabilities $Q_m(\tau) = \Pr(\| \mathbf{D}^{N(\tau)} \| \in d_m)$, m = 1, 2, 3, and 4 of the largest story damage $\| \mathbf{D}^{N(\tau)} \|$ with $\tau = 50\ yr$ starting with various cases of initial states for sites C and D. The tabulated results are obtained by both Markov model (Eq. 7.39) and current estimate (Eq. 7.32). They indicate that the lifetime probabilities based on lifetime largest load effect can be both unconservative and conservative depending on site conditions when compared with that obtained from seismic hazard based on damage accumulation between seismic events.

Table 7.4 illustrates the lifetime probabilities by Markov model in sites C and D for $\tau = 50\ yr$ with a uniform distribution of initial damage state, *i.e.*, when $\mathbf{P}(0) = \frac{1}{244}\{1, 1, \cdots, 1\}$. Due to uncertain initial states, the probabilities can still be obtained directly from Eq. 7.38 and previous transition matrices. Results suggest that the uncertainty in the initial condition can yield significant variation on seismic reliability estimates.

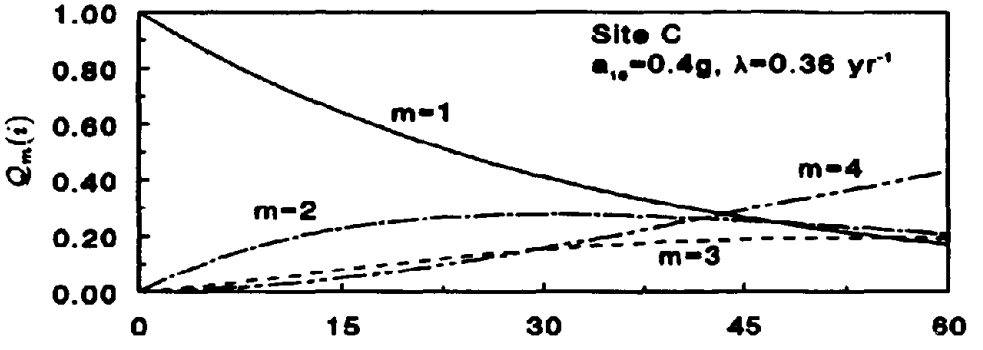

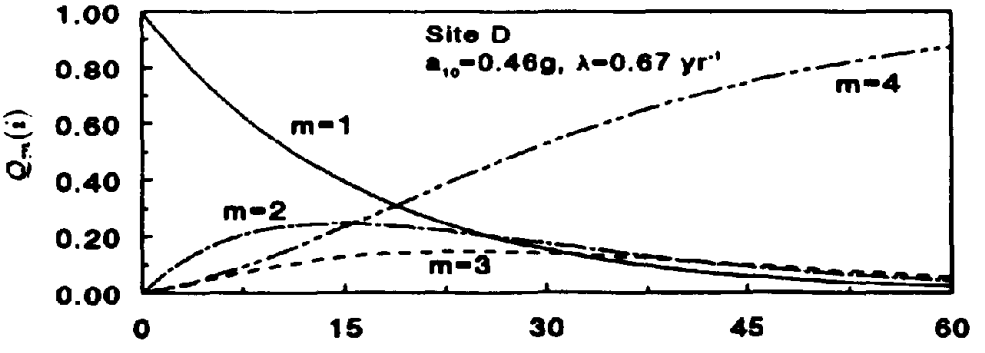

Figure 7.11: Evolution of Distribution of $\| \mathbf{D}^i \|$

Table 7.3: Lifetime Probabilities with Deterministic Initial States

Methods	Cases	$Q_m(\tau) = \Pr(\| \mathbf{D}^{N(\tau)} \| \in d_m)$							
		Site C				Site D			
		$m=1$	$m=2$	$m=3$	$m=4$	$m=1$	$m=2$	$m=3$	$m=4$
Markov	Case-1	0.592	0.241	0.097	0.070	0.132	0.155	0.132	0.581
Model	Case-2	0.000	0.482	0.209	0.309	0.000	0.079	0.065	0.856
(Eq. 7.39)	Case-3	0.000	0.000	0.304	0.696	0.000	0.000	0.015	0.985
Current	Case-1	0.592	0.246	0.036	0.126	0.398	0.355	0.078	0.169
Estimate	Case-2	0.000	0.417	0.292	0.291	0.000	0.299	0.323	0.378
(Eq. 7.32)	Case-3	0.000	0.000	0.185	0.815	0.000	0.000	0.194	0.806

Table 7.4: Lifetime Probabilities with Uncertain Initial States

Sites	$Q_m(\tau) = \Pr(\| \mathbf{D}^{N(\tau)} \| \in d_m)$			
	$m=1$	$m=2$	$m=3$	$m=4$
Site C	0.002427	0.068973	0.427373	0.501227
Site D	0.000539	0.013461	0.060988	0.925012

SECTION 8
Conclusions

8.1 Introduction

Research in this study focused on several important issues of probabilistic seismic performance of structural systems. Three major directions of research had been pursued. They involved (*i*) evaluation of effects of simplifications in reliability-based design codes, (*ii*) development of a new methodology based on Markov model for seismic reliability of degraded structures, and (*iii*) development of an analytical approach to establish relations between local and global damage indices for seismic analysis of shear type buildings. The conclusions from each of these studies are summarized below.

8.2 Reliability-Based Design Codes

One of the major objectives of this study was the evaluation of effects of simplifications used in current seismic design and reliability analysis. The evaluation procedure was based on both static and dynamic reliability methods. They were applied to determine seismic reliability of simple structures modeled as nondegrading systems and multi-story buildings with degrading material models.

8.2.1 Nondegrading Systems

Reliability measures for simple structures designed by *Uniform Building Codes* subjected to earthquake loading were determined using both static and dynamic methods and strength-based and damage-related limit states. Results showed that:

- reliability depends on the mean arrival rate and the intensity of the seismic load process. Sites with frequent small earthquakes have very different reliability indices than those at sites with infrequent large earthquakes, although the sites are characterized by the same value of a_{10};

- *event* and *lifetime* reliabilities of the designs can differ significantly particularly at sites with frequent small earthquakes; and
- designs at sites with frequent small events have larger event reliabilities than those at sites with rare large events. However, lifetime reliability suggest that the design can be either safe or unsafe when the two sites are compared.

8.2.2 Degrading Systems

A 5-story, 3-bay rectangular R/C frame was analyzed and designed in accordance with the appropriate provisions of *1985 Uniform Building Code* (UBC) and *ACI Code 318-83* for Seismic *Zones*-2 and -3. The structural stress analysis was based on linear-elastic static method. The probabilistic analysis involved elementary strength-based failure criteria at a particular structural component and was performed by FORM/SORM and Importance Sampling methods. Effects of structural redundancy, nonlinear dynamic response, and damage accumulation were not included in this simplified approach. It was found by the static reliability method that the minimum member level reliability indices can be as low as 1.50 and 1.30 for seismic zone-2 ($a_{10} = 0.2g$) and zone-3 ($a_{10} = 0.4g$), respectively.

The reliability indices for the above frames were re-evaluated based on nonlinear dynamic analysis of degrading multi-story buildings. The probabilistic analysis involved damage-related failure criteria and was performed by direct Monte Carlo simulation. Results from the dynamic reliability method indicated that the minimum values of component reliability indices were 5.13 and 2.91 for the two seismic zones mentioned earlier. Comparisons between the estimates from the static and dynamic methods indicate that the seismic reliability is underestimated by the static method.

8.3 A Markov Model For Seismic Reliability Analysis

A major goal of this research was the development of guidelines for seismic design that can rationally account for particular features of seismic hazard, mechanical characteristics of structural systems, and likely failure modes. In this regard, a new methodology based

on a Markov model was proposed to evaluate seismic performance and sensitivity to initial state of structural systems and determine the vulnerability of structures exposed to one or more earthquakes. The analysis involved simple but realistic characterization of seismic hazard, nonlinear dynamic analysis for estimating structural response, uncertainty in the initial state of structural systems, and failure conditions incorporating damage accumulation during consecutive seismic events.

The Markov model, developed in this study, is based on theoretical development using general hysteretic restoring force characteristics which can be applied to both reinforced concrete and steel structures. It can estimate both *event* and *lifetime* reliabilities thus providing a designer more control in seismic performance evaluation. It can be used to determine the damage probability evolution during several earthquakes allowing investigation on seismic vulnerability of new and existing structures. The model can be used to compute mean first passage time determining average number of seismic events before the structure will suffer potential damage. It can also evaluate sensitivity of seismic reliability due to the variability in the initial state of structural systems.

The proposed model was applied to evaluate seismic reliability measures of simple code-designed structures. Results showed that the designs by the *Uniform Building Code* can have very different reliabilities at sites with frequent small earthquakes and infrequent large earthquakes, although the sites were characterized by the same value of a_{10}. Similar findings were also obtained when the reliabilities were calculated for nondegrading systems.

The uncertainty regarding initial condition can yield significant variation on seismic reliability. Since, variability regarding initial conditions can play a significant role in seismic reliability estimate, it is desirable that any reliability scheme has provisions of uncertain initial condition(s). Using the Markov structure, this was accomplished here with little effort.

A small increase in the dimension of damage state vector representing state of structural systems is associated with comparatively large increase in the order of transition matrix. Correspondingly, the computational involvement in obtaining transition probabilities may become significant.

8.4 Local and Global Damage Indices

A global hysteretic model was developed and the relations between the parameters of local and global models were established for seismic analysis of multi-story shear buildings. In both models, the analysis involved hysteretic constitutive laws commonly used in earthquake engineering to represent restoring forces and nonlinear dynamic analysis for estimating seismic structural response. From the proposed relations, the local hysteretic behavior and damage can be recovered from analysis based on global models. Using current global indices based on heuristic combination of local damage measures, this was not possible due to the lack of unique relation between local and global damages.

Both nondegrading and degrading systems were considered and several numerical examples on single- and multi-degree-of-freedom systems of shear beam models were presented to illustrate the proposed methodology. First, a single-degree-of-freedom system with both nondegrading and degrading restoring forces was investigated to evaluate the adequacy of global hysteretic model in predicting various seismic response characteristics. Second, a multi-degree-of-freedom system with more realistic design and earthquake loading was studied to compare damage measures by both local and global hysteretic models. In all cases, results showed that the global model can provide satisfactory estimates of seismic response and damage characteristics when compared with those obtained from the analysis based on local model. The plots of restoring forces versus displacement, which represent the hysteretic loops, were also well-predicted by the global model. When the local hysteretic characteristics were recovered from dynamic analysis based on global model, they were found to be in excellent agreement with the results produced by the local model.

In both local and global models, the dynamic stress analysis can be viewed as a nonlinear initial-value problem. However, the dimension of global initial-value problem is much smaller than that of local initial-value problem. Hence, significant savings of computational resources, such as Central Processing Units and core memory, can be achieved by using the proposed global model.

The correlation equations were also applied to implement the Markov model developed in the earlier phase of this study for estimating seismic performance of multi-story

degrading structures. Such model facilitates a systematic investigation on the validity of current seismic reliability practice which are based on lifetime largest seismic hazard without any consideration of cumulative damage during consecutive seismic events. A numerical example based on a 5-story building structure designed by the *1988 Uniform Building Code* was presented. Effects of uncertainty in the initial state of system on the seismic structural performance were also investigated. Results showed that (*i*) seismic reliability based on lifetime largest load effects can differ significantly from that obtained from seismic hazard based on damage accumulation between seismic events and (*ii*) the uncertainty regarding initial condition can yield significant variation in the seismic reliability estimate.

SECTION 9
References

[1] Abrams, D. P., and Sozen, M. A., "Experimental Study of Frame-Wall Interaction in Reinforced Concrete Structures Subjected to Strong Earthquake Motions," Civil Engineering Studies, *Structural Research Series No. 460*, University of Illinois at Urbana-Champaign, Urbana, Illinois, March 1979.

[2] Algermissen, S. T., An Introduction to the Seismicity of the United States, Monograph Series, Earthquake Engineering Research Institute, Berkeley, California, 1983.

[3] Algermissen, S. T., Perkins, D. M., Thenhaus, P. C., Hanson, S. L. and Bender, B. L., "Probabilistic Estimates of Maximum Acceleration and Velocity in Rock in the Contiguous United States," *U.S. Geological Survey Open-File Report*, 82 – 1033, 1982.

[4] Algermissen, S. T., and Perkins, D. M., "A Probabilistic Estimateof Maximum Acceleration in Rock in the Contiguous United States," *U.S. Geological Survey Open-File Report*, 76 – 416, 1976.

[5] Algermissen, S. T., "Seismic Risk Studies in the United States," *Proceedings of the 4th World Conference on Earthquake Engineering*, San Francisco, Vol. IV, pp. 459-466, 1984. Vol. 1, pp. 14-27, Santiago, Chile, 1969.

[6] Akiyama, H., Earthquake Resistant Limit-State Design for Buildings, University of Tokyo Press, 1985.

[7] Allen, F., Darvall, P., "Lateral Load Equivalent Frame," *ACI Journal*, Proceedings, No. 7, pp. 294-299, July 1977.

[8] Allen, D. E., "Limit States Design - A Probabilistic Study, " *Canadian Journal of Civil Engineering*, Vol. 2, No. 1, pp. 36-49, 1976.

[9] American Concrete Institute, "Building Code Requirements for Reinforced Concrete," *ACI Standard 318-83*, Detroit, Michigan.

[10] American National Standard Institute, "Minimum Design Loads for Buildings and Other Structures," ANSI A58.1-1982, New York, New York.

[11] Amin, M., and Ang, A. H.-S., "Nonstationary Stochastic Models of Earthquake," *Journal of Engineering Mechanics*, ASCE, Vol. 94, No. EM2, pp. 559-583, April 1968.

[12] Amin, M., and Ang, A. H.-S., "A Nonstationary Stochastic Model for Strong Motion Earthquakes," *F-UI-306*, University of Illinois, Urbana, 1966.

[13] Anagnostopoulos, S. A., "Non-linear Dynamic Response and Ductility Requirements of Building Structures Subjected to Earthquakes," Optimum Seismic Protection and Building Damage Statistics, Report No. 3, Dept. of Civil Engineering, *MIT Publication No. R72-54*, Cambridge, Massachusetts, September 1972.

[14] Aoyama, H., "A Quick Analysis of the Imperial County Services Building for Seismic Resistance," *Second Meeting on the Evaluation of Structures for Seismic Hazard*, Berkeley Marina, California, 1984.

[15] Aoyama, H., "A Method for the Evaluation of the Seismic Capaciacity of Existing Buildings," *Bull. New Zealand National Society for Earthquake Engineering*, Vol. 14, No. 3, 1981, pp 17 – 42.

[16] Applied Technolgy Council, "Tentative Provisions for the Development of Seismic Regulations for Buildings," *National Bureau of Standards Special Publication No. SP* 510, *ATC*3 – 06, Washington, D.C., June 1978.

[17] Atalay, M. B., and Penzien, J., "The Seismic Behavior of Critical Regions of Reinforced Concrete Components as Influenced by Moment, Shear, and Axial Forces," *Report No. EERC-75-19*, University of California, Berkeley, California, December 1975.

[18] Atalik, T. S., and Utku, S., "Stochastic Linearization of Multidegree of Freedom Nonlinear Systems," *Earthquake Engineering and Structural Dynamics*, Vol. 4., pp. 411-420, 1976.

[19] Baber, T. T., and Noori, M. N., "Random Vibration of Pinching Hysteretic Systems," *Report No. UVA/526378/CE84/102*, University of Virginia, Virginia, September 1983.

[20] Baber, T. T. and Wen, Y. -K., "Random Vibration of Hysteretic Degrading Systems," Jour. of Engr. Mech, ASCE, 107(6), 1069-1087, 1981.

[21] Baber, T. T. and Wen, Y. -K., "Stochastic Equivalent Linearization for Hysteretic Degrading Multistorey Structures", *Structural Research Series No. 471*, Dept. of Civil Engineering, Univ. of Illinois at Urbana-Champaign, 1980.

[22] Banon, H., and Veneziano, D., "Seismic Safety of Reinforced Members in Structures," *Earthquake Eng. Struc. Dyn.*, 10(2), 1982.

[23] Bathe, K. J., Finite Element Procedures in Engineeering Analysis, Prentice-Hall, Inc., Englewood Cliffs, New Jersey, 1982.

[24] Bathe, K. J., and Wilson, E. L., Numerical Methods in Finite Element Analysis, Prentice-Hall, Inc., Englewood Cliffs, New Jersey, 1976.

[25] Bazant Z.P., Kriezek R.J. and Shieh C. L., Hysteretic Endochronic Theory for Sand, J. of Engineering Mech., ASCE, 109(4), pp.1073-1095, 1983.

[26] Berg, G. V., "Response of Multistory Structures to Earthquakes," *Journal of Engineering Mechanics*, ASCE, Vol. 87, No. EM2, pp. 1-16, April 1961.

[27] Berg, G. V., "Dynamic Analysis of Elasto-Plastic Structures," *Journal of Engineering Mechanics*, ASCE, Vol. 86, No. EM2, pp. 35-38, April 1960.

[28] Bertero, V. V., and Bresler, B., "Design and Engineering Decision: Failure Criteria (Limit States), Developing Methodologies for Evaluating the Earthquake Safety of Existing Buildings," *Report No. EERC-77-6*, University of California, Berkeley, California, February 1977.

[29] Bertero, V. V., and Bresler, B., "Developing Methodologies for Evaluating the Earthquake Safety of Existing Buildings," *Report No. UCB-EERC-77-06*, University of California, Berkeley, CA, 1971.

[30] Bjerager, P., "Probability Integation by Directional Simulation," *Journal of Engineering mechanics*, ASCE, Vol. 114, No. 8, pp. 1285-1302, August 1988.

[31] Blejwas, T., and Bresler, B., "Damageability in Existing Buildings," *Report No. EERC-78-12*, University of California, Berkeley, California, August 1979.

[32] Bolotin, V. V., "Statistical Theory of Aseismic Design of Structures," *2nd World Conference on Earthquake Engineering*, 1365-1374, 1960.

[33] Bolt, B. A., "Duration of Strong Motion," Proceedings of *the 5th World Conference on Earthquake Engineering*, Rome, Italy, Vol. 1, pp. 1304-1313, June 1973.

[34] Bouc, R., "Forced Vibration of Mechanical Systems with Hysteresis," Abstract, Proceedings of the 4th Conference on Nonlinear Oscillation, Prague, Czechoslovakia, 1967.

[35] Breitung, K., "Asymptotic Approximation for Multinormal Integrals," *Journal of Engineering Mechanics, ASCE*, 110(3), pp. 357-366, March 1984.

[36] Building Officials and Code Administrators International, *The BOCA Basic Building Code*, Chicago, Illinois, 1950-1981.

[37] Building Officials and Code Administrators International, *The BOCA National Building Code*, Country Club Hills, 1987.

[38] Bulirsch, R., and Stoer, J., "Numerical Treatment of Ordinary Differential Equations by Extrapolation Methods," *Numerische Mathematik*, 8, 1966.

[39] Butcher, J. C., "On the Unattainable Order of Runge-Kutta Methods," *Math. Comp.*, 19, pp. 408-417, 1965.

[40] Butcher, J. C., "Integration Processes based on Radau Quadrature Formulas," *Math. Comp.*, 18, pp. 50-64, 1964.

[41] Butcher, J. C., "On Runge-Kutta Processes of High Order," *J. Austral. Math. Soc*, 4, pp. 179-194, 1964.

[42] Butcher, J. C., "Coefficients for the Study of Runge-Kutta Integration Processess," *J. Austral. Math. Soc*, 3, pp. 185-201, 1963.

[43] Bycroft, G. N., "White Noise Representation of Earthquakes," *Journal of Engineering Mechanics, ASCE*, Vol. 86, No. *EM2*, pp. 1 – 16, April 1960.

[44] Casciati, F. and Faravelli, L., "Stochastic Equivalent Linearization for 3-D Frames," *Journal of Engineering mechanics*, Vol. 114, No. 10, pp. 1760-1771.

[45] Casciati, F., "Smoothed Plasticity Laws and Elasto-Plastic Analysis," *Note Scientifiche in occasione del 70* deg *Compleano*, Pubblicazione n. 179, Dell Universita di Pavia, 1988.

[46] Casciati, F., "Nonlinear Stochastic Dynamics of Large Structural Systems by Equivalent Linearization," Proceedings of *the 5th International Conferenece on Application of Statistics and Probability in Soil and Structural Engineering* (ICASP 5), Vancouver, BC, Canada, Vol. II, pp. 1165-1172, 1987.

[47] Casciati, F. and Faravelli, L., "A Simplified Reliability Approach in Stochastic Non-Linear Dynamics," *Proceedings of the IUTAM Symposium*, October 31-November 6, 1987, ed., Henning, K., Institute of Mechanics at the Academy of Sciences of the Germany Republic, Akadmie-Verlag, Berlin, 1983.

[48] Chung, Y. S., Meyer, C., and Shinozuka, M., "Seismic Damage Assessment of Reinforced Concrete Members," *Technical Report NCEER-87-0022*, National Center for Earthquake Engineering Research, Buffalo, New York, October 1987.

[49] Clough, R. W. and Penzien, J., Dynamics of Structures, McGraw-Hill, New York, N. Y., 1975.

[50] Clough, R. W. and Johnston, S. B., "Effect of Stiffness Degradation on Earthquake Ductility Requirements," *Proceedings of the Second Japan Earthquake Engineering Symposium*, pp. 227-232, Tokyo, October 1966.

[51] Clough, R. W., Benuska, K. L., and Wilson, E. L., "Inelastic Earthquake Response of Tall Buildings," Proceedings of *the 3rd World Conference on Earthquake Engineering*, Auckland, New Zealand, Vol. II, pp. 68-69, 1960.

[52] Cook, R. D., Concepts and Applications of Finite Element Analysis, John Wiley and Sons, Inc., New York, 1981.

[53] Cornell, C. A., "Engineering Seismic Risk Analysis," *Bulletin of the Seismological Society of America*, Vol. 58, No. 5, pp. 1583 – 1606, 1968.

[54] Craig, R. R., Structural Dynamics, John Wiley and Sons, Inc., New York, 1981.

[55] Crede, C. E., Vibration and Shock Isolation, John Wiley and Sons, N.Y., pp. 151-170, 1951

[56] Darwin, D. and Nmai, C. K., "Energy Dissipation in RC Beams under Cyclic Load," *Journal of Structural Division*, ASCE, Vol. 112, No. 8, August 1986.

[57] Davenport, A. G., "Note on the Distribution of the Largest Value of a Random Function with Application to Gust Loading," *Proc. Institute of Civil Engineers*, London, Paper No. 6739, Vol. 28, 1964.

[58] Deak I., "Three Digit Accurate Multiple Normal Probabilities," *Numerische Mathematik*, 35, pp. 369-380, 1980.

[59] DiPasquale, E. and Cakmak, A. S., "Detection of Seismic Structural Damage using Parameter-based Global Damage Indices," *Probabilistic Engineering Mechanics*, Vol. 5., No. 2, pp. 60-65, 1990.

[60] Ditlevsen, O., Olesen, R., and Mohr, G., "Solution of a Class of Load Combination Problems by Directional Simulation,", *Structural Safety*, 4, pp. 95-109, 1986.

[61] Ditlevsen, O., Uncertainty Modeling, McGraw-Hill, New York, New York, 1981.

[62] Drucker, D. C., "On Uniqueness in the Theory of Plasticity", *Quarterly of Applied Mathematics*, Vol. 14, pp. 35-42, 1956.

[63] Duffing, G., "Erzwungene Schwingungen bei Veranderlicher Eigenfrequenz," F. Vieweg u. Sohn: Braunschweig, 1918.

[64] Ellingwood, B., MacGregor, J. C., Galambos, T. V., and Cornell C. A., "Probability Based Load Criteria - Load Factors and Load Combinations," *Journal of Structural Division*, ASCE, Vol. 108, No. ST5, Proc. Paper 17068, pp. 978-997, May 1982.

[65] Ellingwood, B., Galambos, T. V., MacGregor, J. C., and Cornell C. A., "Development of a Probability Based Load Criterion for American National Standard *A*58," *National Bureau of Standards Special Publication No. SP* 577, Washington, D.C., June 1980.

[66] Fiessler, B., Neumann, H. -J., and Rackwitz, R. "Quadratic Limit States in Structural Reliability," *Journal of Engineering Mechanics*, ASCE, 105(EM4), pp. 661-676.

[67] Frazer, R. A., Duncan, W. J., and Collar, A. R., Elementary Matrices, Cambridge University Press, Cambridge, England, 1965.

[68] Freeman, J. R., Earthquake Damage and Earthquake Insurance, McGraw-Hill, New York, 1932.

[69] Fu, G., and Moses, F., "A Sampling Distribution for System Reliability Applications," *Proceedings of the First IFIP WG 7.5 Working Conference on Reliability and Optimization of Structural Systems*, Aalborg, Denmark, pp. 141-155, May 1987.

[70] Fukada, Y., "A Study on the Restoring Force Characteristics of Reinforced Concrete Buildings," Proceedings of *the Kanto District Symposium of AIJ*, Tokyo, Japan, November 1969.

[71] Galambos, T. V., Ellingwood, B., MacGregor, J. G., and Cornell, C. A., "Probability Based Load Criteria: Assessment of Current Design Practice," *Journal of Structural Division*, ASCE, Vol. 108, No. ST5, Proc. Paper 17067, pp. 959-977, May 1982.

[72] Galambos, T. V., and Ravindra, M. K., "Load and Resistance Factor Design," *Journal of Structural Division*, ASCE, ST9, Proc. Paper 14008, pp. 1335-1336, September 1978.

[73] Gallagher, R. H., Finite Element Analysis, Prentice-Hall, Inc., Englewood Cliffs, New Jersey, 1975.

[74] Gear, C. W., Numerical Initial Value Problems in Ordinary Differential Equations, Prentice-Hall, Englewood Cliffs, New Jersey, 1971.

[75] Goel, S. C., and Berg, G. V., "Inelastic Earthquake Response of Tall Steel Frames," *Journal of Structural Division*, ASCE, Vol. 94, No. ST8, pp. 1907-1934, August 1968.

[76] Gosain, N. K., Brown, R. H., and Jirsa, J. O., "Shear Requirements for Load Reversals on RC Members," *Journal of Structural Division*, ASCE, Vol. 103, No. ST7, July 1977.

[77] Grigoriu, M., Ruiz, S., and Rosenblueth, E., "Nonstationary Models of Seismic Ground Acceleration," *Earthquake Spectra*, The Professional Journal of the Earthquake Engineering Research Institute, November, 1988 (*Technical Report* NCEER-88-0043, National Center for Earthquake Engineering Research, Buffalo, July 1988).

[78] Grigoriu, M., Ruiz, S., and Rosenblueth, E., "A New Nonstationary Model of Seismic Ground Acceleration," *Proceedings of the 8th Structures Congress*, Baltimore, Maryland, April 1990.

[79] Grigoriu, M., "Damage Models for Seismic Analysis," *Technical Report* 87-4, Department of Structural Engineering, Cornell University, Ithaca, NY, September 1987.

[80] Grigoriu, M., "Mean-square Response to Stationary Ground Acceleration," *Journal of Engineering Mechanics*, ASCE, Vol. 107, pp. 969-986, October 1981.

[81] Gulkan, P., and Sozen, M. A., "Response and Energy-Dissipation of Reinforced Concrete Frames Subjected to Strong Base Motions," Civil Engineering Studies, *Structural Research Series No. 377*, University of Illinois at Urbana-Champaign, Urbana, Illinois, May 1971.

[82] Gurtin, M. E., An Introduction to Continuum Mechanics, Academic Press, 1981.

[83] Harbitz, A., "An Efficient Sampling Method for Probability of Failure Calculation," *Structural Safety*, Vol. 3, No. 1., pp. 109-115, October 1986.

[84] Harbitz, A., "Efficient and Accurate Probability of Failure Calculation by use of the Importance Sampling Technique," *Proceedings of the 4th International Conference on Applications of Statistics and Probability in Soil and Structural Engineering*, Florence, Italy, 1983.

[85] Hasselman, T. K., Eguchi, R. T., and Wiggins, J. H., "Assessment of Damageability for Existing Buildings in a Natural Hazards Environment," *Technical Report, No. 80-1932-1*, Vol. 1, J. H. Wiggins Company, Redondo Beach, California, September, 1980.

[86] Hasofer, A. M., and Lind, N. C., "An Exact and Invariant First-Order Reliability Format," *Journal of Engineering Mechanics*, ASCE, Vol. 100, No. EM1, pp. 111-121, February 1974.

[87] Heun, K., "Neue Methode zur approximativen Integration der Differentialgleichungen einer unabhängigen Veränderlichen," *Z. Math. Physik.*, 45, pp. 23-38, 1900.

[88] Hindmarsh, A. C., "GEAR:Ordinary Differential Equation System Solver," *Lawrence Livermore Laboratory Report UCID-30001*, Revision 3, 1974.

[89] Hohenbichler, M., "Improvement of Second-Order Reliability Estimates by Importance Sampling," *Journal of Engineering Mechanics*, ASCE, Vol. 114, No. 12, pp. 2195-2199, December 1988.

[90] Hohenbichler, M., "New Light on First- and Second-Order Reliability Methods," *Structural Safety*, 4, pp. 267-284, 1987.

[91] Housner G. W. and Jennings, P. C., "Generation of Artificial Earthquakes," *Journal of Engineering Mechanics*, ASCE, Vol. 90, No. EM1, pp. 113-150, February 1964.

[92] Huebner, K. H., The Finite Element Method for Engineers, John Wiley and Sons, Inc., New York, 1975.

[93] Hull, T. E., Enright, W. H., and Jackson, K. R., "User's Guide for DVERK - A Subroutine for Solving Non-Stiff ODE's," *Technical Report 100*, Department of Computer Science, University of Toronto, Ontario, Canada, 1976.

[94] Hurty, C. W. and Rubinstein, M. F., Dynamics of Structures, Prentice Hall, Inc. Englewood Cliffs, New Jersey, 1964.

[95] Husid, R., "The Effect of Gravity on the Collapse of Yielding Structures with Earthquake Excitation," *Proceedings of the 4th World Conference on Earthquake Engineering*, Santiago, Chile, pp. 31-43, 1969.

[96] Huťa, A., "Contribution à la formule de sixième ordre dans la méthode de Runge-Kutta-Nyström," *Acta Fac. Rerum Natur. Univ. Comenian. Math.*, 2, pp. 21-24, 1957.

[97] Hwang, T. H. and Scribner, C. F., "R/C member Cyclic Responses During Various Loadings," *Journal of Structural Division*, ASCE, Vol. 110, No. 3, March 1984.

[98] Ibrahim, Y. and Rahman, S., "Reliability Analysis of Uncertain Dynamic Systems Using Importance Sampling," *Proceedings of the Sixth International Conference on Applications of Statistics and Probability in Civil Engineering*, Mexico City, Mexico, 1991.

[99] Iglesias, J. *et al.*, "Estudios de las Intensidades del Sismo del 19 de Septiembre en la Ciudad de Mexico," *Universidad Autonoma Metropolitana*, Departmento de Materiales, Junio 1987.

[100] International Conference of Building Officials, *Uniform Building Code*, Whittier, California, 1988.

[101] International Conference of Building Officials, *Uniform Building Code*, Whittier, California, 1985.

[102] International Conference of Building Officials, *Uniform Building Code*, Whittier, California, 1982.

[103] International Conference of Building Officials, *Uniform Building Code*, Whittier, California, 1979.

[104] International Conference of Building Officials, *Uniform Building Code*, Whittier, California, 1970.

[105] Israel, M., Ellingwood, B. W., and Corotis, R. B., "Reliability-based Code Formulations for Reinforced Concrete Buildings," *Journal of Structural Engineering*, Vol. 113, No. 10, pp. 2235-2252, October 1987.

[106] Iwan, W. D., "A Model for the Dynamic Analysis of Deteriorating Structures," *Proceedings of the 5th World Conference on Earthquake Engineering*, Rome, Italy, 1973.

[107] Iwan, W. D., "A Distributed-Element Model for Hysteresis and Its Steady-State Dynamic Response," *Journal of Applied Mechanics*, 33(4), 893-900, 1966.

[108] Iwan, W. D., "The Steady-State Response of the Double Bilinear Hysteretic Model," *Journal of Applied Mechanics*, Vol. 32, Transaction of ASME, Vol. 87, Series E, No. 4, pp. 921-925, December 1965.

[109] Iyengar, R. N. and Iyengar, K. T. S., "A Nonstationary Stochastic Random Process Model for Earthquake Accelerograms," *Bulletin of the Seismological Society of America*, Vol. 59, No. 3, pp. 1163-1188, June 1969.

[110] Jackson, K. R., Enright, W. H., and Hull, T. E., "A Theoretical Criterion for Comparing Runge-Kutta Formulas," *Technical Report 101*, Department of Computer Science, University of Toronto, Ontario, Canada, 1977.

[111] Jayakumar, P. and Beck, J. L., "System Identification Using Nonlinear Structural Models," Proceedings of *the Structural Safety Evaluation based on System Identification Approaches*, Lambrecht, Germany, pp. 82-102, July 1987.

[112] Jennings, P. C., "Periodic Response of a General Yielding Structure," *Journal of Engineering Mechanics*, ASCE, Vol. 90, pp. 131-165, April 1964.

[113] Kanai, K. T., "Semi-Empirical Formula for the Seismic Characteristics of the Ground," *Bull. Earthquake Res. Inst., Univ. Tokyo*, 35, 1957.

[114] Karnopp, D. and Scharton, T. D., "Plastic Deformation in Random Vibration," *Journal of Acoustical Society of America*, Vol. 39, No. 6, pp. 1154 – 1161, 1966

[115] Kato, B., and Akiyama, H., "Theoretical Prediction of the Load-Deflection Relationship of Steel Members and Frames," *IABSE Symposium on Resistance and Ultimate Deformability of Structures Acted on by Well Defined Loads*, Preliminary Publication, Lisboa, 1973.

[116] Khan, F. R., Sbarounis, J. A., "Interaction of Shear Walls and Frames," *Journal of Structural Division*, ASCE, Vol. 90, No. 3, pp. 285-335, June 1964.

[117] Kleijnen, J. P. C., Statistical Techniques in Simulation, Part-I, Marcell Dekker, Inc., New York, 1974.

[118] Kobori, T., Minai, R., and Suzuki, Y., "Stochastic Seismic Response of Hysteretic Structures," *Bulletin of the Disaster Prevention Research Institute*, Kyoto University, Vol. 26, Part 1, pp. 55-70, 1976.

[119] Krawinkler, H. and Zohrei, M., "Cumulative Damage in Steel Structures Subjected to Earthquake Ground Motions," *Computers and Structures*, Vol. 16, No. 14, 1983

[120] Kutta, W., "Beitraz zur näherungsweisen Integration totaler Differentialgleichungen," *Z. Math. Phys.*, 46, 435-453, 1901.

[121] Lai, P. S-S., "Seismic Safety: 10-story UBC Designed Steel Buildings," *Journal of Engineering Mechanics*, ASCE, Vol. 109, No. EM2, pp. 557-575, April 1983.

[122] Lai, P. S-S., "Statistical Characterization of Strong Motions Using Power Spectral Density Functions," *Bulletin of the Seismological Society of America*, Vol. 72, No. 1, pp. 259-274, February 1982.

[123] Lai, P. S-S., "Overall Safety Assessment of Multistory Steel Buildings Subjected to Earthquake Loads," Evaluation of Seismic Safety of Buildings, Final report, Dept. of Civil Engineering, *MIT Publication No. R80-26*, Cambridge, Massachusetts, June 1980.

[124] Lambert, J. D., Computational Methods in Ordinary Differential Equations, London, John Wiley & Sons, 1973.

[125] Langhaar, H. L., Energy Methods in Applied Mechanics, John Wiley and Sons, Inc., New York, 1962.

[126] Larabee, R., and Cornell, C. A., "A Combination Procedure for a Wide Class of Loading Processes," *Probabilistic Mechanics and Structural Reliability*, ASCE, New York, New York, January 1979.

[127] Levy, R., Kozin, F., and Moorman, R. B., "Random Processes for Earthquake Simulation," *Journal of Engineering Mechanics, ASCE*, Vol. 97, No. *EM*2, pp. 495 – 517, April 1971.

[128] Lin, Y. K., Probabilistic Theory of Structural Dynamics, Krieger Publishing Co., Huntington, New York, 1976.

[129] Liu, S. C., "Evolutionary Power Spectral Density of Strong Motion Earthquakes," *Bull. Seismolozical Societv of America*, 60, pp. 891-900, 1970.

[130] MacGregor, J. G., Mirza, S. A., and Ellingwood, B. R., "Statistical Analysis of Resistance of Reinforced and Prestressed Concrete Members," *Journal of American Concrete Institute*, 80(3), pp. 167-176, 1983.

[131] MacGregor, J. G., "Safety and Limit States Design for Reinforced Concrete," *Canadian Journal of Civil Engineering*, Vol. 3, No. 4, pp. 484-513, 1976.

[132] Madsen, H. O., Krenk, S., and Lind, N. C., Methods of Structural Safety, Prentice-Hall, Inc., Englewood Cliffs, New Jersey, 1986.

[133] Malvern, L. E., Introduction to the Mechanics of a Continuous Medium, Prentice-Hall, Inc., 1969.

[134] McCann, W. M., and Shah, H. C., "Determining Strong-Motion Duration of Earthquakes," *Bulletin of the Seismological Society of America*, Vol. 69, No. 4, pp. 1253-1265, August 1979.

[135] McLauchlan, N. W., Ordinary Non-Linear Differential Equations in Engineering and Physical Sciences, Oxford University Press, London, pp. 24-40, 1956.

[136] Meirovitch, L., Analytical methods in Vibration, The Macmillan Co., New York, N.Y., 1967.

[137] Melchers, R. E., "Efficient Monte Carlo Probability Integartion," *Report NO. 7*, Dept. of Civil Engineering, Monash University, Australia, 1984.

[138] Meli, R., "Metodos Simplificados para la Evaluacion de la Seguridad Sismica de Edificios," *private communication*, 1986.

[139] Mizuhata, K., "Evaluation of Seismic Safety for Reinforced Concrete Structures," *Report No. GBRC*, Vol. 10, No. 4, Laboratory of Japanese Architectural Society, Japan, 1985.

[140] Moayyad, P. , and Mohraz, B., "A Study of Power Spectral Density of Earthquake Accelerograms," Civil And Mechanicsl Engineering Department, Southern Methodist University, Dallas, Texas, June 1982.

[141] Moses, F., and Yao, J. T. P., "Safety Evaluation of Buildings and Bridges," *Symposium on Structural Design, Inspection, and Redundancy*, Williamsburg, Virginia, pp. 14-19, November 1983.

[142] Muto, K., Hisada, T., Tsugawa, T., and Bessho, S., "Earthquake Resistant Design of a 20-story Reinforced Concrete Building," Proceedings of *the 5th World Conference on Earthquake Engineering*, Rome, Italy, June 1973.

[143] Nemat-Nasser, S., "On Nonequilibrium Thermodynamics of Continua," *Mechanics Today*, S. Nemat-Nasser, ed., Vol. 2, Pergamon Press, Inc., New York, pp. 94-158, 1975.

[144] Newmark, N. M. and Rosenblueth, E., Fundamentals of Earthquake Engineering, Prentice Hall, Inc. Englewood Cliffs, New Jersey, 1971.

[145] Newmark, N. M., "A Method of Computation for Structural Dynamics," *Journal of Engineering Mechanics Division*, EM3, ASCE, pp. 67-94, July 1959.

[146] Nielsen, S. R. K. and Cakmak, A. S., "Evaluation of Maximum Softening as a Damage Indicator for Reinforced Concrete Under Seismic Excitation," *Proceedings of the First*

International Conference on Computational Stochastic Mechanics, edited by Spanos and Brebbia, pp. 169-184, 1992.

[147] Nielsen, S. R. K., Köylüoğlu, H. U., and Cakmak, A. S., "One- and Two-Dimensional Maximum Softening Damage Indicators for Reinforced Concrete Structures Under Seismic Excitation," *Soil Dynamics and Earthquake Engineering*, Vol. 11, pp. 435-443, 1992.

[148] Nigam, N. C., and Housner, G. W., "Elastic and Inelastic Response of Framed Structures During Earthquakes," Proceedings of the 4th World Conference on Earthquake Engineering, 1969.

[149] O'Connor, M. J., and Ellingwood, B., "Reliability of Nonlinear Structures with Seismic Loading," *Journal of Structural Division*, ASCE, May 1987.

[150] Oden, J. T., Finite Elements of Nonlinear Continua, McGraw-Hill, New York, 1962.

[151] Ogden, R. W., Non-linear Elastic Deformation, Ellis Horwood Ltd., 1983.

[152] Okada, T., "Standard for Evaluation of Seismic Capacity of Existing Reinforced Concrete Buildings," *Seminar notes, Institute of Earthquake Engineering and Engineering Seismology*, Skopje, Yugoslavia, 1985, pps 25.

[153] Oliveria, "Seismic Risk Analysis for a Site and a Metropolitan Area," *EERC Report No. 75-2*, University of California, Berkeley, CA, 1975.

[154] Otani, S., and Sozen, M. A., "Behavior of Multistory Reinforced Concrete Frames During Earthquakes," Civil Engineering Studies, *Structural Research Series No. 392*, University of Illinois at Urbana-Champaign, Urbana, Illinois, 1972.

[155] Park, R., and Paulay, T., Reinforced Concrete Structures, John Wiley and Sons, Inc., New York, 1975.

[156] Park, Y. J., Reinhorn, A. M., and Kunnath, S. K., "IDARC:Inelastic Damage Analysis of Reinforced Concrete Frame-Shear Wall Structures," Technical report, *NCEER-87-0008*, State University of New York at Buffalo, Buffalo, New York, July 1987.

[157] Park, Y. J., Wen, Y- K. and Ang, A. H- S., "Two-Dimensional Random Vibration of Hysteretic Structures," *Journal of Earthquake Engineering and Structural Dynamics*, **14**, pp. 543-557, 1986.

[158] Park, Y. J., Wen, Y. K., and Ang, A. H-S., "Damage Model for Buildings Subjected to Earthquakes," *Structural Safety Studies*, ASCE, pp. 86-95, May 1985.

[159] Park, Y. J. and Ang, A. H-S., "Mechanical Seismic Damage Model for Reinforced Concrete," *Journal of Structural Division*, ASCE, 111(4), 722-739, 1985.

[160] Park, Y. J., Ang, A. H-S., and Wen Y-K., "Seismic Damage Analysis of Reinforced Concrete Buildings," *Journal of Structural Division*, ASCE, 111(4), 740-757, 1985.

[161] Parzen, E., Stochastic Processes, Holden-Day, San Francisco, California, 1962.

[162] Paz, M., Structural Dynamics- Theory and Computation, Van Nostrand Reinhold Company, New York, 1985.

[163] Peng, C. Y., and Iwan, W. D., "Identification of Hysteretic Structural Behavior from Strong Motion Accelerograms," Proceedings of *the Structural Safety Evaluation based on System Identification Approaches*, Lambrecht, Germany, pp. 103-117, July 1987.

[164] Penzien, J., "Elasto-Plastic Response of Idealized Multistory Structures Subjected to Strong Motion Earthquake," Proceedings of *the 2nd World Conference on Earthquake Engineering*, Japan, Vol. II, pp. 739-760, 1960.

[165] Perkins, D. M., "Seismic Risk Maps," *Earthquake Information Bulletin*, Vol.6, U.S. Geological Survey, pp. 10-15, 1974.

[166] Powell, G. H., and Chen, P. F-S., "3-D Beam-Column Element with Generalized Plastic Hinges," *Journal of Engineering Mechanics*, ASCE, 112(76), pp. 627-641, 1986.

[167] Priestley, M. B., "Evolutionary Spectra and Nonstationary Processes," *J. Royal Statist. Soc. B.*, Vol. 27, pp. 204-237, 1965.

[168] Rackwitz, R. and Fiessler, B., "Structural Reliability under Combined Random Load Sequences," *Computer and Structures*, Vol. 9, pp. 484-494, 1978.

[169] Rahman, S. and Grigoriu, M., "Markov Model for Seismic Reliability Analysis of Degrading Structures," *Journal of Structural Engineering*, Vol. 119, No. 6, pp. 1844-1865, June 1993.

[170] Rahman, S. and Grigoriu, M., "Local and Global Models for Nonlinear Dynamic Analysis of Multi-Story Shear Buildings Subject to Earthquake Loading," accepted for publication in the *Computers & Structures: An International Journal*, 1994 (in press).

[171] Rahman, S., "A Markov Model for Local and Global Damage Indices in Seismic Analysis," Ph.D. Dissertation, Department of Structural Engineering, Cornell University, Ithaca, NY, 1991.

[172] Rahman, S. and Ibrahim, Y., "Adequacy of Statistical Linearization for Nonlinear Degrading Structural Systems," *Proceedings of ASCE Engineering Mechanics Speciality Conference*, Columbus, Ohio, 1991.

[173] Rahman, S., "Evaluation of Effects of Simplifications Used in Current Seismic Reliability Analysis," *Proceedings of 3rd International Conference on Earthquake, Blast & Impact*, Manchester, United Kingdom, 1991.

[174] Rahman, S., "Uncertainty in System Modeling for Seismic Performance of Structural Systems," *Proceedings of 6th Canadian Conference on Earthquake Engineering*, Toronto, Canada, 1991.

[175] Rahman, S., and Grigoriu, M., "Effects of Model Uncertainty on Seismic Response and Reliability of Structural Systems" *Proceedings of the 9th Structures Congress*, Indianapolis, Indiana, 1991.

[176] Rahman, S. and Grigoriu, M., "Local and Global Damage Indices in Seismic Analysis," *Proceedings of 9th Symposium on Earthquake Engineering*, University of Roorkee, Roorkee, India, December 1990.

[177] Rahman, S. and Grigoriu, M., "Probabilistic Evaluation of Seismic Performance of Structural Systems," *Proceedings of 4th U. S. National Conference on Earthquake Engineering*, Palm Springs, California, May 1990.

[178] Rahman, S. and Saif, M., "Stochastic Modeling of Damage Accumulation Due to Mode-I Propagation of Fatigue Cracks," *Proceedings of AIAA 31st Structures, Structural Dynamics & Materials Conference*, Long Beach, California, 1990.

[179] Rahman, S., and Grigoriu, M., "Reliability Based Design Codes," *Proceedings of the International Conference of Structural Safety and Reliability*, San Francisco, California, August 1989.

[180] Rahman, S., Turkstra, C., Grigoriu, M., and Kim H-J, "Seismic Performance of Existing Building in New York City," Proceedings of the *7th Structures Congress*, San Francisco, California, 1989.

[181] Ralston, A., A First Course in Numerical Analysis, McGraw-Hill, 1965.

[182] Reinhorn, A. M., Kunnath, S. K., Bracci, J., Mander, J. B., "Normalized Damage Index for Evaluation of Buildings," Proceedings of *the 7th Structures Congress*, San Francisco, California, May 1989.

[183] Richter, C. F.,"Seismic Regionalization," *Bulletin of Seismological Society of America*, pp. 123-162, July 1959.

[184] Rice, S. O., "Mathematical Analysis of Random Noise," *Bell System Technical Journal*, Part II, Vol. 24, pp. 46-156, 1945.

[185] Rice, S. O., "Mathematical Analysis of Random Noise," *Bell System Technical Journal*, Part I, Vol. 23, pp. 282-332, 1944.

[186] Roberts, E. B. and F. P. Ulrich, "Seismological Activities of the U.S. Coast and Geodetic Survey in 1949," *Bulletin of Seismological Society of America*, pp. 205-220, July 1951.

[187] Ronfaid, M. S. K., and Meyer, C., "Analysis of Damaged Concrete Frame Buildings," *Technical Report No. MSF-CEE-81-21359-1*, Columbia University, New York, New York, 1981.

[188] Rosenblatt, M., "Remarks on a Multivariate Transformation," *Ann. Math. Statistics*, Vol. 23, pp. 470-472, 1952.

[189] Roufaiel, M. S. L. and Meyer, C., "Analytical Modeling of Hysteretic Behavior of R/C Frames," *Journal of Structural Division*, ASCE, Vol. 113, No. 3, March1987.

[190] Rubinstein, R. Y., Simulation and the Monte Carlo Method, John Wiley & Sons, New York, New York, 1981.

[191] Runge, C., "Über die numerische Auflösung von Differentialgleichungen," *Math. Ann.*, 46, pp. 167-178, 1895.

[192] Safak, E., and Boore, D. M., "On Nonstationary Stochastic Models for Earthquakes," *Proceedings of the Third U.S. National Conference on Earthquake Engineering*, Charleston, South Carolina, pp. 137-148, Aug. 24-28, 1986.

[193] Saragoni, G. R., and Hart, G. C., "Simulation of Artificial Earthquakes," *Earthouake Enzineerinz and Structural Dvnamics*, 2, pp. 249-267, 1974.

[194] Shampine, L. F., and Gear, C. W., "A User's View of Solving Stiff Ordinary Differential Equations," *SIAM Review*, 21, 1979.

[195] Shibata, A., and Sozen, M. A., "Substitute Structure Method for Seismic Design in R/C," *Journal of Structural Division*, ASCE, 1976.

[196] Shiga, T., Shibata, A., and Takahashi, T., "Earthquake Damage and Wall Index of Reinforced Concrete Buildings (in Japanese)," *Proc. Tohoku District Symposium*, Architectural Institute of Japan, No. 12, December 1968, pp. 29 – 32.

[197] Shinozuka, M. and Sato, Y., "Simulation of Nonstationary Random Processes," *Journal of Engineering Mechanics*, ASCE, Vol. 93, No. EM1, pp. 11-40, February 1966.

[198] Southern Building Code Congress International, *Standard Building Code*, Birmingham, Alabama, 1985.

[199] Sozen, M. A., "Review of Earthquake Response of Reinforced Concrete Buildings with a View to Drift Control," *State-of-the-Art in Earthquake Engineering*, Turkish National Committee on Earthquake Engineering, Istanbul, Turkey, pp. 383-418, 1981.

[200] Spencer, R. A., "Stiffness and Damping of Cyclically Loaded Prestressed Concrete Members," *Segundo Congreso Nacional de Ingenieria Sismica*, Veracruz, Mexico, 1968.

[201] Stephens, J. E. "A Damage Function Using Structural Response Measurements," *Structural Safety Studies*, ASCE, May 1985, pp. 22-39.

[202] Stephens, J. E., and Yao, J. T. P., "Estimation of Interstory Load- Deformation Relations for Damaged Structures," *Fourth International Conference on Structural Safety and Reliability*, Kobe, Japan, 1985.

[203] Stratonovich, R. L.,Topics in the Theory of Random Noise, Vols. 1 & 2, Gordon and Breach, New York, 1963.

[204] Sues, R. H., Mau, S. T., and Wen, Y. -K., "System Identification of Degrading Hysteretic Restoring Forces," *Journal of Engineering Mechanics*, Vol. 114, No. 5, pp. 833-846, 1988.

[205] Sues, R. H., Wen, Y. -K., and Ang, A. H-S., "Stochastic Seismic Performance Evaluation of Buildings," Civil Engineering Studies, *Structural Research Series No. 506*, University of Illinois at Urbana-Champaign, Urbana, Illinois, May 1983

[206] Suko, M., and Adams, P. F., "Dynamic Analysis of Multibay Multistory Structures," *Journal of Structural Division*, ASCE, Vol. 97, No. ST10, October 1971.

[207] Suzuki, Y. and Minai, R., "Application of stochastic differential equation to seismic reliability analysis of hysteretic structures," *Proceedings of US-Japan joint seminar on stochastic approaches in earthquake engineering*, pp. 334-356, Boca Raton, Florida, May 1987.

[208] Suzuki, Y. and Minai, R., "A Method of seismic Response Analysis of Hysteretic Structures Based on Stochastic Differential Equations," *Proceedings of the 8th World Conference on Earthquake Engineering*, San Francisco, Vol. IV, pp. 459-466, 1984.

[209] Tajimi, H, "A Statistical Method of Determining the Maximum Response of a Building Structure During an Earthquake," *Proceedings of the 2nd World Conference on Earthquake Engineering*, vol. 11, Tokyo, Japan, 1960.

[210] Takeda, T., Sozen, M. A., and Nielsen, N. N., "Reinforced Concrete Response to Simulated Earthquakes," *Journal of Structural Division*, ASCE, Vol. 96, No. ST12, pp. 2557-2573, 1970.

[211] Takizawa, H., and Aoyama, H., "Biaxial Effects in Modeling Earthquake Response of R/C Structures," *Journal of Earthquake Engineering and Structural Dynamics*, 4, 523-552, 1976.

[212] Takizawa, H., "Notes on Some Basic Problems in Inelastic Analysis of Planar R/C Structures (Parts I & II)," *Trans. of the Arch. Inst. of Japan*, No. 240, 1976.

[213] Takizawa, H., "Nonlinear Models for Simulating the Dynamic Damaging Process of Low Rise Reinforced Concrete Buildings During Severe Earthquakes," *Journal of Earthquake Engineering and Structural Dynamics*, Vol. 4, pp. 73-94, 1975.

[214] Tanabashi, R., and Kaneta, K., "On the Relation between the Restoring Force Characteristics of Structures and the Pattern of Earthquake Ground Motions," *Proceedings of Japan National Symposium on Earthquake Engineering*, pp. 57-62, Tokyo, November 1962.

[215] Toussi, S., and Yao, J. T. P., "Assessment of Structural Damage Using the Theory of Evidence," *Structural Safety*, 1, Elsevier Publishing Co., Amsterdam, Netherland, pp. 107-121, 1982.

[216] Trifunac, M. D., and Brady, A. G., "A Study of the Duration of Strong Earthquake Ground Motions," *Bulletin of the Seismological Society of America*, Vol. 65, No. 3, pp. 581-626, June 1975.

[217] Tucker, M. J., Challenor, P. G. and Carter, D. J. T., "Numerical Simulation of a Random sea: A Common Error and its Effect Upon Wave Group Statistics," *Applied Ocean Research*, Vol. 6, 1984.

[218] Turkstra, C., Kim, H-J., Grigoriu, M., and Rahman, S., "Simple Damage Predictors for Large-Scale Seismic Risk Mapping," Proceedings of the *5th International Conference on Structural Safety and Reliability*, San Francisco, California, 1989.

[219] Turkstra, C. J., "Theory of Structural Design Decisions," *Solid Mechanics Study No. 2*, University of Waterloo, Waterloo, Ontaio, Canada, 1972.

[220] Valanis, K. C., "A Theory of Viscoplasticity without a Yield Surface," *Archiwum Mechaniki Stossowanig*, Vol. 23, pp. 517-551, 1971.

[221] Vanmarcke, E. H., and Lai, P. S-S., "Strong-Motion Duration and RMS Amplitude of Earthquake Records," *Bulletin of the Seismological Society of America*, Vol. 70, No. 4, pp. 1293-1307, August 1980.

[222] Vanmarcke, E. H. and Veneziano, D., "Probabilistic Seismic Response of Simple Inelastic Systems," *Proc. 5th WCEE*, Rome, Italy, pp. 2851 – 2863, 1973.

[223] Vanmarcke, E. H., "First Passage and Other Failure Criteria in Narrow Band Random Vibration: A Discrete State Approach," Thesis presented to the Massachusetts Institute of Technology, Cambridge, Massachusetts, in partial fulfillment of the requirements for the degree of Doctor of Philosophy, 1969.

[224] Vanmarcke, E. H., Yanev, P. I., and De Estrada, M. B., "Response of Simple Hysteretic Systems to Random Excitation," *M.I.T. Dept. of Civil Engineering Research Report R70-66*, September 1970.

[225] Wempner, G. and Aberson, J., "A Formulation of Inelasticity from Thermal and Mechanical Concepts," *International Journal of Solids and Structures*, 12, 705-721, 1976.

[226] Wen, Y. -K., "Methods of Random Vibration for Inelastic Structures," *Journal of Applied Mechanics*, Vol. 42, No. 2, pp. 39-52, February 1989.

[227] Wen, Y. -K., and Ang, A. H-S., "Inelastic Modeling and System Identification," Proceedings of *the Structural Safety Evaluation based on System Identification Approaches*, Lambrecht, Germany, pp. 142-160, July 1987.

[228] Wen, Y. -K., "Equivalent Linearization for Hysteretic Systems Under Random Excitations," *J. Appl. Mech., trans.* ASME, 47(1), pp. 150-154, 1980.

[229] Wen, Y. -K., "Statistical Combination of Extreme Loads," *Journal of Structural Division*, ASCE, Vol. 103, No. ST6, Proc. Paper 12930, pp. 1079-1095, May 1977.

[230] Wen, Y. -K., "Method for Random Vibration of Hysteretic Systems" *Journal of Engineering Mechanics*, ASCE, Vol. 102, pp. 249-263, April 1976.

[231] Withman, R. V., Biggs, J. M., Brennan, J. E., Cornell, C. A., de Neufville, R. L., and Vanmarcke, E., "Seismic Design Decision Analysis," *Journal of Structural Division*, ASCE, Vol. 101, No.ST.5, pp. 1067-1084, May 1979.

[232] Yanev, P. I., "Response of Simple Inelastic Systems to Random Excitation," Thesis presented to the Massachusetts Institute of Technology, Cambridge, Massachusetts, in partial fulfillment of the requirements for the degree of Master of Science, 1970.

[233] Yang, Y., and Yang, L., "Empirical Relationship Between Damage to Multistorey Brick Buildings and Strength of Walls During the Tangshan Earthquake," *Proc. 7 WCEE*, Vol. 6, Instanbul, 1980, pp. 501 – 508.

[234] Yao, J. T. P., and Munse, W., "Low Cycle Axial Fatigue Behavior of Mild Steel," *ASTM Special Publication*, No. 338, 1962, pp. 5-24.

[235] Yao, J. T. P., Wen. Y. -K., Yang, J. -N., Schueller, G. I., and Ditlevsen, 0., "Stochastic Fatigue, Fracture, and Damage Analysis," *Structural Safety*, 3, 1986, pp. 231-267.

[236] Zienkiewicz, O. C., The Finite Element Method, McGraw-Hill, New York, 1977.

APPENDIX A
FORM/SORM and Importance Sampling

A.1 First- and Second-Order Reliability Methods

Consider a transformation $H : \mathbf{X} \rightarrow \mathbf{U}$ where $\mathbf{U} \in \Re^n$ denotes an independent standard Gaussian random vector. The transformation H is necessary if originally, the basic uncertainty vector $\mathbf{X}$ has arbitrary joint distribution function $\mathbf{F_X(x)}$. For example, when the Rosenblatt transformation [188] is used, the explicit form of above mapping from original $\mathbf{x}$ space to $\mathbf{u}$ space becomes

$$H : \begin{cases} u_1 &= \Phi^{-1}[F_{X_1}(x_1)] \\ u_2 &= \Phi^{-1}[F_{X_2}(x_2|x_1)] \\ . & . \\ . & . \\ u_n &= \Phi^{-1}[F_{X_n}(x_n|x_1, x_2, ..., x_{n-1})] \end{cases} \tag{A.1}$$

in which $F_{X_i}(x_i|x_1, x_2, ..., x_{i-1})$ is the cumulative distribution function of X_i conditional on $X_1 = x_1,\ X_2 = x_2,\ \cdots X_{i-1} = x_{i-1}$ and can be obtained from

$$F_{X_i}(x_i|x_1, x_2, ..., x_{i-1}) = \frac{\int_{-\infty}^{x_i} f_{X_1, X_2, \cdots, X_{i-1}, X_i}(x_1, x_2, \cdots, x_{i-1}, s)ds}{f_{X_1, X_2, \cdots, X_{i-1}}(x_1, x_2, \cdots, x_{i-1})} \tag{A.2}$$

where $f_{X_1, X_2, \cdots, X_{i-1}}(x_1, x_2, \cdots, x_{i-1})$ is the joint probability density function of $\{X_1, X_2, \cdots, X_{i-1}\}^T$. The inverse transformation can be obtained in a stepwise manner as

$$H^{-1} : \begin{cases} x_1 &= {F_{X_1}}^{-1}[\Phi(u_1)] \\ x_2 &= {F_{X_2}}^{-1}[\Phi(u_2)|x_1] \\ . & . \\ . & . \\ x_n &= {F_{X_n}}^{-1}[\Phi(u_n)|x_1, x_2, ..., x_{n-1}] \end{cases} \tag{A.3}$$

which when substituted in Eq. 3.18 yields

$$P_F = \Pr[g_U(\mathbf{U}) < 0] = \int_{g_U(\mathbf{u})<0} \phi(\mathbf{u}) d\mathbf{u} \tag{A.4}$$

where $\phi(\mathbf{u})$ is the standard multivariate Gaussian density function defined as

$$\phi(\mathbf{u}) = (2\pi)^{-\frac{n}{2}} \exp\left(-\frac{1}{2}\mathbf{u}^T\mathbf{u}\right) \tag{A.5}$$

and $g_U(\mathbf{u}) = 0$ is the new limit state surface in the image $\mathbf{u}$ of space $\mathbf{x}$.

First-Order Reliability Method (FORM)

Consider a tangential linearization at the point $\mathbf{u}^*$ of the limit state surface $g_U(\mathbf{u}) = 0$ which is given by

$$g_L(\mathbf{u}) = \alpha^T(\mathbf{u} - \mathbf{u}^*) = 0 \tag{A.6}$$

where $\mathbf{u}^*$ is the closest point (known as the design point, beta point, etc.) of $g_U(\mathbf{u}) = 0$ to the origin of $\mathbf{u}$ space, and $\alpha \in \Re^n$ is the vector of direction cosines obtained from

$$\alpha = \frac{\nabla g_U(\mathbf{u}^*)}{\| \nabla g_U(\mathbf{u}^*) \|} \tag{A.7}$$

in which

$$\nabla = \begin{Bmatrix} \frac{\partial}{\partial u_1} \\ \frac{\partial}{\partial u_2} \\ \cdot \\ \cdot \\ \cdot \\ \frac{\partial}{\partial u_n} \end{Bmatrix} \tag{A.8}$$

with $\nabla g_U(\mathbf{u}^*)$ as the gradient of scalar field g_U at $\mathbf{u}^*$, and

$$\| \nabla g_U(\mathbf{u}^*) \| = \sqrt{\sum_{i=1}^{n} \left| \frac{\partial g_U}{\partial u_i}(\mathbf{u}^*) \right|^2} \tag{A.9}$$

is the *Euclidean* $\mathcal{L}_2$-norm of a n-tuple vector $\nabla g_U(\mathbf{u}^*)$. The distance β_{HL} of this point $\mathbf{u}^*$ to the origin of u space is referred to as *Hasofer-Lind reliability index* [86] and is shown in Fig. 3.2. β_{HL} can be obtained from a nonlinear optimization scheme

$$\beta_{HL} = \inf_{g_U(\mathbf{u})} \| \mathbf{u} \| = \| \mathbf{u}^* \| = \boldsymbol{\alpha}^T \mathbf{u}^* \tag{A.10}$$

When the linear approximation of limit state in Eq. A.6 is substituted in Eq. A.4, the estimates of P_F and β_G by FORM becomes [168]

$$\begin{aligned} P_{F,1} &= \int_{\boldsymbol{\alpha}^T(\mathbf{u}-\mathbf{u}^*)<0} \phi(\mathbf{u}) d\mathbf{u} \\ &= \int_{\boldsymbol{\alpha}^T\mathbf{u}-\beta_{HL}<0} \phi(\mathbf{u}) d\mathbf{u} \\ &= \Phi(-\beta_{HL}) \end{aligned} \tag{A.11}$$

and

$$\beta_{G,1} = \beta_{HL}. \tag{A.12}$$

Second-Order Reliability Method (SORM)

Consider a suitable rotational transformation from u space to v space so that the the mapped design point $\mathbf{v}^*$ has coordinates $(0, 0, \cdots, -\beta_{HL})$. Suppose, the transformed vector $\mathbf{v} = \{v_1, v_2, \cdots, v_n\}^T = \{\bar{\mathbf{v}}, v_n\}^T$ where $\bar{\mathbf{v}} = \{v_1, v_2, \cdots, v_{n-1}\}^T$ and $v_n = h_V(\bar{\mathbf{v}})$ which is the root of the mapped limit state surface $g_V(\bar{\mathbf{v}}, v_n) = 0$ in v space. In this way, the limit state surface $g_V(\mathbf{v}) = g_V(\bar{\mathbf{v}}, v_n) = 0$ can be alternatively represented by $v_n = h_V(\bar{\mathbf{v}})$ in the v space. Consider a second-order approximation $g_Q(\mathbf{v}) = 0$ to $g_V(\mathbf{v}) = 0$ or rather an approximation $v_n = h_Q(\bar{\mathbf{v}})$ to $v_n = h_V(\bar{\mathbf{v}})$ of the limit state surface. If the quadratic approximant is of special form such as the rotational hyperparaboloid, it can be shown that [89]

$$h_Q(\bar{\mathbf{v}}) = -\beta_{HL} + \frac{1}{2} \sum_{i=1}^{n-1} \kappa_i v_i^2 \tag{A.13}$$

where κ_i is the ith principal curvature of the limit state surface at the design point. The above quadratic is equivalent to the actual $v_n = h_V(\bar{\mathbf{v}})$ in the sense that

$$h_Q(\bar{\mathbf{v}}^*) = h_V(\bar{\mathbf{v}}^*) \tag{A.14}$$

$$\frac{\partial h_Q}{\partial v_i}(\bar{\mathbf{v}}^*) = \frac{\partial h_V}{\partial v_i}(\bar{\mathbf{v}}^*) \tag{A.15}$$

$$\frac{\partial^2 h_Q}{\partial v_i \partial v_j}(\bar{\mathbf{v}}^*) = \frac{\partial^2 h_V}{\partial v_i \partial v_j}(\bar{\mathbf{v}}^*) \tag{A.16}$$

for $i, j = 1, 2, \cdots, n-1$. When the actual limit state surface is approximated by the hyperparaboloid in Eq. A.13, the estimate of P_F by SORM becomes [35]

$$P_{F,2} \simeq \Phi(-\beta_{HL}) \prod_{i=1}^{n-1} (1 - \kappa_i \beta_{HL})^{-\frac{1}{2}} \tag{A.17}$$

which is asymptotically exact when $\beta_{HL} \nearrow \infty$. An improvement over above probability estimate has also been proposed by Hohenbichler [89] which gives

$$P_{F,2} \simeq \Phi(-\beta_{HL}) \prod_{i=1}^{n-1} (1 - \kappa_i \Psi(-\beta_{HL}))^{-\frac{1}{2}} \tag{A.18}$$

where

$$\Psi(-\beta_{HL}) = \frac{\phi(-\beta_{HL})}{\Phi(-\beta_{HL})}. \tag{A.19}$$

Note that when $\beta_{HL} \nearrow \infty$, $\Psi(-\beta_{HL}) \nearrow \beta_{HL}$ and Eq. A.18 degenerates to Eq. A.17 as expected. Finally, the corresponding estimate of β_G becomes

$$\beta_{G,2} = \Phi^{-1}\left(-P_{F,2}\right). \tag{A.20}$$

A.2 Importance Sampling

Consider the Eq. A.4 which can be rewritten in the form

$$P_F = \Pr[g_{app}(\mathbf{U}) < 0] \frac{\Pr[g_U(\mathbf{U}) < 0]}{\Pr[g_{app}(\mathbf{U}) < 0]} = \Pr[g_{app}(\mathbf{U}) < 0]\ C_F \tag{A.21}$$

where $g_{app}(\mathbf{U})$ is either the linear or quadratic approximation to $g_U(\mathbf{U})$ and $C_F = \Pr[g_U(\mathbf{U}) < 0] / \Pr[g_{app}(\mathbf{U}) < 0]$ is the correction factor improving the reliability estimate by $g_{app}(\mathbf{U})$. When the quadratic approximation in Eq. A.13 is used, C_F can be approximated by simulation with importance sampling. According to Hohenbichler [89], it is given by

$$C_F \simeq \frac{1}{N_{IS}} \sum_{j=1}^{N_{IS}} C_{F,j} \tag{A.22}$$

in which

$$C_{F,j} = \frac{\Phi\left(h_Q(\hat{\mathbf{v}}_j)\right)}{\Phi\left(\beta_{HL}\right)} \exp\left[-\frac{1}{2}\Psi\left(\beta_{HL}\right) \sum_{i=1}^{n-1} \kappa_i \hat{v}_{i,j}^2\right], \tag{A.23}$$

$\hat{\mathbf{v}}_j = \{\hat{v}_{1,j}, \hat{v}_{2,j}, \cdots, \hat{v}_{n-1,j}\}^T$ is the jth realization of the independent Gaussian random vector $\hat{\mathbf{V}} \in \Re^{n-1}$ with mean and variance of ith component given by

$$\mathrm{E}(\hat{V}_i) = 0 \tag{A.24}$$

$$\mathrm{Var}(\hat{V}_i) = \frac{1}{[1 - \Psi\left(-\beta_{HL}\right)]} \tag{A.25}$$

and N_{IS} is the total number of samples for simulation. Thus, the estimates of P_F and β_G by simulation with importance sampling become

$$\begin{aligned} P_{F,3} \simeq\ & \Phi(-\beta_{HL}) \prod_{k=1}^{n-1} \{1 - \kappa_k \Psi(\beta_{HL})\}^{-\frac{1}{2}} \frac{1}{N_{IS}} \sum_{j=1}^{N_{IS}} \frac{\Phi\left(h_Q(\hat{\mathbf{v}}_j)\right)}{\Phi\left(\beta_{HL}\right)} \times \\ & \exp\left[-\frac{1}{2}\Psi\left(\beta_{HL}\right) \sum_{i=1}^{n-1} \kappa_i \hat{v}_{i,j}^2\right] \end{aligned} \tag{A.26}$$

and

$$\beta_{G,3} = \Phi^{-1}(-P_{F,3}). \tag{A.27}$$

APPENDIX B
Incremental Dynamic Analysis

B.1 Incremental Form of Equation of Motion

Consider the nonlinear equation of motion in Eq. 5.19. Let the vector functional $\mathbf{g}(\{\mathbf{X}_s, 0 < s < t\}; \boldsymbol{\alpha})$ be expressed in the matrix equation

$$\mathbf{g}\left(\{\mathbf{X}_s, 0 < s < t\}; \boldsymbol{\alpha}\right) = \mathbf{k}_t\left(\{\mathbf{X}_s, 0 < s < t\}; \boldsymbol{\alpha}\right)\mathbf{X}_t \tag{B.1}$$

in which $\mathbf{k}_t$ is the instantaneous stiffness matrix at time t. Note that each component of this matrix $\mathbf{k}_t$ is a functional due to hereditary nature of the restoring force. Consider now the incremental form of equation of motion

$$\mathbf{m}\Delta\ddot{\mathbf{X}}_t + \mathbf{c}\Delta\dot{\mathbf{X}}_t + \mathbf{k}_{t+\Delta t}\mathbf{X}_{t+\Delta t} - \mathbf{k}_t\mathbf{X}_t = -\mathbf{m}\mathbf{d}\Delta W_\tau(t) \tag{B.2}$$

in which Δt is a finite time increment, $\Delta\mathbf{X}_t = \mathbf{X}_{t+\Delta t} - \mathbf{X}_t$, and $\Delta W_\tau(t) = W_\tau(t+\Delta t) - W_\tau(t)$. Eq. B.2 is obtained when the equations of motion at times t and $t + \Delta t$ combined with the the matrix equation for restoring force in Eq.B.1 are subtracted from each other. Suppose, the time step Δt is sufficiently small during which the change in stiffness characteristics of structural components can be neglected. Then, the incremental equation of motion takes the form

$$\mathbf{m}\Delta\ddot{\mathbf{X}}_t + \mathbf{c}\Delta\dot{\mathbf{X}}_t + \mathbf{k}_t\Delta\mathbf{X}_t = -\mathbf{m}\mathbf{d}\Delta W_\tau(t). \tag{B.3}$$

with the approximation

$$\mathbf{k}_{t+\Delta t}\left(\{\mathbf{X}_s, 0 < s < t + \Delta t\}; \boldsymbol{\alpha}\right) = \mathbf{k}_t\left(\{\mathbf{X}_s, 0 < s < t\}; \boldsymbol{\alpha}\right). \tag{B.4}$$

B.2 Numerical Integration of Equation of Motion

Consider the Newmark integration scheme in which the generalized velocity and displacement vector at time $t + \Delta t$ is approximated by following difference equation [23,145]

$$\dot{\mathbf{X}}_{t+\Delta t} = \dot{\mathbf{X}}_t + \Delta t \left[(1-\gamma_1)\ddot{\mathbf{X}}_t + \gamma_1 \ddot{\mathbf{X}}_{t+\Delta t}\right] \tag{B.5}$$

$$\mathbf{X}_{t+\Delta t} = \mathbf{X}_t + \Delta t \dot{\mathbf{X}}_t + \Delta t^2 \left[\left(\frac{1}{2} - \gamma_2\right) \ddot{\mathbf{X}}_t + \gamma_2 \ddot{\mathbf{X}}_{t+\Delta t}\right] \tag{B.6}$$

where γ_1 and γ_2 are parameters determining the accuracy and stability of numerical integration. When $\gamma_1 = 1/2$, $\gamma_2 = 1/6$ and $\gamma_1 = 1/2$, $\gamma_2 = 1/4$ are used, the above equations correspond to the familiar linear acceleration method and constant-average-acceleration method, respectively [23]. From Eqs. B.5 and B.6, the incremental acceleration and velocity vectors can be obtained as

$$\Delta \ddot{\mathbf{X}}_t = \frac{\Delta \mathbf{X}_t}{\gamma_2 \Delta t^2} - \frac{\dot{\mathbf{X}}_t}{\gamma_2 \Delta t} - \frac{\ddot{\mathbf{X}}_t}{2\gamma_2} \tag{B.7}$$

$$\Delta \dot{\mathbf{X}}_t = \left(1 - \frac{\gamma_1}{2\gamma_2}\right) \Delta t \ddot{\mathbf{X}}_t + \frac{\gamma_1}{\gamma_2 \Delta t} \Delta \mathbf{X}_t - \frac{\gamma_1}{\gamma_2} \dot{\mathbf{X}}_t \tag{B.8}$$

which when substituted in the incremental form of equation of motion (Eq. B.2) gives rise to the following system of linear algebraic equation

$$\mathbf{k}_t^* \Delta \mathbf{X}_t = \Delta \mathbf{F}_t^* \tag{B.9}$$

where

$$\mathbf{k}_t^* = \mathbf{k}_t + \frac{1}{\gamma_2 \Delta t^2} \mathbf{m} + \frac{\gamma_1}{\gamma_2 \Delta t} \mathbf{c} \tag{B.10}$$

and

$$\Delta \mathbf{F}_t^* = -\Delta W_r(t) \mathbf{m} \mathbf{d} + \left[\frac{1}{\gamma_2 \Delta t} \dot{\mathbf{X}}_t + \frac{1}{2\gamma_2} \ddot{\mathbf{X}}_t\right] \mathbf{m} + \left[\frac{\gamma_1}{\gamma_2} \dot{\mathbf{X}}_t - \left(1 - \frac{\gamma_1}{2\gamma_2}\right) \Delta t \ddot{\mathbf{X}}_t\right] \mathbf{c} \tag{B.11}$$

When $\Delta \mathbf{X}_t$ is calculated by solving Eq. B.9, the generalized displacement vector $\mathbf{X}_{t+\Delta t}$ at time $t + \Delta t$ can be obtained as

$$\mathbf{X}_{t+\Delta t} = \mathbf{X}_t + \Delta \mathbf{X}_t. \tag{B.12}$$

This numerical scheme with $\gamma_1 = 1/2$ and $\gamma_2 = 1/4$ is unconditionally stable. Thus, the determination of the time step Δt depends only on the accuracy desired in the numerical integration.

APPENDIX C
Runge-Kutta Method

C.1 Initial Value Problem

Consider the initial value problem

$$\begin{aligned} \dot{\theta}(t) &= h(\theta(t), t) \\ \theta(0) &= \theta_0 \end{aligned} \tag{C.1}$$

where $t \in \Re$ and $\theta \in \Re$ are independent and dependent variables, respectively and θ_0 is the initial value of $\theta(t)$. A general explicit one-step method for the solution of Eq. C.1 is given by [124,191,120,87]

$$\theta_{i+1} - \theta_i = \Delta t \varphi(t_i, \theta_i; \Delta t) \tag{C.2}$$

where t_i is a discrete value of independent variable t, $\theta_i = \theta(t_i)$, and $\varphi(\cdot)$ will be defined later. The fact that Eq. C.2 does not mention the function $h(\theta, t)$ which defines the differential equation, makes it impossible to characterize the order of the method independently of the differential equation. Traditionally, Runge-Kutta methods are all explicit, although, recently, implicit Runge-Kutta methods for improving stability characteristics have also been considered. In this study, however, "Runge-Kutta" will be phrased to imply "explicit Runge-Kutta" method.

Definition *The method in Eq. C.2 is said to have* **order** *p if p is the largest integer for which*

$$\theta(t + \Delta t) - \theta(t) - \Delta t \varphi(t, \theta(t); \Delta t) = O\left(\Delta t^{p+1}\right) \tag{C.3}$$

holds, where $\theta(t)$ is the theoretical solution of the initial value problem

C.2 Explicit Runge-Kutta Method

The general R-stage explicit Runge-Kutta method is defined by Eq. C.2 in which

$$\varphi(t,\theta;\Delta t) = \sum_{r=1}^{R} A_r K_r \tag{C.4}$$

where

$$\begin{aligned} K_1 &= h(t,\theta) \\ K_r &= h\left(t + \Delta t \sum_{s=1}^{r-1} B_{rs},\ \theta + \Delta t \sum_{s=1}^{r-1} B_{rs} K_s\right),\quad r = 2,3,\cdots,R \end{aligned} \tag{C.5}$$

with A_r and B_{rs} as appropriate constants. Note that an R-stage Runge-Kutta method involves R function evaluations per step. Each of the functions $K_r(t,\theta;\Delta t)$, $r = 1,2,\cdots,R$, may be interpreted as an approximation to the time derivative $\dot{\theta}$, and the functions $\varphi(t,\theta(t);\Delta t)$ as the weighted average of these approximations.

C.3 Special Cases

There is a great deal of tedious algebraic manipulation involved in deriving the expressions for above constants A_r and B_{rs} for an arbitrary order. Two well-known four-stage fourth order methods are [124,181]

$$\theta_{i+1} - \theta_i = \frac{\Delta t}{6}(K_1 + 2K_2 + 2K_3 + K_4) \tag{C.6}$$

where

$$\begin{aligned} K_1 &= h(t_i,\theta_i) \\ K_2 &= h\left(t_i + \frac{1}{2}\Delta t, \theta_i + \frac{1}{2}\Delta t K_1\right) \\ K_3 &= h\left(t_i + \frac{1}{2}\Delta t, \theta_i + \frac{1}{2}\Delta t K_2\right) \\ K_4 &= h(t_i + \Delta t, \theta_i + \Delta t K_3) \end{aligned} \tag{C.7}$$

and

$$\theta_{i+1} - \theta_i = \frac{\Delta t}{8}(K_1 + 3K_2 + 3K_3 + K_4) \tag{C.8}$$

where

$$\begin{aligned} K_1 &= h(t_i, \theta_i) \\ K_2 &= h\left(t_i + \frac{1}{3}\Delta t, \theta_i + \frac{1}{3}\Delta t K_1\right) \\ K_3 &= h\left(t_i + \frac{2}{3}\Delta t, \theta_i - \frac{1}{3}\Delta t K_1 + \Delta t K_2\right) \\ K_4 &= h(t_i + \Delta t, \theta_i + \Delta t K_1 - \Delta t K_2 + \Delta t K_3) \end{aligned} \tag{C.9}$$

The method in Eq. C.7 is the most popular of all Runge-Kutta methods. It is frequently referred to, somewhat loosely, as "the fourth-order Runge-Kutta method".

Higher-order Runge-Kutta methods usually involve complicated algebra [39,40,41,42]. For examples, the six-stage fifth order method is [124]

$$\theta_{i+1} - \theta_i = \frac{\Delta t}{192}(23K_1 + 125K_3 - 81K_5 + 125K_6) \tag{C.10}$$

where

$$\begin{aligned} K_1 &= h(t_i, \theta_i) \\ K_2 &= h\left(t_i + \frac{1}{3}\Delta t, \theta_i + \frac{1}{3}\Delta t K_1\right) \\ K_3 &= h\left(t_i + \frac{2}{5}\Delta t, \theta_i + \frac{1}{25}\Delta t[4K_1 + 6K_2]\right) \\ K_4 &= h\left(t_i + \Delta t, \theta_i + \frac{1}{4}\Delta t[K_1 - 12K_2 + 15K_3]\right) \\ K_5 &= h\left(t_i + \frac{2}{3}\Delta t, \theta_i + \frac{1}{81}\Delta t[6K_1 + 90K_2 - 50K_3 + 8K_4]\right) \\ K_6 &= h\left(t_i + \frac{4}{5}\Delta t, \theta_i + \frac{1}{75}\Delta t[6K_1 + 36K_2 + 10K_3 + 8K_4]\right) \end{aligned} \tag{C.11}$$

and the eight-stage sixth order method is [96]

$$\theta_{i+1} - \theta_i = \frac{\Delta t}{840}(41K_1 + 216K_3 + 27K_4 + 272K_5 + 27K_6 + 216K_7 + 41K_8) \tag{C.12}$$

where

$$
\begin{aligned}
K_1 &= h\left(t_i, \theta_i\right) \\
K_2 &= h\left(t_i + \frac{1}{9}\Delta t, \theta_i + \frac{1}{9}\Delta t K_1\right) \\
K_3 &= h\left(t_i + \frac{1}{6}\Delta t, \theta_i + \frac{1}{24}\Delta t[K_1 + 3K_2]\right) \\
K_4 &= h\left(t_i + \frac{1}{3}\Delta t, \theta_i + \frac{1}{6}\Delta t[K_1 - 3K_2 + 4K_3]\right) \\
K_5 &= h\left(t_i + \frac{1}{2}\Delta t, \theta_i + \frac{1}{8}\Delta t[-5K_1 + 27K_2 - 24K_3 + 6K_4]\right) \\
K_6 &= h\left(t_i + \frac{2}{3}\Delta t, \theta_i + \frac{1}{9}\Delta t[221K_1 - 981K_2 + 867K_3 - 102K_4 + K_5]\right) \\
K_7 &= h\left(t_i + \frac{5}{6}\Delta t, \theta_i + \frac{1}{48}\Delta t[-183K_1 + 678K_2 - 472K_3 - 66K_4 + 80K_5 \right. \\
&\quad \left. +3K_6]\right) \\
K_8 &= h\left(t_i + \Delta t, \theta_i + \frac{1}{82}\Delta t[716K_1 - 2079K_2 + 1002K_3 + 834K_4 - 454K_5 \right. \\
&\quad \left. -9K_6 + 72K_7]\right). \qquad \text{(C.13)}
\end{aligned}
$$

APPENDIX D
Evaluation of $e^{\mathbf{A}}$

D.1 Preliminaries

Consider a real $K \times K$ square matrix $\mathbf{A}$. A non-zero vector $\mathbf{x} \in \mathcal{C}^K$ satisfying the equation

$$\mathbf{A}\mathbf{x} = \lambda\mathbf{x} \tag{D.1}$$

is called the right eigenvector of $\mathbf{A}$ with the associated eigenvalue λ. When Eq. D.1 is written as

$$\mathbf{x}\mathbf{A} = \lambda\mathbf{x} \tag{D.2}$$

the vector $\mathbf{x}$ is known as the left eigenvector of $\mathbf{A}$. Suppose, there are K linearly independent family $\mathbf{x}^{(1)}, \mathbf{x}^{(2)}, \cdots, \mathbf{x}^{(K)}$ of either right and left eigenvectors of $\mathbf{A}$. Then there exists linearly independent right eigenvectors $\boldsymbol{\phi}^{(1)}, \boldsymbol{\phi}^{(2)}, \cdots, \boldsymbol{\phi}^{(K)}$ and linearly independent left eigenvectors $\boldsymbol{\psi}^{(1)}, \boldsymbol{\psi}^{(2)}, \cdots, \boldsymbol{\psi}^{(K)}$, which satisfies orthogonality condition

$$\left(\boldsymbol{\phi}^{(i)}, \boldsymbol{\psi}^{(j)}\right) \stackrel{\text{def}}{=} \sum_{k=1}^{K} \phi_{ik}\overline{\psi}_{jk} = \delta_{ij} \tag{D.3}$$

where $\boldsymbol{\phi}^{(i)} = \{\phi_{i1}, \phi_{i2}, \cdots, \phi_{iK}\}^T$, $\boldsymbol{\psi}^{(i)} = \{\psi_{i1}, \psi_{i2}, \cdots, \psi_{iK}\}^T$, $\overline{\psi}_{jk}$ is the complex conjugate of ψ_{jk}, and δ_{ij} is the kronecker delta. Assume that $\lambda_1, \lambda_2, \cdots, \lambda_K$ are the eigenvalues (which may not be distinct) corresponding to the eigenvectors $\boldsymbol{\phi}^{(1)}, \boldsymbol{\phi}^{(2)}, \cdots, \boldsymbol{\phi}^{(K)}$. Then the matrix $\mathbf{A}$ can represented by

$$\mathbf{A} = \boldsymbol{\Phi}\boldsymbol{\Lambda}\boldsymbol{\Psi} \tag{D.4}$$

where

$$\mathbf{\Phi} = \begin{bmatrix} \phi_{11} & \phi_{21} & \cdots & \phi_{K1} \\ \phi_{12} & \phi_{22} & \cdots & \phi_{K2} \\ \vdots & \vdots & \ddots & \vdots \\ \phi_{1K} & \phi_{2K} & \cdots & \phi_{KK} \end{bmatrix} \tag{D.5}$$

$$\mathbf{\Psi} = \begin{bmatrix} \psi_{11} & \psi_{12} & \cdots & \psi_{1K} \\ \psi_{21} & \psi_{22} & \cdots & \psi_{2K} \\ \vdots & \vdots & \ddots & \vdots \\ \psi_{K1} & \psi_{K2} & \cdots & \psi_{KK} \end{bmatrix} \tag{D.6}$$

and

$$\mathbf{\Lambda} = \begin{bmatrix} \lambda_1 & 0 & \cdots & 0 \\ 0 & \lambda_2 & \cdots & 0 \\ \vdots & \vdots & \ddots & 0 \\ 0 & 0 & \cdots & \lambda_K \end{bmatrix}. \tag{D.7}$$

From Eq. D.3, it can be shown that

$$\mathbf{\Psi\Phi} = \mathbf{\Phi\Psi} = \mathbf{I} \tag{D.8}$$

where $\mathbf{I}$ is the K-dimensional identity matrix. This immediately gives

$$\mathbf{A}^m = \mathbf{\Phi\Lambda}^m\mathbf{\Psi} \tag{D.9}$$

with

$$\mathbf{\Lambda}^m = \begin{bmatrix} \lambda_1{}^m & 0 & \cdots & 0 \\ 0 & \lambda_2{}^m & \cdots & 0 \\ \vdots & \vdots & \ddots & 0 \\ 0 & 0 & \cdots & \lambda_K{}^m \end{bmatrix}. \tag{D.10}$$

D.2 Expansion of $e^{\mathbf{A}}$

Consider now the expansion of $e^{\mathbf{A}}$ given by

$$e^{\mathbf{A}} = \sum_{m=0}^{\infty} \frac{\mathbf{A}^m}{m!} \tag{D.11}$$

This equation when combined with Eqs. D.9 and D.10 reduces to

$$\begin{aligned} e^{\mathbf{A}} &= \sum_{m=0}^{\infty} \frac{\mathbf{\Phi}\mathbf{\Lambda}^m\mathbf{\Psi}}{m!} \\ &= \mathbf{\Phi}\left(\sum_{m=0}^{\infty} \frac{\mathbf{\Lambda}^m}{m!}\right)\mathbf{\Psi} \\ &= \mathbf{\Phi}e^{\mathbf{\Lambda}}\mathbf{\Psi} \end{aligned} \tag{D.12}$$

where

$$e^{\mathbf{\Lambda}} = \begin{bmatrix} e^{\lambda_1} & 0 & \cdots & 0 \\ 0 & e^{\lambda_2} & \cdots & 0 \\ \vdots & \vdots & \ddots & 0 \\ 0 & 0 & \cdots & e^{\lambda_K} \end{bmatrix}. \tag{D.13}$$

NATIONAL CENTER FOR EARTHQUAKE ENGINEERING RESEARCH
LIST OF TECHNICAL REPORTS

The National Center for Earthquake Engineering Research (NCEER) publishes technical reports on a variety of subjects related to earthquake engineering written by authors funded through NCEER. These reports are available from both NCEER's Publications Department and the National Technical Information Service (NTIS). Requests for reports should be directed to the Publications Department, National Center for Earthquake Engineering Research, State University of New York at Buffalo, Red Jacket Quadrangle, Buffalo, New York 14261. Reports can also be requested through NTIS, 5285 Port Royal Road, Springfield, Virginia 22161. NTIS accession numbers are shown in parenthesis, if available.

NCEER-87-0001 "First-Year Program in Research, Education and Technology Transfer," 3/5/87, (PB88-134275).

NCEER-87-0002 "Experimental Evaluation of Instantaneous Optimal Algorithms for Structural Control," by R.C. Lin, T.T. Soong and A.M. Reinhorn, 4/20/87, (PB88-134341).

NCEER-87-0003 "Experimentation Using the Earthquake Simulation Facilities at University at Buffalo," by A.M. Reinhorn and R.L. Ketter, to be published.

NCEER-87-0004 "The System Characteristics and Performance of a Shaking Table," by J.S. Hwang, K.C. Chang and G.C. Lee, 6/1/87, (PB88-134259). This report is available only through NTIS (see address given above).

NCEER-87-0005 "A Finite Element Formulation for Nonlinear Viscoplastic Material Using a Q Model," by O. Gyebi and G. Dasgupta, 11/2/87, (PB88-213764).

NCEER-87-0006 "Symbolic Manipulation Program (SMP) - Algebraic Codes for Two and Three Dimensional Finite Element Formulations," by X. Lee and G. Dasgupta, 11/9/87, (PB88-218522).

NCEER-87-0007 "Instantaneous Optimal Control Laws for Tall Buildings Under Seismic Excitations," by J.N. Yang, A. Akbarpour and P. Ghaemmaghami, 6/10/87, (PB88-134333). This report is only available through NTIS (see address given above).

NCEER-87-0008 "IDARC: Inelastic Damage Analysis of Reinforced Concrete Frame - Shear-Wall Structures," by Y.J. Park, A.M. Reinhorn and S.K. Kunnath, 7/20/87, (PB88-134325).

NCEER-87-0009 "Liquefaction Potential for New York State: A Preliminary Report on Sites in Manhattan and Buffalo," by M. Budhu, V. Vijayakumar, R.F. Giese and L. Baumgras, 8/31/87, (PB88-163704). This report is available only through NTIS (see address given above).

NCEER-87-0010 "Vertical and Torsional Vibration of Foundations in Inhomogeneous Media," by A.S. Veletsos and K.W. Dotson, 6/1/87, (PB88-134291).

NCEER-87-0011 "Seismic Probabilistic Risk Assessment and Seismic Margins Studies for Nuclear Power Plants," by Howard H.M. Hwang, 6/15/87, (PB88-134267).

NCEER-87-0012 "Parametric Studies of Frequency Response of Secondary Systems Under Ground-Acceleration Excitations," by Y. Yong and Y.K. Lin, 6/10/87, (PB88-134309).

NCEER-87-0013 "Frequency Response of Secondary Systems Under Seismic Excitation," by J.A. HoLung, J. Cai and Y.K. Lin, 7/31/87, (PB88-134317).

NCEER-87-0014 "Modelling Earthquake Ground Motions in Seismically Active Regions Using Parametric Time Series Methods," by G.W. Ellis and A.S. Cakmak, 8/25/87, (PB88-134283).

NCEER-87-0015 "Detection and Assessment of Seismic Structural Damage," by E. DiPasquale and A.S. Cakmak, 8/25/87, (PB88-163712).

NCEER-87-0016 "Pipeline Experiment at Parkfield, California," by J. Isenberg and E. Richardson, 9/15/87, (PB88-163720). This report is available only through NTIS (see address given above).

NCEER-87-0017 "Digital Simulation of Seismic Ground Motion," by M. Shinozuka, G. Deodatis and T. Harada, 8/31/87, (PB88-155197). This report is available only through NTIS (see address given above).

NCEER-87-0018 "Practical Considerations for Structural Control: System Uncertainty, System Time Delay and Truncation of Small Control Forces," J.N. Yang and A. Akbarpour, 8/10/87, (PB88-163738).

NCEER-87-0019 "Modal Analysis of Nonclassically Damped Structural Systems Using Canonical Transformation," by J.N. Yang, S. Sarkani and F.X. Long, 9/27/87, (PB88-187851).

NCEER-87-0020 "A Nonstationary Solution in Random Vibration Theory," by J.R. Red-Horse and P.D. Spanos, 11/3/87, (PB88-163746).

NCEER-87-0021 "Horizontal Impedances for Radially Inhomogeneous Viscoelastic Soil Layers," by A.S. Veletsos and K.W. Dotson, 10/15/87, (PB88-150859).

NCEER-87-0022 "Seismic Damage Assessment of Reinforced Concrete Members," by Y.S. Chung, C. Meyer and M. Shinozuka, 10/9/87, (PB88-150867). This report is available only through NTIS (see address given above).

NCEER-87-0023 "Active Structural Control in Civil Engineering," by T.T. Soong, 11/11/87, (PB88-187778).

NCEER-87-0024 "Vertical and Torsional Impedances for Radially Inhomogeneous Viscoelastic Soil Layers," by K.W. Dotson and A.S. Veletsos, 12/87, (PB88-187786).

NCEER-87-0025 "Proceedings from the Symposium on Seismic Hazards, Ground Motions, Soil-Liquefaction and Engineering Practice in Eastern North America," October 20-22, 1987, edited by K.H. Jacob, 12/87, (PB88-188115).

NCEER-87-0026 "Report on the Whittier-Narrows, California, Earthquake of October 1, 1987," by J. Pantelic and A. Reinhorn, 11/87, (PB88-187752). This report is available only through NTIS (see address given above).

NCEER-87-0027 "Design of a Modular Program for Transient Nonlinear Analysis of Large 3-D Building Structures," by S. Srivastav and J.F. Abel, 12/30/87, (PB88-187950).

NCEER-87-0028 "Second-Year Program in Research, Education and Technology Transfer," 3/8/88, (PB88-219480).

NCEER-88-0001 "Workshop on Seismic Computer Analysis and Design of Buildings With Interactive Graphics," by W. McGuire, J.F. Abel and C.H. Conley, 1/18/88, (PB88-187760).

NCEER-88-0002 "Optimal Control of Nonlinear Flexible Structures," by J.N. Yang, F.X. Long and D. Wong, 1/22/88, (PB88-213772).

NCEER-88-0003 "Substructuring Techniques in the Time Domain for Primary-Secondary Structural Systems," by G.D. Manolis and G. Juhn, 2/10/88, (PB88-213780).

NCEER-88-0004 "Iterative Seismic Analysis of Primary-Secondary Systems," by A. Singhal, L.D. Lutes and P.D. Spanos, 2/23/88, (PB88-213798).

NCEER-88-0005 "Stochastic Finite Element Expansion for Random Media," by P.D. Spanos and R. Ghanem, 3/14/88, (PB88-213806).

NCEER-88-0006 "Combining Structural Optimization and Structural Control," by F.Y. Cheng and C.P. Pantelides, 1/10/88, (PB88-213814).

NCEER-88-0007 "Seismic Performance Assessment of Code-Designed Structures," by H.H-M. Hwang, J-W. Jaw and H-J. Shau, 3/20/88, (PB88-219423).

NCEER-88-0008 "Reliability Analysis of Code-Designed Structures Under Natural Hazards," by H.H-M. Hwang, H. Ushiba and M. Shinozuka, 2/29/88, (PB88-229471).

NCEER-88-0009 "Seismic Fragility Analysis of Shear Wall Structures," by J-W Jaw and H.H-M. Hwang, 4/30/88, (PB89-102867).

NCEER-88-0010 "Base Isolation of a Multi-Story Building Under a Harmonic Ground Motion - A Comparison of Performances of Various Systems," by F-G Fan, G. Ahmadi and I.G. Tadjbakhsh, 5/18/88, (PB89-122238).

NCEER-88-0011 "Seismic Floor Response Spectra for a Combined System by Green's Functions," by F.M. Lavelle, L.A. Bergman and P.D. Spanos, 5/1/88, (PB89-102875).

NCEER-88-0012 "A New Solution Technique for Randomly Excited Hysteretic Structures," by G.Q. Cai and Y.K. Lin, 5/16/88, (PB89-102883).

NCEER-88-0013 "A Study of Radiation Damping and Soil-Structure Interaction Effects in the Centrifuge," by K. Weissman, supervised by J.H. Prevost, 5/24/88, (PB89-144703).

NCEER-88-0014 "Parameter Identification and Implementation of a Kinematic Plasticity Model for Frictional Soils," by J.H. Prevost and D.V. Griffiths, to be published.

NCEER-88-0015 "Two- and Three- Dimensional Dynamic Finite Element Analyses of the Long Valley Dam," by D.V. Griffiths and J.H. Prevost, 6/17/88, (PB89-144711).

NCEER-88-0016 "Damage Assessment of Reinforced Concrete Structures in Eastern United States," by A.M. Reinhorn, M.J. Seidel, S.K. Kunnath and Y.J. Park, 6/15/88, (PB89-122220).

NCEER-88-0017 "Dynamic Compliance of Vertically Loaded Strip Foundations in Multilayered Viscoelastic Soils," by S. Ahmad and A.S.M. Israil, 6/17/88, (PB89-102891).

NCEER-88-0018 "An Experimental Study of Seismic Structural Response With Added Viscoelastic Dampers," by R.C. Lin, Z. Liang, T.T. Soong and R.H. Zhang, 6/30/88, (PB89-122212). This report is available only through NTIS (see address given above).

NCEER-88-0019 "Experimental Investigation of Primary - Secondary System Interaction," by G.D. Manolis, G. Juhn and A.M. Reinhorn, 5/27/88, (PB89-122204).

NCEER-88-0020 "A Response Spectrum Approach For Analysis of Nonclassically Damped Structures," by J.N. Yang, S. Sarkani and F.X. Long, 4/22/88, (PB89-102909).

NCEER-88-0021 "Seismic Interaction of Structures and Soils: Stochastic Approach," by A.S. Veletsos and A.M. Prasad, 7/21/88, (PB89-122196).

NCEER-88-0022 "Identification of the Serviceability Limit State and Detection of Seismic Structural Damage," by E. DiPasquale and A.S. Cakmak, 6/15/88, (PB89-122188). This report is available only through NTIS (see address given above).

NCEER-88-0023 "Multi-Hazard Risk Analysis: Case of a Simple Offshore Structure," by B.K. Bhartia and E.H. Vanmarcke, 7/21/88, (PB89-145213).

NCEER-88-0024 "Automated Seismic Design of Reinforced Concrete Buildings," by Y.S. Chung, C. Meyer and M. Shinozuka, 7/5/88, (PB89-122170). This report is available only through NTIS (see address given above).

NCEER-88-0025 "Experimental Study of Active Control of MDOF Structures Under Seismic Excitations," by L.L. Chung, R.C. Lin, T.T. Soong and A.M. Reinhorn, 7/10/88, (PB89-122600).

NCEER-88-0026 "Earthquake Simulation Tests of a Low-Rise Metal Structure," by J.S. Hwang, K.C. Chang, G.C. Lee and R.L. Ketter, 8/1/88, (PB89-102917).

NCEER-88-0027 "Systems Study of Urban Response and Reconstruction Due to Catastrophic Earthquakes," by F. Kozin and H.K. Zhou, 9/22/88, (PB90-162348).

NCEER-88-0028 "Seismic Fragility Analysis of Plane Frame Structures," by H.H-M. Hwang and Y.K. Low, 7/31/88, (PB89-131445).

NCEER-88-0029 "Response Analysis of Stochastic Structures," by A. Kardara, C. Bucher and M. Shinozuka, 9/22/88, (PB89-174429).

NCEER-88-0030 "Nonnormal Accelerations Due to Yielding in a Primary Structure," by D.C.K. Chen and L.D. Lutes, 9/19/88, (PB89-131437).

NCEER-88-0031 "Design Approaches for Soil-Structure Interaction," by A.S. Veletsos, A.M. Prasad and Y. Tang, 12/30/88, (PB89-174437). This report is available only through NTIS (see address given above).

NCEER-88-0032 "A Re-evaluation of Design Spectra for Seismic Damage Control," by C.J. Turkstra and A.G. Tallin, 11/7/88, (PB89-145221).

NCEER-88-0033 "The Behavior and Design of Noncontact Lap Splices Subjected to Repeated Inelastic Tensile Loading," by V.E. Sagan, P. Gergely and R.N. White, 12/8/88, (PB89-163737).

NCEER-88-0034 "Seismic Response of Pile Foundations," by S.M. Mamoon, P.K. Banerjee and S. Ahmad, 11/1/88, (PB89-145239).

NCEER-88-0035 "Modeling of R/C Building Structures With Flexible Floor Diaphragms (IDARC2)," by A.M. Reinhorn, S.K. Kunnath and N. Panahshahi, 9/7/88, (PB89-207153).

NCEER-88-0036 "Solution of the Dam-Reservoir Interaction Problem Using a Combination of FEM, BEM with Particular Integrals, Modal Analysis, and Substructuring," by C-S. Tsai, G.C. Lee and R.L. Ketter, 12/31/88, (PB89-207146).

NCEER-88-0037 "Optimal Placement of Actuators for Structural Control," by F.Y. Cheng and C.P. Pantelides, 8/15/88, (PB89-162846).

NCEER-88-0038 "Teflon Bearings in Aseismic Base Isolation: Experimental Studies and Mathematical Modeling," by A. Mokha, M.C. Constantinou and A.M. Reinhorn, 12/5/88, (PB89-218457). This report is available only through NTIS (see address given above).

NCEER-88-0039 "Seismic Behavior of Flat Slab High-Rise Buildings in the New York City Area," by P. Weidlinger and M. Ettouney, 10/15/88, (PB90-145681).

NCEER-88-0040 "Evaluation of the Earthquake Resistance of Existing Buildings in New York City," by P. Weidlinger and M. Ettouney, 10/15/88, to be published.

NCEER-88-0041 "Small-Scale Modeling Techniques for Reinforced Concrete Structures Subjected to Seismic Loads," by W. Kim, A. El-Attar and R.N. White, 11/22/88, (PB89-189625).

NCEER-88-0042 "Modeling Strong Ground Motion from Multiple Event Earthquakes," by G.W. Ellis and A.S. Cakmak, 10/15/88, (PB89-174445).

NCEER-88-0043 "Nonstationary Models of Seismic Ground Acceleration," by M. Grigoriu, S.E. Ruiz and E. Rosenblueth, 7/15/88, (PB89-189617).

NCEER-88-0044 "SARCF User's Guide: Seismic Analysis of Reinforced Concrete Frames," by Y.S. Chung, C. Meyer and M. Shinozuka, 11/9/88, (PB89-174452).

NCEER-88-0045 "First Expert Panel Meeting on Disaster Research and Planning," edited by J. Pantelic and J. Stoyle, 9/15/88, (PB89-174460).

NCEER-88-0046 "Preliminary Studies of the Effect of Degrading Infill Walls on the Nonlinear Seismic Response of Steel Frames," by C.Z. Chrysostomou, P. Gergely and J.F. Abel, 12/19/88, (PB89-208383).

NCEER-88-0047 "Reinforced Concrete Frame Component Testing Facility - Design, Construction, Instrumentation and Operation," by S.P. Pessiki, C. Conley, T. Bond, P. Gergely and R.N. White, 12/16/88, (PB89-174478).

NCEER-89-0001 "Effects of Protective Cushion and Soil Compliancy on the Response of Equipment Within a Seismically Excited Building," by J.A. HoLung, 2/16/89, (PB89-207179).

NCEER-89-0002 "Statistical Evaluation of Response Modification Factors for Reinforced Concrete Structures," by H.H-M. Hwang and J-W. Jaw, 2/17/89, (PB89-207187).

NCEER-89-0003 "Hysteretic Columns Under Random Excitation," by G-Q. Cai and Y.K. Lin, 1/9/89, (PB89-196513).

NCEER-89-0004 "Experimental Study of 'Elephant Foot Bulge' Instability of Thin-Walled Metal Tanks," by Z-H. Jia and R.L. Ketter, 2/22/89, (PB89-207195).

NCEER-89-0005 "Experiment on Performance of Buried Pipelines Across San Andreas Fault," by J. Isenberg, E. Richardson and T.D. O'Rourke, 3/10/89, (PB89-218440). This report is available only through NTIS (see address given above).

NCEER-89-0006 "A Knowledge-Based Approach to Structural Design of Earthquake-Resistant Buildings," by M. Subramani, P. Gergely; C.H. Conley, J.F. Abel and A.H. Zaghw, 1/15/89, (PB89-218465).

NCEER-89-0007 "Liquefaction Hazards and Their Effects on Buried Pipelines," by T.D. O'Rourke and P.A. Lane, 2/1/89, (PB89-218481).

NCEER-89-0008 "Fundamentals of System Identification in Structural Dynamics," by H. Imai, C-B. Yun, O. Maruyama and M. Shinozuka, 1/26/89, (PB89-207211).

NCEER-89-0009 "Effects of the 1985 Michoacan Earthquake on Water Systems and Other Buried Lifelines in Mexico," by A.G. Ayala and M.J. O'Rourke, 3/8/89, (PB89-207229).

NCEER-89-R010 "NCEER Bibliography of Earthquake Education Materials," by K.E.K. Ross, Second Revision, 9/1/89, (PB90-125352).

NCEER-89-0011 "Inelastic Three-Dimensional Response Analysis of Reinforced Concrete Building Structures (IDARC-3D), Part I - Modeling," by S.K. Kunnath and A.M. Reinhorn, 4/17/89, (PB90-114612).

NCEER-89-0012 "Recommended Modifications to ATC-14," by C.D. Poland and J.O. Malley, 4/12/89, (PB90-108648).

NCEER-89-0013 "Repair and Strengthening of Beam-to-Column Connections Subjected to Earthquake Loading," by M. Corazao and A.J. Durrani, 2/28/89, (PB90-109885).

NCEER-89-0014 "Program EXKAL2 for Identification of Structural Dynamic Systems," by O. Maruyama, C-B. Yun, M. Hoshiya and M. Shinozuka, 5/19/89, (PB90-109877).

NCEER-89-0015 "Response of Frames With Bolted Semi-Rigid Connections, Part I - Experimental Study and Analytical Predictions," by P.J. DiCorso, A.M. Reinhorn, J.R. Dickerson, J.B. Radziminski and W.L. Harper, 6/1/89, to be published.

NCEER-89-0016 "ARMA Monte Carlo Simulation in Probabilistic Structural Analysis," by P.D. Spanos and M.P. Mignolet, 7/10/89, (PB90-109893).

NCEER-89-P017 "Preliminary Proceedings from the Conference on Disaster Preparedness - The Place of Earthquake Education in Our Schools," Edited by K.E.K. Ross, 6/23/89, (PB90-108606).

NCEER-89-0017 "Proceedings from the Conference on Disaster Preparedness - The Place of Earthquake Education in Our Schools," Edited by K.E.K. Ross, 12/31/89, (PB90-207895). This report is available only through NTIS (see address given above).

NCEER-89-0018 "Multidimensional Models of Hysteretic Material Behavior for Vibration Analysis of Shape Memory Energy Absorbing Devices, by E.J. Graesser and F.A. Cozzarelli, 6/7/89, (PB90-164146).

NCEER-89-0019 "Nonlinear Dynamic Analysis of Three-Dimensional Base Isolated Structures (3D-BASIS)," by S. Nagarajaiah, A.M. Reinhorn and M.C. Constantinou, 8/3/89, (PB90-161936). This report is available only through NTIS (see address given above).

NCEER-89-0020 "Structural Control Considering Time-Rate of Control Forces and Control Rate Constraints," by F.Y. Cheng and C.P. Pantelides, 8/3/89, (PB90-120445).

NCEER-89-0021 "Subsurface Conditions of Memphis and Shelby County," by K.W. Ng, T-S. Chang and H-H.M. Hwang, 7/26/89, (PB90-120437).

NCEER-89-0022 "Seismic Wave Propagation Effects on Straight Jointed Buried Pipelines," by K. Elhmadi and M.J. O'Rourke, 8/24/89, (PB90-162322).

NCEER-89-0023 "Workshop on Serviceability Analysis of Water Delivery Systems," edited by M. Grigoriu, 3/6/89, (PB90-127424).

NCEER-89-0024 "Shaking Table Study of a 1/5 Scale Steel Frame Composed of Tapered Members," by K.C. Chang, J.S. Hwang and G.C. Lee, 9/18/89, (PB90-160169).

NCEER-89-0025 "DYNA1D: A Computer Program for Nonlinear Seismic Site Response Analysis - Technical Documentation," by Jean H. Prevost, 9/14/89, (PB90-161944). This report is available only through NTIS (see address given above).

NCEER-89-0026 "1:4 Scale Model Studies of Active Tendon Systems and Active Mass Dampers for Aseismic Protection," by A.M. Reinhorn, T.T. Soong, R.C. Lin, Y.P. Yang, Y. Fukao, H. Abe and M. Nakai, 9/15/89, (PB90-173246).

NCEER-89-0027 "Scattering of Waves by Inclusions in a Nonhomogeneous Elastic Half Space Solved by Boundary Element Methods," by P.K. Hadley, A. Askar and A.S. Cakmak, 6/15/89, (PB90-145699).

NCEER-89-0028 "Statistical Evaluation of Deflection Amplification Factors for Reinforced Concrete Structures," by H.H.M. Hwang, J-W. Jaw and A.L. Ch'ng, 8/31/89, (PB90-164633).

NCEER-89-0029 "Bedrock Accelerations in Memphis Area Due to Large New Madrid Earthquakes," by H.H.M. Hwang, C.H.S. Chen and G. Yu, 11/7/89, (PB90-162330).

NCEER-89-0030 "Seismic Behavior and Response Sensitivity of Secondary Structural Systems," by Y.Q. Chen and T.T. Soong, 10/23/89, (PB90-164658).

NCEER-89-0031 "Random Vibration and Reliability Analysis of Primary-Secondary Structural Systems," by Y. Ibrahim, M. Grigoriu and T.T. Soong, 11/10/89, (PB90-161951).

NCEER-89-0032 "Proceedings from the Second U.S. - Japan Workshop on Liquefaction, Large Ground Deformation and Their Effects on Lifelines, September 26-29, 1989," Edited by T.D. O'Rourke and M. Hamada, 12/1/89, (PB90-209388).

NCEER-89-0033 "Deterministic Model for Seismic Damage Evaluation of Reinforced Concrete Structures," by J.M. Bracci, A.M. Reinhorn, J.B. Mander and S.K. Kunnath, 9/27/89.

NCEER-89-0034 "On the Relation Between Local and Global Damage Indices," by E. DiPasquale and A.S. Cakmak, 8/15/89, (PB90-173865).

NCEER-89-0035 "Cyclic Undrained Behavior of Nonplastic and Low Plasticity Silts," by A.J. Walker and H.E. Stewart, 7/26/89, (PB90-183518).

NCEER-89-0036 "Liquefaction Potential of Surficial Deposits in the City of Buffalo, New York," by M. Budhu, R. Giese and L. Baumgrass, 1/17/89, (PB90-208455).

NCEER-89-0037 "A Deterministic Assessment of Effects of Ground Motion Incoherence," by A.S. Veletsos and Y. Tang, 7/15/89, (PB90-164294).

NCEER-89-0038 "Workshop on Ground Motion Parameters for Seismic Hazard Mapping," July 17-18, 1989, edited by R.V. Whitman, 12/1/89, (PB90-173923).

NCEER-89-0039 "Seismic Effects on Elevated Transit Lines of the New York City Transit Authority," by C.J. Costantino, C.A. Miller and E. Heymsfield, 12/26/89, (PB90-207887).

NCEER-89-0040 "Centrifugal Modeling of Dynamic Soil-Structure Interaction," by K. Weissman, Supervised by J.H. Prevost, 5/10/89, (PB90-207879).

NCEER-89-0041 "Linearized Identification of Buildings With Cores for Seismic Vulnerability Assessment," by I-K. Ho and A.E. Aktan, 11/1/89, (PB90-251943).

NCEER-90-0001 "Geotechnical and Lifeline Aspects of the October 17, 1989 Loma Prieta Earthquake in San Francisco," by T.D. O'Rourke, H.E. Stewart, F.T. Blackburn and T.S. Dickerman, 1/90, (PB90-208596).

NCEER-90-0002 "Nonnormal Secondary Response Due to Yielding in a Primary Structure," by D.C.K. Chen and L.D. Lutes, 2/28/90, (PB90-251976).

NCEER-90-0003 "Earthquake Education Materials for Grades K-12," by K.E.K. Ross, 4/16/90, (PB91-251984).

NCEER-90-0004 "Catalog of Strong Motion Stations in Eastern North America," by R.W. Busby, 4/3/90, (PB90-251984).

NCEER-90-0005 "NCEER Strong-Motion Data Base: A User Manual for the GeoBase Release (Version 1.0 for the Sun3)," by P. Friberg and K. Jacob, 3/31/90 (PB90-258062).

NCEER-90-0006 "Seismic Hazard Along a Crude Oil Pipeline in the Event of an 1811-1812 Type New Madrid Earthquake," by H.H.M. Hwang and C-H.S. Chen, 4/16/90(PB90-258054).

NCEER-90-0007 "Site-Specific Response Spectra for Memphis Sheahan Pumping Station," by H.H.M. Hwang and C.S. Lee, 5/15/90, (PB91-108811).

NCEER-90-0008 "Pilot Study on Seismic Vulnerability of Crude Oil Transmission Systems," by T. Ariman, R. Dobry, M. Grigoriu, F. Kozin, M. O'Rourke, T. O'Rourke and M. Shinozuka, 5/25/90, (PB91-108837).

NCEER-90-0009 "A Program to Generate Site Dependent Time Histories: EQGEN," by G.W. Ellis, M. Srinivasan and A.S. Cakmak, 1/30/90, (PB91-108829).

NCEER-90-0010 "Active Isolation for Seismic Protection of Operating Rooms," by M.E. Talbott, Supervised by M. Shinozuka, 6/8/9, (PB91-110205).

NCEER-90-0011 "Program LINEARID for Identification of Linear Structural Dynamic Systems," by C-B. Yun and M. Shinozuka, 6/25/90, (PB91-110312).

NCEER-90-0012 "Two-Dimensional Two-Phase Elasto-Plastic Seismic Response of Earth Dams," by A.N. Yiagos, Supervised by J.H. Prevost, 6/20/90, (PB91-110197).

NCEER-90-0013 "Secondary Systems in Base-Isolated Structures: Experimental Investigation, Stochastic Response and Stochastic Sensitivity," by G.D. Manolis, G. Juhn, M.C. Constantinou and A.M. Reinhorn, 7/1/90, (PB91-110320).

NCEER-90-0014 "Seismic Behavior of Lightly-Reinforced Concrete Column and Beam-Column Joint Details," by S.P. Pessiki, C.H. Conley, P. Gergely and R.N. White, 8/22/90, (PB91-108795).

NCEER-90-0015 "Two Hybrid Control Systems for Building Structures Under Strong Earthquakes," by J.N. Yang and A. Danielians, 6/29/90, (PB91-125393).

NCEER-90-0016 "Instantaneous Optimal Control with Acceleration and Velocity Feedback," by J.N. Yang and Z. Li, 6/29/90, (PB91-125401).

NCEER-90-0017 "Reconnaissance Report on the Northern Iran Earthquake of June 21, 1990," by M. Mehrain, 10/4/90, (PB91-125377).

NCEER-90-0018 "Evaluation of Liquefaction Potential in Memphis and Shelby County," by T.S. Chang, P.S. Tang, C.S. Lee and H. Hwang, 8/10/90, (PB91-125427).

NCEER-90-0019 "Experimental and Analytical Study of a Combined Sliding Disc Bearing and Helical Steel Spring Isolation System," by M.C. Constantinou, A.S. Mokha and A.M. Reinhorn, 10/4/90, (PB91-125385).

NCEER-90-0020 "Experimental Study and Analytical Prediction of Earthquake Response of a Sliding Isolation System with a Spherical Surface," by A.S. Mokha, M.C. Constantinou and A.M. Reinhorn, 10/11/90, (PB91-125419).

NCEER-90-0021 "Dynamic Interaction Factors for Floating Pile Groups," by G. Gazetas, K. Fan, A. Kaynia and E. Kausel, 9/10/90, (PB91-170381).

NCEER-90-0022 "Evaluation of Seismic Damage Indices for Reinforced Concrete Structures," by S. Rodriguez-Gomez and A.S. Cakmak, 9/30/90, PB91-171322).

NCEER-90-0023 "Study of Site Response at a Selected Memphis Site," by H. Desai, S. Ahmad, E.S. Gazetas and M.R. Oh, 10/11/90, (PB91-196857).

NCEER-90-0024 "A User's Guide to Strongmo: Version 1.0 of NCEER's Strong-Motion Data Access Tool for PCs and Terminals," by P.A. Friberg and C.A.T. Susch, 11/15/90, (PB91-171272).

NCEER-90-0025 "A Three-Dimensional Analytical Study of Spatial Variability of Seismic Ground Motions," by L-L. Hong and A.H.-S. Ang, 10/30/90, (PB91-170399).

NCEER-90-0026 "MUMOID User's Guide - A Program for the Identification of Modal Parameters," by S. Rodriguez-Gomez and E. DiPasquale, 9/30/90, (PB91-171298).

NCEER-90-0027 "SARCF-II User's Guide - Seismic Analysis of Reinforced Concrete Frames," by S. Rodriguez-Gomez, Y.S. Chung and C. Meyer, 9/30/90, (PB91-171280).

NCEER-90-0028 "Viscous Dampers: Testing, Modeling and Application in Vibration and Seismic Isolation," by N. Makris and M.C. Constantinou, 12/20/90 (PB91-190561).

NCEER-90-0029 "Soil Effects on Earthquake Ground Motions in the Memphis Area," by H. Hwang, C.S. Lee, K.W. Ng and T.S. Chang, 8/2/90, (PB91-190751).

NCEER-91-0001 "Proceedings from the Third Japan-U.S. Workshop on Earthquake Resistant Design of Lifeline Facilities and Countermeasures for Soil Liquefaction, December 17-19, 1990," edited by T.D. O'Rourke and M. Hamada, 2/1/91, (PB91-179259).

NCEER-91-0002 "Physical Space Solutions of Non-Proportionally Damped Systems," by M. Tong, Z. Liang and G.C. Lee, 1/15/91, (PB91-179242).

NCEER-91-0003 "Seismic Response of Single Piles and Pile Groups," by K. Fan and G. Gazetas, 1/10/91, (PB92-174994).

NCEER-91-0004 "Damping of Structures: Part I - Theory of Complex Damping," by Z. Liang and G. Lee, 10/10/91, (PB92-197235).

NCEER-91-0005 "3D-BASIS - Nonlinear Dynamic Analysis of Three Dimensional Base Isolated Structures: Part II," by S. Nagarajaiah, A.M. Reinhorn and M.C. Constantinou, 2/28/91, (PB91-190553).

NCEER-91-0006 "A Multidimensional Hysteretic Model for Plasticity Deforming Metals in Energy Absorbing Devices," by E.J. Graesser and F.A. Cozzarelli, 4/9/91, (PB92-108364).

NCEER-91-0007 "A Framework for Customizable Knowledge-Based Expert Systems with an Application to a KBES for Evaluating the Seismic Resistance of Existing Buildings," by E.G. Ibarra-Anaya and S.J. Fenves, 4/9/91, (PB91-210930).

NCEER-91-0008 "Nonlinear Analysis of Steel Frames with Semi-Rigid Connections Using the Capacity Spectrum Method," by G.G. Deierlein, S-H. Hsieh, Y-J. Shen and J.F. Abel, 7/2/91, (PB92-113828).

NCEER-91-0009 "Earthquake Education Materials for Grades K-12," by K.E.K. Ross, 4/30/91, (PB91-212142).

NCEER-91-0010 "Phase Wave Velocities and Displacement Phase Differences in a Harmonically Oscillating Pile," by N. Makris and G. Gazetas, 7/8/91, (PB92-108356).

NCEER-91-0011 "Dynamic Characteristics of a Full-Size Five-Story Steel Structure and a 2/5 Scale Model," by K.C. Chang, G.C. Yao, G.C. Lee, D.S. Hao and Y.C. Yeh," 7/2/91, (PB93-116648).

NCEER-91-0012 "Seismic Response of a 2/5 Scale Steel Structure with Added Viscoelastic Dampers," by K.C. Chang, T.T. Soong, S-T. Oh and M.L. Lai, 5/17/91, (PB92-110816).

NCEER-91-0013 "Earthquake Response of Retaining Walls; Full-Scale Testing and Computational Modeling," by S. Alampalli and A-W.M. Elgamal, 6/20/91, to be published.

NCEER-91-0014 "3D-BASIS-M: Nonlinear Dynamic Analysis of Multiple Building Base Isolated Structures," by P.C. Tsopelas, S. Nagarajaiah, M.C. Constantinou and A.M. Reinhorn, 5/28/91, (PB92-113885).

NCEER-91-0015 "Evaluation of SEAOC Design Requirements for Sliding Isolated Structures," by D. Theodossiou and M.C. Constantinou, 6/10/91, (PB92-114602).

NCEER-91-0016 "Closed-Loop Modal Testing of a 27-Story Reinforced Concrete Flat Plate-Core Building," by H.R. Somaprasad, T. Toksoy, H. Yoshiyuki and A.E. Aktan, 7/15/91, (PB92-129980).

NCEER-91-0017 "Shake Table Test of a 1/6 Scale Two-Story Lightly Reinforced Concrete Building," by A.G. El-Attar, R.N. White and P. Gergely, 2/28/91, (PB92-222447).

NCEER-91-0018 "Shake Table Test of a 1/8 Scale Three-Story Lightly Reinforced Concrete Building," by A.G. El-Attar, R.N. White and P. Gergely, 2/28/91, (PB93-116630).

NCEER-91-0019 "Transfer Functions for Rigid Rectangular Foundations," by A.S. Veletsos, A.M. Prasad and W.H. Wu, 7/31/91.

NCEER-91-0020 "Hybrid Control of Seismic-Excited Nonlinear and Inelastic Structural Systems," by J.N. Yang, Z. Li and A. Danielians, 8/1/91, (PB92-143171).

NCEER-91-0021 "The NCEER-91 Earthquake Catalog: Improved Intensity-Based Magnitudes and Recurrence Relations for U.S. Earthquakes East of New Madrid," by L. Seeber and J.G. Armbruster, 8/28/91, (PB92-176742).

NCEER-91-0022 "Proceedings from the Implementation of Earthquake Planning and Education in Schools: The Need for Change - The Roles of the Changemakers," by K.E.K. Ross and F. Winslow, 7/23/91, (PB92-129998).

NCEER-91-0023 "A Study of Reliability-Based Criteria for Seismic Design of Reinforced Concrete Frame Buildings," by H.H.M. Hwang and H-M. Hsu, 8/10/91, (PB92-140235).

NCEER-91-0024 "Experimental Verification of a Number of Structural System Identification Algorithms," by R.G. Ghanem, H. Gavin and M. Shinozuka, 9/18/91, (PB92-176577).

NCEER-91-0025 "Probabilistic Evaluation of Liquefaction Potential," by H.H.M. Hwang and C.S. Lee," 11/25/91, (PB92-143429).

NCEER-91-0026 "Instantaneous Optimal Control for Linear, Nonlinear and Hysteretic Structures - Stable Controllers," by J.N. Yang and Z. Li, 11/15/91, (PB92-163807).

NCEER-91-0027 "Experimental and Theoretical Study of a Sliding Isolation System for Bridges," by M.C. Constantinou, A. Kartoum, A.M. Reinhorn and P. Bradford, 11/15/91, (PB92-176973).

NCEER-92-0001 "Case Studies of Liquefaction and Lifeline Performance During Past Earthquakes, Volume 1: Japanese Case Studies," Edited by M. Hamada and T. O'Rourke, 2/17/92, (PB92-197243).

NCEER-92-0002 "Case Studies of Liquefaction and Lifeline Performance During Past Earthquakes, Volume 2: United States Case Studies," Edited by T. O'Rourke and M. Hamada, 2/17/92, (PB92-197250).

NCEER-92-0003 "Issues in Earthquake Education," Edited by K. Ross, 2/3/92, (PB92-222389).

NCEER-92-0004 "Proceedings from the First U.S. - Japan Workshop on Earthquake Protective Systems for Bridges," Edited by I.G. Buckle, 2/4/92, (PB94-142239, A99, MF-A06).

NCEER-92-0005 "Seismic Ground Motion from a Haskell-Type Source in a Multiple-Layered Half-Space," A.P. Theoharis, G. Deodatis and M. Shinozuka, 1/2/92, to be published.

NCEER-92-0006 "Proceedings from the Site Effects Workshop," Edited by R. Whitman, 2/29/92, (PB92-197201).

NCEER-92-0007 "Engineering Evaluation of Permanent Ground Deformations Due to Seismically-Induced Liquefaction," by M.H. Baziar, R. Dobry and A-W.M. Elgamal, 3/24/92, (PB92-222421).

NCEER-92-0008 "A Procedure for the Seismic Evaluation of Buildings in the Central and Eastern United States," by C.D. Poland and J.O. Malley, 4/2/92, (PB92-222439).

NCEER-92-0009 "Experimental and Analytical Study of a Hybrid Isolation System Using Friction Controllable Sliding Bearings," by M.Q. Feng, S. Fujii and M. Shinozuka, 5/15/92, (PB93-150282).

NCEER-92-0010 "Seismic Resistance of Slab-Column Connections in Existing Non-Ductile Flat-Plate Buildings," by A.J. Durrani and Y. Du, 5/18/92.

NCEER-92-0011 "The Hysteretic and Dynamic Behavior of Brick Masonry Walls Upgraded by Ferrocement Coatings Under Cyclic Loading and Strong Simulated Ground Motion," by H. Lee and S.P. Prawel, 5/11/92, to be published.

NCEER-92-0012 "Study of Wire Rope Systems for Seismic Protection of Equipment in Buildings," by G.F. Demetriades, M.C. Constantinou and A.M. Reinhorn, 5/20/92.

NCEER-92-0013 "Shape Memory Structural Dampers: Material Properties, Design and Seismic Testing," by P.R. Witting and F.A. Cozzarelli, 5/26/92.

NCEER-92-0014 "Longitudinal Permanent Ground Deformation Effects on Buried Continuous Pipelines," by M.J. O'Rourke, and C. Nordberg, 6/15/92.

NCEER-92-0015 "A Simulation Method for Stationary Gaussian Random Functions Based on the Sampling Theorem," by M. Grigoriu and S. Balopoulou, 6/11/92, (PB93-127496).

NCEER-92-0016 "Gravity-Load-Designed Reinforced Concrete Buildings: Seismic Evaluation of Existing Construction and Detailing Strategies for Improved Seismic Resistance," by G.W. Hoffmann, S.K. Kunnath, A.M. Reinhorn and J.B. Mander, 7/15/92, (PB94-142007, A08, MF-A02).

NCEER-92-0017 "Observations on Water System and Pipeline Performance in the Limón Area of Costa Rica Due to the April 22, 1991 Earthquake," by M. O'Rourke and D. Ballantyne, 6/30/92, (PB93-126811).

NCEER-92-0018 "Fourth Edition of Earthquake Education Materials for Grades K-12," Edited by K.E.K. Ross, 8/10/92.

NCEER-92-0019 "Proceedings from the Fourth Japan-U.S. Workshop on Earthquake Resistant Design of Lifeline Facilities and Countermeasures for Soil Liquefaction," Edited by M. Hamada and T.D. O'Rourke, 8/12/92, (PB93-163939).

NCEER-92-0020 "Active Bracing System: A Full Scale Implementation of Active Control," by A.M. Reinhorn, T.T. Soong, R.C. Lin, M.A. Riley, Y.P. Wang, S. Aizawa and M. Higashino, 8/14/92, (PB93-127512).

NCEER-92-0021 "Empirical Analysis of Horizontal Ground Displacement Generated by Liquefaction-Induced Lateral Spreads," by S.F. Bartlett and T.L. Youd, 8/17/92, (PB93-188241).

NCEER-92-0022 "IDARC Version 3.0: Inelastic Damage Analysis of Reinforced Concrete Structures," by S.K. Kunnath, A.M. Reinhorn and R.F. Lobo, 8/31/92, (PB93-227502, A07, MF-A02).

NCEER-92-0023 "A Semi-Empirical Analysis of Strong-Motion Peaks in Terms of Seismic Source, Propagation Path and Local Site Conditions, by M. Kamiyama, M.J. O'Rourke and R. Flores-Berrones, 9/9/92, (PB93-150266).

NCEER-92-0024 "Seismic Behavior of Reinforced Concrete Frame Structures with Nonductile Details, Part I: Summary of Experimental Findings of Full Scale Beam-Column Joint Tests," by A. Beres, R.N. White and P. Gergely, 9/30/92, (PB93-227783, A05, MF-A01).

NCEER-92-0025 "Experimental Results of Repaired and Retrofitted Beam-Column Joint Tests in Lightly Reinforced Concrete Frame Buildings," by A. Beres, S. El-Borgi, R.N. White and P. Gergely, 10/29/92, (PB93-227791, A05, MF-A01).

NCEER-92-0026 "A Generalization of Optimal Control Theory: Linear and Nonlinear Structures," by J.N. Yang, Z. Li and S. Vongchavalitkul, 11/2/92, (PB93-188621).

NCEER-92-0027 "Seismic Resistance of Reinforced Concrete Frame Structures Designed Only for Gravity Loads: Part I - Design and Properties of a One-Third Scale Model Structure," by J.M. Bracci, A.M. Reinhorn and J.B. Mander, 12/1/92, (PB94-104502, A08, MF-A02).

NCEER-92-0028 "Seismic Resistance of Reinforced Concrete Frame Structures Designed Only for Gravity Loads: Part II - Experimental Performance of Subassemblages," by L.E. Aycardi, J.B. Mander and A.M. Reinhorn, 12/1/92, (PB94-104510, A08, MF-A02).

NCEER-92-0029 "Seismic Resistance of Reinforced Concrete Frame Structures Designed Only for Gravity Loads: Part III - Experimental Performance and Analytical Study of a Structural Model," by J.M. Bracci, A.M. Reinhorn and J.B. Mander, 12/1/92, (PB93-227528, A09, MF-A01).

NCEER-92-0030 "Evaluation of Seismic Retrofit of Reinforced Concrete Frame Structures: Part I - Experimental Performance of Retrofitted Subassemblages," by D. Choudhuri, J.B. Mander and A.M. Reinhorn, 12/8/92, (PB93-198307, A07, MF-A02).

NCEER-92-0031 "Evaluation of Seismic Retrofit of Reinforced Concrete Frame Structures: Part II - Experimental Performance and Analytical Study of a Retrofitted Structural Model," by J.M. Bracci, A.M. Reinhorn and J.B. Mander, 12/8/92, (PB93-198315, A09, MF-A03).

NCEER-92-0032 "Experimental and Analytical Investigation of Seismic Response of Structures with Supplemental Fluid Viscous Dampers," by M.C. Constantinou and M.D. Symans, 12/21/92, (PB93-191435).

NCEER-92-0033 "Reconnaissance Report on the Cairo, Egypt Earthquake of October 12, 1992," by M. Khater, 12/23/92, (PB93-188621).

NCEER-92-0034 "Low-Level Dynamic Characteristics of Four Tall Flat-Plate Buildings in New York City," by H. Gavin, S. Yuan, J. Grossman, E. Pekelis and K. Jacob, 12/28/92, (PB93-188217).

NCEER-93-0001 "An Experimental Study on the Seismic Performance of Brick-Infilled Steel Frames With and Without Retrofit," by J.B. Mander, B. Nair, K. Wojtkowski and J. Ma, 1/29/93, (PB93-227510, A07, MF-A02).

NCEER-93-0002 "Social Accounting for Disaster Preparedness and Recovery Planning," by S. Cole, E. Pantoja and V. Razak, 2/22/93, (PB94-142114, A12, MF-A03).

NCEER-93-0003 "Assessment of 1991 NEHRP Provisions for Nonstructural Components and Recommended Revisions," by T.T. Soong, G. Chen, Z. Wu, R-H. Zhang and M. Grigoriu, 3/1/93, (PB93-188639).

NCEER-93-0004 "Evaluation of Static and Response Spectrum Analysis Procedures of SEAOC/UBC for Seismic Isolated Structures," by C.W. Winters and M.C. Constantinou, 3/23/93, (PB93-198299).

NCEER-93-0005 "Earthquakes in the Northeast - Are We Ignoring the Hazard? A Workshop on Earthquake Science and Safety for Educators," edited by K.E.K. Ross, 4/2/93, (PB94-103066, A09, MF-A02).

NCEER-93-0006 "Inelastic Response of Reinforced Concrete Structures with Viscoelastic Braces," by R.F. Lobo, J.M. Bracci, K.L. Shen, A.M. Reinhorn and T.T. Soong, 4/5/93, (PB93-227486, A05, MF-A02).

NCEER-93-0007 "Seismic Testing of Installation Methods for Computers and Data Processing Equipment," by K. Kosar, T.T. Soong, K.L. Shen, J.A. HoLung and Y.K. Lin, 4/12/93, (PB93-198299).

NCEER-93-0008 "Retrofit of Reinforced Concrete Frames Using Added Dampers," by A. Reinhorn, M. Constantinou and C. Li, to be published.

NCEER-93-0009 "Seismic Behavior and Design Guidelines for Steel Frame Structures with Added Viscoelastic Dampers," by K.C. Chang, M.L. Lai, T.T. Soong, D.S. Hao and Y.C. Yeh, 5/1/93, (PB94-141959, A07, MF-A02).

NCEER-93-0010 "Seismic Performance of Shear-Critical Reinforced Concrete Bridge Piers," by J.B. Mander, S.M. Waheed, M.T.A. Chaudhary and S.S. Chen, 5/12/93, (PB93-227494, A08, MF-A02).

NCEER-93-0011 "3D-BASIS-TABS: Computer Program for Nonlinear Dynamic Analysis of Three Dimensional Base Isolated Structures," by S. Nagarajaiah, C. Li, A.M. Reinhorn and M.C. Constantinou, 8/2/93, (PB94-141819, A09, MF-A02).

NCEER-93-0012 "Effects of Hydrocarbon Spills from an Oil Pipeline Break on Ground Water," by O.J. Helweg and H.H.M. Hwang, 8/3/93, (PB94-141942, A06, MF-A02).

NCEER-93-0013 "Simplified Procedures for Seismic Design of Nonstructural Components and Assessment of Current Code Provisions," by M.P. Singh, L.E. Suarez, E.E. Matheu and G.O. Maldonado, 8/4/93, (PB94-141827, A09, MF-A02).

NCEER-93-0014 "An Energy Approach to Seismic Analysis and Design of Secondary Systems," by G. Chen and T.T. Soong, 8/6/93, (PB94-142767, A11, MF-A03).

NCEER-93-0015 "Proceedings from School Sites: Becoming Prepared for Earthquakes - Commemorating the Third Anniversary of the Loma Prieta Earthquake," Edited by F.E. Winslow and K.E.K. Ross, 8/16/93.

NCEER-93-0016 "Reconnaissance Report of Damage to Historic Monuments in Cairo, Egypt Following the October 12, 1992 Dahshur Earthquake," by D. Sykora, D. Look, G. Croci, E. Karaesmen and E. Karaesmen, 8/19/93, (PB94-142221, A08, MF-A02).

NCEER-93-0017 "The Island of Guam Earthquake of August 8, 1993," by S.W. Swan and S.K. Harris, 9/30/93, (PB94-141843, A04, MF-A01).

NCEER-93-0018 "Engineering Aspects of the October 12, 1992 Egyptian Earthquake," by A.W. Elgamal, M. Amer, K. Adalier and A. Abul-Fadl, 10/7/93, (PB94-141983, A05, MF-A01).

NCEER-93-0019 "Development of an Earthquake Motion Simulator and its Application in Dynamic Centrifuge Testing," by I. Krstelj, Supervised by J.H. Prevost, 10/23/93.

NCEER-93-0020 "NCEER-Taisei Corporation Research Program on Sliding Seismic Isolation Systems for Bridges: Experimental and Analytical Study of a Friction Pendulum System (FPS)," by M.C. Constantinou, P. Tsopelas, Y-S. Kim and S. Okamoto, 11/1/93, (PB94-142775, A08, MF-A02).

NCEER-93-0021 "Finite Element Modeling of Elastomeric Seismic Isolation Bearings," by L.J. Billings, Supervised by R. Shepherd, 11/8/93, to be published.

NCEER-93-0022 "Seismic Vulnerability of Equipment in Critical Facilities: Life-Safety and Operational Consequences," by K. Porter, G.S. Johnson, M.M. Zadeh, C. Scawthorn and S. Eder, 11/24/93.

NCEER-93-0023 "Hokkaido Nansei-oki, Japan Earthquake of July 12, 1993, by P.I. Yanev and C.R. Scawthorn, 12/23/93.

NCEER-94-0001 "An Evaluation of Seismic Serviceability of Water Supply Networks with Application to San Francisco Auxiliary Water Supply System," by I. Markov, Supervised by M. Grigoriu and T. O'Rourke, 1/21/94.

NCEER-94-0002 "NCEER-Taisei Corporation Research Program on Sliding Seismic Isolation Systems for Bridges: Experimental and Analytical Study of Systems Consisting of Sliding Bearings, Rubber Restoring Force Devices and Fluid Dampers," Volumes I and II, by P. Tsopelas, S. Okamoto, M.C. Constantinou, D. Ozaki and S. Fujii, 2/4/94.

NCEER-94-0003 "A Markov Model for Local and Global Damage Indices in Seismic Analysis," by S. Rahman and M. Grigoriu, 2/18/94.